NASA CONTRACTOR REPORT

NASA CR-1762

EFFECTS OF VIBRATION AND SHOCK ON THE PERFORMANCE OF GAS-BEARING SPACE-POWER BRAYTON CYCLE TURBOMACHINERY.

I – Half-Sine Shock and Sinusoidal Vibration

by Paul R. Spencer, Peter W. Curwen, and Henry B. Tryon

Prepared by
MECHANICAL TECHNOLOGY INCORPORATED
Latham, N.Y. 12110
for

NATIONAL AERONAUTICS AND SPACE ADMINISTRATION • WASHINGTON, D. C. • JULY 1971

1. Report No.	2. Government Accession No.	3. Recipient's Catalog No.
NASA CR-1762		

4. Title and Subtitle	5. Report Date
EFFECTS OF VIBRATION AND SHOCK ON THE PERFORMANCE OF GAS-BEARING SPACE-POWER BRAYTON CYCLE TURBOMACHINERY. I - HALF-SINE SHOCK AND SINUSOIDAL VIBRATION	July 1971
	6. Performing Organization Code
7. Author(s) Paul R. Spencer and Peter W. Curwen, Mechanical Technology Incorporated; and Henry B. Tryon, Lewis Research Center, Cleveland, Ohio.	8. Performing Organization Report No. MTI-70TR19
	10. Work Unit No.
9. Performing Organization Name and Address Mechanical Technology Incorporated 968 Albany-Shaker Road Latham, New York 12110	11. Contract or Grant No. NASw-1713
	13. Type of Report and Period Covered Contractor Report
12. Sponsoring Agency Name and Address National Aeronautics and Space Administration Washington, D.C. 20546	14. Sponsoring Agency Code

15. Supplementary Notes

16. Abstract

Testing of a high-speed gas-bearing-supported rotor assembly has been performed to obtain an initial assessment of the effects of environmental shock and vibration on the mechanical performance of Brayton Cycle space-power turbomachinery. Sinusoidal vibration testing was conducted over a frequency range of 5 to 2000 Hz. Shock testing was performed with 10-millisecond half-sine pulses of approximately 20-g peak acceleration. The vibration and shock conditions were applied in three orthogonal directions. Testing was conducted with and without shaft rotation, and with and without the rotor-bearing assembly mounted on vibration isolators. The test results indicate that the specified shock condition should not be a problem for gas-lubricated Brayton Cycle space-power turbomachinery. Sinusoidal vibration could be a problem, particularly if imposed while the machinery is running. The use of vibration isolators appears to be a solution to the vibration problems during shutdown (nonrotating) conditions. During rotation, the use of isolators greatly reduces, but may not eliminate, the possibility of vibration-induced bearing contacts. Further testing will be required to identify if such contacts would cause bearing damage or degradation of bearing performance.

17. Key Words (Suggested by Author(s))	18. Distribution Statement
Shock and vibration Gas bearings Brayton cycle Space power	Unclassified - unlimited

19. Security Classif. (of this report)	20. Security Classif. (of this page)	21. No. of Pages	22. Price*
Unclassified	Unclassified	203	$3.00

*For sale by the National Technical Information Service, Springfield, Virginia 22151

FOREWORD

The research described in this report was conducted by Mechanical Technology Incorporated under NASA contract NASw-1713. Mr. Henry B. Tryon of the Lewis Research Center Space Power Systems Division was the NASA Project Manager.

The computer program used to calculate transverse vibration response of the rotor-bearing system was developed by Dr. Jorgen Lund of the Technical University of Denmark, Copenhagen, in his capacity as consultant to MTI. The program is an extension of one of MTI's basic rotor-response programs previously developed by Dr. Lund. The axial response computer program was developed by Mr. Paul Spencer of MTI.

The metallurgical analysis reported in Appendix D was conducted by Mr. Charles Nolan of the Watervliet Arsenal, Watervliet, New York.

The report was originally issued as Mechanical Technology Incorporated report MTI-70TR19.

TABLE OF CONTENTS

	Page
SUMMARY	1
INTRODUCTION	6
DESCRIPTION OF EQUIPMENT	8
Instrumentation	10
Test Method	12
AXIAL RESPONSE	15
Analytical Models Used	15
Method of Solution	16
Initial Results	20
Results of 5- to 2,000-Hz Vibration Tests	23
Results of Axial Shock Tests and Calculations	26
TRANSVERSE RESPONSE	30
Analysis Model for Transverse Vibration Calculations	30
Transverse Vibration Tests	34
Discussion of Transverse Vibration Tests and Calculations	34
Transverse Shock Testing	38
PHYSICAL EFFECTS ON BEARING SURFACES AND COMPONENTS	40
CONCLUSIONS	44
Experimental Observations	44
Bearing System Damage and Wear	46
Analytical Study of Shock and Vibration Response	46
Summary of Significant Results	48
RECOMMENDATIONS	52
LIST OF REFERENCES	54

APPENDICES

	Page
A. EQUATIONS OF MOTION FOR AXIAL RESPONSE	55
B. AXIAL RESPONSE COMPUTER PROGRAM	58
C. PHOTOGRAPHS OF BEARING SURFACES AND COMPONENTS	94
D. METALLURGICAL REPORT ON FLEXURE FAILURE	98
MATHEMATICAL SYMBOLS	103
FIGURES	105

LIST OF FIGURES

Figure		Page
1	Schematic of Turbocompressor Simulator Mounted on Test Stand (Vertical Orientation)	105
2	Schematic of Turbocompressor Simulator with Capacitance Probe Designations (Horizontal Orientation)	106
3	Simulator Mounted Vertically on Vibration Table	107
4	Simulator Mounted Horizontally on Vibration Table	108
5	Main Components of Rotor-Bearing Assembly	109
6	Photograph of the Simulator Forward (Primary) Thrust Bearing	110
7	Arrangement of Journal Bearing Pad	111
8	Shock Machine With Simulator Mounted Vertically on Shock and Vibration Isolators	112
9	Vibration Table With Simulator Mounted Horizontally on Shock and Vibration Isolation Isolators	113
10	Arrangement of Simulator Controls, Data Acquisition Equipment and Visual Displays	114
11	Maximum Vibration Test Objectives	115
12	Alternate Presentation of Maximum Vibration Test Objectives	116
13	Comparison Between Actual Shock Pulse and Two Idealized Shock Pulses	117
14	Single-Degree-of-Freedom Representation of Simulator Axial Response Mode	118
15	Three-Degree-of-Freedom Axial Response Model of Simulator on Shock and Vibration Isolators	119
16	Three-Degree-of-Freedom Axial Response Model of Simulator on Rigid Mounts	120
17	General Flowchart of Axial Shock and Vibration Response Computer Program	121
18	Static Load Characteristics of Thrust Bearing	122

Figure		Page
19	Damping Coefficient Characteristics of Thrust Bearing----------	123
20	Comparison Between Theoretical Transmissibility and Catalog Data for a Single Isolator----------	124
21	Measured Static Load Characteristic of a Single Test Isolator----------	125
22	Construction of Shock and Vibration Isolator----------	126
23	Representations of Thrust-Plate Housing for Stiffness Calculations----------	127
24	Measured Stiffness of Thrust-Plate Housing----------	128
25	Typical Computed Thrust Bearing Response to Axial Shock---------	129
26	Calculated Low-Frequency Axial Vibration Response----------	130
27	Measured Modal Behavior at 110 Hz----------	131
28	Lissajous Patterns Indicating 90° Phase Shift at 120 Hz---------	132
29	Test Set-Up to Measure Phase Shift----------	133
30	Measured Modal Behavior at 605 Hz----------	134
31	Measured Modal Behavior at 870 Hz----------	135
32	Response of Thrust Bearing Gas Film at 17 Hz----------	136
33	Maximum Axial Vibration Levels for Safe Operation of the Simulator When Rigidly Mounted on Vibration Table (Shaft Rotating at 39,000 rpm)----------	137
34	Maximum Axial Vibration Levels for Safe Operation of the Simulator When Mounted on Shock and Vibration Isolators (Shaft Rotating at 39,000 rpm)----------	138
35	Calculated and Measured Thrust Bearing Film Response to Axial Vibration About Region of First Resonance (Simulator Rigidly Mounted)----------	139
36	Data Displays for Axial Shock Test of the Simulator When Mounted on Isolation Mounts (Shaft Rotating at 39,000 rpm)------	140
37	Calculated and Measured Thrust Bearing Film Response to Axial Shock (Simulator Rigidly Mounted, Single-Degree-of-Freedom Analysis Model)----------	141
38	Calculated Response of Thrust Bearing Gas Film to a Haversine Approximation of the Axial Shock Pulse to Illustrate Effects of Film Damping----------	142

Figure		Page
39	Calculated and Measured Shock Response During Collapse of the Thrust-Bearing Gas Film	143
40	Damping Ratio of the Thrust-Bearing Gas Film Versus Film Thickness	144
41	Calculated and Measured Thrust-Bearing Gas Film Response to Axial Shock (Simulator Mounted on Isolators, Shafting Rotating at 39,000 rpm)	145
42	Calculated and Measured Thrust-Bearing Gas Film Response to Axial Shock (Simulator Mounted on Isolators, Calculated Values Based on Acceleration of Simulator Casing)	146
43	Parameters of Computer Program Used to Calculate Transverse Vibration Response	147
44	Definitions of Journal Bearing Pad Motions	148
45	Cross-Sectional View of Rotor-Bearing System Simulator	149
46	Model of Rotor and Casing Used in Computer Program to Calculate Transverse Vibration Response	150
47	Frequency Dependence of Normalized Journal-Bearing Stiffness and Damping Coefficients	151
48	Method of Determining Isolator System Parameters Showing Effect of Damping	152
49	Measured Orbits of Rotor at 166 Hz During Transverse Vibration Testing	153
50	Measured Orbits of Rotor at 225 Hz During Transverse Vibration Testing	154
51	Calculated Mode Shapes for the Two Rigid-Body Critical Speeds of the Rotor-Bearing System	155
52	Comparison Between Measured and Calculated Orbits at 166 Hz	156
53	Comparison Between Measured and Calculated Orbits at 225 Hz	157
54	Calculated Transverse Frequency Response Showing Region of First Two Rigid-Body Critical Speeds	158
55	Effect of Isolator Damping on Calculated Transverse Frequency Response	159

Figure		Page
56	Effect of Journal Bearing Damping on Calculated Transverse Frequency Response	160
57	Mode Shape of Casing at First Natural Bending Frequency	161
58	Maximum Transverse Vibration Levels in the T1 Direction for Safe Operation of the Simulator When Rigidly Mounted on Vibration Table (Shaft Rotating at 39,000 rpm)	162
59	Maximum Transverse Vibration Levels in the T1 Direction for Safe Operation of the Simulator When Mounted on Vibration Isolators (Shaft Rotating at 39,000 rpm)	163
60	Maximum Transverse Vibration Levels in the T2 Direction for Safe Operation of the Simulator When Rigidly Mounted on Vibration Table (Shaft Rotating at 39,000 rpm)	164
61	Maximum Transverse Vibration Levels in the T2 Direction for Safe Operation of the Simulator When Mounted on Vibration Isolators (Shaft Rotating at 39,000 rpm)	165
62	Maximum Transverse Vibration Levels in the T1 Direction for Safe Operation of the Simulator With Nonrotating Shaft, and With and Without Vibration Isolators	166
63	Maximum Transverse Vibration Levels in the T2 Direction for Safe Operation of the Simulator With Nonrotating Shaft, and With and Without Vibration Isolators	167
64	Data Displays of Transverse Shock Responses With Simulator Mounted on Vibration and Shock Isolators (Shaft Rotating at 39,000 rpm)	168
65	Forward Thrust Plate and Runner, Inspection 1, After Cleaning	169
66	Forward Thrust Plate and Runner, Inspection 2	170
67	Forward Thrust Plate and Runner, Inspection 3	171
68	Forward Thrust Plate and Runner, Inspection 4, Before Cleaning	172
69	Forward Thrust Plate and Runner Inspection 5, Before Cleaning	173
70	Reverse Thrust Plate and Runner, Inspection 1	174
71	Reverse Thrust Plate and Runner Inspection 5	175
72	Compressor Bearing Journal, Inspection 1	176

Figure		Page
73	Compressor Bearing Journal, Inspection 5	177
74	Compressor Journal Bearing Pads, Face View, Inspection 1	178
75	Compressor Journal Bearing Pads, Face View, Inspection 5	179
76	Compressor Journal Bearing Pads, Rear View with Pivots, Inspection 1	180
77	Compressor Journal Bearing Pads, Rear View with Pivots, Inspection 4	181
78	Compressor Journal Bearing Pad Pivot Surfaces, Inspection 4	182
79	Compressor Journal Bearing Pads, Rear View with Pivots, Inspection 5	183
80	Turbine Bearing Journal, Inspection 1	184
81	Turbine Bearing Journal, Inspection 5	185
82	Turbine Journal Bearing Pads, Face View, Inspection 1	186
83	Turbine Journal Bearing Pads, Face View, Inspection 2	187
84	Turbine Journal Bearing Pads, Rear View with Pivots, Inspection 1	188
85	Turbine Journal Bearing Pads, Rear View with Pivots, Inspection 4	189
86	Turbine Journal Bearing Pads, Rear View with Pivots, Inspection 5	190
87	Views of Fractured Flexure	191
88	Magnified Views of Fractured Flexure Surfaces	192
89	Electron Micrographs of Fractured Surfaces, 6500X	193
90	Grain Structure Micrographs	194

SUMMARY

Testing of a high-speed gas-bearing-supported rotor assembly has been performed to obtain an initial assessment of the effects of environmental shock and vibration on the mechanical performance of Brayton Cycle space-power turbomachinery. The rotor-bearing assembly consisted of a 10.5-pound, 39,000-rpm rotor, supported by two self-acting, pivoted-pad journal bearings and a self-acting, spiral-grooved thrust bearing. Sinusoidal vibration testing was conducted over a frequency range of 5 to 2000 Hz. Shock testing was performed with 10-millisecond half-sine pulses of approximately 20-g peak acceleration. The vibration and shock conditions were applied in three orthogonal directions: along the rotor axis (axial response), and transverse to the rotor axis in two directions (transverse response). Testing was conducted with and without shaft rotation, and with and without the rotor-bearing assembly mounted on vibration isolators. Dynamic displacements of the assembly were measured throughout the tests with capacitance probe equipment.

Further objectives of the investigation were as follows: to identify the design factors which most strongly influence shock and vibration response of gas lubricated space-power turbomachinery, and to validate analytical methods for predicting dynamic response of such turbomachinery. To this end, an analytical study of the shock and vibration response of the high-speed rotor-bearing test assembly was performed*. For axial response calculations, a nonlinear three-degree-of-freedom analytical model was developed. The equations of motion were programmed for digital computer solution using a fourth-order Runge-Kutta numerical integration procedure. Solutions can be obtained for various types of excitations: sinusoidal vibration, half-sine or haversine shock pulses, or any arbitrary vibration or shock characteristic expressed in terms of displacement (or acceleration) and time coordinates.

Analysis of transverse response was performed only for the case of sinusoidal

---

* The analytical study was performed only for the condition of shaft rotation (i.e., for the condition of hydrodynamic gas-film lubrication).

vibration excitation. A digital computer program was used to calculate steady-state vibration amplitudes of the rotor-bearing system based on a finite-element model of both the rotor and the rotor casing. A total of eight, frequency-dependent, linearized coefficients were used to represent the stiffness and damping characteristics of each journal bearing.

The significant results of this investigation are summarized below. From a quantitative standpoint, it must be remembered that the results apply to one specific rotor-bearing system. From a phenomenological standpoint, however, the system response characteristics are indicative of those which would be exhibited by similarly configured gas-lubricated rotor-bearing systems.

Shock Tests

1. Gas-lubricated rotor-bearing systems of the type tested can satisfactorily survive at least a limited number of externally imposed 10-millisecond, 20-g shock impulses*, both with and without shaft rotation, and with or without isolation mounts. For the system tested, momentary contacts between the rotating and stationary bearing surfaces were observed under all test conditions. However, there was no surface damage or degradation of bearing performance as a result of these contacts**.

Sinusoidal Vibration Tests – Shutdown Condition (Nonrotating Shaft)

1. Under shutdown (nonrotating) conditions, gas-bearing-supported rotor systems of the type tested can satisfactorily survive, at least for a limited period of time, axial imposition of the specified sinusoidal vibration conditions, either with or without isolation mounts.

---

* A total of 73 shock pulses were accumulated during the test program. Four of the axial pulses were inadvertently conducted at 60-g peak acceleration.

** Based on previous work, it is known that the ability of gas bearings to successfully survive repeated high-speed contacts is strongly dependent upon the bearing materials used. The experimental results reported herein were all obtained using bearing parts whose mating surfaces were coated with plasma-sprayed chrome oxide. Based on considerable testing, chrome oxide is the optimum gas-bearing surfacing material thus far identified for operation at temperatures up to 600°F.

2. For transversely imposed vibration under shutdown (nonrotating) conditions, vibration isolation may be required to survive the specified sinusoidal excitation conditions. During the nonrotating transverse vibration tests without isolators, the objective input excitation levels could not be achieved in the frequency range from 190 to 235 Hz, this being the region of one of the critical speeds (resonant frequencies) of the nonrotating shaft. The limiting factor in this frequency range was deflection (overstressing) of the flexures used to support the individual journal bearing pads. With isolators installed, excitation of the flexures was greatly reduced and the objective input vibration levels could be safely imposed in the two transverse directions.

3. A total of 27 minutes of vibration testing was accumulated under nonrotating conditions. No damage to the bearing surfaces nor degradation of bearing performance was detected as a result of the nonrotating tests.

Sinusoidal Vibration Tests — Normal Operation (Rotating Shaft)

1. Under normal rotating conditions, gas-lubricated rotor-bearing systems of the type tested may have to be vibration isolated to survive the specified sinusoidal vibration conditions. During the shaft rotation tests without isolation, rotor-to-bearing contacts became imminent, over broad regions of the frequency spectrum, at input vibration levels considerably below the test objectives. However, with isolators installed, the objective vibration input levels were achieved, without bearing contacts, over most of the frequency range. Only in the vicinity of the isolator resonant frequency (approximately 12 Hz), and in the vicinity of the rotor critical speeds (130, 166, and 225 Hz), did bearing contact become imminent at less than the objective vibration input levels.

2. Input vibration levels were carefully controlled during the rotating vibration tests to prevent the occurrence of bearing contacts. Consequently, it is not known whether bearing performance would have

been degraded under vibration-induced contact conditions.

Calculated Shock and Vibration Response

1. Accurate predictions of the axial shock and vibration response of gas-bearing machinery can be obtained using a three-degree-of freedom analytical model of the rotor-bearing system with nonlinear representation of the load and damping characteristics of the thrust bearing gas film. An approximate, simplified method of representing the gas-film nonlinearities can be used which yields both accurate and economic (in terms of computer cost) solutions. The only drawback of the herein presented axial response analysis is the modeling of the vibration isolators in terms of linear stiffness and damping coefficients. Under shock conditions (i.e., large displacement conditions) the isolators are quite nonlinear and must be so modeled*.

2. Accurate predictions of the transverse resonant frequencies of the rotor-bearing test system were obtained using the finite-element analysis model of the rotor and rotor casing, together with the linearized journal bearing stiffness and damping coefficients. There was, however, considerable discrepancy between the calculated and measured amplitudes of vibration, and of the rotor-to-casing orbit shapes. Calculated amplitudes were considerably higher than the measured amplitudes. The discrepancy in calculated amplitudes may be due to "large amplitude" nonlinear stiffness and damping effects in the journal bearings which were not represented in the analysis. There was also a small amount of horizontal vibration (cross talk) in the vibration table which was neglected in the calculations. Finally, there may have been significant damping from the thrust bearing and from the shaft labyrinth seals. These sources of damping were also neglected in the analysis.

---

* The axial-response computer program has, in fact, been modified during Task 3 of the present contract to permit nonlinear representation of the isolator deflection and damping characteristics. The results of additional Task 3 calculations with the nonlinear isolator model will be reported in Part II of this Final Report.

3. The analysis results clearly show the beneficial effects of gas-bearing squeeze-film damping on minimizing the severity of shock-induced bearing contacts. Gas-bearing systems which must operate under shock conditions should be optimized to take maximum advantage of this effect.

The above listed results indicate that 10-millisecond, 20-g shock pulses should not be a problem for gas-lubricated Brayton Cycle space-power turbomachinery. Sinusoidal vibration could be a problem, particularly if imposed during shaft rotation. The use of vibration isolators appears to be a solution to the vibration problems during shutdown (nonrotating) conditions. During rotation, the use of isolators greatly reduces, but may not eliminate, the possibility of vibration-induced bearing contacts. Further testing will be required to identify if such contacts would cause bearing damage or degradation of bearing performance.

INTRODUCTION

As America's space capabilities grow, it becomes more and more apparent that a long-life, reliable space-power source is required for the 10-15 kilowatt range. One likely candidate for a space-power system of this range is the Brayton Cycle System. This consists of an inert gas in a closed loop which, after being heated in a recuperator and a heat source, drives one or more turbines turning an alternator and a compressor before being cooled again in the recuperator and radiator. To avoid the problems associated with an oil-lubricated bearing system, the rotating equipment can be supported by gas bearings utilizing the working gas as a lubricant. These bearings have the added advantage of long life since bearing and shaft are separated during rotation by a film of gas.

Several items of Brayton Cycle rotating equipment have been built during recent years. This equipment has been tested by the NASA Lewis Research Center and by the associated contractors under both design and off-design conditions with excellent results. However, an assessment of the effects of environmental shock and vibration was not included in these initial tests. Although some low-frequency vibration and shock testing for Naval applications has been successfully conducted on a 62-pound, 8,000-rpm gas-bearing rotor [1], it was not felt that this experience was applicable to the dynamic environment associated with space-power applications. In particular, it was not known whether the latter environment might cause sufficient displacements of the shaft or bearing support assembly to result in contact between moving parts, fatigue, deformation, or fracture of parts with resulting failure of the machine.

In order to gain insight into the effects of shock and vibration upon gas-bearing machinery for space-power applications, the NASA Lewis Research Center contracted with Mechanical Technology Incorporated to conduct a combined analytical and experimental investigation using a high-speed, gas-bearing machine representative of the type under consideration. This was an especially opportune time, since a turbocompressor gas-bearing simulator of the general size, weight, and speed required had recently been made available from another NASA contract [2]. With minor modifications and some added instrumentation, the machine was well suited

for the experimental portion of this investigation.

The analytical portion of the investigation was devoted to developing calculation techniques and computer programs to the point where the effects of shock and vibration could be analytically predicted for a given rotor-bearing system. The experimental portion of the investigation consisted of subjecting the modified gas-bearing simulator to shock and vibration. This was done with the machine mounted in each of three mutually perpendicular positions, both with and without the shaft rotating, and with and without the use of isolators. The analytical results are compared with the measured results in this report, and the comparisons are used to validate the analytical procedures.

DESCRIPTION OF EQUIPMENT

A schematic of the turbocompressor simulator mounted on the test stand is shown in Figure 1. The rotor, shown in cross-hatching, consists of the following components:

a) The drive turbine
b) The turbine-end journal
c) A center section (which would normally hold a six-stage, axial compressor)
d) The compressor-end journal
e) The thrust runner.

Cross-sections AA and BB of Figure 1 show the configuration of the gas-lubricated, compressor-end and turbine-end journal bearings respectively. Self-acting, pivoted-pad bearings are used. Each pad is individually supported by a mechanical flexure to permit the bearings to accommodate radial centrifugal growth of the journals and differential, radial, thermal expansions between the various bearing parts. Details of the journal-bearing designs are given in Reference 2.

The gas-lubricated thrust-bearing assembly consists of a thrust runner, a reverse-thrust stator, a forward-thrust plate, and a support flexure and support housing for the forward-thrust plate. The forward bearing is the primary thrust bearing; the reverse bearing is used only during turbocompressor start-up. The forward bearing is a self-acting, spiral-groove type. The reverse bearing is an externally pressurized type. Design details for the complete thrust-bearing assembly are likewise documented in Reference 2.

Highly successful operation of the simulator gas bearings, up to 60,000 rpm, was demonstrated under static environmental conditions on a previous NASA contract [2]. For the shock-and-vibration testing described herein, the simulator was operated between 38,000 and 39,000 rpm, this being close to the design speed of a Brayton-cycle, space-power system currently being

investigated by NASA [3].

Figure 2 is a schematic of the turbocompressor simulator oriented horizontally. Also shown in Figure 2 is the capacitance probe coding scheme, which applies to the probes shown in Figure 1 as well.

Figure 3 is a photograph of the simulator and test stand mounted on the vibration shaker ready for testing. In this photograph, the simulator casing is rigidly mounted to the test stand. To perform tests with the casing on isolators, the two mounting blocks shown in Figure 3 were removed, two additional legs were added to the test stand, and a shock-and-vibration isolator was installed between the top of each leg and the simulator casing. The isolator mounting arrangement was symmetric about the rotor axis.

Figure 4 shows the tripod mounting arrangement used to mount the simulator, in a horizontal attitude, on the vibration table (shaker). The rigid mounting block on the right side of the photo has a hidden counterpart away from the viewer. These mounting blocks were interchangeable with the isolators used when the simulator was tested in the vertical as well as the horizontal attitude.

Figure 5 is a photograph of the main components of the rotor-bearing assembly. Here we see the forward-thrust bearing in some detail. The self-lubricating action of this bearing may be visualized by imagining the face of the thrust runner being placed upon the thrust plate and rotating clockwise at high speed. The runner drags or pumps the ambient gas inwardly along the lighter-appearing spiral grooves causing a high-pressure region at the sealed end of the grooves. This pressure produces the load-carrying capacity required to support the steady-state axial loads (aerodynamic thrust and rotor weight, for example) as well as the dynamic loads resulting from externally-imposed axial shock and vibration.

The simulator was designed to also support thrust loads with the rotor in a non-rotating condition. This is accomplished by supplying externally-pressurized gas to orifices in the thrust plate during startup and shutdown (hydrostatic operation). Figure 6 shows the size and location of these orifices, along with the spiral grooves which provide the hydrodynamic operation when the rotor achieves operating speed and the external pressure is withdrawn. A similar

arrangement of hydrostatic orifices was used in the reverse thrust bearing.

Figure 7 shows the arrangement of a typical journal-bearing pad. Four such pads were situated around each of the two journal bearings. A capacitance-probe lead is shown along with the pivot assembly. The pivot itself is not visible in Figure 7, but is located between the convex surface of the pad and the pivot assembly. The two short beams protruding from the assembly constitute the flexure when the two lugs are bolted to the casing.

Figure 8 shows the shock machine used in the experimental phase of the program. The simulator is shown mounted vertically on isolators. The operation of the shock machine is as follows: the table is raised pneumatically and then released to fall onto the elastomer pad shown resting on the anvil. The resulting impact produces a shock pulse that is roughly half-sine in shape.

Figure 9 shows the vibration shaker with the simulator mounted horizontally on isolators. In this position it was necessary to add lead weights to the compressor end of the casing in order to properly load the isolators without modification of the simulator casing.

Instrumentation

A permanent complement of capacitance probes was used to measure diaplacements of the rotating journals relative to the simulator casing, as well as film thickness in the journal and thrust bearings. Additional probes were used to measure relative displacements between various nonrotating parts of the bearing and casing assemblies. The capacitance probes are schematically indicated (in solid black) in Figure 1. The ends of the probes, mounted in the forward-thrust plate and the turbine-end journal-bearing pads, can be seen in Figures 5 and 6 (similar probes were mounted in the compressor-end jounal-bearing pads). These probes, used to measure instantaneous film thickness, had a linear range of 5 mils. All of the capacitance-probe instrumentation channels had a flat frequency response to 8 kHz.

The most significant transducer signals obtained in any given test were permanently documented on the multichannel tape recorder shown as part of the data

acquisition equipment in Figure 10. Dynamic responses were recorded on nine frequency-modulated (FM) channels, while a direct-record channel was used for voice recording. Most of the recording was done at 7.5 inches-per-second tape speed. Response of the FM channels at this speed was flat from DC to 2.5 kHz. Different combinations of transducer outputs to be recorded could be set up via the selector-switch panel.

The semi-circular cutouts in two of the turbine-end journal pads, shown in Figure 5, provide clearance for two capacitance probes used to measure dynamic motions of the journal in orthogonal directions. (Similar probes were used in the compressor-end bearing). These probes had a linear range of 10 mils and were used to display the orbital motions of the journals.

Crystal accelerometers were used at different points on the simulator casing and the test stand. Figure 3 shows several accelerometers mounted on the casing. Frequency response of the accelerometers and related signal-conditioning equipment was flat from 2 Hz to 9 kHz, based on catalog data.

Strain gages were mounted on several of the journal-bearing flexures, and on the forward-thrust-plate flexure, to measure dynamic strain in the flexures. Frequency response of the strain-gage system was flat to 3 kHz, based on catalog information.

Additional simulator transducers included pressure pickups to record simulator internal pressures, and a magnetic speed pickup to measure rotor speed.

Figure 10 also shows the simulator control station and the instrumentation display and recording equipment. At the simulator control station, rotor speed was indicated by an electronic counter located above the control panel. Speed was manually regulated by controlling air flow through the simulator drive turbine via a regulating valve located on the panel. Also located on the panel are two control valves for independent hydrostatic operation of the forward and reverse thrust bearings. During simulator startup, both bearings were operated hydrostatically (i.e., air pressure was supplied to the small orifices in the bearings). When sufficient speed was attained for hydrodynamic (self-acting) operation of the forward bearing, the hydrostatic pressure was shut off.

At this point the entire rotor became hydrodynamically supported, since the journal bearings are of the self-acting type.

The test personnel normally monitored the eight dual-beam oscilloscopes shown in Figure 10 during simulator operation. Four of the scopes displayed the journal-bearing film clearances between each of the eight pads and the journals, while two scopes displayed the journal orbits relative to the casing. One scope monitored the clearance of the thrust runner with respect to both the forward thrust plate and the reverse-thrust stator. The eighth scope was generally used to monitor a shock or vibration input accelerometer, and a simulator response accelerometer. The locations of these accelerometers were arbitrary, but they were usually chosen to be representative of the input, located near the test-stand base, and the output, located on the simulator itself. Although the above transducers were routinely monitored, certain circumstances required other sets of visual information. The selector-switch panel, shown in the center of the rack below the tape recorder, was used to obtain various combinations of transducer readout. A bank of charge amplifiers for the accelerometers was located just above the selector-switch panel.

Test Method

The vibration and shock tests were conducted independently. Each type of test was performed with and without isolation of the simulator casing, and with and without rotation of the shaft. Finally, the test combinations were conducted along each of three orthogonal axes of the simulator.

The vibration testing was entirely sinusoidal in nature. For purposes of this first exploration with the turbocompressor simulator, the following schedule was used:

5-33 Hz	-	140 mils double amplitude
33-140 Hz	-	8 g's peak
140-190 Hz	-	8 mils double amplitude
190-2000 Hz	-	15 g's peak.

This vibration schedule was not a qualification test specification used to determine whether the equipment would fail or pass. It was, rather, a set of

maximum vibration test objectives serving as a guideline while conducting the exploratory investigation of the vibration characteristics of the simulator. The maximum vibration test objectives are outlined in Figures 11 and 12. The former is an acceleration plot which forms the basis of actual performance limits discussed in this report. Figure 12 is simply a restatement of the objectives in terms of displacement, which is a form commonly encountered in MIL-Specs. The original specification was slightly modified to provide continuity at the 190-Hz crossover point, which was previously set at 240 Hz.

The shock-test objective calls for a half-sine pulse of 20-g peak acceleration and 10-milliseconds duration. This idealized shock pulse is shown in Figure 13, together with the actual pulse obtained from the shock machine, and a haversine approximation to the actual pulse. It is seen that the haversine is the better idealized approximation because it represents the case of elastic impact, which is nearly the situation of the shock table striking the elastomer pad on the anvil.

The nonrotating vibration tests were conducted by sweeping through the 5- to 2000-Hz range in accordance with the Figure 11 vibration amplitude schedule. During these tests, the signals from the strain gages mounted on the journal and thrust bearing flexures were continuously monitored to prevent overstressing of the flexures. For the rotating tests, an additional test criterion was imposed. The criterion required that the gas bearings always be maintained in a "contact-free" operating condition such that the three-axis vibration survey could be completed with a minimum possibility of damaging the bearings. This criterion was satisfied by limiting the minimum operating film thickness of the bearings to 0.1 mil.

To satisfy the above film thickness criterion during the rotating vibration tests, the vibration table was manually controlled such that the vibration conditions could be investigated slowly and carefully. If, as the 5- to 2000-Hz total frequency range was manually traversed, minimum dynamic film thickness in any one of the bearings approached 0.1 mil, the vibration-table amplitude was reduced to prevent the minimum film value from dropping below 0.1 mil. In this manner, vibration amplitude schedules for "contact-free" bearing operation were determined as a function of frequency. These "contact-free" amplitude

schedules did not meet the vibration objectives, as is discussed in a later section of this report.

Vibration-table amplitudes were also limited during the nonrotating tests to avoid excessive flexure stress. This problem would have to be corrected by redesign if the machine were to be flight rated.

The shock testing was performed on the pneumatically raised vertical-shock machine shown in Figure 8. A typical shock pulse was obtained with a table drop height of about one inch.

AXIAL RESPONSE

The shock and vibration tests were conducted along each of three orthogonal axes, one axial and two transverse. There was very little observed interaction between the axial and the transverse vibration modes; therefore, they are considered to be separate and distinct throughout the remainder of this report.

Analytical Models Used

To be easily usable as a design tool, the analytical model of a physical system should be kept as simple as possible. At the same time, the model must be capable of realistically describing, within acceptable limits of engineering accuracy, the effects that are of interest to the designer. The simplest possible model for describing axial response of the simulator is the single-degree-of-freedom model shown in Figure 14. This model is comprised of the rotor mass, m, and the non-linear gas force, $G(h,\dot{h})$, while the remainder of the simulator (the "base") is considered to be entirely rigid. This one-degree-of-freedom model is adequate to describe the response of the rigidly-mounted simulator to axial shock, but it is inadequate (as discussed later) to describe the response to axial vibration for rigid-mount conditions. Furthermore, the model cannot be used to describe either the axial shock or vibration response when the simulator is mounted on isolators.

Based on further consideration of the simulator design, as well as examination of the initial axial vibration test results, two three-degree-of-freedom analytical models were evolved which could satisfactorily describe the axial responses for all test conditions. These models are shown in Figures 15 and 16.

Figure 15 shows the three-degree-of-freedom model used to calculate the axial response of the simulator when mounted on isolators. The base is taken to be a rigid platform to which the shock or vibration excitation is applied. The shock and vibration isolators are assumed to have axial symmetry, as is the entire simulator, including symmetrical application and distribution of all applied forces. The isolators are also assumed to be representable by a linear spring, k_1, and a viscous damper, c_1, connected in parallel as shown. The entire casing

is considered sufficiently rigid to be represented by the lumped mass, m_1. The thrust-bearing housing and the thrust-bearing flexure are considered as two simple springs in series having an equivalent spring constant, k_2. Since these components are all metallic, they are considered to have negligible damping. The mass of the thrust plate, together with the effective combined mass of the thrust-plate flexure and the thrust-plate housing, are lumped into m_2. The mass of the rotor is lumped as m_3, which is connected to m_2 by the nonlinear gas-film force, $G(h,\dot{h})$. G is a function both of the film thickness, h, and its time derivative, $\dot{h}$.

In order to use three lumped masses to represent the simulator on rigid mounts, a slightly different set of assumptions is required. The method of modeling the simulator on rigid mounts is shown in Figure 16. The base is considered to include the entire test fixture and simulator casing. The input shock and vibration is thus applied directly to the mounting flange of the thrust-plate housing. The stiffness of the thrust-plate housing is represented by k_1 (c_1 is now considered to be negligibly small), and m_1 is taken as the effective mass of the housing. The stiffness of the thrust-plate flexure is lumped into k_2, while the mass of the thrust plate is combined with one-third of the mass of the flexure to produce m_2. The rest of the model is identical of the previous case; that is, G represents the nonlinear gas forces while m_3 represents the mass of the rotor. Again, complete axial symmetry is assumed with regard to properties and forces.

Method of Solution

A computer program was written to solve the equations of motion which describe the responses of the systems shown in Figures 14, 15, and 16. The derivation of these equations is presented in Appendix A. The computer program is described in a general way by the flow chart of Figure 17, while the details of the program, including program listing and operating instructions, are given in Appendix B.

The first decision indicated on the flow chart of Figure 17 is whether to use the system representation shown in Figure 16 (rigidly mounted complete model), Figure 15 (model on isolators), or Figure 14 (the simple model). The user may then select any of the following types of nonlinear functions to represent the load capacity and the damping coefficient characteristics of the thrust-bearing gas film

a) An exponential function of the form:

$$Ae^{-Bh}$$

where h = mean thickness of thrust bearing gas film

e = base of natural logarithms,

and A and B are constants selected by the user to give the best practical approximation to the nonlinear characteristics of the gas film as predetermined by applying rigorous lubrication theory.

b) A power function of the form:

$$Ch^{-D}$$

where C and D are the arbitrary constants used to obtain a curve fit.

The program will handle any of the four different types of forcing functions shown in Figure 17, which may be expressed either as base displacement or base acceleration. These forcing functions include sinusoidal vibration and three types of shock pulses.

The haversine pulse is the best simple idealization of the main shock pulse produced by the type of shock machine used, which relies on quasi-elastic impact to generate the required levels of acceleration. The half-sine pulse, as called for in the specification, is closely approximated by the haversine pulse, since the latter falls within the half-sine shock pulse tolerance limits given in Figure 516-2 of MIL-STD-810B, dated June 15, 1967. The half-sine pulse is physically unrealizable because the discontinuous derivatives at the end points imply a system with zero response time. The arbitrary shock-pulse excitation option adds considerable flexibility to the program. This option was used to describe the actual shock-machine pulse since it was necessary to include the acceleration values during the drop interval of the table.

In order to calculate the response of the simulator using the computer program, it is necessary to assign values to the parameters appearing in the equations of motion, as well as to define the nonlinear load capacity and damping characteristics of the thrust bearing gas film. Figure 18 shows curves of the static

load carrying capacity of the thrust-bearing as a function of film thickness. The solid curves were calculated by gas lubrication theory using Reynolds equation with appropriate boundary conditions for our particular bearing design operating under the conditions stated in the figure. The upper curve is based on calculations assuming flat and parallel surfaces. The effect of crowning (convex distortion) of the thrust plate results in a loss of load carrying capacity as is shown by the lower solid curve. Based on experience, it is not unreasonable to expect the amount of distortion represented by this lower curve, but we note that the curve still does not intersect a known load capacity point of the thrust bearing (10.5 pounds at a measured film thickness of 0.9 mils). Therefore, an exponential curve was assumed which was parallel to the original curve but displaced by a sufficient amount to agree with experimental evidence. The additional displacement is justifiable because of thermal effects. This dashed curve is the one used in the computer program.

Figure 19 shows the coefficient of viscous damping for the thrust bearing as a function of frequency and film thickness. The solid curves, which are rigorously correct only for "small" amplitude sinusoidal motions, are also based on gas lubrication theory under the same conditions as noted on Figure 18. The dashed curve is the power function approximation to the damping characteristic that was used in the computer program to calculate shock response, as well as to calculate vibration response at 200 Hz and below. Both the damping coefficient and the load capacity approximations begin to diverge from the theoretical curves at bearing clearances in excess of 2 mils, a fact which should be realized in interpreting some of the shock results presented later in this paper.

The above approach of treating the gas film has been made deliberately empirical. Alternatively, a more rigorous attack would have been to solve the Reynolds equation of gas dynamics [4], which is a nonlinear, partial-differential equation, to produce the thrust-bearing gas film force on a point-to-point basis. However, the rigorous solution would have required an increase in computer time by a considerable amount over the method evolved here. The intent here was instead to develop an economical design tool to determine the axial dynamic response of the rotor-bearing system.

In addition to the thrust bearing load capacity and damping characteristics, there are several other parameters required for axial response computations, such as the coefficients for isolator damping and stiffness, and for the housing stiffness.

The isolator properties were initially determined by taking manufacturer's data in the vicinity of peak transmissibility and performing a curve fit with the isolator representation shown in Figure 20. The good correlation obtained with the simple linear isolator representation is deceptive, however, when applied to field test conditions, as we shall show later. The principal deficiency in the simple model lies in its linearity.

Figure 21 presents the measured static-load characteristics of an individual shock-and-vibration isolator, presumed to be representative of the four that were used to isolate the simulator in the vertical attitude. It reveals the inadequacy of the simple linear representation. Although the isolator spring constant is essentially linear within its design static-load range, it exhibits strong nonlinearities under the conditions of shock previously stated. The total static load of the simulator was about 120 pounds, which initially loaded each isolator to 30 pounds. As the isolators go into tension shortly after shock-table release, they exhibit a spring-hardening characteristic.

This nonlinear load characteristic is due to two factors — the construction of the isolators, and the nonlinear modulus of the rubber used. The construction of an individual isolator is shown in Figure 22. The initial preload is carried by the concentric springs E and F. This load is applied through the specimen support mount G. For small deflections there is little compliance of the rubber spring inherent in the cylindrical section of A. The initial damping is primarily due to the relative motion between the split ring, C, which is loaded against the cup, B, via the split spring, D. After springs E and F have compressed, the rubber column of A provides some compliance and gives rise to a spring hardening characteristic when the deflection exceeds 0.5 inches. The rubber also provides the damping mechanism at these large deflections. The snubbers protruding above the retaining plate A transmit the load directly through the rubber column at very large deflections.

The stiffness of the thrust-plate housing is an important parameter required to calculate the response of the three-degree-of-freedom representation of the simulator on rigid mounts. This stiffness was initially calculated with the aid of Reference 5 for the three models shown in Figure 23. The spread of stiffness values shown was sufficient to require actual measurement to obtain sufficient accuracy and confidence. The methods of stiffness measurement along with the results obtained are presented in Figure 24. The method shown in the lower half of the figure is thought to be more representative of the actual attachment situation (the housing was bolted to the casing with three No. 10-32 screws) and therefore the lower stiffness value of 53,300 lb/in was used in the response calculations.

Initial Results

The static measurements and design values established in the foregoing section provide sufficient data to utilize the axial response computer program to generate some initial results.

A typical computer result is shown in Figure 25, which was produced by the computer program on an automatic plotter. The legend and axis scaling are entirely performed by the program. This particular response was obtained with a three-degree-of-freedom representation of the system. The lower right hand corner of the figure indicates the time of contact, at which point the rotor bottoms against the thrust plate. No subsequent calculations are performed beyond this point and the computer program automatically terminates because the analysis has no provision for bearing contact.

Figure 26 is also a typical example of the computer program output. This time, the excitation is a sinusoidal vibration applied to the single-degree-of-freedom representation of the system. Note that the nature of the solution required calculating the transient response all the way up through the steady-state solution. Scrutiny of this steady-state response after 0.04 seconds in Figure 26, reveals the calculated effect of the nonlinear gas film characteristic which amounts to an asymmetrical periodic motion about the equilibrium film thickness. As we shall see later, the measured asymmetry was even more pronounced than the

calculated value.

Figure 27 shows a typical set of data that were obtained during the vibration test program. The oscilloscope photos presented were taken at 110 Hz with an input vibration amplitude of approximately 0.1 g's peak. This frequency, while slightly below the resonance point, was representative of the resonance region. The photos show the modal behavior which prevailed up to about 300 Hz. The upper oscilloscope photo reveals that the gaps on each side of the thrust runner are moving out of phase and have equal total excursions. The middle photo shows that the reverse thrust plate has virtually no response relative to the housing except for a slight, high-frequency ripple corresponding to the running speed of the rotor.

The bottom photo shows that diametric positions of the thrust-bearing gas film are responding in phase and are of about equal amplitude. These three photos, taken collectively, lead to the conclusion that this modal behavior consists of axial motion of the rotor with no noticeable wobble and no detectable participation of other components, such as the thrust plate or the housing.

The undamped first natural frequency of the simulator was determined experimentally by observing the Lissajous pattern formed by the signals of a gas-film-thickness probe and a probe measuring base motion. Figures 28 and 29 indicate the method used. The Lissajous patterns of Figure 28 were obtained from the setup of Figure 29. The latter figure shows the capacitance probe "looking" at the displacement of the casing relative to the rigid piece of channel iron attached to the stationary portion of the vibration shaker. The signal obtained was fed into one channel of a dual beam scope while the gas film thickness was fed into the other channel. The relative amplitudes were adjusted to produce a circle at the 90-degree phase position to facilitate identification of this phase condition, which is depicted by the center Lissajous pattern in Figure 28. All three patterns were obtained with the same amplitude setting. The departure from ideal ellipses is due to the waveform departure from an ideal sinusoid. As noted on Figure 28, the undamped first natural frequency of the rotor was 120 Hz.

The computer program was used to predict both undamped and damped first natural axial frequencies of the rotor on the thrust bearing. An equivalent linear stiffness of the gas film was determined to be 27,000 lb/in by taking the derivative of the load curve at the point of static equilibrium corresponding to a rotor weight of 10.5 pounds. These values of stiffness and weight give a calculated undamped natural frequency of 158 Hz for a single-degree-of-freedom system. The discrepancy between this and the measured, undamped natural frequency (120 Hz) indicates that a single-degree-of-freedom representation is inadequate. The inadequacy cannot be ascribed to the gas-film nonlinearity because the axial response computer program yielded an undamped natural frequency of 150 Hz for the single-degree-of-freedom nonlinear representation.

A three-degree-of-freedom representation of the system was therefore considered. The equivalent lumped weight of m_2 was determined from a design drawing to be 1.4 pounds, and the equivalent value of m_1 was found by weighing the parts to be 0.4 pound. The measured value of k_1 was 53,300 lb/in while the design value of 670,000 lb/in was used for k_2. These values produced calculated undamped natural frequencies of 128 Hz, 685 Hz, and 4,654 Hz for a linear three-degree-of-freedom system. The first of these frequencies shows good agreement with the 120 Hz measured value.

Beyond the first natural frequency, two other distinct axial vibration modes were observed during the vibration test program. One of these is shown in Figure 30 which displays data from the same probes described in Figure 27. Figure 30 shows the modal behavior that occurred in the second distinct resonance region. These photos were taken at 605 Hz with about 0.5 g's peak input. The three displays are not simultaneous; therefore, amplitude comparisons cannot be made from photo to photo because of slight variations in vibration-table amplitude. Again, the mode is representative of the frequency region, and not necessarily at the resonance point. The upper photo shows that the probe readings on either side of the thrust runner are out of phase, and that the forward thrust-bearing gas film exhibits the greater of the excursions. The middle photo reveals that there is now some relative motion between the housing and the thrust plate. It further reveals that this relative motion is approximately 180 degrees out of phase with the thrust-bearing gas film. It is also worth noting that the second,

undamped, natural frequency for the linearized model was 685 Hz and lies within this second, observed resonance region. Furthermore, the gas film's total excursion is about equal to the sum of the other two relative motions, which implies that the thrust-plate housing itself is not participating in this mode. The lower photo, again, shows no significant wobbling of the thrust runner. These three photos, taken collectively, imply that the second mode consists of axial motion of both the rotor and the thrust plate, with the rotor exhibiting the greater amplitude.

A third mode, shown in Figure 31, was observed in the vicinity of 870 Hz. Oscilloscope photos obtained were similar to those of the second mode except that the reverse thrust bearing gap now displays an excursion one-third as large as the forward-thrust-bearing gas film variation. This implies that this third mode involved some flexing of the housing, or some relative motions between the housing, the casing, and the reverse-thrust plate. At any rate this third mode is not as readily explained as were the first and second modes.

The waveform of the thrust bearing response seen in Figures 27, 30, and 31, although not a pure sine wave, is reasonably sinusoidal. This condition prevailed throughout the frequency spectrum above 80 Hz. At lower excitation frequencies, however, the wave form became asymmetrical due to the film nonlinearity. This is shown in an idealized way in Figure 26.

Figure 32 shows that the actual asymmetry is considerably more severe. In fact, the waveform is highly irregular indicating the influence of effects not calculated by the simple theory. This study does not delve into the causes of the erratic waveform at low frequencies, but merely documents observation of the effect.

Results of 5- to 2,000-Hz Vibration Tests

Figures 33 and 34 show the input vibration levels which could be sustained, without and with isolators, while maintaining contact-free operation of the

thrust bearing. It is seen that considerably higher levels of input vibration could be sustained when using isolators. However, even with isolators, the desired levels of input acceleration were not achieved at low vibration frequencies due to resonance of the isolator-casing system at 12 Hz, and resonance of the thrust bearing at 130 Hz. Because of our decision to maintain contact-free bearing operation during the vibration tests with shaft rotation, we know only that bearing contacts would probably have occurred (with or without isolators) in the frequency regions where the objective input levels were not achieved. Further testing would be needed to determine whether sustained, vibration-induced, rotor-bearing contacts would significantly degrade bearing performance.

A series of computer runs was conducted using the nonlinear load and damping characteristics of the gas film to explore the region around the first natural frequency. The results are presented in Figure 35, which compares the vibration response of the three-degree-of-freedom system with that of the single-mass system and with actual measured values. In order to make these comparisons as consistent as possible, all the measurements were taken with a 0.2 mil peak-to-peak shaker amplitude, the same value used in the computer runs.* The single-degree-of-freedom results predict a peak at about 160 Hz. Observation of the phase angle between the input and response indicated a calculated undamped natural frequency of about 150 Hz. This is consistent with simple linear theory for a single mass system which predicts that the effect of damping is to shift the peak response of the relative displacement above the undamped natural frequency [6].

The three-degree-of-freedom model results in considerably better agreement with measured values than does the single-mass approximation. The three-mass model produces a peak response at 130 Hz which is consistent with the previously mentioned, measured, undamped frequency of 120 Hz. The effect of the gas-film non-linearity is to lower the first natural frequency of the three-mass model by a few percent. The foregoing is summarized in Table I.

The final series of axial vibration tests were performed with a nonrotating shaft, with and without vibration isolators. For either condition of mounting, the specified vibration excitation could be imposed over the complete 5- to 2,000-Hz range

*A common input amplitude was necessary because the natural frequencies of nonlinear systems are amplitude dependent.

TABLE I

Comparison of Values for the First
Natural Frequency of the
Simulator Rotor-Bearing System in the
Axial Response Mode (hydrodynamic operation at 38,500 rpm)

	Undamped Natural Frequency (Hz)	Resonant Frequency (Hz)
Analytical Model	Calculated	Calculated
1 mass linearized	158	–
1 mass nonlinear*	150	160
3 mass linearized	128	–
3 mass nonlinear*	125	130
	Measured	Measured
	120	Between 120 & 150

*The undamped natural frequency for the nonlinear system is actually a function of response amplitude; frequency decreases with increased amplitude. Values stated are based on 0.2 mils peak-to-peak input.

without exceeding safe dynamic stress levels in the thrust or journal bearing flexures. After each nonrotating vibration sweep, the simulator was started up and operating clearances of all bearings carefully checked. No significant change in bearing system performance was detected as a result of the nonrotating vibration tests.

Results of Axial Shock Tests and Calculations

Figure 36 shows a typical set of test data displays for axially imposed shock with the simulator mounted on isolators and the shaft rotating at 39,000 rpm. The top traces of photos A and B show the relative motions between the rotor and journal-bearing pads. Photos C and E are accelerometer traces. Photo D depicts the casing-to-thrust-plate motion in the top trace, and the relative motion between the casing and the reverse side of the thrust runner in the bottom trace.

Figure 37 shows a comparison of measured and calculated shock response of the thrust-bearing film thickness for the rigidly mounted simulator with the shaft rotating at 38,500 rpm. The calculated results were obtained using the axial response computer program described earlier. The initial response is a gradual increase in film thickness occurring as a result of the shock-table drop interval preceding the impact. As the impact occurs, however, the gas film undergoes a reversal, followed by a rapid decrease in film thickness. It is of interest to note that a slight hump appears in the calculated response curve during the final period of the gas-film collapse just prior to contact. It was initially thought that this hump was due to an irregularity of the shock pulse, which was modeled as a straight line during the drop interval. Therefore, the response was recalculated using the closed-form expression for a haversine as a pulse approximation.

Figure 38A shows the calculated undamped response of the thrust-bearing gas film using the haversine shock pulse approximation. Figure 38B is a repeat of the same calculation, but with the normal nonlinear thrust bearing damping restored. It is concluded from these two calculations that the inflection in the thrust bearing film thickness curve in Figure 38B results from the nonlinear property of the gas film rather than from a quirk of the shock pulse. This characteristic is of significant importance because, as illustrated by Figure 38B, the film

damping results in a slower approach velocity of the runner just prior to contact. This may result in far greater shock resistance for this type of gas bearing than one might otherwise expect.

Figure 39 furnishes further experimental evidence of the precontact inflection, together with further comparisons of the calculated shock response during collapse of the thrust-bearing gas film. Before film collapse, the three-degree-of-freedom model and the single-mass model yield similar calculated responses. The essential difference during the collapse interval, shown in Figure 39, is that the three-mass model predicts a simple inflection rather than the hump exhibited by the single-mass model. The simple inflection bears a closer resemblance to measured results and also appears for the three-mass model when a haversine approximation is used to represent the shock pulse. It is interesting to note that there is only a spread of about one millisecond in the contact time regardless of the model used to represent either the simulator or the shock pulse.

Figure 40 gives further explanation of the low velocity thrust bearing contact. The nonlinear film stiffness and damping functions are such that the damping ratio of the rotor-gas-film system becomes very large at small values of film clearances.

Figure 41 shows the measured shock response of the thrust-bearing gas film with the simulator mounted on shock-and-vibration isolators. For comparison, calculated results are shown using two different values of isolator stiffness. The agreement between calculated and measured response is considerably worse than was indicated for the rigidly mounted case shown in Figures 27 and 39. There is only a general agreement with respect to the gross behavior when the stiffer value of k_1 (16,000 lb/in) is used. For example, an initial peak occurs, with a noticeable discrepancy in amplitude, in both measured and calculated responses at about 70 milliseconds after shock-table release. This comment also applies to the dips occurring at about 77 milliseconds and the subsequent rise. Beyond 82 milliseconds, the calculated and measured responses diverge considerably. At about 87 milliseconds, the experimental data indicates that the thrust runner contacts the reverse-thrust plate. The computed response, however, does not even approach a contact amplitude until 110 milliseconds after table release.

The poor correlation evidenced in Figure 41 stands in sharp contrast to the close agreement between measured and calculated results shown in Figure 37. The fundamental difference in the measured behavior in the two cases is as follows: when rigid mounts are used (Figure 37), the initial collision occurs between the thrust runner and forward-thrust plate during the table-impact interval, with subsequent collisions between the thrust runner and reverse thrust plate; however, when shock-and-vibration isolators are used (Figure 41), the initial collision occurs between the thrust runner and reverse-thrust plate before the main pulse of the table-impact interval.

The computer program was not able to predict this contact with the reverse-thrust plate even when using a meticulous representation of the shock pulse with measured values of acceleration obtained every millisecond during the table-drop interval. The manner in which the isolators produce this sudden rise in film thickness to cause reverse contact can be qualitatively discussed as follows: initially, the shock table is released and begins to fall; the inertia of the low-frequency system (consisting of the simulator on the isolators), along with release of the preload on the isolators, cause an inherent response delay. Eventually the isolators are fully extended and begin to "snap back" so as to impart a sudden downward acceleration to the simulator casing. The reverse-thrust plate then collides with the thrust runner, which has its own inertia by virtue of the 10.5-pound rotor, as we shall see presently. An accelerometer attached to the casing verified that this was indeed the sequence of events.

The poor quantitative correlation shown in Figure 41 results from the inadequacy of the simple linear model used to represent the isolators. As Figure 41 indicates, adjustment of the linear spring constant, k_1, will not, by itself, give good correlation of results.

When table impact occurs at about 107 milliseconds after table release, the base acceleration reverses direction and tends to drive the isolators into compression. The subsequent g-levels on the simulator become large enough to produce compressive loads in excess of those shown in Figure 21. These loads, which are of the order of the product of the simulator weight (120 pounds) and the g-level (17 g's), place the operating point above the steep region near the upper right hand corner of Figure 21. In fact, the effective stiffness is in excess of the value

indicated because, as is shown in Reference 7, the dynamic modulus of rubber, having the hardness measured for the subject isolator (Durometer hardness = 67), is about twice the static modulus.

Figure 42 provides verification that the linear isolator modeling is the primary cause for the discrepancy shown in Figure 41. In order to get the results shown in Figure 42, the computer program was run using the measured casing accelerometer as the shock input, thereby effectively bypassing the isolators. By so doing, it was possible to analytically predict the salient features of the thrust-bearing gas-film response up to the point where the thrust runner collides against the reverse-thrust plate. Beyond this point the computer results would not be valid because the program contains no provision for bottoming in the form of bearing surface contact.

TRANSVERSE RESPONSE

As was previously mentioned, the axial and transverse responses exhibited very little interaction. Hence, the discussion of transverse response deals primarily with rotor and bearing motions in the vicinity of the journal bearings, with less relative significance attached to the thrust-bearing response.

The shock and vibration testing was conducted in two transverse directions, which are distinguishable by the dead-load position of the rotor with respect to the journal bearing pads. Each journal bearing consists of four identical pads supported by individual flexures. Two adjacent pads are supported by substantially stiffer flexures than are the remaining two. The two former pads will be referred to as "rigid" pads, and the two latter as "compliant" pads. The pad arrangement is seen in cross section in Figure 2. The two transverse directions in which dynamic loading was applied are defined as follows:

1. The "T1" direction, this being transverse rotor excitation in a direction parallel to the plane containing the rotor centerline and passing midway between the pivots of the two "rigid" pads;
2. The "T2" direction, this being transverse rotor excitation in a direction perpendicular to the "T1" direction (i.e., parallel to the plane containing the rotor centerline and passing midway between the pivots of one "rigid" pad and one "compliant" pad).

Analysis of transverse response was performed for the T1 direction only, and the only forcing function considered was that of steady-state vibration.

Analysis Model For Transverse Vibration Calculations

A distributed-parameter model of the rotor-bearing assembly was used to analyze system response to transversely applied vibration. This model, implemented in a MTI computer program, describes the rotor and casing in much the same way as one would consider a beam of varying cross section having continuously distributed mass and modulus of elasticity. The basic analysis is thoroughly described in

Reference 8 and will not be discussed in detail here.

The more significant capabilities of the computer program are pointed out in Figure 43 which specifies the parameters used to calculate transverse vibration response. In addition to the large number (theoretically limitless) of degrees of freedom arising from modeling the casing and rotor as continuous finite elements, other vibration modes result from the isolators and from the motions of the journal bearing pads. There are a total of eight pads in the journal bearing system and each pad has four degrees of freedom as shown in Figure 44. The translational mode and each of the three rotational modes may be excited, thereby giving rise to a number of frequencies at which various resonances might occur. The various frequencies that are associated with the particular bearing design used in the simulator are presented in tabular form in Table II.

A cross-section view of the rotor-bearing system simulator is shown in Figure 45. The details concerning each of the significant features shown are presented in Reference 2 and will not be dealt with here. We will consider primarily the analytical modeling of the rotor and casing as shown in Figure 46. This latter representation was obtained from the drawing of Figure 45 by dividing the rotor and casing into segments of an inch or two in length. At each segment, identified by a station number, values were assigned to the equivalent physical dimensions of that particular segment. In this way, complex regions could be very closely approximated by short sections of uniform, cylindrical cross section. The journal-bearing pad mass and inertia properties were also specified along with the gas film characteristics. It should be emphasized that the computer program used to determine transverse response is a sophisticated tool that has evolved from previously successful programs to calculate unbalance response of flexible rotors.

The gas film stiffnesses and damping characteristics of each journal bearing pad may be expressed in terms of eight linear coefficients. Thus, K_{xy} refers to the change in force in the x-direction due to an incremental motion in the y-direction. Similarly, B_{yx} refers to the change in viscous damping force in the y-direction due to an incremental velocity in the x-direction. These coefficients are commonly treated in normalized form as follows:

$$\bar{K}_{xy} = \frac{CK_{xy}}{P_a LD} \qquad \bar{B}_{yx} = \frac{C\omega B_{yx}}{P_a LD}$$

where C is the radial (machined) pad clearance, P_a is the ambient pressure, and L and D are the nominal bearing length and diameter, respectively. These coefficients are not constants, but vary both with journal eccentricity and with frequency of applied vibration. This frequency is commonly normalized by dividing it by the rotor speed. The resulting variation of the normalized coefficients is shown in Figure 47.

Another set of properties required by the analysis consisted of the isolator stiffness and damping values. An attempt was made to obtain these experimentally by vibrating the simulator transversely, with isolators, in the vicinity of the natural frequency of the isolator system. Accelerometer readings were obtained simultaneously to represent the input and output of the isolators. The former accelerometer was located on a reasonably rigid region of the base while the latter was located on the isolated simulator.

The results of these measurements, along with a series of curve-fit approximations, are presented in Figure 48. Comparison with Figure 20 reveals that, again, the measured values are generally below the curves obtained by a linear system representation. The effect of increasing the damping coefficient is to lower the analytical transmissibility values. The damping coefficient was adopted as C = 33. It was felt that higher values tended to flatten the curve excessively, thereby diluting the pronounced peak that was actually observed. As in the vertical case, the nonlinearity of the isolator introduces considerable error in attempting to describe the response with a linear model. At any rate, we have, at this point, determined the basic data that are required as input to the computer program. They are:

1) Model of rotor and casing
2) Journal bearing properties and gas film characteristics
3) Isolator properties.

Table II

Calculated Natural Frequencies of
Journal Bearing Pads

Bearing	Pad Flexure	Mode	Frequency* (Hz)
Compressor	Compliant	Radial	2100
Compressor	Compliant	Pitch	880
Compressor	Compliant	Roll	1170
Compressor	Compliant	Yaw	245
Compressor	Rigid	Radial	3580
Compressor	Rigid	Pitch	1300
Compressor	Rigid	Roll	1720
Compressor	Rigid	Yaw	370
Turbine	Compliant	Radial	1460
Turbine	Compliant	Pitch	625
Turbine	Compliant	Roll	860
Turbine	Compliant	Yaw	177
Turbine	Rigid	Radial	2820
Turbine	Rigid	Pitch	1000
Turbine	Rigid	Roll	1400
Turbine	Rigid	Yaw	290

*Shaft rotating at 39,000 rpm in air at 14.7 psia and 70°F.

Results of the transverse vibration response calculations are discussed starting on page 38.

Transverse Vibration Tests

The simulator transverse vibration tests were conducted in much the same way as were the axial vibration tests. That is, all bearing clearances were monitored while conducting a frequency sweep and continuously adjusting the amplitude to maximum values within the predetermined test envelope.

The most pronounced effect of vibrating the system transversely was to induce orbital motion of the rotor that was observed at both journal bearings. Two distinct orbital resonances were observed during the tests. The first of these occurred at 166 Hz, and the precise nature of the rotor orbits is shown in Figure 49. Figure 49a shows the relative displacement between the rotor and the casing at the position of the compressor journal bearing while Figure 49b shows the simultaneously occurring orbit in the vicinity of the turbine journal bearing.

The other distinct orbital resonance occurred at 225 Hz; the response is shown in Figure 50. As before, Figure 50a shows the rotor-to-casing displacement at the compressor journal bearing while Figure 50b shows the corresponding turbine bearing orbit taken simultaneously. Comparisons and further discussion of these orbits will be deferred to the next section.

Discussion of Transverse Vibration Tests and Calculations

It has been shown, in Figures 49 and 50, that rotor-bearing system resonances were excited at 166 and 225 Hz. These were subsequently identified as the rotor first and second rigid-body critical speeds, respectively.

A previously developed MTI rotor lateral critical speed computer program was used to calculate the modal shapes corresponding to these two frequencies and the results are presented in Figure 51 which is based on Figure II-21 of Reference 2. Examination of Figure 49 indicates that the first rigid-body mode

has a noticeably greater amplitude at the turbine journal bearing compared with the compressor bearing. This is predicted qualitatively in Figure 51.

The measured data of Figure 50 shows that, conversely, the second rigid-body mode produces a greater amplitude at the compressor bearing. This also is exhibited qualitatively in Figure 51.

It is not surprising that, at each frequency, the ratio of measured maximum orbital values is lower than what Figure 51 would indicate. The apparent discrepancy arises from the fact that pure modes are not excited in isolated ways. The two modal frequencies are quite close together and there is probably a substantial participation of the second mode at the lower forcing frequency and vice versa.

When the previously described rotor-casing model and bearing properties were used in the computer program to calculate transverse response, the orbits shown in Figure 52 resulted. The input steady-state sinusoidal vibration is 12 g's peak amplitude at 166 Hz, the same condition used to obtain the measured orbits of Figure 49. These measured orbits are presented in Figure 52 in an idealized form in order to make a direct comparison between measured and calculated paths. We observe only qualitative agreement in the sense that the major dimension, or orientation, lies roughly in the same general direction for the calculated and measured orbits. It should also be noted that the larger orbit occurs in the vicinity of the turbine journal bearing for both the calculated and measured responses.

Figure 53 is similar to Figure 52 except that the applied vibration condition is now 12 g's peak at 225 Hz, the critical speed of the second rigid body mode. Again, we get the relatively larger calculated orbit occurring at the compressor journal bearing as was observed in Figure 50 and predicted in Figure 51. A very significant discrepancy, however, is noted in Figure 53: the orientations of the measured orbits are off by about 90 degrees at the compressor journal bearing and by about 45 degrees at the turbine journal bearing.

One would expect that the rotor orbits would generally have their major axes

aligned with the direction of applied vibration. A slight perpendicular component would arise from gyroscopic effects due to a slope along the shaft which might occur in the vicinity of a heavy disk such as the turbine or thrust bearing. Indeed such forces produce the slight elliptical broadening seen in the calculated orbits in Figures 52 and 53. Some horizontal vibration component was probably present, although no measurement of it was attempted. In each case, however, the measured response component perpendicular to the direction of motion was observed to be noticeably greater than that calculated. The discrepancy is documented here, but no further attempt is made to explain it.

Although the computer program for transverse response yielded poor amplitude and orbital orientation data, it did yield remarkably good predictions of the resonant frequencies. This is evidenced in Figure 54 which shows the calculated peak amplitude of the relative displacement between the rotor and the housing as a function of frequency in the vicinity of the first and second rigid body critical speeds. The measured amplitudes at the observed critical speeds are spotted in on the graph, to show the poor amplitude agreement and the excellent frequency correlation.

The first parameter that was examined in an attempt to account for the amplitude discrepancy was the damping coefficient of the isolator. A decrease in damping causes a decrease in the transmissibility of the isolator within the frequency range of interest. The sensitivity of the response to this parameter is shown in Figure 55. Comparison between Figures 54 and 55 reveals that isolator damping is a relatively sensitive parameter for high damping values but it becomes less sensitive at the lower values. In fact, Figure 56 shows that regardless of how small we consider the isolator damping coefficient to be, it is impossible to explain the amplitude discrepancy at the turbine journal bearing solely in terms of isolator system damping.

The next parameter to be investigated was the damping value of the journal bearing gas films. Figure 56 shows that film damping is a very sensitive parameter throughout a wide range of values. The figure shows that it was possible to account for the discrepancy in amplitude at the compressor bearing by doubling the damping in this bearing. The turbine journal bearing, on the other hand,

requires a damping increase by a factor of 4 or 5 to bring the calculated amplitude down to the observed experimental value.

It thus appears that a source of discrepancy in the results is damping in the turbine region that is not properly accounted for in the computer program. This overlooked damping may possibly arise from the dissipation of energy in the turbine labyrinth seals.

Another interesting effect that was encountered as part of the transverse response calculations was identification of the first bending mode of the casing, the resonance of which corresponds to a forcing frequency of about 1440 Hz. The mode shape of the casing is shown in Figure 57 which presents the rotor-to-housing relative clearance for a one-mil amplitude sinusoidal input to the simulator on rigid mounts.

The other calculated natural frequencies, which are associated primarily with transverse response, are the individual journal bearing pad resonances. These frequencies are tabulated in Table II, and the terminology for the various vibration modes was previously defined in Figure 44. The majority of the pad resonances were not severely excited during the test. In fact, the only pad resonance that was clearly identified was the radial mode of one of the compliant pads in the turbine journal bearing. This resonance was so severe that the flexure failed during testing at 1365 Hz. It is interesting to note that this frequency is about 6.5% below the theoretical value as presented in Table II. The details concerning the failure are discussed in Appendix D.

Figures 58 through 61 summarize the vibration test results for transverse response in much the same way as Figures 33 and 34 did for the axial testing. Figure 58 presents the maximum safe operating levels for the rigidly mounted simulator with vibration applied in the T1 direction. No attempt was made to identify the individual component resonances while taking this data, but there was a general tendency toward severe reaction by the compressor journal bearing at the lower frequencies while the turbine journal bearing participated in the higher frequency region (above 800 Hz).

Figure 59 shows the response with vibration again applied in the T1 direction,

but this time the simulator was mounted on shock and vibration isolators. It is evident that the isolators performed their function well except for two narrow regions. The first of these occurred at the natural frequency of the isolators (between 6 Hz and 15 Hz). The second critical region occurred between 190 Hz and 235 Hz. Within this range of frequencies the rotor exhibited the same type of orbital motion discussed previously.

Figure 60 presents the maximum safe operating levels when vibration was applied in the T2 direction without isolators. The same general response descriptions for the T1 direction are also applicable here. In fact, the only essential difference is that there is some loading asymmetry inherent to the T2 direction.

Figure 61 shows that, once again, the isolators performed their intended function. In fact, even the orbital motions in the region between 190 and 235 Hz remained small enough to permit testing at the maximum test envelope. This is probably due to more of the orbital energy going into the perpendicular component because of the asymmetrical loading. The only region that could not be met was a one-Hz band width between 7 and 8 Hz.

We see from Figures 62 and 63 that isolators are also required in the presence of transverse vibration with a nonrotating rotor. With the simulator rigidly mounted, vibration within the frequency range from 190 to 235 Hz produced large amplitude levels in the journal bearing flexures, regardless of whether the vibration was applied in the T2 or the T1 direction. However, when the simulator was mounted on isolators and the rotor was inert, the full test objective could be safely accommodated in any direction.

Transverse Shock Testing

Shock testing in the transverse direction required that transducers be more closely monitored than was the case for the axial direction, as may be seen by comparing Figure 64 with Figure 36. The additional data presented in Figure 64 results from two factors: 1) orbital motion between the rotor and casing is excited, as indicated in oscilloscope photos b, c and d; and 2) the journal bearing pad-to-rotor motions are significantly induced by transverse shock, as is seen in photos a, e, f, and h.

The remaining photo, g, presents an accelerometer reading on the input side of the isolators (lower trace) and one on the output side (upper trace). These simultaneous traces, taken collectively, indicate that the effect of the isolators was to reduce the amplitude of transversely applied shock by a factor of two. A secondary effect was to spread the shock pulse over a longer time, which indicates that much of the shock energy was transferred rather than immediately dissipated by the isolators. Figure 64 also gives a good indication of the type of data that was displayed on the screens of the oscilloscopes shown in the "Data-Displays" section of Figure 10. Although the nature of the responses were completely different for the axial and transverse excitations, the same displays were monitored. The only circumstance in which basically different monitoring was required was when the nonrotating tests were conducted, as these required paying considerable attention to strain-gage data.

PHYSICAL EFFECTS ON BEARING SURFACES AND COMPONENTS

At the start of this study, the turbocompressor simulator, which had previously been used for training purposes, was disassembled and overhauled by replacing worn or defective components. Then the active bearing surfaces were refurbished and photographed for later comparisons ("before-and-after"). The condition of these surfaces, at various intervals in the test program, is fully documented in Appendix C.

After the machine was reassembled, adjusted, and brought up to operating speed (39,000 rpm), testing was begun by applying vibration in the axial direction with the simulator rigidly mounted. Toward the end of these tests, one of the pad supports in the turbine-end journal bearing failed. The location of this support, referred to as a pad flexure, is shown schematically in Figure 2 adjacent to probe PF22 in the upper-right-hand corner of Section BB. The flexure and its associated pad were in resonance at 1365 Hz, the frequency of applied vibration, when the failure occurred.

Figure D1 of Appendix D presents two views of the failed turbine-end journal-bearing flexure. The failure was detected from the instrumentation signals which describe the position of the journal relative to the casing, as well as from the signals which describe the film thickness between each pad and the journal. These signals indicated a sudden displacement of the journal, followed by repeated contacting between the pads and journal. The simulator was shut down without difficulty. The broken flexure was located, removed, and replaced with a spare during a partial disassembly of the simulator. Visual inspection of the journal at this time did not reveal any debris nor any damage to the journal or pad as a result of the failure; the simulator was reassembled and testing was resumed.

Appendix D contains a complete report on the failed flexure. The report concludes that the failure resulted from the propagation of a crack which was formed during the quenching operation of the heat treatment process used when fabricating the part. Since the failure occurred when a resonance of this particular component was being explored, it seems reasonable to conclude that the amplitude of the

dynamic deflection at resonance resulted in a stress level of sufficient magnitude to permit accelerated crack propagation. It should be noted that materials, design techniques, and heat treatment techniques exist that permit the avoidance of this particular type of failure in future flexure designs. The following paragraphs document the sequence in which the vibration and shock testing was performed, and the results of the periodic checks and inspections of the bearing parts made during the tests.

The first series of vibration tests, as identified below, were all conducted with the simulator running at 39,000 rpm:

1. Axial vibration, rigid mounts
2. Axial vibration, isolation mounts
3. Transverse (T1)* vibration, rigid mounts
4. Transverse (T1) vibration, isolation mounts.

At the conclusion of the above tests, a complete disassembly and inspection of the bearing parts was performed. The results of this inspection are documented in Appendix C. The bearing surfaces appeared to have collected some dust and other fine debris as the result of moisture and incomplete filtering of the air used to drive the rotor. The surfaces were cleaned with soap and water, then with alcohol. The simulator was then reassembled and adjusted in preparation for the nonrotating (rotor inert) tests.

The following series of vibration tests were next conducted with the rotor in a nonrotating condition:

1. Transverse (T1) vibration, isolation mounts
2. Transverse (T1) vibration, rigid mounts
3. Transverse (T2) vibration, isolation mounts
4. Transverse (T2) vibration, rigid mounts
5. Axial vibration, isolation mounts
6. Axial vibration, rigid mounts.

*Recall that (T1) refers to the transverse direction with the rotor supported by the two adjacent "rigid" pads, while the (T2) direction is also transverse but with the rotor supported by one "rigid" and one adjacent "compliant" pad.

At the conclusion of the transverse testing indicated above, one journal bearing pad was removed and inspected because a small, but noticeable, increase in the housing-to-rotor clearance had occurred. The pad surface was lightly covered with a small amount of chrome oxide (coating) dust and the pad pivot had slight wear marks. These indications were not considered significant, so the pad was replaced, adjusted, and testing continued.

Upon completion of all the above indicated nonrotating tests, a complete stripdown and inspection of bearing parts was performed, including photographing the bearing surfaces. This stripdown is also documented in Appendix C. It includes photos of the pivot surfaces. Parts were thoroughly cleaned, and the machine was reassembled for resumption of tests. The vibration testing was concluded by conducting the following test series at a rotor speed of 39,000 rpm:

1. Transverse (T2) vibration, isolation mounts
2. Transverse (T2) vibration, rigid mounts.

At the conclusion of these tests, another disassembly, inspection, and reassembly (without cleaning) was accomplished before shock testing. All pad pivots were replaced at this point in order that the shock effects could be assessed independent of the vibration history of these components. The pads, on the other hand, were left intact because of the expense involved in their replacement.

As was mentioned earlier, the shock-test objective was to apply a 20-g, 10-millisecond, half-sine pulse to the simulator in each of three directions, using both rigid mounts and isolators, and with the rotor running and then inert. Early in the shock-test program, however, an error in the setting of a pressure regulating valve on the shock-test machine resulted in four axial impacts being imposed at a 60-g level, instead of the specified 20-g level. The shaft was rotating during these 60-g impacts and the simulator was mounted on isolators.

No change in bearing performance was noted as a result of this high level of shock. During an inspection following the last of these high impacts, it was noted that the dynamic deflection of the simulator on the isolators was approximately one inch. Also, a fitting was nearly sheared off from the piping which provided external pressure to the thrust bearing for startup purposes. Since this fitting was one of two which were connected in parallel, it was removed, the hole was plugged, and testing was resumed. Clearance checks were

performed and, as has been stated, no damage or deterioration was detected from the excessively high shock pulses.

A total of 73 impacts were imposed on the simulator before the shock testing was completed and the machine was stripped down for the final inspection. Results of the final inspection are shown in Appendix C. Other than a few minor wear areas and rub spots, the bearing surfaces were unaffected by all of the testing, even though repeated rotor-bearing contacts occurred during the shock testing. Furthermore, there was no apparent degradation in performance as a result of the engine shock-and-vibration test program. A breakdown of the 73 impacts imposed on the simulator is as follows:

1. 42 impacts in the axial direction
2. 18 impacts in the T1 transverse direction
3. 13 impacts in the T2 transverse direction.

With respect to the nonrotating vibration tests (these being the only vibration tests during which bearing contact occurred), a total of 27 minutes of test time was accumulated; approximately 17 minutes in the transverse directions and 10 minutes in the axial direction.

Throughout the test program, the journal bearings were operated hydrodynamically during simulator startup and shutdown. This means that there was dry sliding of the journal bearing surfaces during the intervals of initial startup and final shutdown (i.e., during the intervals when shaft speed was not sufficient to generate a hydrodynamic gas film). In excess of 40 hydrodynamic startups were accumulated with the simulator horizontal (i.e., with shaft weight supported by the journal bearings). Many more startup cycles were accumulated with the simulator vertical. As has been demonstrated in previous material evaluation studies, the plasma-sprayed chrome oxide coating used on all of the bearing surfaces survived the start-stop sliding and the vibration- and shock-induced contacts in excellent condition.

CONCLUSIONS

The objective of this study was to obtain an initial assessment of the effects of environmental shock and vibration on the mechanical performance of gas-lubricated Brayton Cycle turbomachinery for space-power applications. A threefold approach was used to make this assessment:

1. Experimental observation of the effects of shock and vibration on the performance of a gas-lubricated rotor-bearing system of known characteristics;
2. Periodic inspection of the bearing parts and bearing surfaces during the course of the shock and vibration test program, to determine the extent of rotor-bearing system damage and/or wear resulting from the shock- and vibration-induced dynamic stresses and bearing contacts;
3. Development of analytical methods for predicting shock and vibration response of gas-lubricated rotor-bearing systems, and validation of the analytical methods via comparison of predicted and measured responses for the experimental shock and vibration test system.

Observations and conclusions resulting from this threefold assessment are presented in the following paragraphs.

Experimental Observations

Observations of the rotor-bearing system response during the sinusoidal vibration tests with shaft rotation and rigid mounts, revealed a strong susceptibility for bearing contacts over a broad frequency range encompassing the three rigid-body critical speeds of the rotor. These critical speeds, all occurring below the 650 Hz rotational speed of the simulator, were as follows:

1. An axial critical speed of the rotor on the thrust bearing at about 130 Hz which produced large dynamic amplitudes in the thrust bearing film;

2. Transverse critical speeds of the rotor on the journal bearings at 166 and 225 Hz which produced large orbital motions of the rotor.

At excitation frequencies above the rotor speed, there were likewise broad frequency ranges where the susceptibility for bearing contacts was high. These frequency regions were associated with the individual journal bearing pads, with the rotor casing, with the simulator test stand, and with the vibration test machine itself.

The use of vibration isolation mounts greatly reduced the susceptibility for bearing contacts. At excitation frequencies above rotor speed, the vibration test objectives were fully achieved (for the conditions of shaft rotation and contact-free operation of the bearings) when isolators were used. However, except for the T2 transverse direction, the objective input vibration amplitudes still could not be achieved in narrow frequency bands around the three rigid-body critical speeds of the rotor. Furthermore, the isolators aggravated the rotor-bearing system response in the frequency region below 20 Hz because of the low-frequency casing resonance associated with the isolators.

Application of 20-g, 10-millisecond shock pulses to the running simulator caused rotor-bearing contacts for all three directions of the applied shock loads. The use of isolators did not prevent the contacts, but did change the nature of the shock response. For example, axially applied shock without the isolators caused the initial bearing contact to occur between the thrust runner and the forward thrust plate, whereas the initial contact occurred between the runner and the reverse thrust plate when isolators were used.

A subtle, but noticeable and significant, effect was observed during axial shock testing without isolation mounts. Initially the runner would rapidly approach the thrust plate as the gas film collapsed. Then, quite suddenly, the velocity appreciably decreased just before contact. This braking action (which has been identified by the analysis results to be due to gas-film damping) greatly reduces the thrust bearing susceptibility to shock damage.

Bearing System Damage and Wear

Early in the vibration test program, there was a failure of one of the pad-support flexures in the turbine-end journal bearing. This failure occurred while purposely exciting the resonant frequency of the flexure. The cause of the failure is fully documented in Appendix D. Improved design and manufacturing procedures, as well as improved materials, are available which can eliminate this type of flexure failure.

Aside from the flexure failure, there was no significant effect of the shock and vibration testing on the condition of the bearing surfaces and bearing parts. Excluding a few minor wear areas and polished rub spots, the surfaces were essentially unaffected by the testing even though several rotor-bearing contacts occurred during each of the 73 shock tests, and continuous contacting occurred during the nonrotating vibration tests. In addition, "dry" (hydrodynamic) starts and stops of the simulator were performed without difficulty throughout the shock and vibration test program.

It should be recognized that the ability of gas bearings to operate reliably under repeated contact and sliding conditions is strongly influenced by the surfacing materials used on the bearings. This has been demonstrated by tests reported in References 1, 2, 9 and 10. The bearing parts used in the simulator for the shock and vibration tests were all surfaced with plasma-sprayed chrome oxide. Chrome oxide is the optimum surfacing material thus far identified for gas bearings for temperatures up to 600^{o}F.

Analytical Study of Shock and Vibration Response

Separate analyses were performed for the axial and the transverse responses. The axial analysis dealt with response of the rotor/thrust-bearing system, both with and without isolation of the rotor casing. Both axial shock and axial vibration excitation were considered. The transverse analysis dealt with response of the rotor/journal-bearing system, both with and without isolators. Only transverse vibration excitation was treated.

The adequacy of the shock and vibration analyses were assessed by comparing

measured and calculated responses for the rotor-bearing system simulator. A single computer program was developed and used to perform all of the axial response calculations with the simulator considered either as a three-mass system or a one-mass system. Using the three-mass model for the rigidly mounted simulator, the first axial critical speed, and the corresponding response amplitudes, were accurately predicted. Accurate predictions of the axial critical speed could not be obtained with the single-mass model.

The axial shock response, in terms of amplitude/time history, total time to contact, and the nature of the braking effect which occurs just before rotor bottoming, was accurately calculated using the three-mass model of the simulator on rigid mounts. Reasonably good agreement with the measured responses could also be obtained with the single-mass model of the rigidly mounted simulator. However, for the case of the simulator mounted on isolators (for which the three-mass model must be used), only qualitiative agreement was obtained between the calculated and measured axial shock response. The poor quantitative correlation was found to be due to the fact that the isolators were modeled as linear elements. Subsequent measurements showed the isolator load characteristics to be highly nonlinear. This source of error was verified by bypassing the isolators and using the measured casing acceleration as the input shock function for the computer program. The resulting response calculation was in close agreement with the measured response.

Simply expressed, the fundamental conclusion relating to the axial response calculations is that the masses, stiffnesses, and nonlinear-gas-film properties were all adequately modeled; the shock-and-vibration isolators were not.

The most significant aspect of the analytical approach used to predict the axial response is the application of simple, frequency-independent, nonlinear functions to approximate the theoretical static load capacity and small-amplitude (sinusoidal) viscous damping characteristics of the thrust-bearing gas film. This simplified approach eliminates having to perform a step-by-step solution of the Reynolds equation simultaneously with the ordinary differential equations of the mechanical elements. The simplified approach can be solved much more rapidly than can the rigorous system equations.

Calculations of transverse response were made only for the case of steady-state vibration applied to the simulator through vibration isolators. The significant frequencies calculated were:

1. All journal bearing pad resonances
2. First resonant bending frequency of the rotor casing
3. First and second transverse critical speeds of the rotor.

The only pad resonant frequency that was experimentally identified was within seven percent of the calculated value. The casing resonance was not clearly identified experimentally, but there were indications that it occurred in the vicinity of the calculated resonance.

The first and second transverse critical speeds of the rotor-bearing system were calculated to within one percent of the measured values. However, amplitudes and orientation of the rotor-to-casing displacements were considerably in error. This could be due to several reasons, listed in the following order of likelihood:

1. "Large amplitude" nonlinear stiffness and damping effects in the journal bearings which were not represented in the analysis;
2. The effect of damping from the thrust bearing and from the shaft labyrinth seals which was also neglected in the calculations;
3. The effect of "cross talk" (a small amount of horizontal vibration) which was present in the vibration table, but not accounted-for in the analysis.

Summary of Significant Results

The significant results of this investigation are summarized below. From a quantitative standpoint, it must be remembered that the results apply to one specific rotor-bearing system. From a phenomenological standpoint, however, the system response characteristics are indicative of those which would be exhibited by similarly configured gas-lubricated rotor-bearing systems.

Shock Tests

1. Gas-lubricated rotor-bearing systems of the type tested can satisfactorily survive at least a limited number of externally imposed 10-millisecond, 20-g shock impulses, both with and without shaft rotation, and with or without isolation mounts. For the system tested, momentary contacts between the rotating and stationary bearing surfaces were observed under all test conditions. However, there was no surface damage or degradation of bearing performance as a result of these contacts.

Sinusoidal Vibration Tests — Shutdown Condition (Nonrotating Shaft)

1. Under shutdown (nonrotating) conditions, gas-bearing-supported rotor systems of the type tested can satisfactorily survive, at least for a limited period of time, axial imposition of the specified sinusoidal vibration conditions, either with or without isolation mounts.

2. For transversely imposed vibration under shutdown (nonrotating) conditions, vibration isolation may be required to survive the specified sinusoidal excitation conditions. During the nonrotating transverse vibration tests without isolators, the objective input excitation levels could not be achieved in the frequency range from 190 to 235 Hz, this being the region of one of the critical speeds (resonant frequencies) of the nonrotating shaft. The limiting factor in this frequency range was deflection (overstressing) of the flexures used to support the individual journal bearing pads. With isolators installed, excitation of the flexures was greatly reduced and the objective input vibration levels could be safely imposed in the two transverse directions.

3. A total of 27 minutes of vibration testing was accumulated under nonrotating conditions. No damage to the bearing surfaces nor degradation of bearing performance was detected as a result of the nonrotating tests.

Sinusoidal Vibration Tests — Normal Operation (Rotating Shaft)

1. Under normal rotating conditions, gas-lubricated rotor-bearing systems

of the type tested may have to be vibration isolated to survive the specified sinusoidal vibration conditions. During the shaft rotation tests without isolation, rotor-to-bearing contacts became imminent, over broad regions of the frequency spectrum, at input vibration levels considerably below the test objectives. However, with isolators installed, the objective vibration input levels were achieved, without bearing contacts, over most of the frequency range. Only in the vicinity of the isolator resonant frequency (approximately 12 Hz), and in the vicinity of the rotor critical speeds (130, 166, and 225 Hz), did bearing contact become imminent at less than the objective vibration input levels.

2. Input vibration levels were carefully controlled during the rotating vibration tests to prevent the occurrence of bearing contacts. Consequently, it is not known whether bearing performance would have been degraded under vibration-induced contact conditions.

Calculated Shock and Vibration Response

1. Accurate predictions of the axial shock and vibration response of gas-bearing machinery can be obtained using a three-degree-of freedom analytical model of the rotor-bearing system with nonlinear representation of the load and damping characteristics of the thrust bearing gas film. An approximate, simplified method of representing the gas-film nonlinearities can be used which yields both accurate and economic (in terms of computer cost) solutions. The only drawback of the herein presented axial response analysis is the modeling of the vibration isolators in terms of linear stiffness and damping coefficients. Under shock conditions (i.e., large displacement conditions) the isolators are quite nonlinear and must be so modeled.

2. Accurate predictions of the transverse resonant frequencies of the rotor-bearing test system were obtained using the finite-element analysis model of the rotor and rotor casing, together with the linearized journal bearing stiffness and damping coefficients. There was,

however, considerable discrepancy between the calculated and measured amplitudes of vibration, and of the rotor-to-casing orbit shapes. Calculated amplitudes were considerably higher than the measured amplitudes. The discrepancy in calculated amplitudes may be due to "large amplitude" nonlinear stiffness and damping effects in the journal bearings which were not represented in the analysis. There was also a small amount of horizontal vibration (cross talk) in the vibration table which was neglected in the calculations. Finally, there may have been significant damping from the thrust bearing and from the shaft labyrinth seals. These sources of damping were also neglected in the analysis.

3. The analysis results clearly show the beneficial effects of gas-bearing squeeze-film damping on minimizing the severity of shock-induced bearing contacts. Gas-bearing systems which must operate under shock conditions should be optimized to take maximum advantage of this effect.

The above listed results indicate that 10-millisecond, 20-g shock pulses should not be a problem for gas-lubricated Brayton Cycle space-power turbomachinery. Sinusoidal vibration could be a problem, particularly if imposed during shaft rotation. The use of vibration isolators appears to be a solution to the vibration problems during shutdown (nonrotating) conditions. During rotation, the use of isolators greatly reduces, but may not eliminate, the possibility of vibration-induced bearing contacts. Further testing will be required to identify if such contacts would cause bearing damage or degradation of bearing performance.

RECOMMENDATIONS

This report describes the results of work performed under Tasks I and II of NASA Contract NASw-1713. Additional work is currently being performed under Tasks III and IV of the contract as follows:

Task III - Extension of the axial response computer program to permit nonlinear modeling of isolation mounts; Development of an axial response computer program for random vibration excitation.

Task IV - Experimental test and evaluation of the Brayton Rotating Unit (BRU) simulator under vibration and shock conditions, including random vibration.

As a result of the above on-going contract tasks it is somewhat premature to formulate a list of recommendations until these tasks are completed. There is, however, one important question identified by the herein reported work which will have to be investigated at some point.

During all of the vibration tests performed while the simulator shaft was rotating, the input vibration amplitudes were always controlled to maintain contact-free operation of the simulator bearings. Because of this intentional desire to prevent bearing contacts, there were numerous instances when the objective input vibration amplitudes were not attained because of the imminence of contacts. Figures 33, 58 and 60 show that without isolation, there were broad frequency ranges over which the objective input amplitudes were not attained. Figures 34 and 59 show that even with isolators, there were a few narrow frequency ranges where, again, the objective input levels were not attained.

An important question naturally arises from these results. If the vibration tests had been conducted at the objective input levels over the total 5- to 2,000-Hz frequency range, there undoubtedly would have been bearing contacts within certain frequency regions. The question is, would there have been bearing damage, or degradation of bearing performance, as a results of the

vibration-induced contacts? It appears that the effects of vibration-induced contacts during shaft rotation must be experimentally assessed in the near future.

LIST OF REFERENCES

1. Curwen, P. W., and Frost, A., "An Investigation of the Performance of Gas Bearing Machinery Subjected to Low Frequency Vibration and Shock", The Shock and Vibration Bulletin, Vol. 38, Part 3, Nov. 1968, pp. 221-234.

2. Curwen, P. W., "Research and Development of High-Performance Axial-Flow Turbomachinery", Volume 2 — Design of Gas Bearings, Mechanical Technology Inc.; NASA Contractor Report CR-801, Lewis Research Center, Cleveland, Ohio, May 1968 (Originally issued under NASA Contract NAS 3-4179 as Pratt and Whitney Report No. PWA 2977, Vol. 2).

3. Brown, W. J., "Brayton-B Power System — A Progress Report", Paper No. 16b, presented at the 4th Intersociety Energy Conversion Engineering Conference, Washington, D.C., September 24, 1969.

4. DiPrima, R.C., "The Reynolds Equation", Design of Gas Bearings, Vol. 1, Supplemental Textbook to the RPI-MTI Course on Gas Bearing Design, Mechanical Technology Inc., 1967.

5. Roark, R. J., "Formulas for Stress and Strain", 3rd Edition, McGraw-Hill, New York, 1954, Table 10.

6. Jacobsen, L. S., and Ayre, R. S., "Engineering Vibrations with Applications to Structures and Machinery", McGraw-Hill, New York, 1958, Chapter 5, Section 5-6.

7. Harris, C. M., and Crede, C. E., "Shock and Vibration Handbook — Volume 2", McGraw-Hill, New York, 1961, Chapter 32, Figure 32-23.

8. Lund, J. W., and Orcutt, F. K., "Calculations and Experiments on the Un-Balance Response of a Flexible Rotor", Transactions of the ASME, Vol. 87, Series E, No. 4, Dec. 1965, pp. 911-920.

9. Murray, S. F., "Material Combinations for Hydrodynamic Inert Gas-Lubricated Bearings", Transactions of the ASME, Vol. 90, Series F, No. 1, January 1968, pp. 49-55.

10. Murray, S. F., "Research and Development of High-Temperature Gas Bearings, Part II — Selection and Evaluation of Gas Bearing Materials in Argon at 900 F and 1400 F", Mechanical Technology Inc., NASA Contractor Report CR-1477, Lewis Research Center, Cleveland, Ohio, Dec. 1969.

APPENDIX A

EQUATIONS OF MOTION FOR AXIAL RESPONSE

If we represent the displacement of the three masses shown in Figure 15 as x_1, x_2, and x_3 and represent the displacement of the base as x_b in the same inertial frame, then the three equations of motion may be written directly from Newton's laws. If we introduce an aerodynamic force, F_a, acting on m_3, (the rotor), and take g to be the local gravitational acceleration, the equations are:

$$m_1\ddot{x}_1 = k_2(x_2 - x_1) - k_1(x_1 - x_b) - c_1(\dot{x}_1 - \dot{x}_b) - m_1 g \tag{A1}$$

$$m_2\ddot{x}_2 = -G(h,\dot{h}) - k_2(x_2 - x_1) - m_2 g \tag{A2}$$

$$m_3\ddot{x}_3 = F_a + G(h,\dot{h}) - m_3 g \tag{A3}$$

These equations can be expressed in a form more amenable to laboratory measurements by some redefinition. Resolving the generalized gas force G into an elastic load component and a damping (dissipative) component, we get:

$$G(h,\dot{h}) = W(h) - \dot{h}\, B(h) \tag{A4}$$

Note that initial conditions may be obtained by considering the system to be in static equilibrium for which (A1), (A2), and (A3) become

$$0 = k_2(\bar{x}_2 - \bar{x}_1) - k_1(\bar{x}_1 - \bar{x}_b) - m_1 g \tag{A5}$$

$$0 = -W(\bar{h}) - k_2(\bar{x}_2 - \bar{x}_1) - m_2 g \tag{A6}$$

$$0 = F_a + W(\bar{h}) - m_3 g \tag{A7}$$

where $\bar{x}_1$, $\bar{x}_2$, $\bar{x}_3$, and $\bar{x}_b$ are the values of the coordinates at static equilibrium. The equations of motion can also be written in terms of coordinates referenced to the static equilibrium position of the system by means of the transformation:

$$y_1 = x_1 - \bar{x}_1 \tag{A8}$$

and similarly for the coordinates locating m_2, m_3, and the base, b. We also define an initial film clearance, $\bar{h}$, by

$$\bar{h} = \bar{x}_3 - \bar{x}_2 \tag{A9}$$

The actual value of $\bar{h}$ is determined by the weight of the rotor, the force, F_a, and the thrust-bearing static-load characteristic to be discussed shortly. Applying the relationships (A4) through (A9) to Equations (A1), (A2), and (A3) produces a set of equations of motion whose coordinates are referenced to static equilibrium:

$$m_1\ddot{y}_1 = k_2(y_2 - y_1) - k_1(y_1 - y_b) - c_1(\dot{y}_1 - \dot{y}_b) \tag{A10}$$

$$m_2\ddot{y}_2 = -W[y_3 - y_2 + \bar{h}] + W[\bar{h}] + (\dot{y}_3 - \dot{y}_2)\, B[y_3 - y_2 + \bar{h}] - k_2(y_2 - y_1) \tag{A11}$$

$$m_3\ddot{y}_3 = -W[\bar{h}] + W[y_3 - y_2 + \bar{h}] - (\dot{y}_3 - \dot{y}_2)\, B[y_3 - y_2 + \bar{h}] \tag{A12}$$

Note!! The expressions in square brackets immediately following W and B are arguments of the nonlinear functions W and B. For example, the value of B, in general, depends upon the value of the film thickness, h. The value of B determined in Equation (A12) is that which occurs when $h = [y_3 - y_2 + \bar{h}]$.

Equations (A10) through (A12) were expressed as a set of six, simultaneous, first-order, nonlinear differential equations. These equations were programmed on a digital computer using a fourth-order, Runge-Kutta, integration technique supplemented by an error control method which continuously adjusted the integration step size to maintain solution accuracy within prescribed limits.

In certain instances, computer time is saved without significant loss in accuracy by representing the system with a single-degree-of-freedom model. This is permissible when the thrust-bearing gas film provides substantially all of the compliance in the system. The analysis of such a simplified system results in a single, second-order, nonlinear, differential equation which describes the motion of a single lumped mass, m (the rotor), in terms of a displacement coordinate, x, in an inertial reference frame:

$$\dot{m}\ddot{x} = F_a + W(h) - \dot{h}B(h) - mg \qquad \text{(A13)}$$

As before, the motion is better expressed with respect to the position of static equilibrium. Using the same manipulations previously performed we arrive at:

$$\dot{m}\ddot{y} = W(h) - W(\bar{h}) - (\dot{y} - \dot{y}_b)\, B(h) \qquad \text{(A14)}$$

where y defines the position of the rotor with respect to static equilibrium. Since the equations of motion are written for all three representations of the system, (i.e., three-mass rigid mount, three-mass isolation mount, and one-mass rigid mount) in terms of general base motion, the computer program was written to handle any of the following four types of forcing functions expressed as either base acceleration or as base displacement: continuous vibration, half-sine shock, haversine shock, or arbitrary shock pulse read in as a table of amplitude and time values.

As shall be shown in Appendix B, the computer program user can either elect to represent his system by Figure 15 or 16, which results in simultaneous solution of (A10), (A11), and (A12); or he may elect to use the representation of Figure 14 which requires only the solution of (A14).

APPENDIX B

AXIAL RESPONSE COMPUTER PROGRAM

This appendix presents a complete listing of the computer program, (written in the FORTRAN IV language), used to calculate axial response of the system as represented by Figures 14, 15, or 16. It also provides detailed instructions for preparing the input data cards, along with sample input and sample printed output Some of the typical graphical output has already been presented in the main text.

PROGRAM INPUT

Card 1 Read NCASE, TITLE
FORMAT (I5, 75H)
Set NCASE = Any nonzero character to sequentially identify the case being computed (a blank here will stop the program)
Title = Any message to describe case being computed. If computer graphs are requested, this message will appear at top of graph.

Card 2 Read MODEL, LOADF, IDAMP, IFOFT, ICC, MOTION
FORMAT (6I5)

These are options as follows:

Physical Model
MODEL = 1. Complete system on isolators
MODEL = 2. Complete system on rigid mounts with flexible lower casing.
MODEL = 3. Simple model, gas film with nonlinear stiffness and damping; rigid casing and mounts.

Gas film properties
LOADF = 4 Exponential load
LOADF = 5 Power function load
IDAMP = 6 Exponential damping
IDAMP = 7 Power function damping

Type of Excitation Function
IFOFT = 8 Continuous sine function
IFOFT = 9 Shock function half sine
IFOFT = 10 Shock function haversine
IFOFT = 11 Shock function (table)

Calcomp desired?
ICC = 12 Yes
ICC = 13 No

Is forcing function described in terms of displacement or acceleration?

MOTION = 0 if forcing function input represents displacement in inches.

MOTION = 1 if forcing function input represents acceleration in g's.

Card 3 - data is dependent upon "MODEL" option as follows:

If MODEL = 3

Read M3

FORMAT (20X, E10.4)

M3 = weight of rotor (lb)

If MODEL = 2

Read M1, M2, M3, K1, C1, K2

FORMAT (6E10.4)

M1 = Weight of "lumped" mass assigned to lower region of casing (lb)

M2 = Weight of thrust bearing stator (lb)

M3 = Weight of rotor (lb)

K1 = Value of "lumped" stiffness assigned to lower region of casing (lb/in.)

C1 = 0.0

K2 = Stiffness of thrust bearing flexure (lb/in)

If MODEL = 1

Read M1, M2, M3, K1, C1, K2

FORMAT (6E10.4)

M1 = Weight of casing (lb)

M2 = Weight of thrust bearing stator (lb)

M3 = Weight of rotor (lb)

K1 = Total stiffness of isolators (lb/in.)

C1 = Total damping of isolators (lb sec/in.)

K2 = Stiffness of thrust bearing flexure (lb/in.)

Card 4 - data is dependent upon "LOADF" and "IDAMP" options as follows:

READ ALOAD, BLOAD, CLOAD, DLOAD, ADAMP, BDAMP, CDAMP, DDAMP

FORMAT (8E10.4)

If LOADF = 4 the expression used to represent the nonlinear load characteristic of the gas film is

$W(h) = Ae^{Bh}$

where:

ALOAD = A

BLOAD = B

CLOAD = 0.

DLOAD = 0.

If LOADF = 5 the expression used to represent the nonlinear load characteristic is

$W(h) = Ch^{D}$

where:

ALOAD = 0.

BLOAD = 0.

CLOAD = C

DLOAD = D

If IDAMP = 6 the gas film damping is given by

$B(h) = Ae^{Bh}$

where:

ADAMP = A

BDAMP = B

CDAMP = 0.

DDAMP = 0.

If IDAMP = 7 the gas film damping is given by

$B(h) = Ch^{D}$

where:

ADAMP = 0

BDAMP = 0

CDAMP = C

DDAMP = D

Card 5 - Read GL, FA, ELIM

FORMAT (3E10.4)

GL = Local gravitation acceleration in "g's"

(GL = 1.0 on earth's surface.)

FA = Net aerodynamically induced axial force on rotor (positive, if force is upward)

ELIM = Nonlinear load and damping functions are held constant at film thicknesses less than "ELIM" inches

Card 6 - Data is dependent upon options chosen for IFOFT and MOTION.

If IFOFT = 8 Read AMPLD, FREQ

FORMAT (2E10.4)

AMPLD = amplitude of sinusoidal forcing function.

If MOTION = 0, AMPLD = displacement in inches

If MOTION = 1, AMPLD = acceleration in g's.

FREQ = frequency of forcing function in Hertz (cps)

If IFOFT = 9 Read PEAKS, PDURS

FORMAT (2E10.4)

PEAKS = peak value of half sine shock pulse

If MOTION = 0, PEAKS = displacement in inches

If MOTION = 1, PEAKS = acceleration in g's

PDURS = duration of half sine shock pulse (seconds)

If IFOFT = 10 Read PEAKH, PDURH

FORMAT (2E10.4)

PEAKH = peak value of haversine (shock machine half sine) pulse

If MOTION = 0, PEAKH = displacement in inches

If MOTION = 1, PEAKH = acceleration in g's

PDURH = duration of haversine shock pulse (seconds)

If IFOFT = 11 Read NINC, TINCP

FORMAT (I5, E10.4)

NINC = number of evenly spaced intervals in pulse

TINCP = time interval of each of the above increments

This data card must be followed by as many data cards as are necessary to represent the shock pulse. Call these cards 6A, 6B, etc.

Cards 6A, 6B, etc: Read PUVAL

FORMAT (8E10.4)

PUVAL = values of the shock pulse at each increment specified above. Values must be contiguous starting with the first increment.
If MOTION = 0, PUVAL = displacement in inches.
If MOTION = 1, PUVAL = acceleration in g's.

Note, if more than one increment size is desired, a different case may be run for each step size by using the conditions at the change point as restart values.

Card 7 Read IPSTEP, M, MAXINC, NCYCLS, TPRINT, TMAX, H, E, HM, RERR
FORMAT (4I5, 6E10.4)
This card controls the precision and duration of the internal computation and output.

IPSTEP = ratio of printed to plotted output points. In most cases IPSTEP = 1.

M = number of integrations performed internally before step size is automatically adjusted. Usually M = 2. This will result in the best trade off between precision and economy.

MAXINC = the maximum number of internal integrations before program shuts itself off. This is a safety control to prevent exorbitant computer charges due to unforeseeable misbehavior of the solution. Recommended MAXINC = 1000.

NCYCLS = the number of cycles for which the solution will be calculated beyond the first minimum and maximum after the shock pulse ceases to act. NCYCLS has meaning only for shock pulses. Usually NCYCLS = 0.

TPRINT = output control which establishes the step size of printed and plotted output (seconds). May be any convenient interval into which we want to divide the time range of the solution, generally a few hundred points or so. Example: If we expect the range of interest to be between 0 and 2 seconds and we think 200 solution points are adequate to describe the system behavior in detail, we select

$$\text{TPRINT} = \frac{2 \text{ seconds}}{200} = 0.01$$

and will get results at 10 milliseconds, 20 milliseconds, etc.

TMAX = maximum time value (seconds for which solutions will be computed. This is another safety feature designed to prevent excessive computational charges resulting from some unforeseeable characteristic of the solution. Normally this value should be twice as large as we expect the solution to run.

H = time increment (seconds for which to begin internal computations. Recommended value is 1/4 of TPRINT.

E = maximum absolute error permitted in internal computation. Recommended value is .01

HM = minimum step size (seconds) for internal calculation. This parameter is another safety measure which keeps the step size from approaching zero in order to strive for greater accuracy. Recommended minimum value: 1/100 of TPRINT

RERR = comparable to E, except that RERR represents relative error whereas, E represents absolute error. Recommended value 0.01.

Card 8 Initial value or RESTART CARDS

See analysis section for definition of these coordinates

READ TINIT, Y1IN, Y2IN, Y3IN, V1IN, V2IN, V3IN

FORMAT (7E10.4)

TINIT = initial or restart time (seconds)

Y1IN = initial value of Y_1 (inches)

Y2IN = initial value of Y_2 (inches)

Y3IN = initial value of Y_3 (inches)

V1IN = initial value of V_1 (inches/sec)

V2IN = initial value of V_2 (inches/sec)

V3IN = initial value of V_3 (inches/sec)

Repeat all above cards for each case. Insert a blank card as the last data card. This will stop the program gracefully.

DATA INPUT EXAMPLE

```
 35 FIG     CALCULATED LOW-FREQUENCY VIBRATION RESPONSE
  3    4     7     8    12     0
                              10.5
105.      -2554.84          0.          0.          0.          0.     3.11123E-4 -1.49842
  1.            0.          .00005
.015          17.
  1     2 1000     0     .002        .5          .001        .01         .00001        .01
```

PN999. RESPONSE OF VERTICAL THRUST BEARING TO AXIALLY-APPLIED SHOCK OR VIBRATION

46 HAVERSINE APPROXIMATION TO HARD MOUNT SHOCK PULSE. REF CASE 23

7-21-1969

PROGRAM OPTIONS

OPTIONS SELECTED FOR THIS PARTICULAR RUN ARE DESIGNATED BY

OPTION

CHOICE OF VIBRATION MODEL

1 = THREE-DEGREE OF FREEDOM SYSTEM USING ISOLATORS

2 = THREE-DEGREE OF FREEDOM SYSTEM USING RIGID MOUNTS

3 = SIMPLE MODEL, ENTIRELY RIGID EXCEPT FOR GAS FILM

GAS FILM FUNCTIONAL REPRESENTATION

LOAD CHARACTERISTIC

4 = EXPONENTIAL LOAD CHARACTERISTIC

5 = POWER FUNCTION LOAD CHARACTERISTIC

DAMPING CHARACTERISTIC

6 = EXPONENTIAL DAMPING COEFFICIENT

7 = POWER FUNCTION DAMPING COEFFICIENT

DESCRIPTION OF GAS FILM

THE EXPONENTIAL LOAD CHARACTERISTIC IS OF THE FORM

LOAD (LB) = A*EXP(B*H)

WHERE

H = FILM THICKNESS (INCHES)
A = .1050+03 (LB)
B = -.2555+04 (1/IN)

THE POWER FUNCTION DAMPING COEFFICIENT IS OF THE FORM
B(LB*SEC/IN) = C*H**D
WHERE
H = FILM THICKNESSS (INCHES)
C= . .3111-03 LB-SEC/IN
D= . -.1498+01 (1/IN)

NON-LINEAR LOAD AND DAMPING FUNCTIONS ARE HELD CONSTANT AT FILM THICKNESSES LESS THAN .5000-04 INCHES.

****

EQUILIBRIUM FILM THICKNESS IS .90126 MILS

ASSUMING STEADY-STATE AERODYNAMIC FORCES ON THE ROTOR OF .00000 LB
AND A LOCAL GRAVITATIONAL FIELD OF 1.00000 TIMES STANDARD

****

PARAMETERS OF THE SYSTEM ON RIGID MOUNTS ARE AS FOLLOWS

EFFECTIVE MASS OF LOWER HOUSING (MASS1),(LB)	EFFECTIVE MASS OF STATOR + FLEXURE (MASS2),(LB)	MASS OF ROTOR (MASS3),(LB)	STIFFNESS OF LOWER HOUSING (LB/IN)	FLEXURE STIFFNESS (LB/IN)
1.4000	.4000	10.500	.5800+05	.6700+06

****

TYPE OF EXCITATION FUNCTION

8 = STEADY SINUSOIDAL INPUT

9 = HALF SINE SHOCK

10 = HAVERSINE SHOCK

11 = ARBITRARY SHOCK (TABLE)

****

IS CALCOMP OUTPUT DESIRED-

12 = YES

```
                13 = NO
**********************************************************************************************************
      INPUT MOTION IS HAVERSINE SHOCK PULSE

          PULSE DURATION IS      .0146 SECONDS

          PEAK AMPLITUDE IS   15.7000 G'S ACCELERATION


**********************************************************************************************************

      PROGRAM CONTROL PARAMETERS

          DESIRED TERMINATION
               TIME VALUE WILL NOT EXCEED      .0300 SECONDS
               AS A SAFETY MEASURE WE WILL NOT PERMIT MORE THAN 8000 STEPS
               CALCULATION WILL CONTINUE     1 CYCLES AFTER PULSE DURATION
          STEP SIZE
               INITIAL STEP SIZE FOR CALCULATION PURPOSES IS   .1000-03 SECONDS
               VALUES ARE PRINTED OUT EVERY   .5000-03 SECONDS
               EVERY     1TH POINT IS PLOTTED IF CALCOMP IS USED
               ERROR CRITERION FOR INTEGRATION TECHNIQUE   .2000-02
               MINIMUM STEP-SIZE =.    .1000-05 SECONDS
               NO. OF INTEGRATIONS BEFORE STEP-SIZE IS DOUBLED=     2
               NORMALIZED ERROR LIMIT FOR INTEGRATION TECHNIQUE      .0100

      INITIAL OR RESTART CONDITIONS
               INITIAL TIME              =   .0000     SECONDS
               DISPLACEMENT OF MASS 1    =   .0000     INCHES
               VELOCITY OF MASS 1        =   .0000     IN/SEC
               DISPLACEMENT OF MASS 2    =   .0000     INCHES
               VELOCITY OF MASS 2        =   .0000     IN/SEC
               DISPLACEMENT OF MASS 3    =   .0000     INCHES
               VELOCITY OF MASS 3        =   .0000     IN/SEC
```

```
 000   U   U  TTTTT  PPPP   U   U  TTTTT
0   0  U   U    T    P   P  U   U    T
0   0  U   U    T    PPPP   U   U    T
0   0  U   U    T    P      U   U    T
 000    UUU     T    P       UUU     T
```

TIME (SEC)	FILM THICKNESS (INCHES)	DISPLACEMENT OF MASS 1 (INCHES)	DISPLACEMENT OF MASS 2 (INCHES)	DISPLACEMENT OF ROTOR (INCHES)	VELOCITY OF MASS 1 (IN/SEC)	VELOCITY OF MASS 2 (IN/SEC)	VELOCITY OF ROTOR (IN/SEC)	RELATIVE DISP. BET. MASS2 + MASS1 (INCHES)	FORCING FUNCTION (INCHES)
.0005	.9012-03	.1344-06	.9436-07	.3015-08	.1511-02	.1151-02	.4443-04	.4002-07	.1459-05
.0010	.8965-03	.5943-05	.5139-05	.4007-06	.3123-01	.2789-01	.2712-02	.8042-06	.2324-04
.0015	.8648-03	.4640-04	.4228-04	.5825-05	.1503-00	.1395-00	.2500-01	.4126-05	.1168-03
.0020	.7716-03	.1784-03	.1657-03	.3604-04	.4006-00	.3756-00	.1125+00	.1272-04	.3651-03
.0025	.6066-03	.4689-03	.4383-03	.1437-03	.7833-00	.7351-00	.3538-00	.3062-04	.8790-03
.0030	.4118-03	.9898-03	.9280-03	.4385-03	.1342+01	.1265+01	.8882-00	.6183-04	.1792-02
.0035	.2435-03	.1873-02	.1766-02	.1108-02	.2270+01	.2168+01	.1880+01	.1068-03	.3255-02
.0040	.1952-03	.3287-02	.3136-02	.2430-02	.3717+01	.3511+01	.3494+01	.1504-03	.5426-02
.0045	.1720-03	.5663-02	.5448-02	.4718-02	.6069+01	.5806+01	.5740+01	.2156-03	.8468-02
.0050	.1317-03	.9302-02	.9043-02	.8274-02	.8721+01	.8626+01	.8528+01	.2584-03	.1254-01
.0055	.8279-04	.1438-01	.1412-01	.1330-01	.1161+02	.1170+02	.1159+02	.2671-03	.1778-01
.0060	.3330-04	.2098-01	.2073-01	.1986-01	.1465+02	.1477+02	.1468+02	.2529-03	.2432-01
.0065	-.1201-04	.2909-01	.2886-01	.2794-01	.1768+02	.1771+02	.1762+02	.2363-03	.3226-01

RUN COMPLETE AT THIS POINT. ROTOR HAS BOTTOMED.

```
C                MECHANICAL TECHNOLOGY INCORPORATED
C                      968 ALBANY-SHAKER ROAD
C                      LATHAM, NEW YORK 12110
C
C      THIS PROGRAM CALCULATES THE RESPONSE OF A THRUST BEARING-ROTOR
C      SYSTEM TO EXTERNALLY APPLIED SHOCK AND VIBRATION.
C      IT TREATS THE SYSTEM AS A THREE-DEGREE-OF-FREEDOM VIBRATION MODEL.
C
C      THIS PROGRAM USES THE FOLLOWING SUBROUTINES -
C      INPUT, SIMINI, SOLVE, DIFEQ, TLU, FUNCTION, FORMT, FILM, CALCOM,
C      RONKU
C
      PROGRAM PN457(INPUT,OUTPUT,TAPE5=INPUT,TAPE6=OUTPUT,TAPE22)
      COMMON TPRINT,TMAX,IPSTEP,NCYCLS,MOTION,TITLE(15),YBA,YBINT(200)
      COMMON NR,NW,NCASE,MODEL,LOADF,IDAMP,IFOFT,ICC,
     1               M1,M2,M3,K1,C1,K2,GL,FA,ALOAD,ADAMP,BLOAD,BDAMP,
     2CLOAD,CDAMP,DLOAD,DDAMP,HINIT,IFM7,AMPLD,FREQ,PEAKS,PDURS,PEAKH,
     3PDURH,NINCP,TINCP,TP(200),PUVAL(200),PULDOT(200),TINIT,Y1IN,Y2IN,
     4Y3IN,V1IN,V2IN,V3IN,TIME(6000),Y1,Y2,Y3,V1,V2,V3,N,VEC(6),DVEC(6),
     5MAXINC,H,HM,M,E,AKO,NE,T,                ELIM,INDX,      YB,YBDOT,
     6OMEGA,WHO,WY3Y2H,BY3Y2H
      COMMON FILMT(6000),Y2MY1(6000),VAPEAK(6000),YBPLOT(6000)
      COMMON  IBUF(1000)
      NR=5
      NW=6
      IFLAG=1
    5 READ(NR,1010) NCASE,(TITLE(I),I=1, 8)                              CDC
      IF(NCASE) 10,6,10
    6 IF(IFLAG.EQ.2)  CALL PLOT(18.,0.,999)
    9 CALL EXIT
   10 WRITE(NW,1000)
      WRITE(NW,1015)
      CALL SDATE(DATE)                                                   CDC
      WRITE(NW,1005) NCASE,(TITLE(I),I=1, 8),DATE                        CDC
      CALL INPUT
      IF(IFLAG.EQ.2)   GO TO 24
   20 IF(ICC.EQ.13)  GO TO 25
      IFLAG=2
      CALL PLOTS(IBUF,1000,22)
      GO TO 25
   24 CALL PLOT(18.,0.,-3)
   25 CALL SOLVE
      GO TO 5
 1000 FORMAT( 7H1PN457,10X,73HRESPONSE OF VERTICAL THRUST BEARING TO AXI
     1ALLY-APPLIED SHOCK OR VIBRATION//)
 1005 FORMAT(I5,7A10,A5,2X,A8)                                           CD
 1010 FORMAT(I5,7A10,A5)
 1015 FORMAT(// 1X,119(1H*))
      END
```

```
      SUBROUTINE INPUT
C     THIS SUBROUTINE CALLS SUBROUTINE *FILM* WHICH FINDS EQUILIBRIUM
C     FILM THICKNESS.
C
      COMMON TPRINT,TMAX,IPSTEP,NCYCLS,MOTION,TITLE(15),YBA,YBINT(200)
      COMMON NR,NW,NCASE,MODEL,LOADF,IDAMP,IFOFT,ICC,
     1              M1,M2,M3,K1,C1,K2,GL,FA,ALOAD,ADAMP,BLOAD,BDAMP,
     2CLOAD,CDAMP,DLOAD,DDAMP,HINIT,IFM7,AMPLD,FREQ,PEAKS,PDURS,PEAKH,
     3PDURH,NINCP,TINCP,TP(200),PUVAL(200),PULDOT(200),TINIT,Y1IN,Y2IN,
     4Y3IN,V1IN,V2IN,V3IN,TIME(6000),Y1,Y2,Y3,V1,V2,V3,N,VEC(6),DVEC(6),
     5MAXINC,H,HM,M,E,AKO,NE,T,              ELIM,INDX,     YB,YBDOT,
     6OMEGA,WHO,WY3Y2H,BY3Y2H
      COMMON FILMT(6000),Y2MY1(6000),VAPEAK(6000),YBPLOT(6000)
      REAL M1,M2,M3,C1,K1,K2
      LOGICAL O1,O2,O3,O4,O5,O6,O7,O8,O9,O10
      WRITE(NW,1500)
C PRINT A ROW OF ASTERISKS
      WRITE(NW,1030)
      WRITE(NW,1020)
      WRITE(NW,1031)
C
C
C CHOOSE OPTIONS
C
      READ(NR,30) MODEL,LOADF,IDAMP,IFOFT,ICC,MOTION
   30 FORMAT(6I5)
C
C
C SET LOGICAL VARIABLES AND TEST FOR CORRECTNESS OF INPUT
C
C
      O1=MODEL.LT.1
      O2=MODEL.GT.3
      O3=LOADF.LT.4
      O4=LOADF.GT.5
      O5=IDAMP.LT.6
      O6=IDAMP.GT.7
      O7=IFOFT.LT.8
      O8=IFOFT.GT.11
      O9=ICC.LT.12
      O10=ICC.GT.13
      IF(O1.OR.O2)WRITE(NW,40)
      IF(O3.OR.O4)WRITE(NW,50)
      IF(O5.OR.O6)WRITE(NW,60)
      IF(O7.OR.O8)WRITE(NW,70)
      IF(O9.OR.O10)WRITE(NW,80)
```

```
C  ERROR MESSAGES
   40 FORMAT(    35H0     IMPROPER INPUT CARD 2,COL 5.  )
   50 FORMAT(    35H0     IMPROPER INPUT CARD 2,COL10.  )
   60 FORMAT(    35H0     IMPROPER INPUT CARD 2,COL15.  )
   70 FORMAT(    35H0     IMPROPER INPUT CARD 2,COL20.  )
   80 FORMAT(    35H0     IMPROPER INPUT CARD 2,COL25.  )
      IF(01.OR.02.OR.03.OR.04.OR.05.OR.06.OR.07.OR.08.OR.09.OR.010)
     1CALL EXIT
      IF(MODEL.EQ.1) WRITE(NW,1040)
      IF(MODEL.EQ.1) WRITE(NW,1050)
      IF(MODEL.EQ.1) WRITE(NW,1040)
      IF(MODEL.EQ.1) WRITE(NW,1400)
      IF(MODEL.EQ.1) WRITE(NW,1060)
      IF(MODEL.EQ.1) WRITE(NW,1400)
      IF(MODEL.EQ.1) WRITE(NW,1070)
      IF(MODEL.EQ.2) WRITE(NW,1050)
      IF(MODEL.EQ.2) WRITE(NW,1400)
      IF(MODEL.EQ.2) WRITE(NW,1040)
      IF(MODEL.EQ.2) WRITE(NW,1060)
      IF(MODEL.EQ.2) WRITE(NW,1040)
      IF(MODEL.EQ.2) WRITE(NW,1400)
      IF(MODEL.EQ.2) WRITE(NW,1070)
      IF(MODEL.EQ.2) WRITE(NW,1400)
      IF(MODEL.EQ.3) WRITE(NW,1050)
      IF(MODEL.EQ.3) WRITE(NW,1400)
      IF(MODEL.EQ.3) WRITE(NW,1060)
      IF(MODEL.EQ.3) WRITE(NW,1400)
      IF(MODEL.EQ.3) WRITE(NW,1040)
      IF(MODEL.EQ.3) WRITE(NW,1070)
      IF(MODEL.EQ.3) WRITE(NW,1040)
C
C
C
C PHYSICAL PARAMETERS I/O
      READ(NR,90)M1,M2,M3,K1,C1,K2
90    FORMAT(8E10.4)
C CORRECTION TO CHECK FOR M3=0
      IF (M3) 902,900,902
C  M3=0
  900 WRITE(NW,901) M3
      CALL EXIT
  901 FORMAT(24H0   IMPROPER INPUT M3 = ,E10.4)
  902 WRITE(NW,1020)
       WRITE(NW,1080)
      IF(LOADF.EQ.4) WRITE(NW,1040)
      IF(LOADF.EQ.4) WRITE(NW,1090)
      IF(LOADF.EQ.4) WRITE(NW,1040)
      IF(LOADF.EQ.4) WRITE(NW,1400)
      IF(LOADF.EQ.4) WRITE(NW,1100)
      IF(LOADF.EQ.4) WRITE(NW,1400)
```

```
      IF(LOADF.EQ.5) WRITE(NW,1090)
      IF(LOADF.EQ.5) WRITE(NW,1400)
      IF(LOADF.EQ.5) WRITE(NW,1040)
      IF(LOADF.EQ.5) WRITE(NW,1100)
      IF(LOADF.EQ.5) WRITE(NW,1040)
      WRITE(NW,1110)
      IF(IDAMP.EQ.6) WRITE(NW,1040)
      IF(IDAMP.EQ.6) WRITE(NW,1120)
      IF(IDAMP.EQ.6) WRITE(NW,1040)
      IF(IDAMP.EQ.6) WRITE(NW,1400)
      IF(IDAMP.EQ.6) WRITE(NW,1130)
      IF(IDAMP.EQ.6) WRITE(NW,1400)
      IF(IDAMP.EQ.7) WRITE(NW,1120)
      IF(IDAMP.EQ.7) WRITE(NW,1400)
      IF(IDAMP.EQ.7) WRITE(NW,1040)
      IF(IDAMP.EQ.7) WRITE(NW,1130)
      IF(IDAMP.EQ.7) WRITE(NW,1040)
      WRITE(NW,1531)
      WRITE(NW,1020)
      WRITE(NW,1400)
C READ LOAD AND DAMPING PARAMETERS
      READ(NR,90) ALOAD,BLOAD,CLOAD,DLOAD,ADAMP,BDAMP,CDAMP,DDAMP
      IF(LOADF.EQ.4) WRITE(NW,1230)ALOAD,BLOAD
      IF(LOADF.EQ.5)  WRITE(NW,1235) CLOAD,DLOAD
      IF(IDAMP.EQ.6) WRITE(NW,1245) ADAMP,BDAMP
      IF(IDAMP.EQ.7) WRITE(NW,1240) CDAMP,DDAMP
C READ THE LOCAL GRAVITATIONAL ACCELERATION UNITS) AND AERODYNAMIC
C  FORCES
      READ(NR,90)  GL,FA,ELIM
C CALCULATE THE EQUILIBRIUM GAS FILM THICKNESS VIA A SUBPROGRAM ≠FILM≠
      CALL FILM
C PRINT FILM THICKNESS AND STEADY STATE ROTOR FORCES
      IF(ELIM.GT.0.0)  GO TO 110
      ELIM=.0002
  110 WRITE(NW,1251)  ELIM
      WRITE(NW,1500)
      WRITE(NW,1020)
C CONVERT HINIT TO MILS FOR PRINTOUT PURPOSES
      HINIT=HINIT*1000.
      WRITE(NW,1250)HINIT,FA,GL
C RECONVERT TO INCHES FOR CALCULATION PURPOSES
      HINIT=HINIT/1000.
      WRITE(NW,1020)
      IF(MODEL.EQ.1)WRITE(NW,1220)M1,M2,M3,K1,C1,K
      IF(MODEL.EQ.2)WRITE(NW,1340)M1,M2,M3,K1,K2
      IF(MODEL.EQ.3) WRITE(NW,1330)M3
C CHANGE UNITS
      M1=M1 /386.069
      M2=M2/ 386.069
      M3=M3/ 386.069
```

```
      WRITE(Nw,1020)
      WRITE(Nw,1140)
      IF(IFOFT.EQ.8)  WRITE(Nw,1040)
      IF(IFOFT.EQ.8)  WRITE(Nw,1150)
      IF(IFOFT.EQ.8)  WRITE(Nw,1040)
      IF(IFOFT.EQ.8)  WRITE(Nw,1400)
      IF(IFOFT.EQ.8)  WRITE(Nw,1160)
      IF(IFOFT.EQ.8)  WRITE(Nw,1400)
      IF(IFOFT.EQ.8)  WRITE(Nw,1170)
      IF(IFOFT.EQ.8)  WRITE(Nw,1400)
      IF(IFOFT.EQ.8)  WRITE(Nw,1180)
      IF(IFOFT.EQ.9)  WRITE(Nw,1400)
      IF(IFOFT.EQ.9)  WRITE(Nw,1150)
      IF(IFOFT.EQ.9)  WRITE(Nw,1400)
      IF(IFOFT.EQ.9)  WRITE(Nw,1040)
      IF(IFOFT.EQ.9)  WRITE(Nw,1160)
      IF(IFOFT.EQ.9)  WRITE(Nw,1040)
      IF(IFOFT.EQ.9)  WRITE(Nw,1400)
      IF(IFOFT.EQ.9)  WRITE(Nw,1170)
      IF(IFOFT.EQ.9)  WRITE(Nw,1400)
      IF(IFOFT.EQ.9)  WRITE(Nw,1180)
      IF(IFOFT.EQ.10)  WRITE(Nw,1400)
      IF(IFOFT.EQ.10)  WRITE(Nw,1150)
      IF(IFOFT.EQ.10)  WRITE(Nw,1400)
      IF(IFOFT.EQ.10)  WRITE(Nw,1160)
      IF(IFOFT.EQ.10)  WRITE(Nw,1400)
      IF(IFOFT.EQ.10)WRITE(Nw,1040)
      IF(IFOFT.EQ.10)WRITE(Nw,1170)
      IF(IFOFT.EQ.10)WRITE(Nw,1040)
      IF(IFOFT.EQ.10)  WRITE(Nw,1400)
      IF(IFOFT.EQ.10)  WRITE(Nw,1180)
      IF(IFOFT.EQ.10)  WRITE(Nw,1400)
      IF(IFOFT.EQ.11)  WRITE(Nw,1400)
      IF(IFOFT.EQ.11)  WRITE(Nw,1150)
      IF(IFOFT.EQ.11)  WRITE(Nw,1400)
      IF(IFOFT.EQ.11)  WRITE(Nw,1160)
      IF(IFOFT.EQ.11)  WRITE(Nw,1400)
      IF(IFOFT.EQ.11)  WRITE(Nw,1170)
      IF(IFOFT.EQ.11)  WRITE(Nw,1400)
      IF(IFOFT.EQ.11)WRITE(Nw,1040)
      IF(IFOFT.EQ.11)WRITE(Nw,1180)
      IF(IFOFT.EQ.11)WRITE(Nw,1040)
      WRITE(Nw,1531)
      WRITE(Nw,1020)
      WRITE(Nw,1190)
      IF(ICC.EQ.12)  WRITE(Nw,1040)
      IF(ICC.EQ.12)  WRITE(Nw,1200)
      IF(ICC.EQ.12)  WRITE(Nw,1040)
      IF(ICC.EQ.12)  WRITE(Nw,1400)
      IF(ICC.EQ.12)  WRITE(Nw,1210)
```

```
      IF(ICC.EQ.13) WRITE(NW,1200)
      IF(ICC.EQ.13) WRITE(NW,1400)
      IF(ICC.EQ.13) WRITE(NW,1040)
      IF(ICC.EQ.13) WRITE(NW,1210)
      IF(ICC.EQ.13) WRITE(NW,1040)
      WRITE(NW,1400)
      WRITE(NW,1020)
C PRINT PARAMETERS ASSOCIATED WITH FORCING FUNCTION
      IFM7=IFOFT-7
      GO TO (120,130,140,150),IFM7
C STEADY STATE SINE FORCE
120   READ(NR,90) AMPLD,FREQ
      WRITE(NW,1320) FREQ
      IF(MOTION.EQ.0) WRITE(NW,1520) AMPLD
      IF(MOTION.EQ.1) WRITE(NW,1530) AMPLD
      GO TO 160
130   READ(NR,90) PEAKS,PDURS
      WRITE(NW,1310) PDURS
      IF(MOTION.EQ.0) WRITE(NW,1520) PEAKS
      IF(MOTION.EQ.1) WRITE(NW,1530) PEAKS
      GO TO 160
140   READ(NR,90)PEAKH,PDURH
      WRITE(NW,1300) PDURH
      IF(MOTION.EQ.0) WRITE(NW,1520) PEAKH
      IF(MOTION.EQ.1) WRITE(NW,1530) PEAKH
      GO TO 160
150   WRITE(NW,1260)
      IF(MOTION.EQ.0)  WRITE(NW,1261)
      IF(MOTION.EQ.1)   WRITE(NW,1262)
C ABOVE IS HEADING FOR SHOCK PULSE TABLE
C NOW READ THE NUMBER OF INCREMENTS IN THE PULSE AND THE INCREMENTAL
C TIME INTO WHICH PULSE IS DIVIDED
      READ(NR,154) NINCP,TINCP
  154 FORMAT(I5,F10.4)
C INITIALIZE FIRST YB VALUE
      INCPO=NINCP+1
      READ(NR,90) (PUVAL(I),I=2, INCPO)
  151 PUVAL(1) =0.0
      TP(1)=0.0
  153 DO 159 I=2,INCPO
      EYE=I-1
      TP(I)=EYE*TINCP
      IM1=I-1
      IP1=I+1
  159 IF(.NOT.(I.EQ.1.OR.I.EQ.INCPO)) PULDOT(I)=(PUVAL(IP1)-
     1PUVAL(IM1))/(2.*TINCP)
      DO 158 I=1,INCPO
      MAPGE=(I/45)*45-I
      IF(MAPGE.EQ.0)  WRITE(NW,1531)
  158 WRITE(NW,1265) TP(I),PUVAL(I)
```

```
      WRITE(NW,1500)
      ANINCP=NINCP
      PDURT=ANINCP*TINCP
      WRITE(NW,1510) PDURT
 1265 FORMAT(13X,2F12.7)
      PULDOT(1)=(PUVAL(2)-PUVAL(1))/TINCP
      PULDOT(INCPO)=(PUVAL(INCPO)-PUVAL(NINCP))/TINCP
C FORM A NEW TABLE FOR THE INTEGRAL OF YB
      IF (MOTION.EQ.1)  CALL FORMT
      WRITE(NW,1531)
C READ PROGRAM CONTROL CARDS
  160 READ(NR,91) IPSTEP,M,MAXINC,NCYCLS,TPRINT,TMAX,H,E,HM,BOGUS
   91 FORMAT(4I5,6E10.4)
      WRITE (NW,1500)
      WRITE(NW,1020)
      NCONE=NCYCLS
      IF(NCYCLS.EQ.0)  NCONE= NCYCLS+1
      WRITE(NW,1280) TMAX,MAXINC,NCONE,H,TPRINT,IPSTEP,E,HM,M,BOGUS
C READ AND WRITE INITIAL CONDITIONS
      READ(NR,90)TINIT,Y1IN,Y2IN,Y3IN,V1IN,V2IN,V3IN
      WRITE(NW,1270) TINIT,Y1IN,V1IN,Y2IN,V2IN,Y3IN,V3IN
 1010 FORMAT(I5,75H
     1                          )
1020  FORMAT(1H ,119(1H*))
 1030 FORMAT(40X,15HPROGRAM OPTIONS/20X,58HOPTIONS SELECTED FOR THIS PAR
     1TICULAR RUN ARE DESIGNATED BY/70X,8H--------/71X,6HOPTION/70X,
     28H--------)
 1031 FORMAT(10X,25HCHOICE OF VIBRATION MODEL/)
 1040 FORMAT(20X,50H--------------------------------------------------)
 1050 FORMAT(20X,50H1 = THREE-DEGREE OF FREEDOM SYSTEM USING ISOLATORS)
 1060 FORMAT(20X,53H2 = THREE-DEGREE OF FREEDOM SYSTEM USING RIGID MOUNT
     1S)
 1070 FORMAT(20X,52H3 = SIMPLE MODEL, ENTIRELY RIGID EXCEPT FOR GAS FILM
     1)
 1080 FORMAT(/10X,34HGAS FILM FUNCTIONAL REPRESENTATION/15X,19HLOAD CHAR
     1ACTERISTIC/)
 1090 FORMAT(20X,35H4 = EXPONENTIAL LOAD CHARACTERISTIC)
 1100 FORMAT(20X,38H5 = POWER FUNCTION LOAD CHARACTERISTIC)
 1110 FORMAT(10X,22HDAMPING CHARACTERISTIC/)
 1120 FORMAT(20X,35H6 = EXPONENTIAL DAMPING COEFFICIENT)
 1130 FORMAT(20X,38H7 = POWER FUNCTION DAMPING COEFFICIENT)
 1140 FORMAT(1H0,9X,27HTYPE OF EXCITATION FUNCTION/)
 1150 FORMAT(20X,      27H8 = STEADY SINUSOIDAL INPUT)
 1160 FORMAT(20X,      19H9 = HALF SINE SHOCK)
 1170 FORMAT(20X,     44H10 = HAVERSINE SHOCK
 1180 FORMAT(20X,     44H11 = ARBITRARY SHOCK (TABLE)
 1190 FORMAT(1H0, 9X,26HIS CALCOMP OUTPUT DESIRED-)
 1200 FORMAT(20X, 8H12 = YES)
 1210 FORMAT(20X, 7H13 = NO)
 1220 FORMAT(1H0,20X,53HPARAMETERS OF THE THREE-DEGREE SYSTEM USING ISOL
```

```
     1ATORS//12X, 7HMASS OF.        5X,14HEFFECTIVE MASS, 4X,7HMASS OF,
     2 6X,9HSTIFFNESS, 6X,7HDAMPING, 7X, 7HFLEXURE/13X,6HCASING,9X
     3    , 8HOF PLATE, 7X,6HROTOR ,10X,2HOF,12X,2HOF, 9X, 9HSTIFFNESS/
     426X,11HAND FLEXURE,18X, 9HISOLATORS, 5X, 9HISOLATORS/
     514X,4H(LB),10X,4H(LB),10X,4H(LB), 9X, 7H(LB/IN), 5X,11H(LB-SEC/IN)
     6, 4X, 7H(LB/IN)//10X,5(G10.3,4X),E12.4)
1230 FORMAT(1H0, 9X,23HDESCRIPTION OF GAS FILM//
     120X,50HTHE EXPONENTIAL LOAD CHARACTERISTIC IS OF THE FORM/
     225X,22HLOAD (LB) = A*EXP(B*H)/20X,5HWHERE/
     325X,27HH = FILM THICKNESS (INCHES)/25X, 4HA = ,E12.4,5H (LB)/
     425X, 4HB = ,E12.4, 7H( 1/IN))
1240 FORMAT(1H0,9X,53HTHE POWER FUNCTION DAMPING COEFFICIENT IS OF THE
     1FORM/20X,21HB(LB*SEC/IN) = C*H**D/10X,5HWHERE/
     220X,28HH = FILM THICKNESSS (INCHES)/
     320X, 4HC= ,E12.4,10H LB-SEC/IN /
     420X, 4HD= ,E12.4, 7H (1/IN))
1250 FORMAT(10X,29HEQUILIBRIUM FILM THICKNESS IS,G12.5, 5H MILS//
     115X,56HASSUMING STEADY-STATE AERODYNAMIC FORCES ON THE ROTOR OF,
     2G12.5, 3H LB/ 15X,34HAND A LOCAL GRAVITATIONAL FIELD OF,G12.5,
     315H TIMES STANDARD)
1251 FORMAT(/10X,85HNON-LINEAR LOAD AND DAMPING FUNCTIONS ARE HELD CONS
     1TANT AT FILM THICKNESSES LESS THAN,G10.3,8H INCHES.)
1260 FORMAT(10X,62HINPUT MOTION IS A SHOCK PULSE DESCRIBED BY THE FOLLO
     1WING TABLE)
1261 FORMAT(/20X,4HTIME,2X,12HDISPLACEMENT/19X,5H(SEC),4X,
     1 8H(INCHES))
1262 FORMAT(/20X,4HTIME,2X,12HACCELERATION/19X,5H(SEC),4X,5H(G≠S))
1270 FORMAT(1H0,9X,29HINITIAL OR RESTART CONDITIONS/
     120X,12HINITIAL TIME,11X,1H=,G10.3,8H SECONDS/
     220X,24HDISPLACEMENT OF MASS 1 =,G10.3, 7H INCHES/
     320X,18HVELOCITY OF MASS 1,5X,1H=,G10.3, 7H IN/SEC/
     420X,24HDISPLACEMENT OF MASS 2 =, G10.3, 7H INCHES/
     520X,18HVELOCITY OF MASS 2,5X,1H=,G10.3, 7H IN/SEC/
     620X,24HDISPLACEMENT OF MASS 3 =,G10.3, 7H INCHES/
     720X,18HVELOCITY OF MASS 3,5X,1H=,G10.3,7H IN/SEC/)
1280 FORMAT(/ 10X,26HPROGRAM CONTROL PARAMETERS//15X,19HDESIRED TERMINA
     1TION/20X,26HTIME VALUE WILL NOT EXCEED,F10.4,8H SECONDS/20X,
     248HAS A SAFETY MEASURE WE WILL NOT PERMIT MORE THAN,I5,6H STEPS/
     320X,25HCALCULATION WILL CONTINUE,I5,28H CYCLES AFTER PULSE DURATIO
     4N/15X,9HSTEP SIZE/20X,45HINITIAL STEP SIZE FOR CALCULATION PURPOSE
     5S IS,G10.3,8H SECONDS/20X,28HVALUES ARE PRINTED OUT EVERY ,G10.3,
     68H SECONDS/20X,5HEVERY,I5,38HTH POINT IS PLOTTED IF CALCOMP IS USE
     7D/20X,41HERROR CRITERION FOR INTEGRATION TECHNIQUE,G10.3/ 20X,20HM
     8INIMUM STEP-SIZE =,G12.5,8H SECONDS/20X,48HNO. OF INTEGRATIONS BEF
     9ORE STEP-SIZE IS DOUBLED=,I5/20X,48HNORMALIZED ERROR LIMIT FOR INT
     1EGRATION TECHNIQUE,F10.4)
1300 FORMAT(10X,37HINPUT MOTION IS HAVERSINE SHOCK PULSE/
     215X,17HPULSE DURATION IS,F10.4, 8H SECONDS/ )
1310 FORMAT(10X,37HINPUT MOTION IS HALF-SINE SHOCK PULSE/
     215X,17HPULSE DURATION IS,F10.4,8H SECONDS/)
```

```
 1320 FORMAT(10X,59HDESCRIPTION OF INPUT MOTION IS STEADY-STATE SINE EXC
     1ITATION/
     315X,12HFREQUENCY IS,F10.4, 3H HZ/ )
 1330 FORMAT(10X,58HTHRUST BEARING ON RIGID FLEXURE (SINGLE DEGREE OF FR
     1EEDOM)/10X,13HMASS OF ROTOR/13X,4H(LB)/10X,G10.3/)
 1340 FORMAT(10X,55HPARAMETERS OF THE SYSTEM ON RIGID MOUNTS ARE AS FOLL
     10WS//13X,50HEFFECTIVE MASS    EFFECTIVE MASS     MASS OF ROTOR,
     26X,9HSTIFFNESS,9X,8HFLEXURE /12X,16HOF LOWER HOUSING,2X,19HOF STAT
     30R + FLEXURE,16X,16HOF LOWER HOUSING,6X,9HSTIFFNESS/
     416X,12H(MASS1),(LB),4X,12H(MASS2),(LB),7X,12H(MASS3),(LB),6X,
     5 7H(LB/IN),11X,7H(LB/IN)/ 16X,G10.3,6X,G10.3,9X,G10.3,2(5X,E12.4))
 1350 FORMAT(30X,14HPROGRAM OUTPUT)
 1360 FORMAT(14X,4HTIME, 6X, 8HGAS FILM, 4X, 8HPEDESTAL, 7X,2HY1,10X,
     12HY2,10X,2HY3,10X,2HV1,10X,2HV2,10X,2HV3/
     224X, 9HTHICKNESS, 2X,10HDEFLECTIVE/25X, 7H(Y3-Y2), 5X, 7H(Y2-Y1)/
     3    12X, 9H(SECONDS), 4X,6H(MILS), 6X,6H(MILS), 6X,6H(MILS), 6X,
     46H(MILS), 6X,6H(MILS), 4X,10H(MILS/SEC), 2X,10H(MILS/SEC), 2X,
     510H(MILS/SEC))
 1370 FORMAT(10X,9(F10.4,2X))
 1380 FORMAT(25X,50HRESTART CONDITIONS (FINAL) AND IDENTIFICATION CODE/
     114X,4HTIME, 9X,2HY1,10X,2HY2,10X,2HY3,10X,2HV1,10X,2HV2,10X,2HV3,
     2 6X,5HNCASE/ 14X,5H(SEC), 6X,6H(MILS), 6X,6H(MILS), 6X,6H(MILS),
     3 4X,10H(MILS/SEC), 2X,10H(MILS/SEC), 2X,10H(MILS/SEC)/
     411X,7(F10.4,2X),I5)
 1235 FORMAT(1H0,9X,27HCHARACTERISTICS OF GAS FILM//
     120X,53HTHE POWER FUNCTION LOAD CHARACTERISTIC IS OF THE FORM//
     225X,18HLOAD (LB) = C*H**D    /20X,5HWHERE/
     325X,27HH = FILM THICKNESS (INCHES)/25X, 4HC = ,E12.4,
     418H LB-SEC/IN.**(1+D)/
     525X, 4HD = ,E12.4            )
1245  FORMAT(1H0,9X,53HTHE EXPONENTIAL DAMPING COEFFICIENT IS OF THE FOR
     1M   /20X,25HB(LB*SEC/IN) = C*EXP(D*H)/10X,5HWHERE/
     220X,28HH = FILM THICKNESSS (INCHES)/
     320X, 4HC = ,E12.4,15H LB-SEC/(IN**2)/
     420X, 4HD = ,E12.4,21H(DIMENSIONLESS UNITS))
 1400 FORMAT(/)
 1500 FORMAT(//)
 1510 FORMAT(// 10X,16HPULSE DURATION =, G12.5,4H SEC)
 1520 FORMAT(15X,17HPEAK AMPLITUDE IS,F10.4,20H INCHES DISPLACEMENT)
 1530 FORMAT(15X,17HPEAK AMPLITUDE IS,F10.4,17H G*S ACCELERATION)
 1531 FORMAT(1H1)
  999 RETURN
      END
      SUBROUTINE SIMINI(SI,FX,A,E,REL,MAXIT,FK,MRET)
      EXTERNAL FX
      LOGICAL REL
      DIMENSION A(2)
      AA=A(1)
      BB=A(2)
      H = (BB-AA) / 6.0
```

```
      XMID = (AA+BB) * .5
      Q = 2. * FX(XMID,FK)
      S1 = FX(AA,FK) + Q + FX(BB,FK)
      PR = H*(S1+Q)
      IF(MAXIT.EQ.1) GO TO 150
      DO 100 IT=2,MAXIT
      ISTOP = 2**IT - 1
      H= .5*H
      S=0.
      DO 80 M=1,ISTOP,2
      X=AA+3.0*M*H
   80 S=S+FX(X,FK)
      SI=H*(4.*S +S1)
      DIFF=ABS(SI-PR)
      IF(REL) DIFF=DIFF/ABS(SI)
      IF(DIFF.LE.E) GO TO 160
      PR=SI
      S1=S1+S+S
  100 CONTINUE
      RETURN
  150 SI=PR
  160 MRET=0
      RETURN
      END


      SUBROUTINE SOLVE
      REAL M1,M2,M3,C1,K1,K2
      COMMON TPRINT,TMAX,IPSTEP,NCYCLS,MOTION,TITLE(15),YBA,YBINT(200)
      COMMON NR,NW,NCASE,MODEL,LOADF,IDAMP,IFOFT,ICC,
     1              M1,M2,M3,K1,C1,K2,GL,FA,ALOAD,ADAMP,BLOAD,BDAMP,
     2CLOAD,CDAMP,DLOAD,DDAMP,HINIT,IFM7,AMPLD,FREQ,PEAKS,PDURS,PEAKH,
     3PDURH,NINCP,TINCP,TP(200),PUVAL(200),PULDOT(200),TINIT,Y1IN,Y2IN,
     4Y3IN,V1IN,V2IN,V3IN,TIME(6000),Y1,Y2,Y3,V1,V2,V3,N,VEC(6),DVEC(6),
     5MAXINC,H,HM,M,E,AKO,NE,T,              ELIM,INDX,     YB,YBDOT,
     6OMEGA,WHO,WY3Y2H,BY3Y2H
      COMMON FILMT(6000),Y2MY1(6000),VAPEAK(6000),YBPLOT(6000)
      COMMON T2,ITIME,YBPREV
C THIS SUBROUTINE SOLVES THE EQUATIONS OF MOTION,WHICH WILL BE DEFINED
C   IN SUBROUTINE DIFFEQ
C
C INITIALIZE THE VECTORS
C INITIALIZE STORAGE FOR MAX AND MIN VALUES
      ITIME=1
      IVAL=1
      IMAXIM=0
      IFM7= IFOFT-7
      ISTEAD=1
      WRITE(NW,1111)
      IF(MODEL.EQ.3)  GO TO 10
```

```
      WRITE(NW,1112)
      N=6
      VEC(1)=V1IN
      VEC(2)=V2IN
      VEC(3)=V3IN
      VEC(4)=Y1IN
      VEC(5)=Y2IN
      VEC(6)=Y3IN
      GO TO 20
   10 WRITE(NW,1113)
      N=2
      VEC(1)=V3IN
      VEC(2)=Y3IN
   20 T=TINIT
C SAVE VALUE OF M= NO. OF INTEGRATIONS BEFORE STEP SIZE IS DOUBLED
      MOLD =M
C INITIALIZE STORAGE FOR T- PRINT VALUES
      TPRVAL=T+TPRINT
      KELP=1
      DO  200 KOUNT=1,MAXINC
C SET FLAG OFF FOR PRINT
      IPRINT=2
C INITIALIZE M AND NE
      M=MOLD
      IF(KOUNT.EQ. 1) NE=0
      IF(KOUNT.NE.1 ) NE=1
      TADINC=T+2.*H
      IF(TADINC.LT.TPRVAL)  GO TO 1200
      TOINC=T+H
      IF(TOINC.LT.TPRVAL)  GO TO 1190
C T+  DT WILL EXCEED PRINT VALUE
C SAVE OLD DT VALUE, I.E.  SAVE H
      HOLD=H
      H=TPRVAL -T
C SAVE NEW DT VALUE
      HNEW=H
C TURN PRINT FLAG ON
      IPRINT=1
C SET M=10,000  , SO THAT DT WILL NOT BE DOUBLED
 1190 M=10000
C RONKU INTEGRATION
 1200 TZ=T
      CALL RONKU(T,VEC,DVEC,H,HM,N,NE,M,E,AKO)
      YBPREV=YB
C TEST PRINT FLAG ON, 1=ON,  2=OFF
      IF(IPRINT.EQ.2)  GO TO 1536
C TEST DT =NEW DT
      IF(H-HNEW)  1536,1210,1536
C RESET DT TO OLD DT
 1210 H=HOLD
```

```
C INCREASE FOR NEXT PRINT VALUE
      TPRVAL=T+TPRINT
C FORM AN INDEX TO TAG NO. OF ITERATIONS
      INDX=KELP
      IF(MOTION.EQ.0)    YBPLOT(KELP)=YB
      IF(MOTION.EQ.1)  YBPLOT(KELP) =YBA
      TIME(KELP)=T
      MAPGE=(KELP/45)*45-KELP
      IF(MAPGE.EQ.0)  WRITE(NW,1118)
      IF(MODEL.EQ.3) GO TO 1490
      Y2MY1(KELP)=VEC(4)-VEC(5)
      FILMT(KELP)=HINIT+VEC(6)-VEC(5)
      WRITE(NW,2222) T,FILMT(KELP),(VEC(IO),IO=4,6),(VEC(IO),IO=1,3),
     1Y2MY1(KELP),YB
      GO TO 1530
1490  FILMT(KELP)=HINIT+VEC(2)-YB
      WRITE(NW,2222) T,FILMT(KELP),VEC(2),VEC(1),YB,YBA
 1530 IF(FILMT(KELP).LT.0.0)  GO TO 1531
      GO TO (400,500,600,700),IFM7
 1531 IF(IFOFT.EQ.8)  GO TO 400
      WRITE(NW,1115)
 1115 FORMAT(/5X,47HRUN COMPLETE AT THIS POINT. ROTOR HAS BOTTOMED.)
      GO TO 666
  400 IF(KELP.LT.3)  GO TO 1535
      D1=FILMT(KELP)
      D2=FILMT(KELP-1)
      D3=FILMT(KELP-2)
      IF(D1.LT.D2.AND.D2.GT.D3)  GO TO 410
      IF(D1.GT.D2.AND.D2.LT.D3)  GO TO 420
      GO TO 1535
  410 IMAXIM = 1
      GO TO 425
  420 IMAXIM=2
  425 VAPEAK(IVAL)=D2
      IVAL=IVAL+1
C TEST FOR MIN OR MAX
      GO TO (1535,430),IMAXIM
C TEST FOR STEADY-STATE
  430 IF(ISTEAD.NE.1)  GO TO 661
      IF(IVAL.LE.5) GO TO 1535
      ERRC=(VAPEAK(IVAL-3)-VAPEAK(IVAL-5))/VAPEAK(IVAL-3)
      IF(ABS(ERRC).GT..01) GO TO 1535
      ISTEAD= 2
      GO TO 1535
C IFOFT = 9
  500 IF (T.LT.PDURS)  GO TO 1535
  510 IF(KELP.LT.3)  GO TO 1535
      D1=FILMT(KELP)
      D2=FILMT(KELP-1)
      D3=FILMT(KELP-2)
```

```
      IF(D1.LT.D2.AND.D2.GT.D3)  GO TO 515
      IF(D1.GT.D2.AND.D2.LT.D3)  GO TO 515
      GO TO 1535
  515 IMAXIM=IMAXIM+1
      IF(NCYCLS.EQ.0) GO TO 520
      IF(IMAXIM.GT.(2*NCYCLS))  GO TO 666
      GO TO 1535
  520 IF(IMAXIM.GE.2) GO TO 666
      GO TO 1535
C IFOFT = 10
  600 IF(T.LT.PDURH)  GO TO 1535
      GO TO 510
  700 ANINCP=NINCP
      IF(T.LT.ANINCP*TINCP)   GO TO 1535
      GO TO 510
 1535 KELP=KELP+1
 1536 IF(T.GT.TMAX)  GO TO 660
200   CONTINUE
      WRITE(NW,1114)  MAXINC
      GO TO 666
C MAKE A HEADING AND PRINT RESULTS
1111  FORMAT(1H1,19X,43H  000   U   U  TTTTT  PPPP   U   U  TTTTT  /
     1         20X, 43H O   O  U   U    T    P   P  U   U    T    /
     2         20X, 43H O   O  U   U    T    PPPP   U   U    T    /
     3         20X, 43H O   O  U   U    T    P      U   U    T    /
     4         20X, 43H  000    UUU     T    P       UUU     T    ////
     5)
 1112 FORMAT(120H   TIME      FILM     DISPLACEMENT DISPLACEMENT DISPLAC
     1EMENT  VELOCITY    VELOCITY    VELOCITY    RELATIVE    FORCING   /
     2       120H            THICKNESS   OF MASS 1    OF MASS 2    OF ROT
     3OR    OF MASS 1   OF MASS 2    OF ROTOR   DISP. BET.   FUNCTION  /
     4        120H   (SEC)   (INCHES)     (INCHES)      (INCHES)      (INCHE
     5S)    (IN/SEC)    (IN/SEC)      (IN/SEC)  MASS2 +MASS1 (INCHES)   )
 1113 FORMAT(95H0   TIME    FILM    DISPLACEMENT   VELOCITY      FORCING
     1    FORCING                                                      /
     2       75H          THICKNESS   OF ROTOR      OF ROTOR     FUNCTION
     3    FUNCTION        /
     4       75H   (SEC) (INCHES)     (INCHES)      (IN/SEC)     (INCHES)
     5    (G≠S)           /)
 1114 FORMAT( /5X,38HMAXIMUM NO. OF TIME STEPS HAS EXCEEDED,I5)
 2222 FORMAT(1X,F7.4,E11.4,3E13.4,5E12.4)
 1116 FORMAT(/5X,42HSTEADY-STATE CRITERION HAS BEEN SATISFIED.)
 1117 FORMAT(/5X,33HSPECIFIED TIME HAS BEEN ATTAINED.)
 1118 FORMAT(1H1)
  660 WRITE(NW,1117)
      GO TO 666
  661 WRITE(NW,1116)
666   IF(ICC.EQ.12) CALL CALCOM
      RETURN
      END
```

```
      SUBROUTINE DIFEQ(N,T,VEC,DVEC)
      REAL M1,M2,M3,C1,K1,K2
      DIMENSION VEC(6),DVEC(6)
      COMMON TPRINT,TMAX,IPSTEP,NCYCLS,MOTION,TITLE(15),YBA,YBINT(200)
      DIMENSION A(2)
      COMMON NR,NW,NCASE,MODEL,LOADF,IDAMP,IFOFT,ICC,
     1              M1,M2,M3,K1,C1,K2,GL,FA,ALOAD,ADAMP,BLOAD,BDAMP,
     2CLOAD,CDAMP,DLOAD,DDAMP,HINIT,IFM7,AMPLD,FREQ,PEAKS,PDURS,PEAKH,
     3PDURH,NINCP,TINCP,TP(200),PUVAL(200),PULDOT(200),TINIT,Y1IN,Y2IN,
     4Y3IN,V1IN,V2IN,V3IN,TIME(6000),Y1,Y2,Y3,V1,V2,V3,
     5NDUM,DDUM(6),DVUM(6),
     5MAXINC,H,HM,M,E,AKO,NE,TTDUM,          ELIM,INDX,     YB,YBDOT,
     6OMEGA,WHO,WY3Y2H,BY3Y2H
      COMMON FILMT(6000),Y2MY1(6000),VAPEAK(6000),YBPLOT(6000)
      COMMON TZ,ITIME,YBPREV
      EXTERNAL FX
C THIS SUBROUTINE DEFINES THE DIFFERENTIAL EQUATIONS SOLVED BY RONKU
      DATA MAXIT,ERR/100,.01/
      WEX(X)=ALOAD*EXP(BLOAD*X)
      WPF(X)=CLOAD*X**DLOAD
      BEX(X)=ADAMP*EXP(BDAMP*X)
      BPF(X)=CDAMP*X**DDAMP
      PI=3.1415926535
      IFM7=IFOFT-7
      IF(MODEL.EQ.3) GO TO 20
      DVEC(4)=VEC(1)
      DVEC(5)=VEC(2)
      DVEC(6)=VEC(3)
   20 GO TO (30,60,90,120),IFM7
30    OMEGA=2.*PI*FREQ
      YB=AMPLD*SIN(OMEGA*T)
      YBDOT=OMEGA*AMPLD*COS(OMEGA*T)
      YBA=-YB*(2.*PI*FREQ)**2/386.069
      IF(MOTION.EQ.0)   GO TO 130
      YB=-386.069/OMEGA**2*AMPLD*SIN(OMEGA*T)
      YBDOT=-386.069/OMEGA*AMPLD*COS(OMEGA*T)
      GO TO 130
60    YB=0.
      IF(T.LT.PDURS) YB=PEAKS*SIN(PI*T/PDURS)
      YBDOT=0.
      YBA=YB
      IF(MOTION.EQ.1) GO TO 65
      IF(T.LT.PDURS) YBDOT=PI/PDURS*PEAKS*COS(PI*T/PDURS)
      GO TO 130
   65 IF(T.LT.PDURS) YB=386.069*PEAKS*PDURS/PI*(T-PDURS/PI*
     1 SIN(PI*T/PDURS))
      IF(T.LT.PDURS) YBDOT=386.069*PEAKS*PDURS/PI*(1.-COS(PI*T/PDURS))
      IF(.NOT.(T.LT.PDURS)) YBDOT=772.138*PEAKS*PDURS/PI
      IF(.NOT.(T.LT.PDURS)) YB=386.069*PEAKS*PDURS**2/PI+YBDOT*(T-PDURS)
      GO TO 130
```

```
90      YB=0.
        IF(T.LT.PDURH) YB=0.5*PEAKH*(1.-COS(2.*PI*T/PDURH))
        YBDOT=0.
        YBA=YB
        IF(MOTION.EQ.1)  GO TO 95
        IF(T.LT.PDURH) YBDOT=PI/PDURH*SIN(2.*PI*T/PDURH)*PEAKH
        GO TO 130
   95   IF(T.LT.PDURH) YB=386.069/4.*PEAKH*(T**2-PDURH**2/(2.*PI**2)*
       1 (1.-COS(2.*PI*T/PDURH)))
         IF(T.LT.PDURH) YBDOT=386.069/4.*PEAKH*(2.*T-PDURH/PI*
       1 SIN(2.*PI*T/PDURH))
        IF(.NOT.(T.LT.PDURH)) YBDOT=193.035*PEAKH*PDURH
        IF(.NOT.(T.LT.PDURH)) YB=386.069/4.*PEAKH*PDURH**2+YBDOT*(T-PDURH)
        GO TO 130
  120   ANINCP=NINCP
        PDURT=ANINCP*TINCP
        IF(T.GT.PDURT)  YB=0.0
        IF(T.GT.PDURT)  YBDOT=0.0
        IF(T.GT.PDURT.AND.MOTION.EQ.0) GO TO 130
         IF(T.GT.PDURT.AND.MOTION.EQ.1)  GO TO 125
        NP1=NINCP+1
        CALL TLU(T,YB,TP,PUVAL,NP1)
        IF(MOTION.EQ.1) GO TO 125
        CALL TLU(T,YBDOT,TP,PULDOT,NP1)
        GO TO 130
  125   YBA=YB
 1240   A(1)=TZ
        A(2)=T
        IOP=1
        IF(T.GT.PDURT)  GO TO 1270
        IF(ITIME.EQ.1)   GO TO 1260
 1250   MRET=126
        CALL SIMINI(YB,FX,A,ERR,0,MAXIT,1.,MRET)
        IF(MRET.EQ. 126) GO TO 126
        YB=386.069*YB+YBPREV
        GO TO (127,1280,1265),IOP
 1260   ITIME=2
        IGR=1
        YBPREV=0.0
        IF(TZ) 1261,1250,1261
 1261   A(1)=0.0
        A(2)=TZ
        IOP=3
        GO TO 1250
 1265   YBPREV=YB
        GO TO 1240
C  SAVE YB VALUE
C T GREATER THAN PDURT
 1270   IF(IGR.EQ.3)  GO TO 1275
        A(2)=PDURT
```

```
      IGR=2
      IOP=2
      GO TO 1250
 1275 YB=YBPDUR
      GO TO 2126
 1280 YBPDUR=YB
      GO TO 127
  126 WRITE(NW,102) MAXIT,ERR
      WRITE(NW,103)
  127 IF(T.LT.PDURT.OR.IGR.LE.2)   GO TO 2127
 2126 YBDOT=DOTDUR
      GO TO 2128
 2127 CALL TLU(T,YBDOT,TP,YBINT,NP1)
      YBDOT=YBDOT*386.069
      IF(IGR.NE.2)   GO TO 130
      IGR=3
      DOTDUR=YBDOT
 2128 YB=YB+YBDOT*(T-PDURT)
130   IF(MODEL.NE.3) GO TO 150
      ARGU=VEC(2)-YB+HINIT
      IF(ARGU.LT..0002)  ARGU=ELIM
      IF(LOADF.EQ.4) WY3Y2H=WEX(ARGU)
      IF(LOADF.EQ.4) WHO=WEX(HINIT)
       IF(LOADF.EQ.5) WY3Y2H=WPF(ARGU)
      IF(LOADF.EQ.5) WHO=WPF(HINIT)
      IF(IDAMP.EQ.6) BY3Y2H=BEX(ARGU)
      IF(IDAMP.EQ.7) BY3Y2H=BPF(ARGU)
      GO TO 190
C SELECT FUNCTIONS
  150 ARGU=VEC(6)-VEC(5)+HINIT
      IF(ARGU.LT..0002) ARGU=ELIM
      IF(LOADF.EQ.4)  WY3Y2H=WEX(ARGU)
      IF(LOADF.EQ.4) WHO=WEX(HINIT)
      IF(LOADF.EQ.5)  WY3Y2H=WPF(ARGU)
      IF(LOADF.EQ.5) WHO=WPF(HINIT)
       IF(IDAMP.EQ.6)  BY3Y2H=BEX(ARGU)
      IF(IDAMP.EQ.7)  BY3Y2H=BPF(ARGU)
C NOW DEFINE DIFFERENTIAL EQUATIONS
190   IF(MODEL-2) 200,300,400
200   DVEC(1)=(K2/M1)*(VEC(5)-VEC(4))-(K1/M1)*(VEC(4)-YB)-C1/M1*(DVEC
     1 (4)-YBDOT)
300   DVEC(2)=-(1./M2)*WY3Y2H+(1./M2)*WHO+(1./M2)*(DVEC(6)-DVEC(5))
     1 *BY3Y2H-(K2/M2)*(VEC(5)-VEC(4))
      DVEC(3)=-(1./M3)*WHO+(1./M3)*WY3Y2H-(1./M3)*(DVEC(6)-DVEC(5))*BY3Y
     12H
      IF(MODEL.EQ.2) DVEC(1)=(K2/M1)*(VEC(5)-VEC(4))-(K1/M1)*(VEC(4)-
     1 YB)
      GO TO 401
  400 DVEC(2)=VEC(1)
      DVEC(1)=-WHO+WY3Y2H-(DVEC(2)-YBDOT)*BY3Y2H
      DVEC(1)=DVEC(1)/M3
  401 RETURN
```

```
  100 FORMAT(/ 6(3X,3HVEC,I3),5X,1H7,6(3X,4HDVEC,I3))
  101 FORMAT(1X,6E9.3,F5.4,6E10.4)
  102 FORMAT(1H0,29HMAXIMUM NUMBER OF ITERATIONS,I3,25H WAS REACHED BEFO
     1RE EPS =,E11.4)
  103 FORMAT( 5X,6HFOR YB)
  104 FORMAT(5X,9HFOR YBDOT)
      END

      SUBROUTINE TLU(A,B,C,D,N)                                          TLU     1
C           LINEAR INTERPOLATION ROUTINE                                 TLU     2
C     A= INDEPENDENT VARIABLE                                            TLU  0003
C     B= DEPENDENT VARIABLE  (ANSWER)                                    TLU  0004
C     C= INDEPENDENT TABLE                                               TLU  0005
C     D= DEPENDENT TABLE                                                 TLU  0006
C     N= NUMBER OF POINTS IN TABLE                                       TLU  0007
C     INDEPENDENT TABLE MUST BE SORTED, EITHER ASCENDING OR DESCENDING   TLU  0008
      DIMENSION C(1),D(1)                                                TLU  0009
      IF(N-1)1,2,3                                                       TLU  0010
    1 B=0.                                                               TLU  0011
      GO TO 100                                                          TLU  0012
    2 B=D(1)                                                             TLU  0013
      GO TO 100                                                          TLU  0014

    3 ML=1                                                               TLU  0015
      MU=N                                                               TLU  0016
    8 IF(MU-ML-1) 15,15,9                                                TLU  0017
    9 M=(MU+ML)/2                                                        TLU  0018
      IF(C(1)-C(2))11,2,10                                               TLU  0019
   10 IF(C(M)-A)13,12,14                                                 TLU  0020
   11 IF(A-C(M))13,12,14                                                 TLU  0021
   12 B=D(M)                                                             TLU  0022
      GO TO 100                                                          TLU  0023
   13 MU=M                                                               TLU  0024
      GO TO 8                                                            TLU  0025
   14 ML=M                                                               TLU  0026
      GO TO 8                                                            TLU  0027
   15 B=D(ML)+(D(MU)-D(ML))*((A-C(ML))/(C(MU)-C(ML)))                    TLU  0028
  100 RETURN                                                             TLU  0029
      END                                                                TLU  0030

      FUNCTION FX(X,FK)
      COMMON TPRINT,TMAX,IPSTEP,NCYCLS,MOTION,TITLE(15),YBA,YBINT(200)
      COMMON NR,NW,NCASE,MODEL,LOADF,IDAMP,IFOFT,ICC,
     1              M1,M2,M3,K1,C1,K2,GL,FA,ALOAD,ADAMP,BLOAD,BDAMP,
     2CLOAD,CDAMP,DLOAD,DDAMP,HINIT,IFM7,AMPLO,FREQ,PEAKS,PDURS,PEAKH,
     3PDURH,NINCP,TINCP,TP(200),PUVAL(200),PULDOT(200),TINIT,Y1IN,Y2IN,
     4Y3IN,V1IN,V2IN,V3IN,TIME(6000),Y1,Y2,Y3,V1,V2,V3,N,VEC(6),DVEC(6),
     5MAXINC,H,HM,M,E,AKO,NE,T,              ELIM,INDX,     YB,YBDOT,
     6OMEGA,WHO,WY3Y2H,BY3Y2H
```

```
      COMMON FILMT(6000),Y2MY1(6000),VAPEAK(6000),YBPLOT(6000)
      REAL M1,M2,M3,C1,K1,K2
      K=FK
      NP1=NINCP+1
      GO TO (1,2) ,K
    1 CALL TLU(X,F1,TP,YBINT ,NP1)
      FX=F1
      RETURN
    2 CALL TLU(X,F2,TP,PUVAL,NP1)
      FX=F2
      RETURN
      END


      SUBROUTINE FORMT
      DIMENSION A(2)
      COMMON TPRINT,TMAX,IPSTEP,NCYCLS,MOTION,TITLE(15),YBA,YBINT(200)
      COMMON NR,NW,NCASE,MODEL,LOADF,IDAMP,IFOFT,ICC,
     1              M1,M2,M3,K1,C1,K2,GL,FA,ALOAD,ADAMP,BLOAD,BDAMP,
     2CLOAD,CDAMP,DLOAD,DDAMP,HINIT,IFM7,AMPLD,FREQ,PEAKS,PDURS,PEAKH,
     3PDURH,NINCP,TINCP,TP(200),PUVAL(200),PULDOT(200),TINIT,Y1IN,Y2IN,
     4Y3IN,V1IN,V2IN,V3IN,TIME(6000),Y1,Y2,Y3,V1,V2,V3,N,VEC(6),DVEC(6),
     5MAXINC,H,HM,M,E,AKO,NE,T,              ELIM,INDX,     YB,YBDOT,
     6OMEGA,WHO,WY3Y2H,BY3Y2H
      COMMON FILMT(6000),Y2MY1(6000),VAPEAK(6000),YBPLOT(6000)
      DATA MAXIT,ERR/100,.01/
      EXTERNAL FX
      REAL M1,M2,M3,C1,K1,K2
      NP1=NINCP +1
      YBINT(1)=0.0
      DO 10 I=2,NP1
      A(1)=TP(I-1)
      A(2)=TP(I)
      MRET=5
      CALL SIMINI(TEMP,FX,A,ERR,0,MAXIT,2.,MRET)
      IF(MRET.EQ.5) GO TO 5
      GO TO 10
    5 WRITE(NW,102) MAXIT,ERR
      WRITE(NW,101)
   10 YBINT(I)=YBINT(I-1)+TEMP
      RETURN
  101 FORMAT(5X,49HFOR FORMATION OF NEW TABLE FOR THE INTEGRAL OF YB)
  102 FORMAT(1H0,29HMAXIMUM NUMBER OF ITERATIONS,I3,25H WAS REACHED BEFO
     1RE EPS =,E11.4)
      END
```

```
      SUBROUTINE FILM
C     THIS SUBROUTINE CALCULATES THE EQUILIBRIUM GAS FILM THICKNESS.
      COMMON TPRINT,TMAX,IPSTEP,NCYCLS,MOTION,TITLE(15),YBA,YBINT(200)
      COMMON NR,NW,NCASE,MODEL,LOADF,IDAMP,IFOFT,ICC,
     1              M1,M2,M3,K1,C1,K2,GL,FA,ALOAD,ADAMP,BLOAD,BDAMP,
     2CLOAD,CDAMP,DLOAD,DDAMP,HINIT,IFM7,AMPLD,FREQ,PEAKS,PDURS,PEAKH,
     3PDURH,NINCP,TINCP,TP(200),PUVAL(200),PULDOT(200),TINIT,Y1IN,Y2IN,
     4Y3IN,V1IN,V2IN,V3IN,TIME(6000),Y1,Y2,Y3,V1,V2,V3,N,VEC(6),DVEC(6),
     5MAXINC,H,HM,M,E,AKO,NE,T,                ELIM,INDX,     YB,YBDOT,
     6OMEGA,WHO,WY3Y2H,BY3Y2H
      COMMON FILMT(6000),Y2MY1(6000),VAPEAK(6000),YBPLOT(6000)
      REAL M1,M2,M3,C1,K1,K2
      W=-FA+M3*GL
      IF(LOADF-4)11,11,21
11    BH=ALOG(W)-ALOG(ALOAD)
      B=BLOAD
      IF(ABS(BLOAD).LT..00001.AND.BLOAD.LT.0.0) B=-.00001
      IF(ABS(BLOAD).LT..00001.AND.BLOAD.GT.0.0)     B=.00001
      HINIT=BH/B
      RETURN
   21 CABIN =W/CLOAD
      D=DLOAD
      IF(ABS(DLOAD).LT..00001.AND.DLOAD.GT.0.0)     D=.00001
      IF(ABS(DLOAD).LT..00001.AND.DLOAD.LT.0.0) D=-.00001
      ONENT=ALOG(CABIN)/D
      IF(ABS(ONENT).GT.88.0) GO TO 30
      HINIT=EXP(ONENT)
      RETURN
   30 WRITE(NW,100) DLOAD
      CALL EXIT
  100 FORMAT(25H0DLOAD IS TOO BIG. DLOAD=,E15.5)
      END



      SUBROUTINE CALCOM
      DIMENSION CLX(20),CLY(20)
      COMMON TPRINT,TMAX,IPSTEP,NCYCLS,MOTION,TITLE(15),YBA,YBINT(200)
      COMMON NR,NW,NCASE,MODEL,LOADF,IDAMP,IFOFT,ICC,
     1              M1,M2,M3,K1,C1,K2,GL,FA,ALOAD,ADAMP,BLOAD,BDAMP,
     2CLOAD,CDAMP,DLOAD,DDAMP,HINIT,IFM7,AMPLD,FREQ,PEAKS,PDURS,PEAKH,
     3PDURH,NINCP,TINCP,TP(200),PUVAL(200),PULDOT(200),TINIT,Y1IN,Y2IN,
     4Y3IN,V1IN,V2IN,V3IN,TIME(6000),Y1,Y2,Y3,V1,V2,V3,N,VEC(6),DVEC(6),
     5MAXINC,H,HM,M,E,AKO,NE,T,                ELIM,INDX,     YB,YBDOT,
     6OMEGA,WHO,WY3Y2H,BY3Y2H
      COMMON FILMT(6000),Y2MY1(6000),VAPEAK(6000),YBPLOT(6000)
      COMMON IBUF(1000)
      DATA XORIG,YORIG,AXLEN,AYLEN/2.,1.5,12.,6./
      WRITE(Nw,202)
  202 FORMAT(1H1,30HROAD MARKERS FOR CALCOMP PLOTS)
      NVALS=INDX
```

```
      NPTS=NVALS/IPSTEP
      I=NPTS*IPSTEP+1
      J=I+IPSTEP
      WRITE(NW,200) NVALS,NPTS,I,J
      CALL FACTOR(.75)
C CHANGES IN CALCOM. INSERT AFTER CALL TO PLOTS
C STOMP OUT NEGATIVE FILM THICKNESSES. TAG FIRST VAL FOR ERROR MESSAGE.
      ITAG=0
      CALL PLOT(XORIG,YORIG,-3)
      DO 20 K=1,NPTS
      IF(ITAG) 15,15,16
15    IF(FILMT(K) .LT. 0.) ITAG=K
16    IF(FILMT(K) .LT. 0.)  FILMT(K)=0.
20    CONTINUE
      CALL SCALE(TIME,AXLEN,NPTS,IPSTEP)
      WRITE(NW,201) TIME(I),TIME(J)
      IF(ITAG) 22,22,21
   21 XPAGE=TIME(ITAG)/TIME(J)
      CALL SYMBOL(XPAGE,0.,.14,7HCONTACT,30.,7)
C SCALE THE AXIS ACCORDING TO THE DATA BUT FORCE THE MINIMUM FILMT TO 0.
C  DEFINE AN ADDITIONAL FILMT TO INSURE AT LEASE ONE ZERO
22    FILMT(I)=0.
C CALL SCALE USING I POINTS. IT WILL STORE 0. AS FILM(J) AND DELTAV IN
C   FILMT(J+IPSTEP)
      NP1=NPTS+1
      CALL SCALE(FILMT,AYLEN,NP1,IPSTEP)
      II=NP1*IPSTEP+1
      JJ= II+IPSTEP
      WRITE(NW,203) FILMT(II),FILMT(JJ)
C NOW MOVE FIRSTV AND DELTAV BACK WHERE THEY BELONG.
      FILMT(I)=FILMT(J)
      FILMT(J)=FILMT(J+IPSTEP)
C SCALE DATA FOR TIME AND INPUT MOTION
      CALL SCALE(TIME,AXLEN,NPTS,IPSTEP)
      CALL SCALE(YBPLOT,AYLEN,NPTS,IPSTEP)
      CALL PLOT(-XORIG,-YORIG,-3)
      WRITE(NW,204)  YBPLOT(I),YBPLOT(J)
C DRAW THE AXIS FOR THE APPROPRIATE INPUT MOTION
     0IF(MOTION .EQ. 0 .AND. IFOFT .EQ. 8)CALL AXIS(1.,1.5,24HINPUT VIBR
     1ATION - INCHES,24,AYLEN,90.,YBPLOT(I),YBPLOT(J))
     0IF(MOTION .EQ. 1 .AND. IFOFT .EQ. 8)CALL AXIS(1.,1.5,37HINPUT VIBR
     1ATION - ACCELERATION IN G#S,37,AYLEN,90.,YBPLOT(I),YBPLOT(J))
     0IF(MOTION .EQ. 0 .AND. IFOFT .GT. 8)CALL AXIS(1.,1.5,20HINPUT SHOC
     1K - INCHES,20,AYLEN,90.,YBPLOT(1),YBPLOT(J))
     0IF(MOTION .EQ. 1 .AND. IFOFT .GT. 8)CALL AXIS(1.,1.5,33HINPUT SHOC
     1K - ACCELERATION IN G#S,33,AYLEN,90.,YBPLOT(I),YBPLOT(J))
      WRITE(NW,205)
C DRAW THE AXIS FOR FILM THICKNESS
     0CALL AXIS(XORIG,YORIG,31HBEARING FILM THICKNESS - INCHES,
     131,AYLEN,90.,FILMT(I),FILMT(J))
      WRITE(NW,206)
C DRAW TIME AXIS
     0CALL AXIS(XORIG,YORIG,     14HTIME - SECONDS,-14,AXLEN,0.,
```

```
     1TIME(I),TIME(J))
      CALL PLOT(XORIG,YORIG,-3)
      WRITE(NW,207)
C PLOT THE GRAPHS
      IF(NPTS.LT.30) NOPON=1
      IF(NPTS.GE.30)  NOPON=NPTS/30
      CALL  LINE(TIME,YBPLOT, NPTS,IPSTEP,NOPON,3)
      CALL  LINE(TIME,FILMT, NPTS,IPSTEP,NOPON,1)
      WRITE(NW,208)
C DRAW A CENTERLINE TO REPRESENT EQUILIBRIUM FILM THICKNESS
   98 CALL PLOT(-XORIG,-YORIG,-3)
      WRITE(NW,209)
      DO 99 K=1,13
      CLY(K)=YORIG+HINIT/FILMT(J)
99    CLX(K)=XORIG+FLOAT(K-1)/12.*AXLEN
      CLX(14)=0.0
      CLX(15)=1.0
      CLY(14) =0.
      CLY(15)=1.
      CALL CNTRLN(CLX,CLY,13,1)
      WRITE(NW,210)
C
C RETURN REFERENCE TO LOWER LEFT HAND CORNER AND LETTER TITLE
C
  100 CALL SYMBOL(2.50,0.50,.14,TITLE,0.,75)
      FNCASE=NCASE
      CALL SYMBOL(11.5,.30,.100,11HCASE NO. = ,0.,11)
      CALL NUMBER(999.,0.30,.10,FNCASE,0.,-1)
      CALL SDATE(DATE)                                                    CD
      CALL SYMBOL(11.5,0.15,.10,DATE,0.,8)                                CD
C PERFORM ANNOTATION
     0IF(MODEL .EQ. 1) CALL SYMBOL(4.50,9.65,.14,
     1 53HSIMULATOR VERTICAL ON ISOLATORS                          ,0.,53)
     0IF(MODEL .EQ. 2) CALL SYMBOL(4.50,9.65,.14,
     1 53HSIMULATOR VERTICAL ON RIGID MOUNTS                       ,0.,53)
     0IF(MODEL .EQ. 3) CALL SYMBOL(4.50,9.65,.14,
     1 55HSIMULATOR VERTICAL ON RIGID MOUNTS, CASING, AND FLEXURE,0.,55)
      CALL SYMBOL(4.50,9.25,.14,19HINPUT FUNCTION IS  ,0.,19)
     0IF(IFOFT .EQ. 8) CALL SYMBOL(999.,9.25,.14,
     1 40HSTEADY-STATE VIBRATION                          ,0.,40)
      IF(IFOFT.EQ. 9.AND.MOTION.EQ.0) CALL SYMBOL(999.,9.25,.14,
     140HHALF SINE DISPLACEMENT SHOCK                     ,0.,40)
      IF(IFOFT.EQ. 9.AND.MOTION.EQ.1) CALL SYMBOL(999.,9.25,.14,
     140HHALF SINE ACCELERATION SHOCK                     ,0.,40)
      IF(IFOFT.EQ.10.AND.MOTION.EQ.0) CALL SYMBOL(999.,9.25,.14,
     140HHAVERSINE DISPLACEMENT SHOCK                     ,0.,40)
      IF(IFOFT.EQ.10.AND.MOTION.EQ.1) CALL SYMBOL(999.,9.25,.14,
     140HHAVERSINE ACCELERATION SHOCK                     ,0.,40)
      IF(IFOFT.EQ.11.AND.MOTION.EQ.0) CALL SYMBOL(999.,9.25,.14,
     141HSHOCK DISPLACEMENT VALUES READ IN AS DATA,0.,41)
      IF(IFOFT.EQ.11.AND.MOTION.EQ.1) CALL SYMBOL(999.,9.25,.14,
     141HSHOCK ACCELERATION VALUES READ IN AS DATA,0.,41)
      GO TO (110,120,130,140),IFM7
```

```
110 CALL SYMBOL(4.50,8.85,.14,13HAMPLITUDE IS ,0.,13)
    CALL NUMBER(999.,8.85,.14,AMPLD,0.,5)
111 IF(MOTION.EQ.0) CALL SYMBOL(999.,8.85,.14,7H INCHES,0.,7)
    IF(MOTION.EQ.1) CALL SYMBOL(999.,8.85,.14,7H G≠S   ,0.,7)
    GO TO (112,116,116,140),IFM7
112 CALL SYMBOL(999.,8.85,.14,17H    FREQUENCY IS ,0.,17)
    CALL NUMBER(999.,8.85,.14,FREQ,0.,5)
    CALL SYMBOL(999.,8.85,.14,3H HZ,0.,3)
    GO TO 150
115 CALL SYMBOL(4.50,8.85,.14,14HPEAK VALUE IS ,0.,14)
    CALL NUMBER(999.,8.85,.14,OPEAK,0.,5)
    GO TO 111
116 CALL SYMBOL(999.,8.85,.14,24H      PULSE DURATION IS ,0.,24)
    CALL NUMBER(999.,8.85,.14,ODOR,0.,5)
    CALL SYMBOL(999.,8.85,.14,8H SECONDS,0.,8)
    GO TO 150
120 OPEAK=PEAKS
    ODOR=PDURS
    GO TO 115
130 OPEAK=PEAKH
    ODOR=PDURH
    GO TO 115
140 ODOR=FLOAT(NINCP)*TINCP
    CALL SYMBOL(4.50,8.85,.14,25HPEAK VALUE IS SHOWN      ,0.,25)
    GO TO 116
150 CALL SYMBOL(4.57,8.32,.14,3,0.,-1)
    CALL SYMBOL(5.00,8.25,.14,17H = INPUT FUNCTION,0.,17)
    CALL SYMBOL(4.57,8.07,.14,1,0.,-1)
    CALL SYMBOL(5.00,8.00,.14,32H = THRUST BEARING FILM THICKNESS,0.,
   132)
    WRITE(Nw,211)
    CLX(16)=4.50
    CLY(16)=7.82
    CLX(17)=5.25
    CLY(17)=7.82
    CLX(18)=0.
    CLY(18)=0.
    CLX(19)=1.
    CLY(19)=1.
    CALL CNTRLN(CLX(16),CLY(16),2,1)
    CALL SYMBOL(5.42,7.75,.14,26HEQUILIBRIUM FILM THICKNESS,0.,26)
    CALL PLOT(-.4,0.,-3)
    CALL DASHPT(0.,11.3,.113)
    CALL DASHPT(14.7,11.3,.147)
    CALL DASHPT(14.7,0.,.113)
    WRITE(Nw,212)
200 FORMAT(/5X,6HNVALS=,I5,6H NPTS=,I5,3H I=,I5,3H J=,I5)
201 FORMAT(/5X,8HTIME(I)=,E12.5,8HTIME(J)=,E12.5)
203 FORMAT(/5X,10HFILMT(II)=,E12.5,10HFILMT(JJ)=,E12.5)
204 FORMAT(/5X,10HYBPLOT(I)=,E12.5,10HYBPLOT(J)=,E12.5)
```

```
205 FORMAT(/5X,25HDIAG VERT AXIS-1 DRAWN    )
206 FORMAT(/5X,25HDIAG VERT AXIS-2 DRAWN    )
207 FORMAT(/5X,25HDIAG HORIZ AXIS DRAWN     )
208 FORMAT(/5X,25HCURVES  PLOTTED           )
209 FORMAT(/5X,25HORIGIN SHIFTED            )
210 FORMAT(/5X,25HCENTERLINE DRAWN          )
211 FORMAT(/5X,25HANNOTATION  ALMOST DONE   )
212 FORMAT(/5X,25HANNOTATION DONE           )
    RETURN
    END



    SUBROUTINE RONKU    (X,Y,DY,H,HM,N,NE,M,E,AKO)
    DIMENSION Y(6),DY(6),Y1(6),YD(6),YP(6,5),QP(6,5),A(4),B(4),C(4)
 30 IF(NE) 1,1,2
  1 A(1)=0.5
    A(2)= .2928932
    A(3)=      1.7071068
    A(4)=1.0/6.0
    B(1)=2.0
    B(2)=1.0
    B(3)=1.0
    B(4)=2.0
    C(1)=0.5
    C(2)=A(2)
    C(3)=A(3)
    C(4)=0.5
    IF (NE) 32,11,2
 11 DO 3 I=1,N
    YP(I,1)=Y(I)
  3 QP(I,1)=0.0
 32 K1=0
  2 X1=X
    HH=H
    K=1
 12 X50 = X1
    DO 4 J=2,5
    DO 17 I=1,N
 17 YD(I)=YP(I,J-1)
    CALL DIFEQ(N,X1,YD,DY)
    IF (J-3) 151,153,152
151 X1=X1+0.5*HH
    GO TO 153
152 X1=X1+0.5*HH
153 CONTINUE
    DO 5 I=1,N
    TERM=A(J-1)*(DY(I)-B(J-1)*QP(I,J-1))
    YP(I,J)=YP(I,J-1)+HH*TERM
```

```
 5 QP(I,J)=QP(I,J-1)+3.0*TERM-C(J-1)*DY(I)
 4 CONTINUE
   X1 =X50
   IF (K-2) 6,7,8
 6 DO 61 J=1,N
   Y1(J)=YP(J,5)
   YP(J,1)=Y(J)
61 QP(J,1)=0.0
   K=K+1
   HH=H/2.0
   GO TO 12
 7 K=K+1
   X1=X1+HH
   DO 71 J=1,N
   QP(J,1)=QP(J,5)
71 YP(J,1)=YP(J,5)
   GO TO 12
 8 DO 81 J=1,N
   T1=SQRT(Y1(J)**2+YP(J,5)**2)
   IF(T1) 18,81,18
18 TEST=ABS (Y1(J)-YP(J,5))/T1
   IF (TEST-E) 81,81,9
81 CONTINUE
   K1=K1+1
   AKO=TEST
   IF (K1-M) 10,13,13
 9 K1=0
   IF (ABS (H/2.0)-ABS (HM))14,15,15
14 AKO=TEST
   GO TO 10
15 H=H/2.0
   DO 16 J=1,N
16 YP(J,1)=Y(J)
   GO TO 2
13 K1=0
   H=H+H
10 X=X1    +HH
   DO 82 J=1,N
   QP(J,1)=QP(J,5)
   YP(J,1)=YP(J,5)+(YP(J,5)-Y1(J))/15.0
82 Y(J)=YP(J,1)
   CALL DIFEQ(N,X,Y,DY)
   RETURN
   END
```

APPENDIX C

PHOTOGRAPHS OF BEARING SURFACES AND COMPONENTS

Introduction

This appendix contains a thorough documentation of the condition of the bearings during various inspections defined by the following sequence of test events:

1. Inspection 1 - Beginning of program before any externally applied shock or vibration.

2. Tests as follows:

   a) axial vibration, rigid mounts, 39,000 rpm
   b) axial vibration, isolation mounts, 39,000 rpm
   c) transverse (T1) vibration, rigid mounts, 39,000 rpm
   d) transverse (T1) vibration, isolation mounts, 39,000 rpm

3. Inspection 2

4. Tests as follows:

   e) transverse (T1) vibration, isolation mounts, rotor inert
   f) transverse (T1) vibration, rigid mounts, rotor inert
   g) transverse (T2) vibration, isolation mounts, rotor inert
   h) transverse (T2) vibration, rigid mounts, rotor inert
   i) axial vibration, isolation mounts, rotor inert
   j) axial vibration, rigid mounts, rotor inert

5. Inspection 3

6. Tests as follows:

   k) transverse (T2) vibration, isolation mounts, 39,000 rpm
   l) transverse (T2) vibration, rigid mounts, 39,000 rpm

7. Inspection 4

8. All Shock Testing

9. Inspection 5

At the conclusion of each inspection, except the final one, all bearing surfaces were cleaned for reasons which will soon become apparent. The photographs presented in this appendix display each significant bearing surface, in turn, in a time sequence of events which, more or less, affected the apparent condition of that surface.

Figures 65 through 69 display the apparent condition of the surfaces of the thrust plate and runner which form two opposing interfaces with the thrust-bearing gas film.

Figure 65 shows the surfaces at the beginning of the test program. Note, that some previous wear is evident around the center of the thrust plate (shown on the left). The face of the thrust runner, on the other hand, shows little or no indication of wear.

Figure 66 shows the condition of the thrust-bearing surfaces during Inspection 2. The radial striations and inner circumferential band shown in part a) on the thrust runner are primarily the result of fine debris rather than wear. Verification is presented in part b) which shows the same surfaces after being cleaned. Figure 67 shows these surfaces at the beginning of Inspection 3. Again the surfaces are dirty but noticeably less so than they were at the beginning of Inspection 2. This is because a substantially cleaner air supply was used to drive the simulator turbine after Inspection 2. Figure 67 shows that some circumferential scratches now appear on the thrust runner which are not removable by washing. These were shallow surface markings and did not affect bearing performance. Figure 68 again shows a small amount of debris accumulation between Inspection 3 and Inspection 4. Figure 69 shows these surfaces at the conclusion of all the shock and vibration testing. The five spots lying in a circle on the thrust runner resulted from suspending the runner in a stationary position by feeding pressurized air through the five small orifices in the thrust plate.

Figure 70 shows the condition of the reverse-thrust bearing and opposing runner face at the beginning of the program, and Figure 71 presents the same surfaces at the conclusion of the testing. The outer circumferential scratch was

present to begin with. The difference in the two Figures is attributable to debris accumulation between Inspection 4 and Inspection 5.

Figures 72 and 73 form a before-and-after set for the compressor bearing journal. Except for occasional debris accumulation, there was no noticeable change in the surface condition throughout the program.

Figure 74 shows the condition of the faces of the compressor journal-bearing pads at the beginning of the program. The pad numbering convention is defined with respect to Figure 2 as follows:

> In Section AA (Bearing #1), beginning with the pad containing PF8, the pad numbers increase in the direction of rotation shown by the curved arrow;
>
> The pad numbers also increase in this direction in Section BB (Bearing #2) starting with the pad containing PF22.

Figure 75 shows the same bearing surfaces at the conclusion of all the shock-and-vibration testing. Again, the only difference is in the small amount of debris accumulation shown in Figure 75.

Figure 76 shows the outer surfaces of the compressor journal-bearing pads along with their corresponding pivots. These photos were taken before commencement of the testing. Figure 77 shows these same surfaces at the conclusion of all vibration testing. The only significant effect that the vibration testing produced was creation of two elongated wear spots on the surfaces of the pivot ball and pivot socket. The effect of this wear was a slight, but noticeable increase in the overall diametral clearance at each journal bearing. This did not produce any observable degradation in machine performance, however. Although the wear is detectable in Figure 77, it is shown in better detail in the magnified views of Figure 78. At this point, the pivot balls were replaced with new ones and shock testing was begun. At the end of the tests the photographs of Figure 79 were taken--showing that the shock testing did not result in the same amount of wear as did the vibration testing.

Figures 80 and 81 document the condition of the turbine bearing journal before and after all the testing. As was the case for the compressor journal, the turbine journal is virtually unaffected by the testing.

Figures 82 through 86 are the turbine journal-bearing counterparts of Figures 74 through 79 . The turbine journal-pad faces exhibited no signs of wear (Figures 82 , 83), while the pivot balls received some wear spots during the vibration testing (Figures 84 and 85), were subsequently replaced, and were not damaged nor worn by the shock testing (Figure 86).

In summary, all the primary bearing surfaces showed no deterioration as a result of the vibration and shock testing. Considerable debris was picked up by the pad faces and thrust-bearing surfaces in the interval between the first two inspections. Lesser, but still noticeable debris accumulated between each successive inspection interval. The pivot-ball surfaces showed some wear resulting from the vibration testing, but their replacements were virtually unaffected by the shock tests. Aside from the flexure which fraccured during a resonance condition, no damage to the machinery resulted from the test program. The simulator was performing just as well at the end of the test program as it was at the beginning.

APPENDIX D

METALLURGICAL REPORT ON FLEXURE FAILURE

The rotor-bearing system used in the simulator accurately represented the turbocompressor rotor-bearing system except for the materials from which certain of the parts were fabricated. Because of the long delivery time involved in obtaining the specific alloys selected for the turbocompressor design, several material substitutions were made for the simulator design. These substitutions were permissible since the simulator, unlike the turbocompressor, would be operated at low temperature conditions. One of the simulator components fabricated from materials other than the materials specified for use in the turbocompressor were the flexures used to support the turbine-end journal bearing. The simulator flexures were fabricated from AISI 4130 steel instead of Discalloy which was specified for the turbocompressor flexures.

During the vibration test with the simulator oriented vertically and running at 39,000 rpm, the test instrumentation indicated the presence of a resonance in one of the turbine-end flexure-supported bearing-pad assemblies. While investigating the nature of this resonance, which occurred at a shake table frequency of 1365 Hz and an input acceleration level of 7 g's, the journal bearing flexure failed.

The failure was detected from the instrumentation signals which describe the position of the journal relative to the casing, and from the signals which describe the film thickness between each bearing pad and the journal. At the instant of the failure, the signals indicated a sudden displacement of the journal and several brief contacts between the pads and journal. The simulator was shut down without difficulty. The broken flexure was located and removed during a partial disassembly of the simulator. Visual inspection of the journal and bearing pads did not reveal any damage to parts other than

to the flexure; therefore, the simulator was reassembled with a new flexure and the test program continued. No further failures of the flexures have been experienced during vibration testing.

The purpose of this appendix is to present a failure analysis of the AISI 4130 steel flexure.

Discussion

The fractured flexure is shown in Figure 87a (side view) and Figure 87b (top view). It is readily apparent that the failure occurred at the radius between the beam and shoulder sections of the flexure. This particular section of the component is in effect a notch and, as would be expected, is susceptible to resultant stress magnification effects. The relevant metallurgical data is given in Table III.

In Figure 88a, the macro-appearance of the fractured surface is given. There is a notable absence of fibrosity or shear lip indicating a brittle type of failure. Figure 88b is a transverse view of the cracked area in the "as polished" condition at 100-power magnification. It is important to note the rather heavy oxide layer present in the crack itself. This indicates that considerable oxidation occurred before the catastrophic failure.

Two different areas of the fractured surface are depicted in the electron micrographs presented in Figures 89a and 89b, respectively. In both figures, the predominance of flat surfaces can be observed; the absence of clear-cut dimpling is also apparent. This further substantiates the brittle nature of the fracture.

The grain size associated with the temperature of the flexure at the time of quenching (prior austenitic grain size) and the microstructure are shown in the optical microphotographs of the failed area shown in Figures 90a and 90b. The grain size shown in Figure 90a is extremely fine and is a reflection of a low austenitizing temperature. This is a highly desirable grain structure,

Table III

RELEVANT METALLURGICAL DATA

CHEMISTRY

C	Mn	Si	Cr	Mo
.32	.55	.29	.86	.19

HARDNESS

Rc 29-32

CLEANLINESS

Satisfactory. Primary inclusions are manganese sulfides and lesser amounts of silicates.

GRAIN SIZE

Extremely fine, smaller than ASTM-9

MICROSTRUCTURE

Duplex - Predominately tempered lower bainite and tempered martensite.

FRACTURE APPEARANCE

Brittle

particularly from toughness considerations. However, the microstructure shown in Figure 90b is duplex in nature, consisting of a mixture of bainite, martensite, and carbide. The presence of these microstructural aggregates is a manifestation of the shallow hardenability characteristics of AISI 4130 steel. Duplex microstructures invariably exhibit lower toughness and greater notch sensitivity than either lower bainite or tempered martensite. The physical properties of toughness and notch ductility at a given strength level collectively play an important role in determining the fatigue behavior of a given material. The microstructure which develops the optimum level of these physical properties must be developed, if possible, during heat treatment.

Metallurgical Observations

1. The metallurgical cleanliness of the AISI 4130 material is satisfactory and representative of good melting and deoxidation practice.

2. The grain size is acceptable.

3. The microstructure is duplex in nature consisting of bainite, martensite, and carbide. This is a highly undesirable microstructure due primarily to its low toughness, its higher transition temperature, and its notch sensitivity.

4. The failure was brittle in nature with very little evidence of plastic deformation present.

5. Considerable oxidation occurred in the crack area before failure.

Conclusions

During the quenching of low alloy steels from their austenitizing temperature, differences in thermal contraction and expansion occur as a result of the austenite transformation. These conditions result in large macroscopic

(measureable) stresses which must be relieved by plastic yielding. Upon occasion, these macroscopic stresses exceed the fracture stress of the material, particularly when stress raisers are present, such as the fillet radius at the ends of the beam section of the flexure. Where relatively large transitions in material volume occur in a given part, the susceptibility to quench cracking is greatly increased.

The most probable cause of the flexure failure was the propagation of a crack at the abrupt change in section between the flexure beam section and end shoulder. Initial formation of the crack is believed to have occurred during fabrication of the flexure; specifically, during the heat-treat quenching operation.

MATHEMATICAL SYMBOLS

A = Arbitrary constant used to obtain curve fit; acceleration amplitude, g's.

B = Coefficient of viscous damping of thrust-bearing gas film, a nonlinear function of arguments indicated in suffixed parentheses, lb-sec/in; arbitrary constant used to obtain curve fit.

C = Arbitrary constant used to obtain curve fit; acceleration amplitude, g's.

c = Coefficient of linear viscous damping, lb-sec/in.

D = Arbitrary constant used to obtain curve fit; acceleration amplitude, g's.

e = Base of natural logarithms.

F_a = Net aerodynamic force acting on rotor, lb.

G = Net force exerted by thrust-bearing gas film, a nonlinear function of arguments usually indicated in suffixed parentheses, lb.

g = Local gravitational acceleration, in/sec^2.

h = Thrust-bearing gas-film thickness, in.

K = Journal-bearing gas-film stiffness, lb/in.

k = Linear spring stiffness, lb/in.

m = Mass, $lb\text{-}sec^2/in$.

T = Time parameter associated with shock pulse, sec.

t = Time, sec.

v = Velocity, in/sec.

W = Static component of thrust-bearing gas-film force, a nonlinear function of arguments usually listed in suffixed parentheses, lb.

x = Displacement with respect to inertial reference frame, in.

y = Displacement relative to position of static equilibrium, in.

Subscripts

1, 2, 3 = first, second, or third mass elements respectively.

b = Base

Superscript Conventions

- = Condition at static equilibrium

$\dot{} = \frac{d}{dt}$

$\ddot{} = \frac{d^2}{dt^2}$

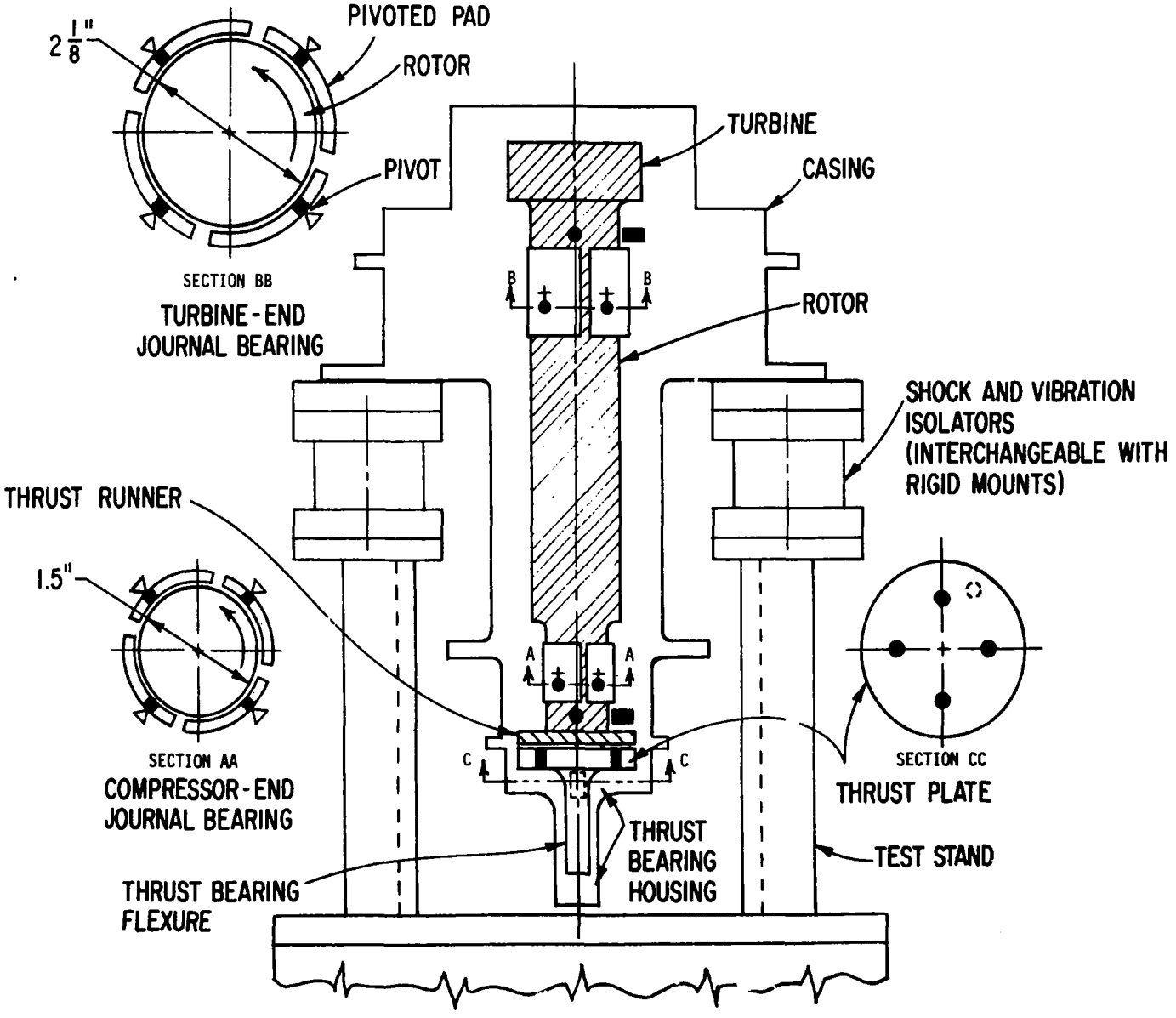

Fig. 1 Schematic of Turbocompressor Simulator Mounted On Test Stand (Vertical Orientation)

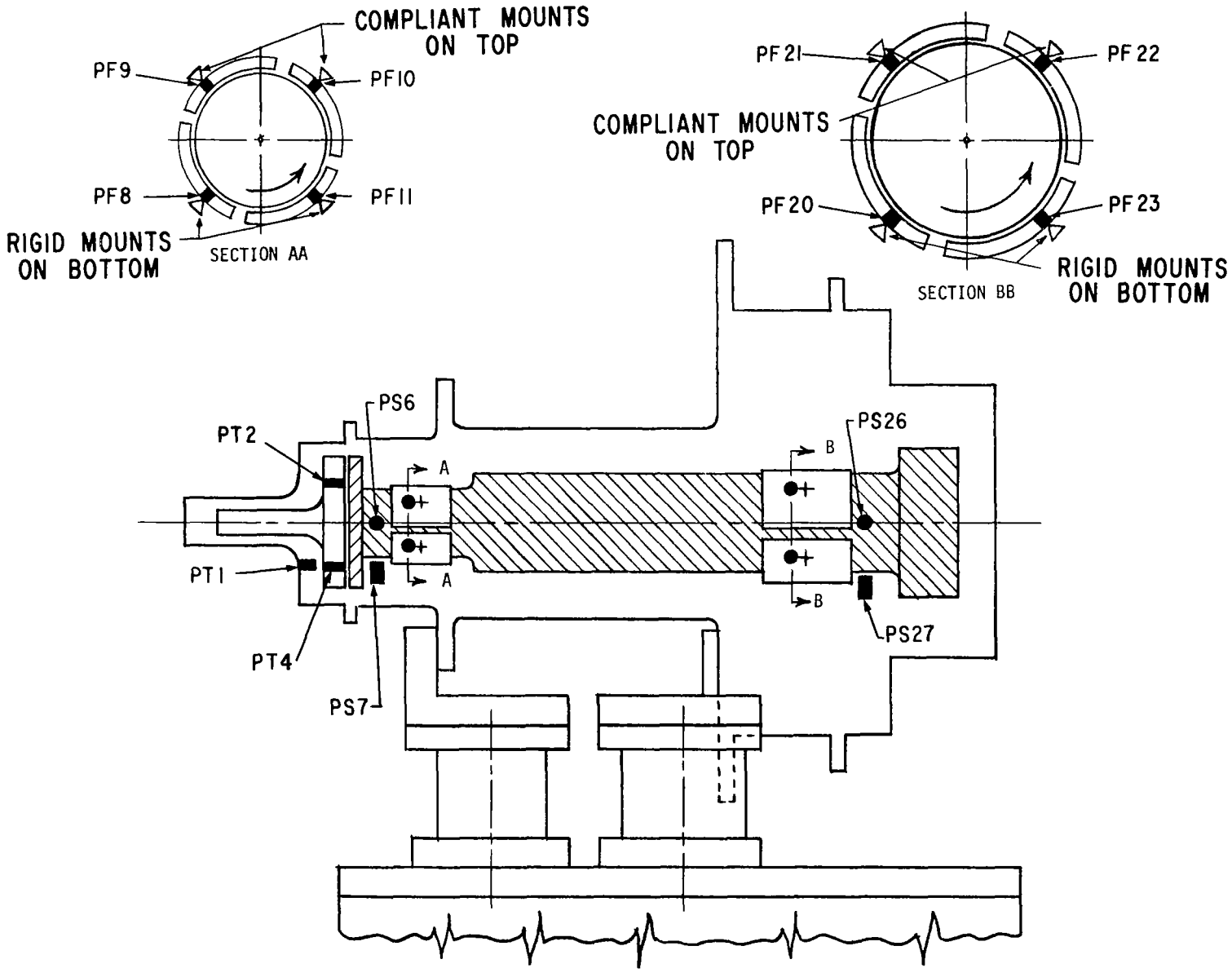

Figure 2 Schematic of Turbocompressor Simulator With Capacitance Probe Designation (Horizontal Orientation)

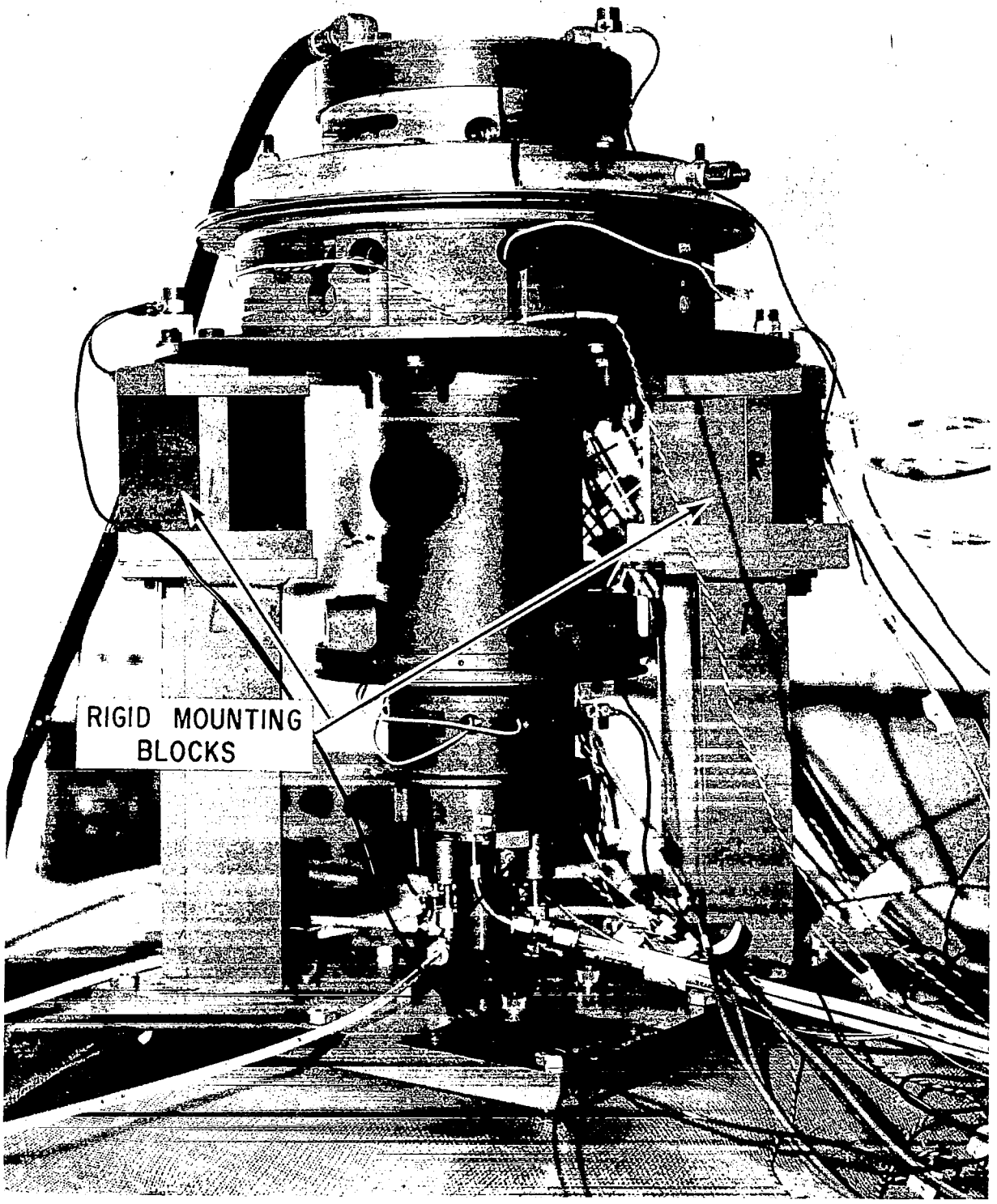

Fig. 3 Simulator Mounted Vertically on Vibration Table

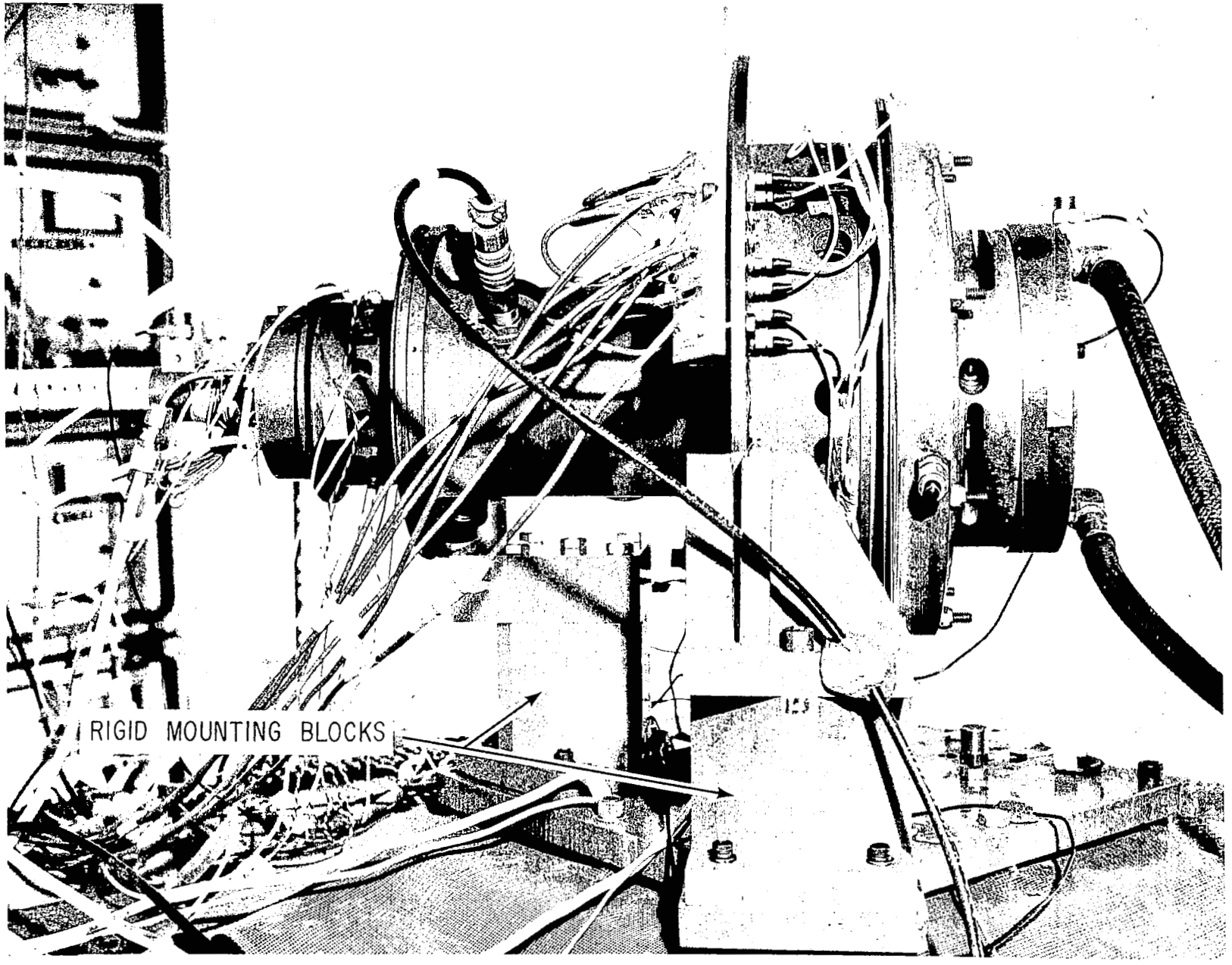

Fig. 4 Simulator Mounted Horizontally on Vibration Table

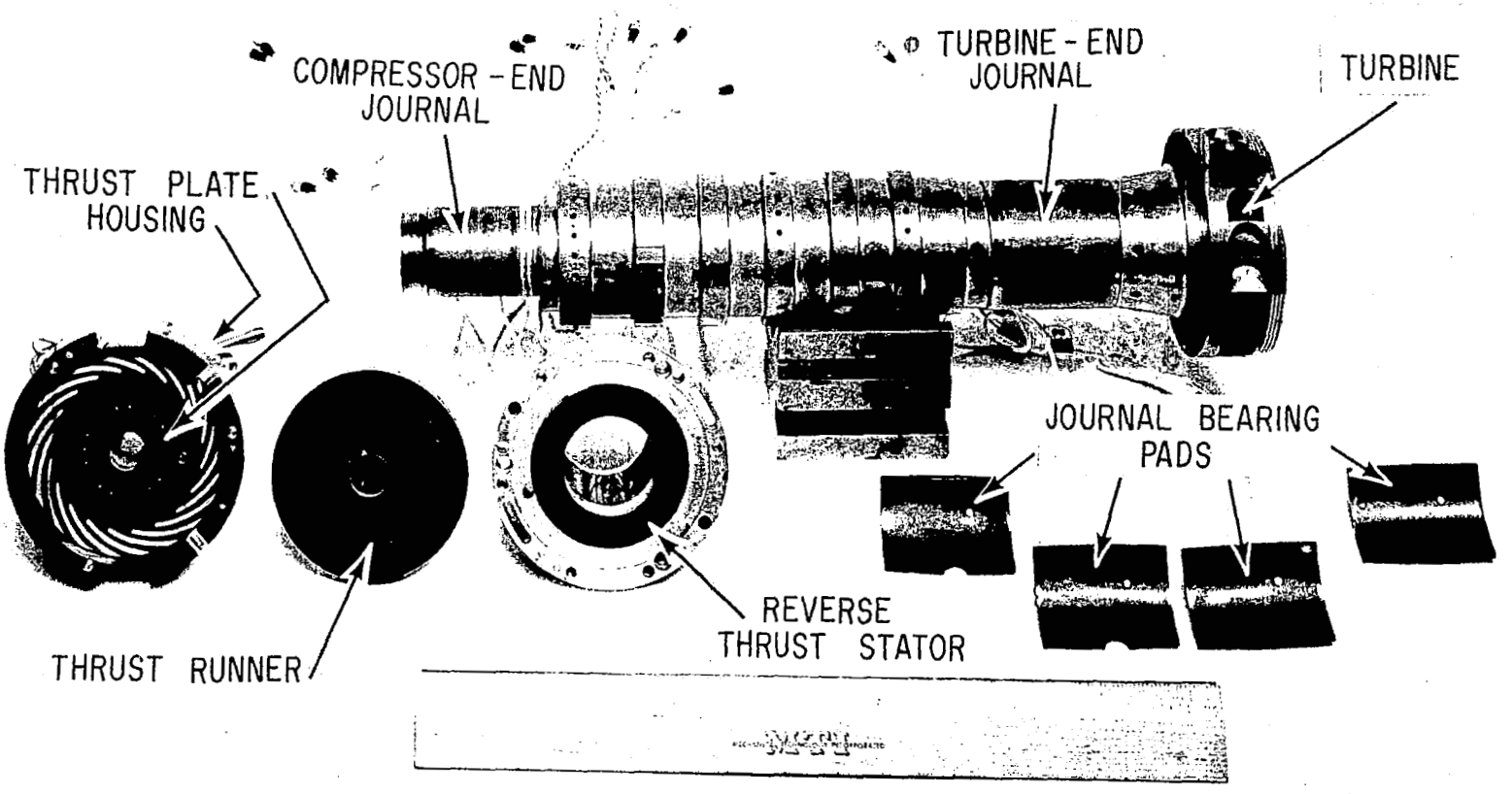

Fig. 5 Main Components of Rotor-Bearing Assembly

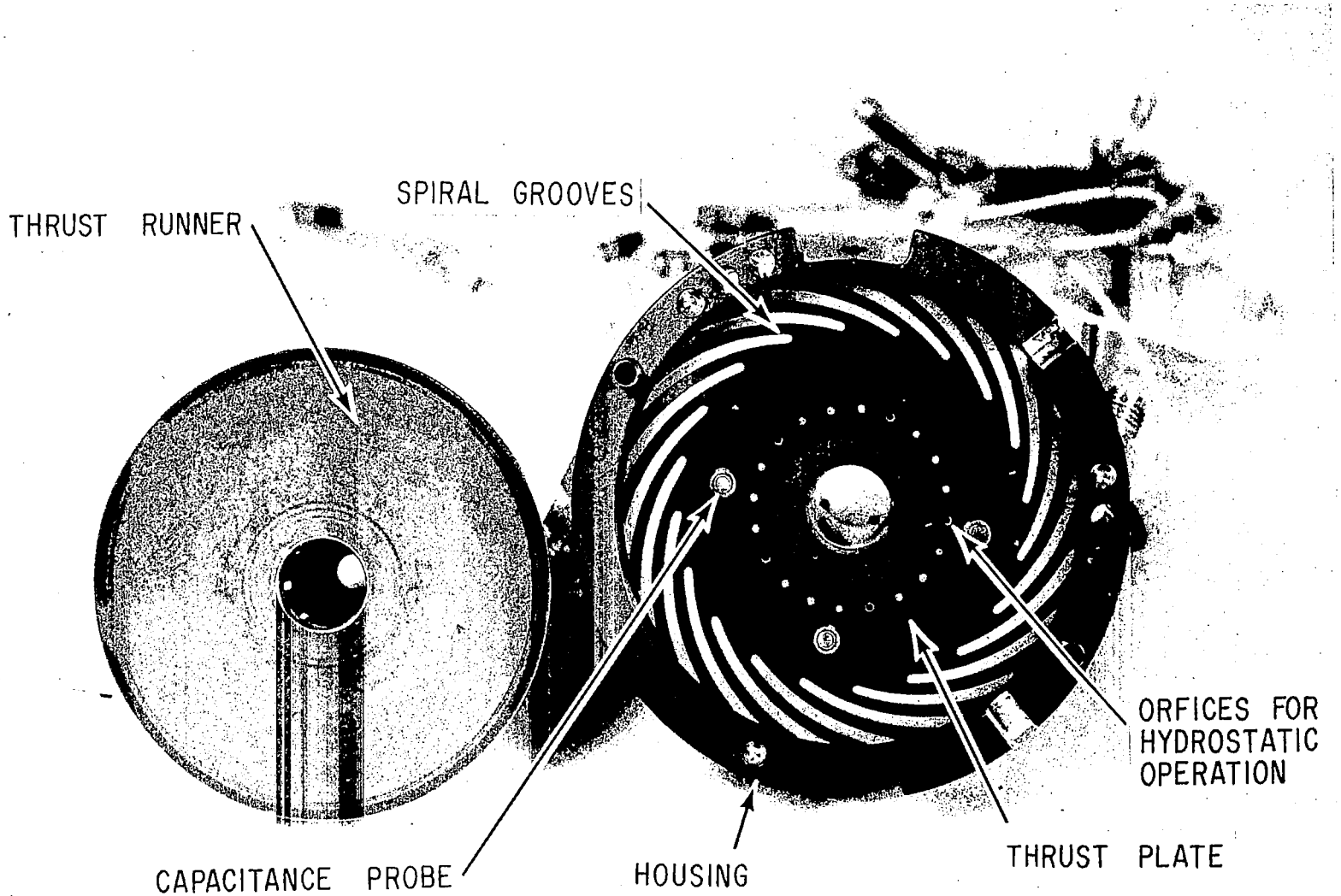

Fig. 6 Photograph of the Simulator Forward (Primary) Thrust Bearing

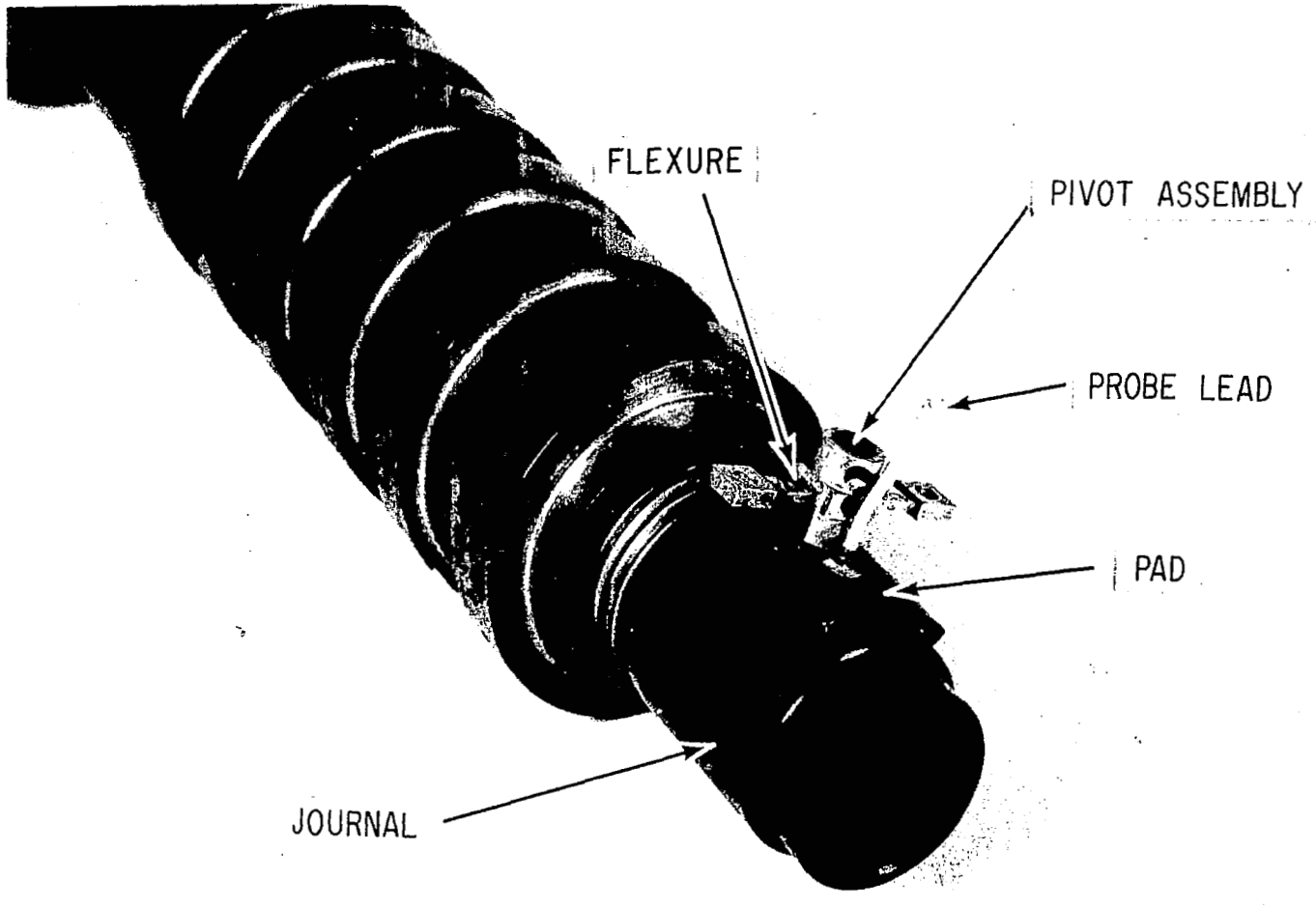

Fig. 7 Arrangement of Journal Bearing Pad

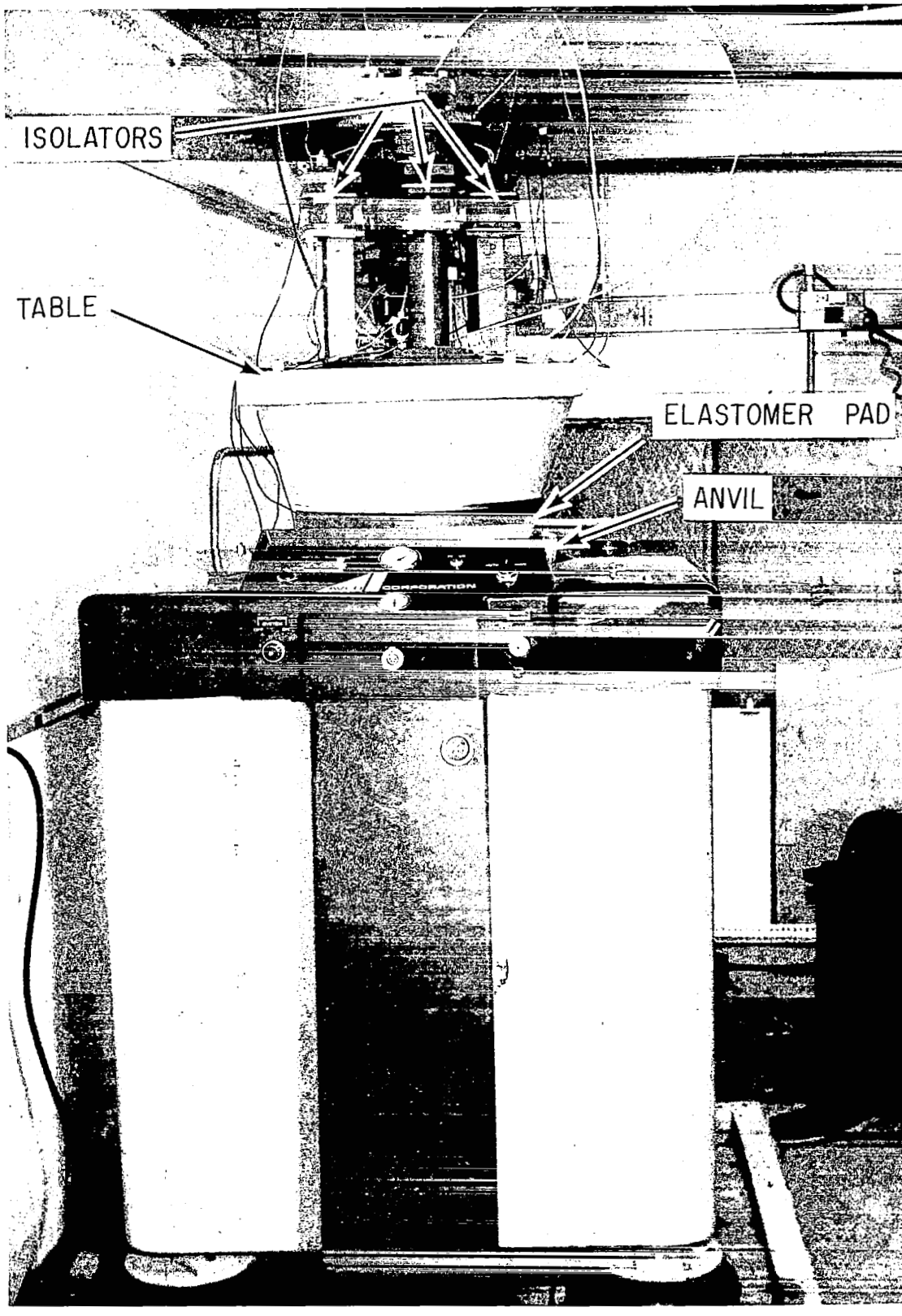

Fig. 8 Shock Machine With Simulator Mounted Vertically On Shock and Vibration Isolators

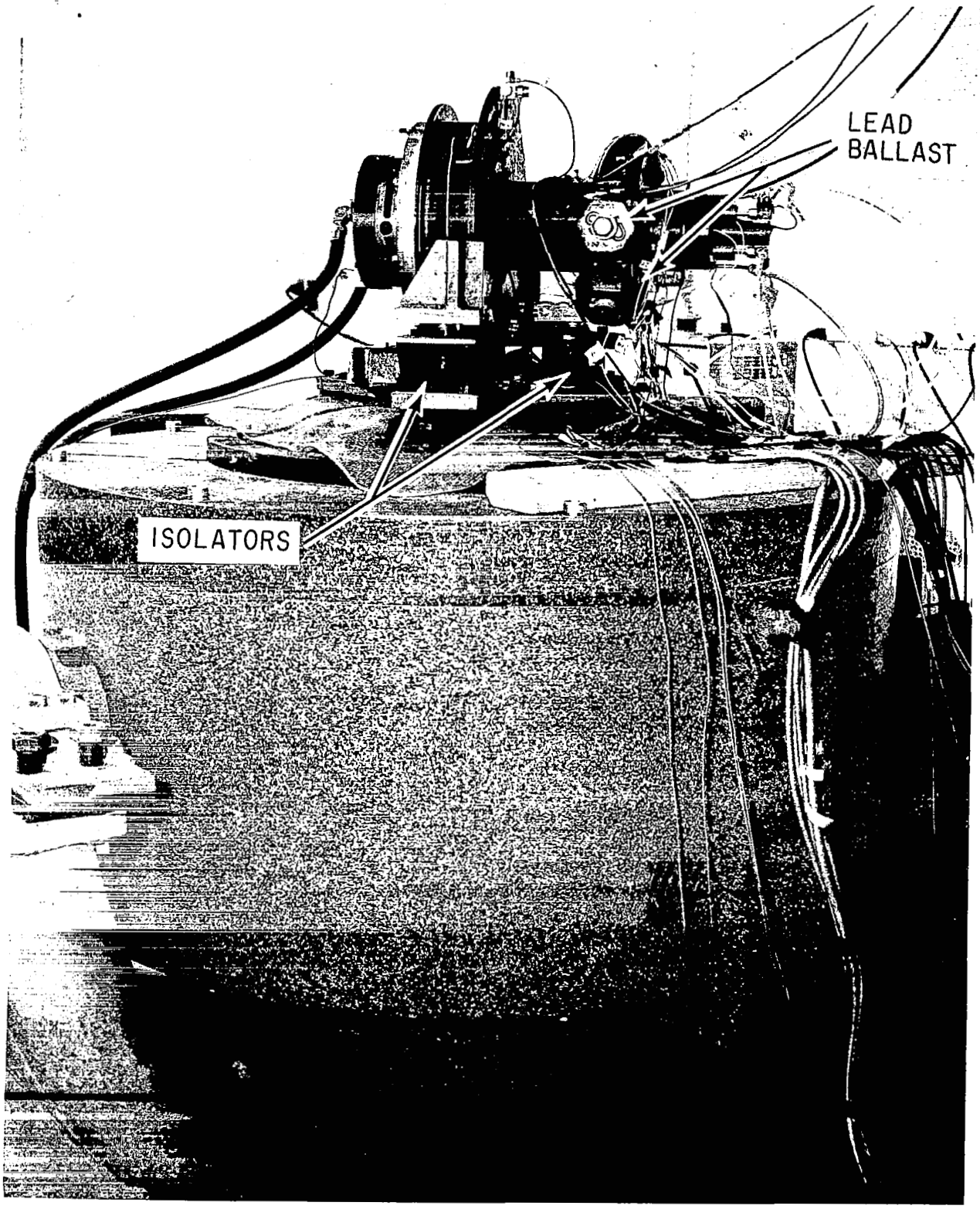

Fig. 9 Vibration Table With Simulator Mounted Horizontally On Shock and Vibration Isolation Isolators

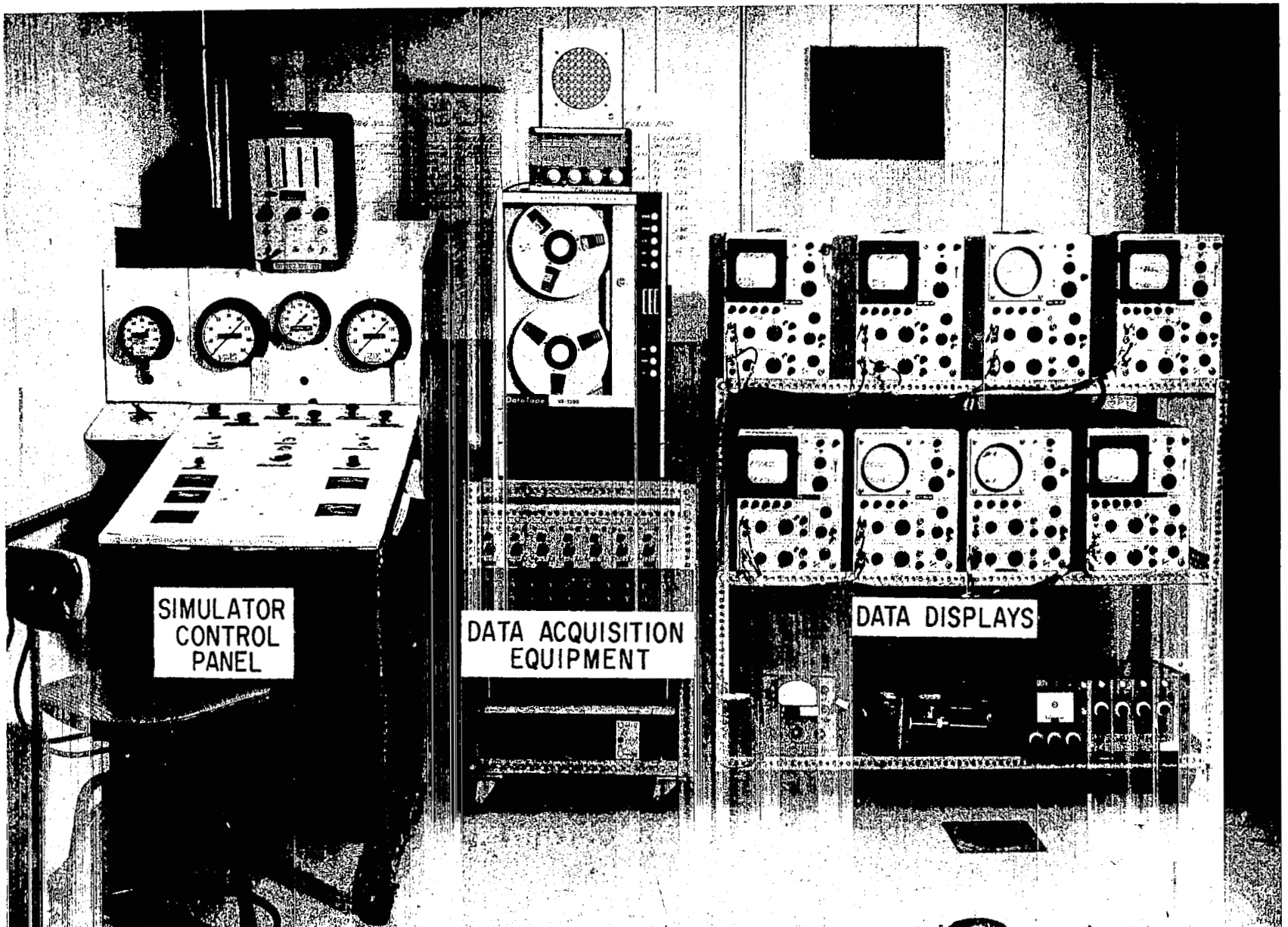

Fig. 10 Arrangement of Simulator Controls, Data Acquisition Equipment and Visual Displays

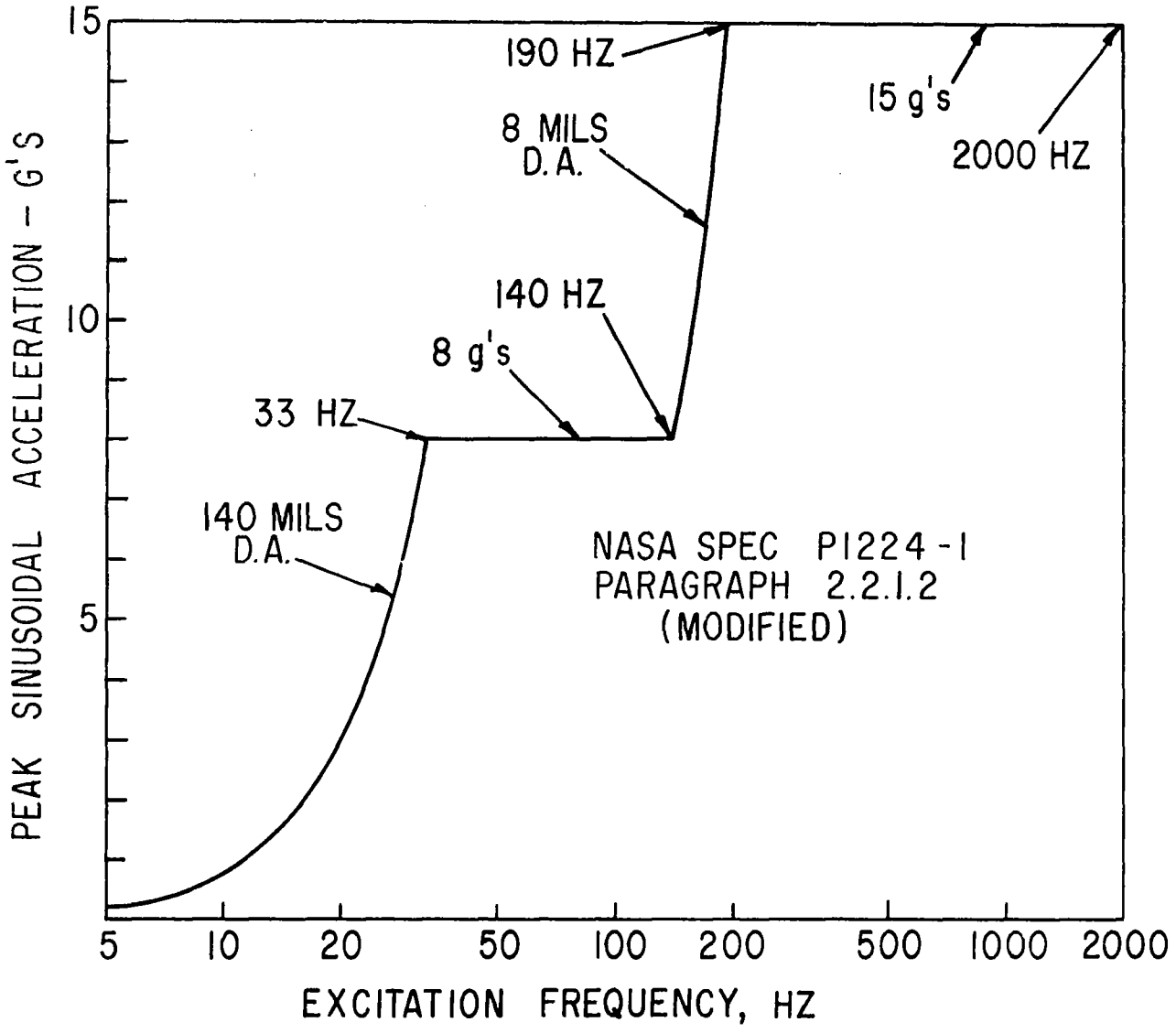

Fig. 11 Maximum Vibration Test Objectives

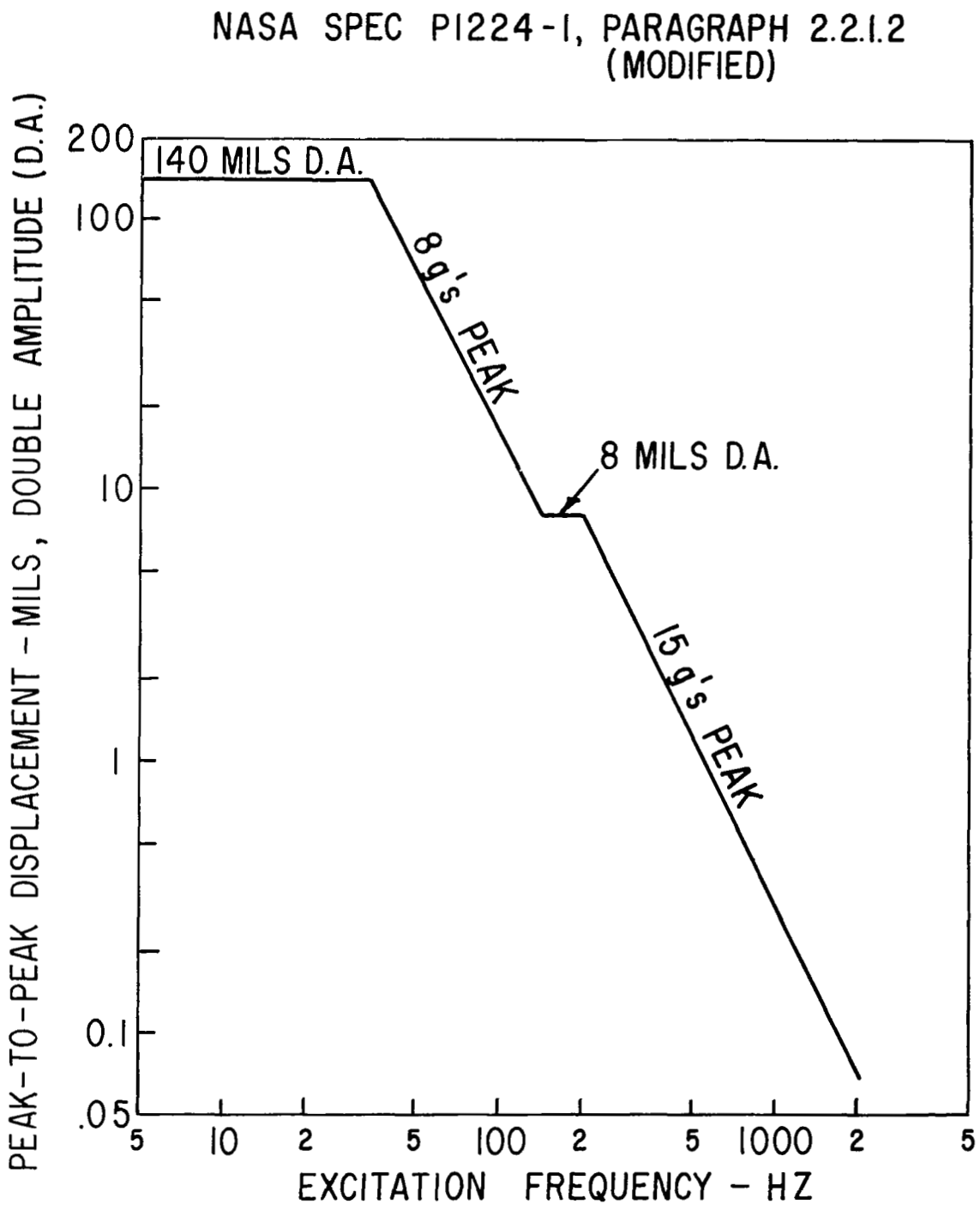

Fig. 12 Alternate Presentation of Maximum Vibration Test Objectives

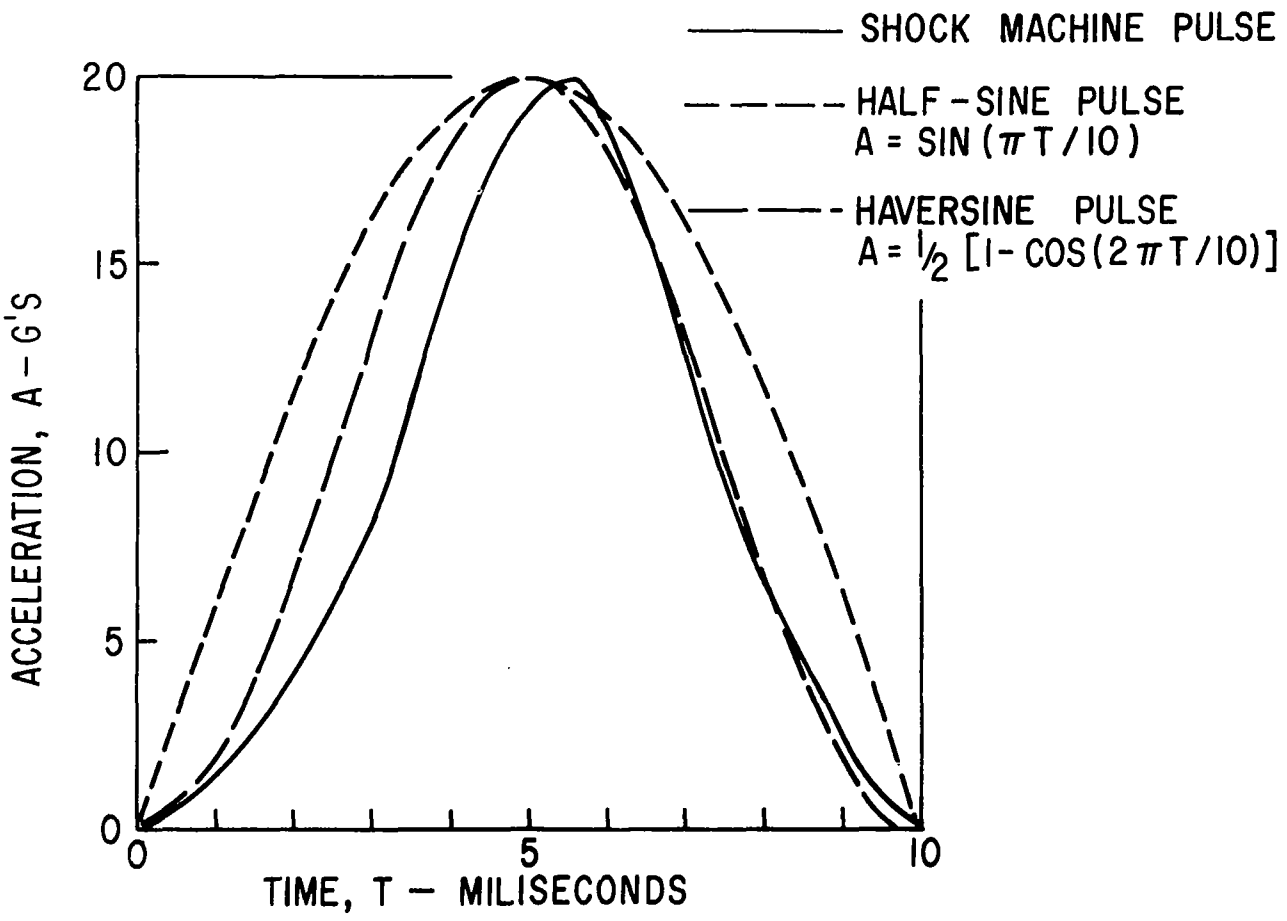

Fig. 13 Comparison Between Actual Shock Pulse and Two Idealized Shock Pulses

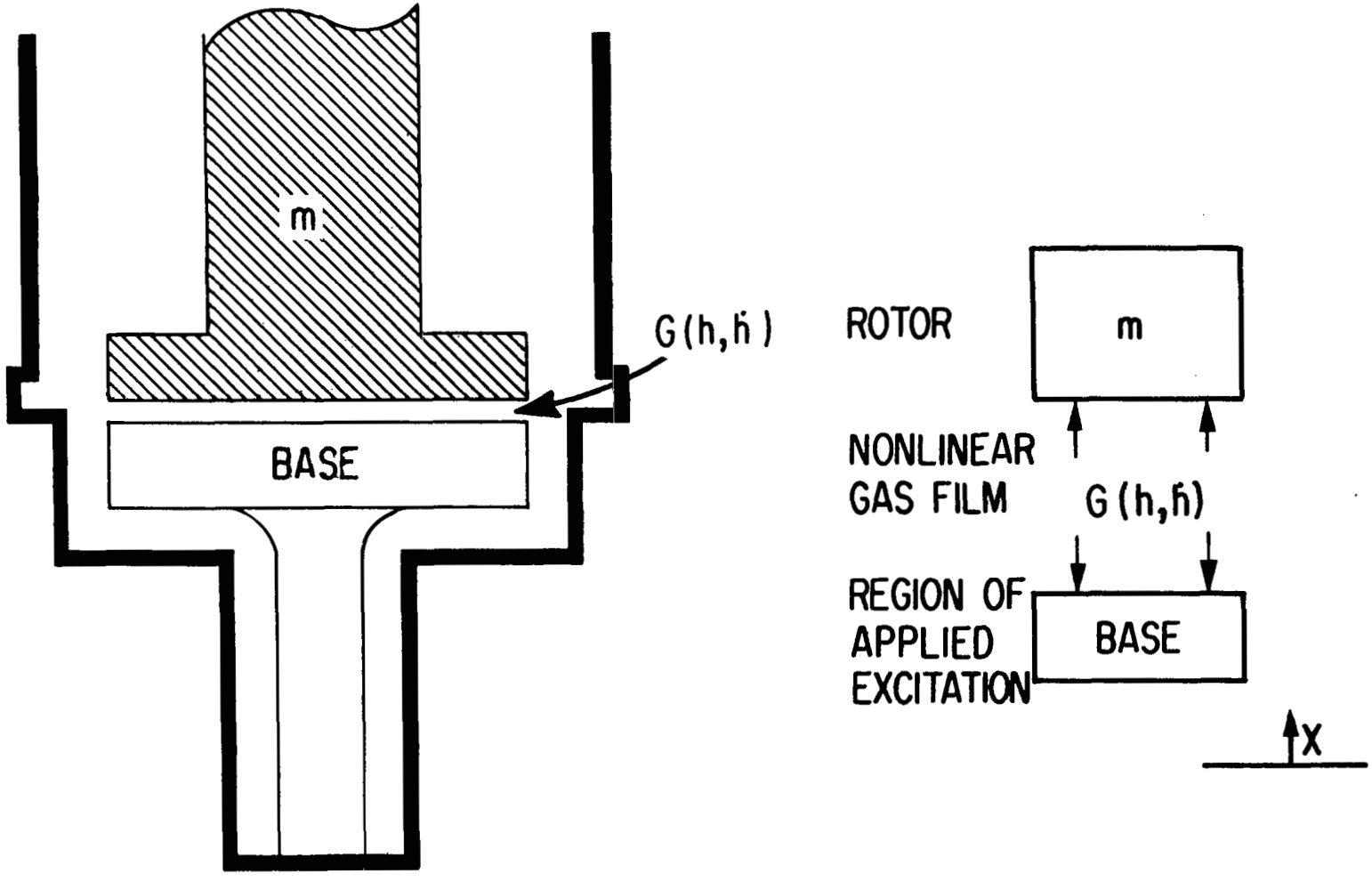

Fig. 14 Single-Degree-of-Freedom Representation of Simulator Axial Response Mode

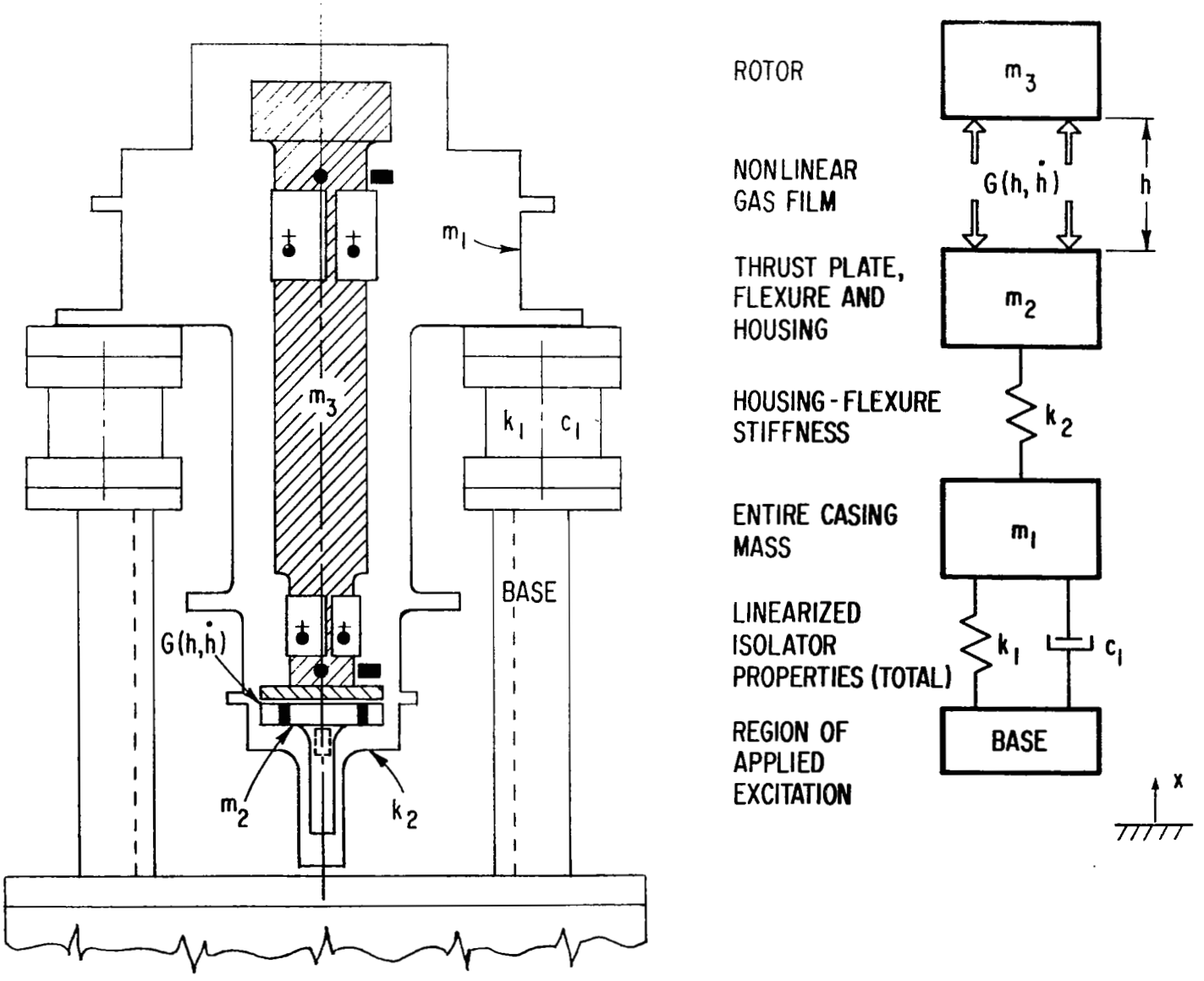

Fig. 15 Three-Degree-of-Freedom Axial Response Model of Simulator on Shock and Vibration Isolators

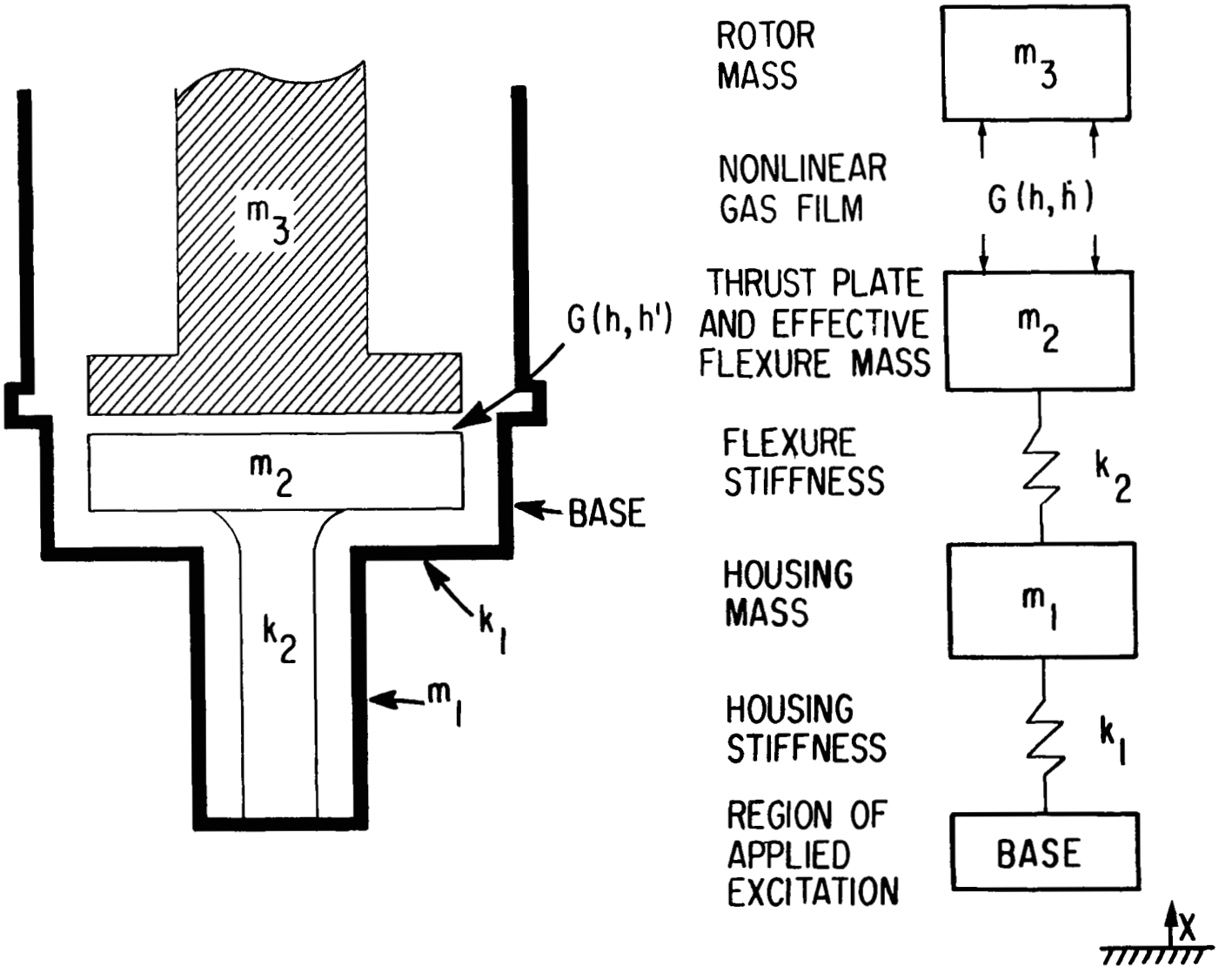

Fig. 16 Three-Degree-of-Freedom Axial Response Model of Simulator on Rigid Mounts

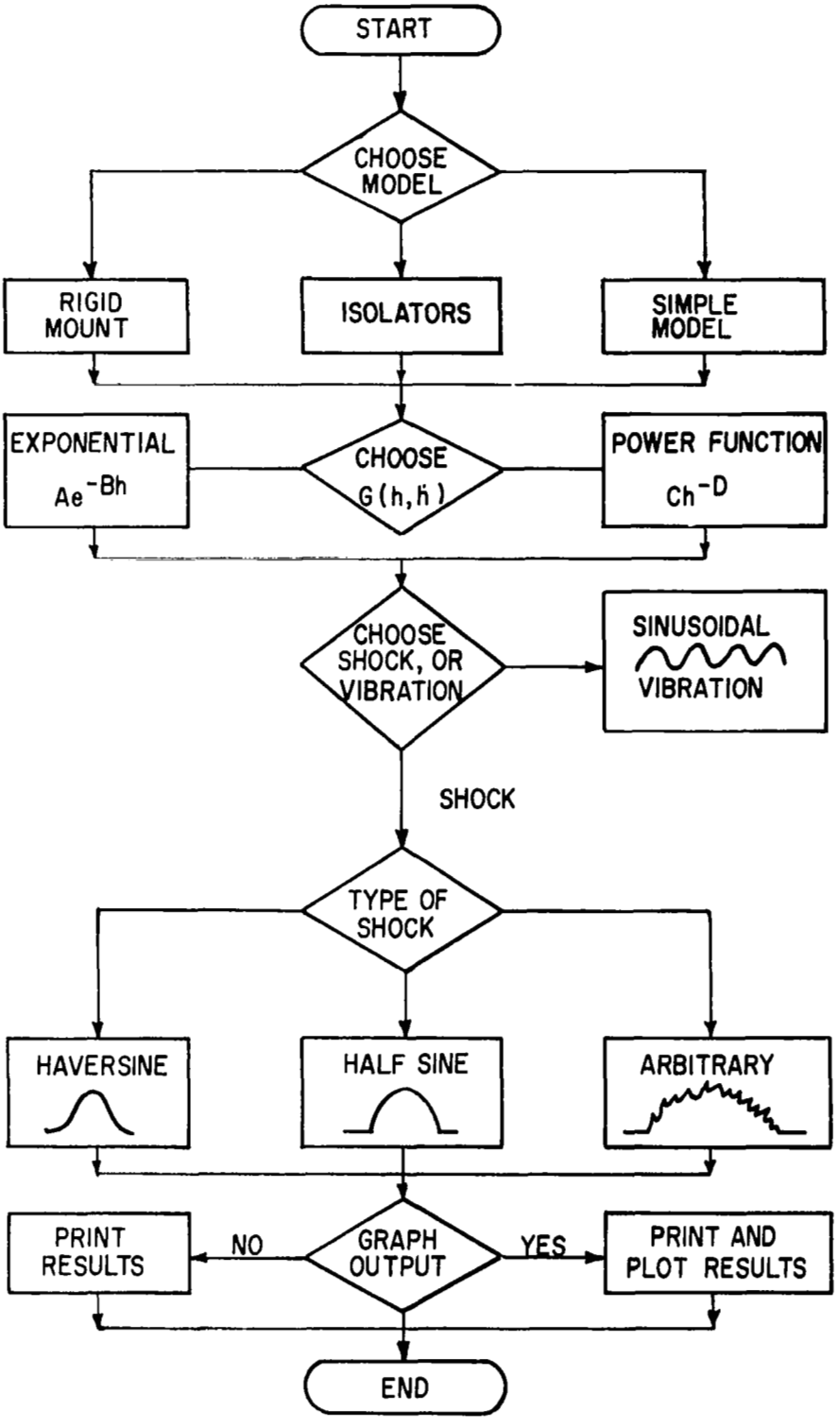

Fig. 17 General Flowchart of Axial Shock and Vibration Response Computer Program

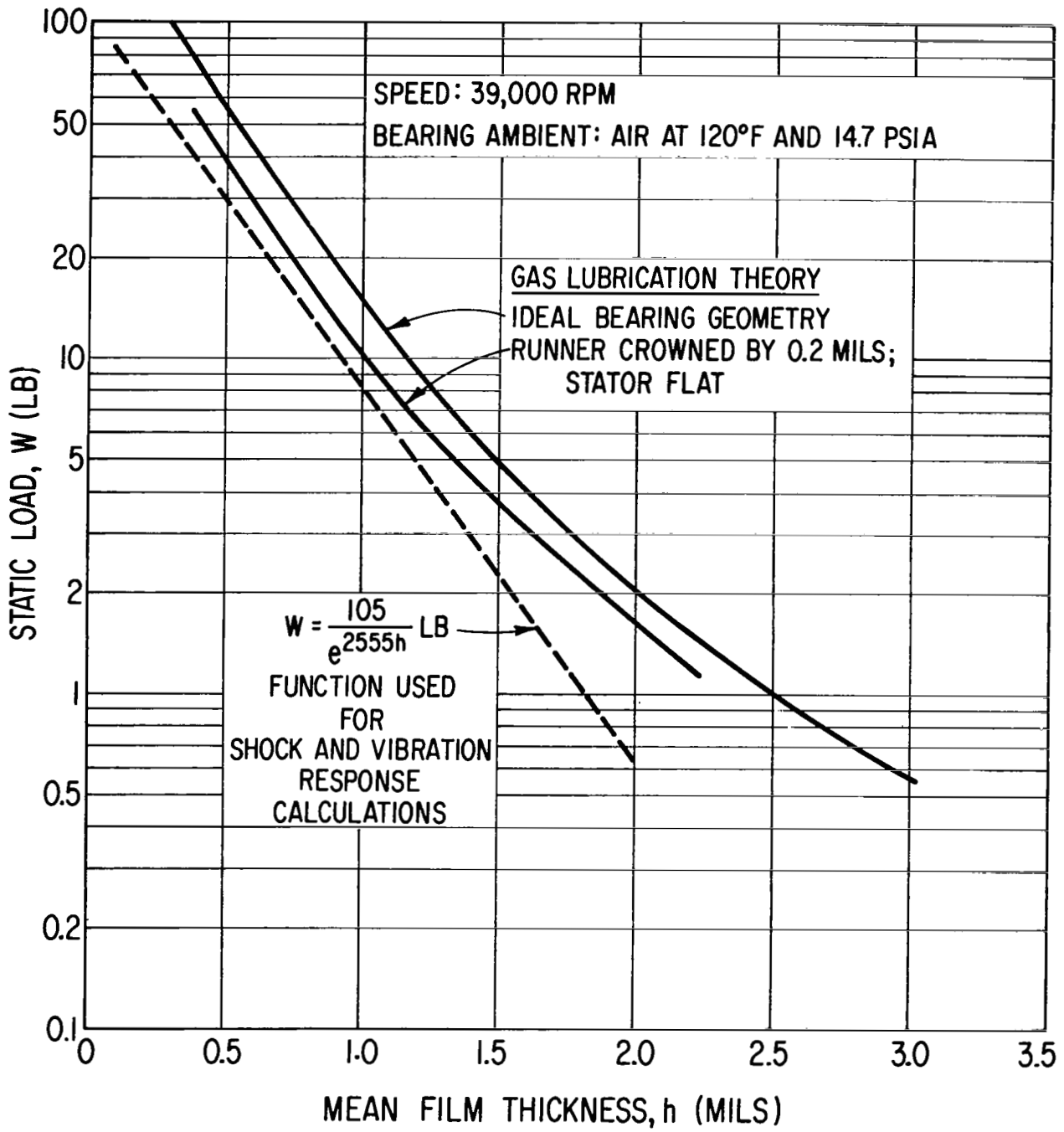

Fig. 18 Static Load Characteristics of Thrust Bearing

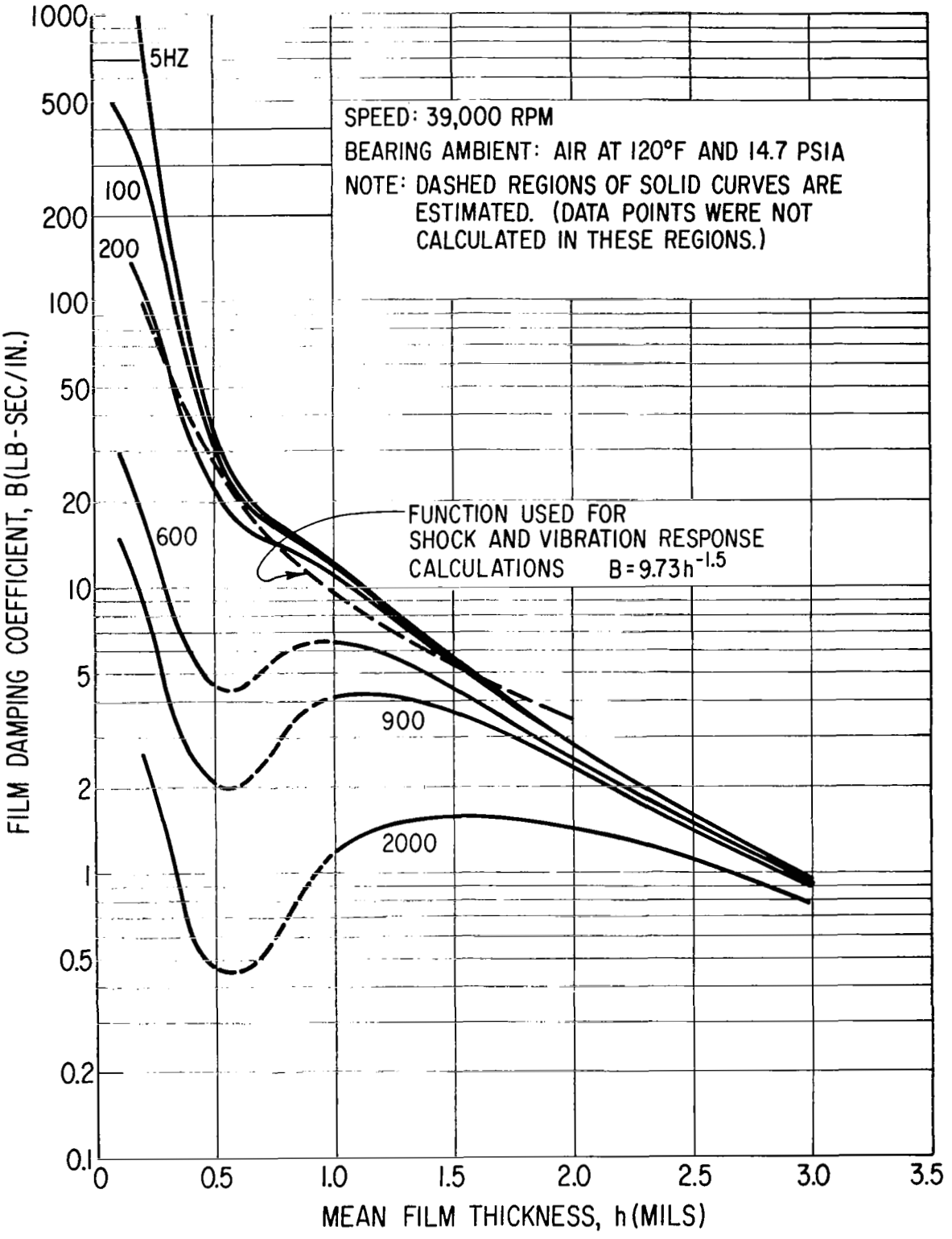

Fig. 19 Damping Coefficient Characteristics of Thrust Bearing

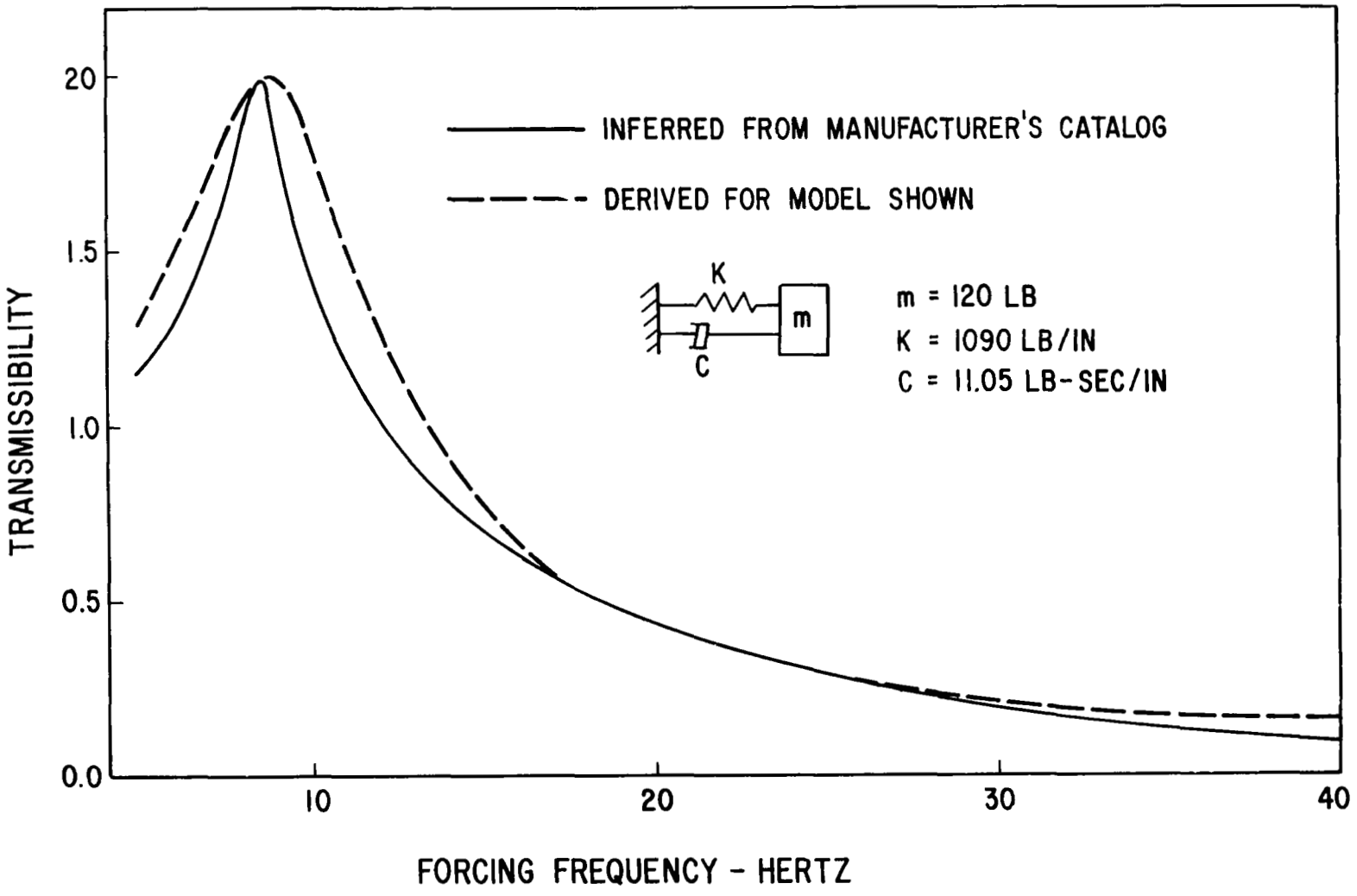

Fig. 20 Comparison Between Theoretical Transmissibility and Catalog Data for a Single Isolator

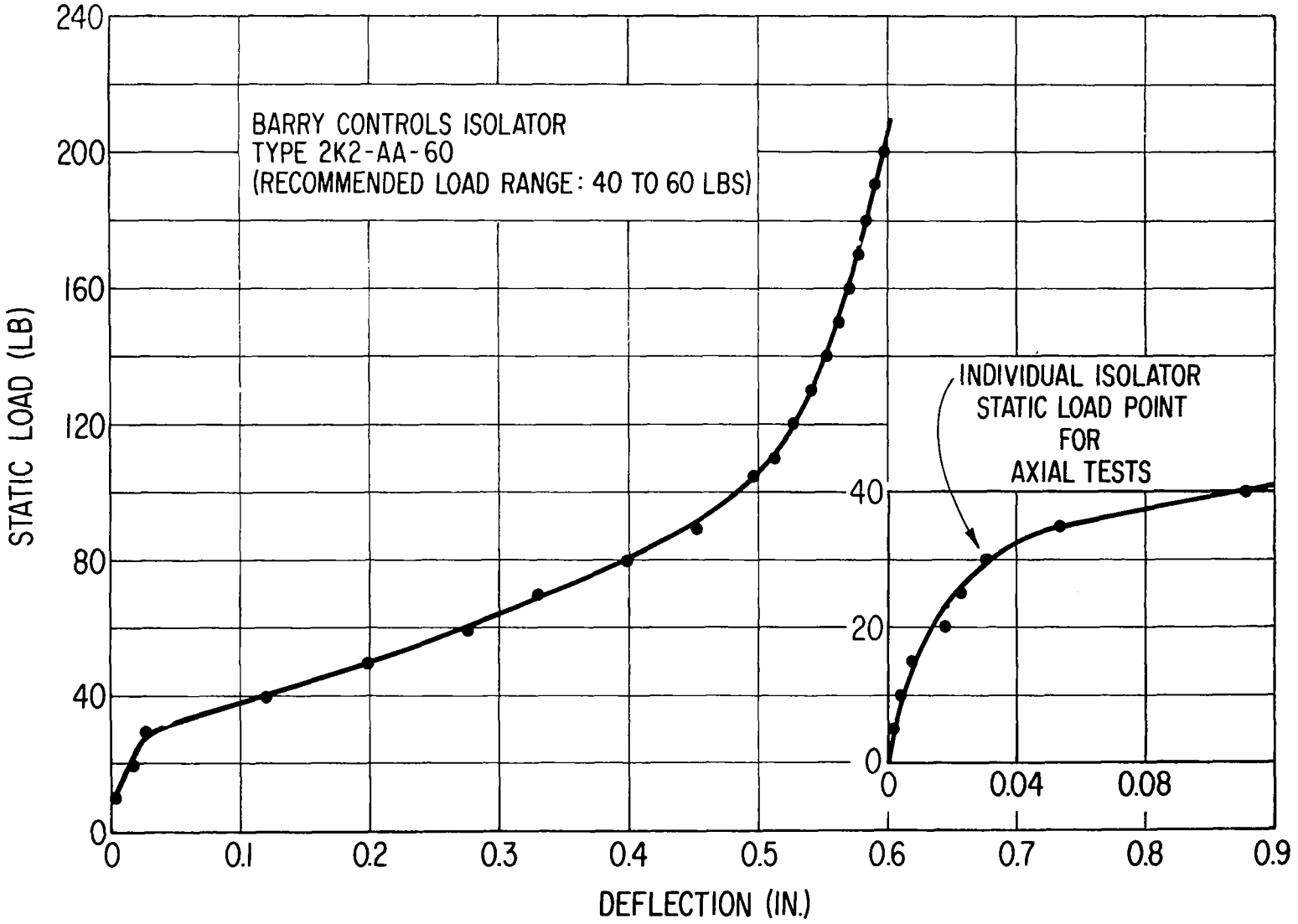

Fig. 21 Measured Static Load Characteristic of a Single Test Isolator

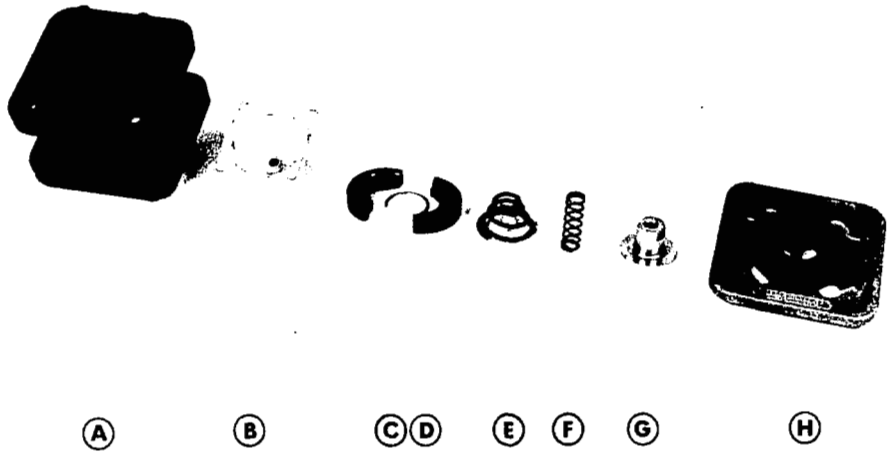

(a) ISOLATOR COMPONENTS

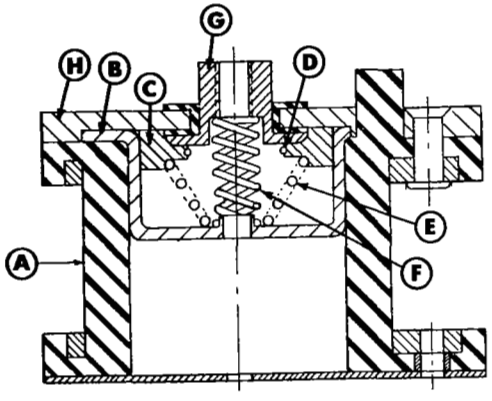

(b) CROSS SECTION

(c) ASSEMBLED ISOLATOR

Fig. 22 Construction of Shock and Vibration Isolator

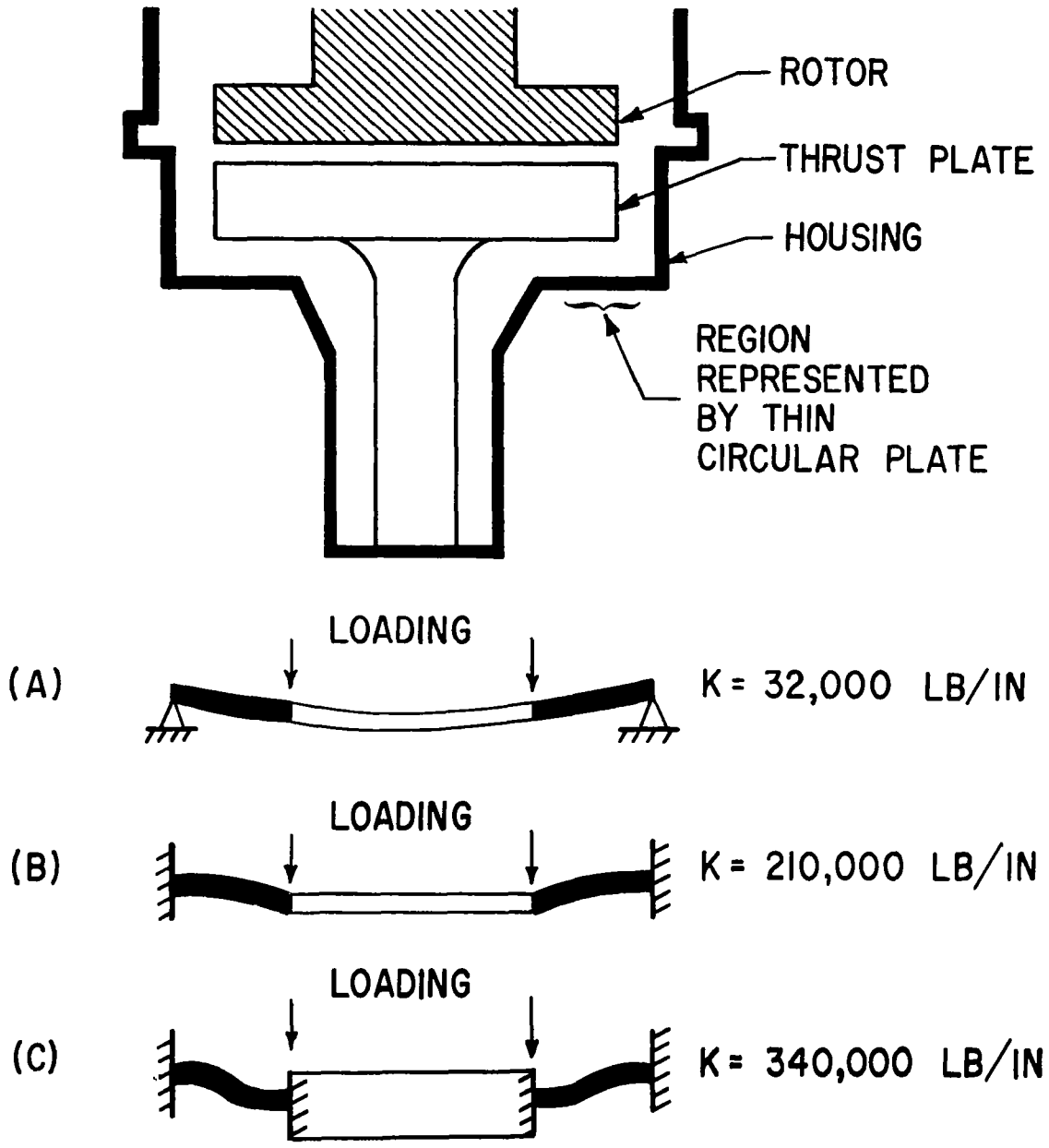

Fig. 23 Representations of Thrust-Plate Housing for Stiffness Calculations

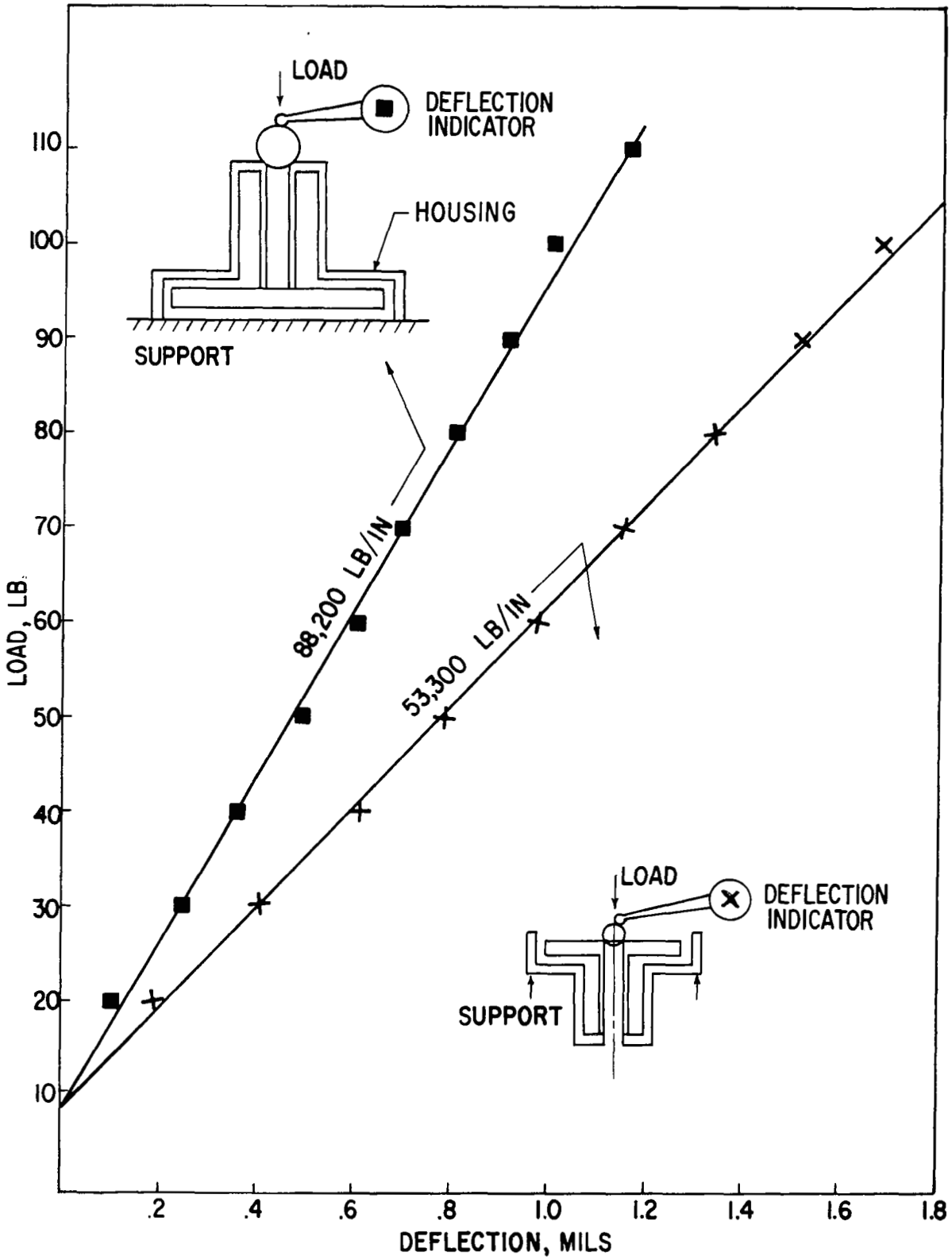

Fig. 24 Measured Stiffness of Thrust-Plate Housing

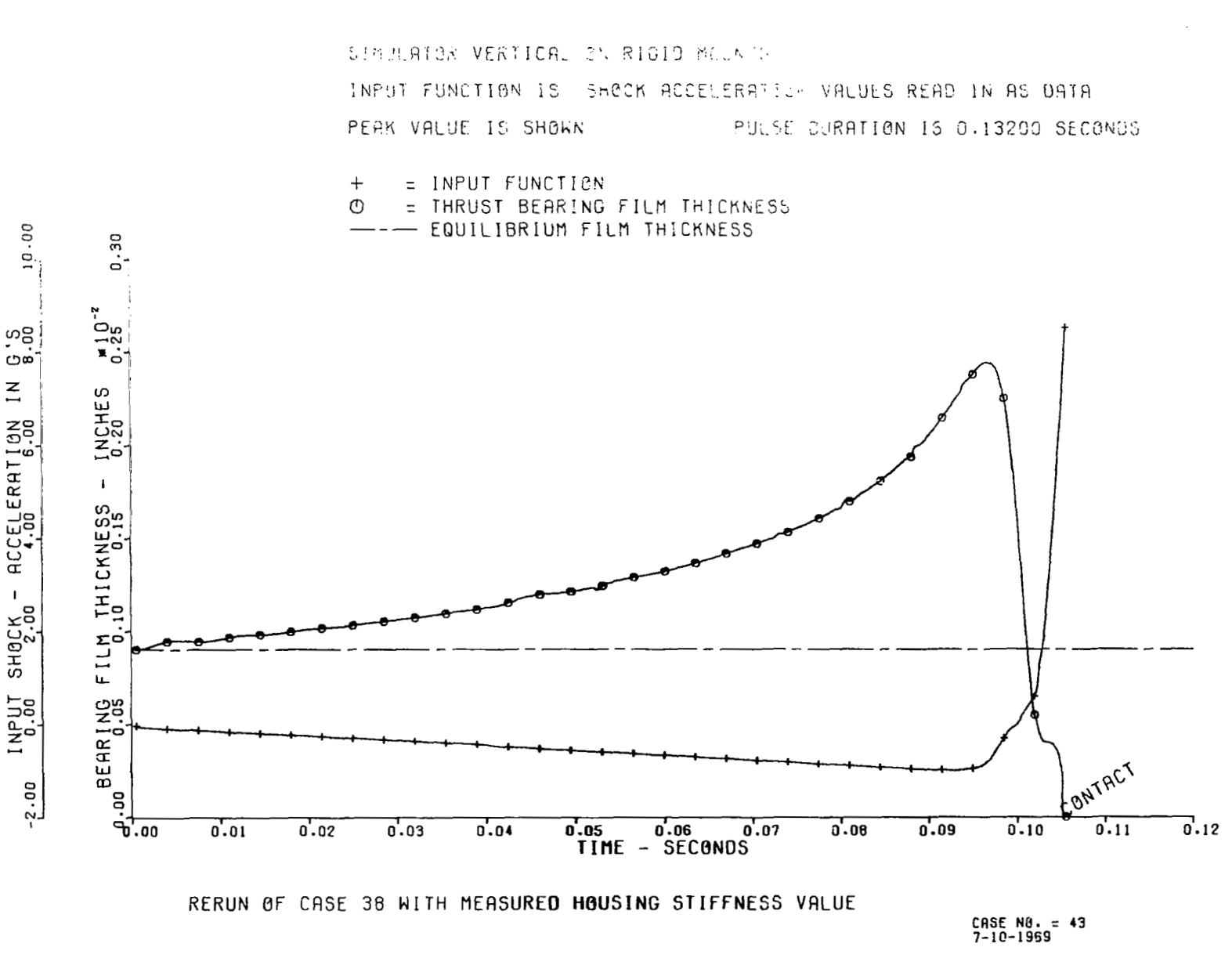

Fig. 25 Typical Computed Thrust Bearing Response to Axial Shock

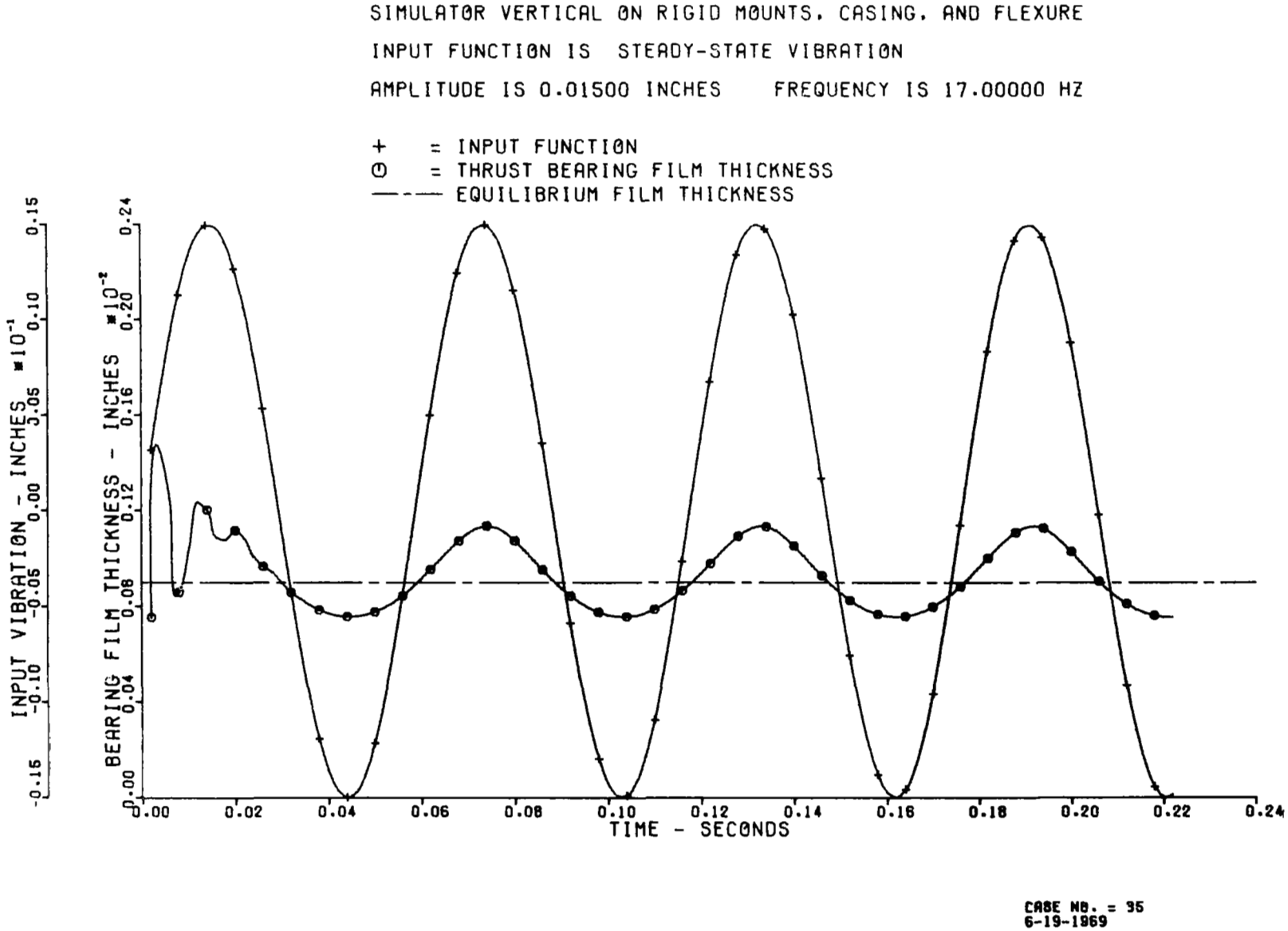

Fig. 26 Calculated Low-Frequency Axial Vibration Response

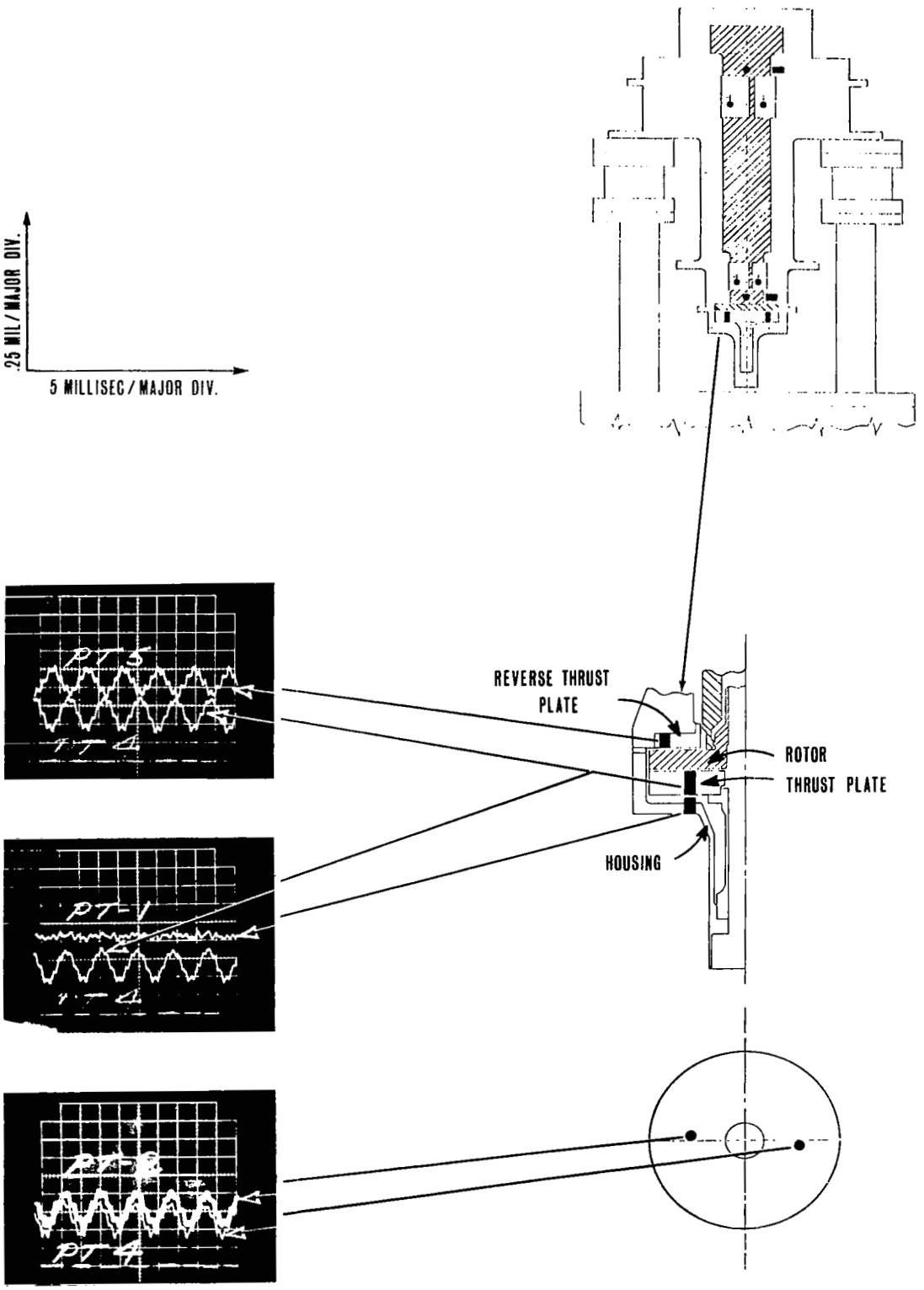

Fig. 27 Measured Modal Behavior at 110 Hz

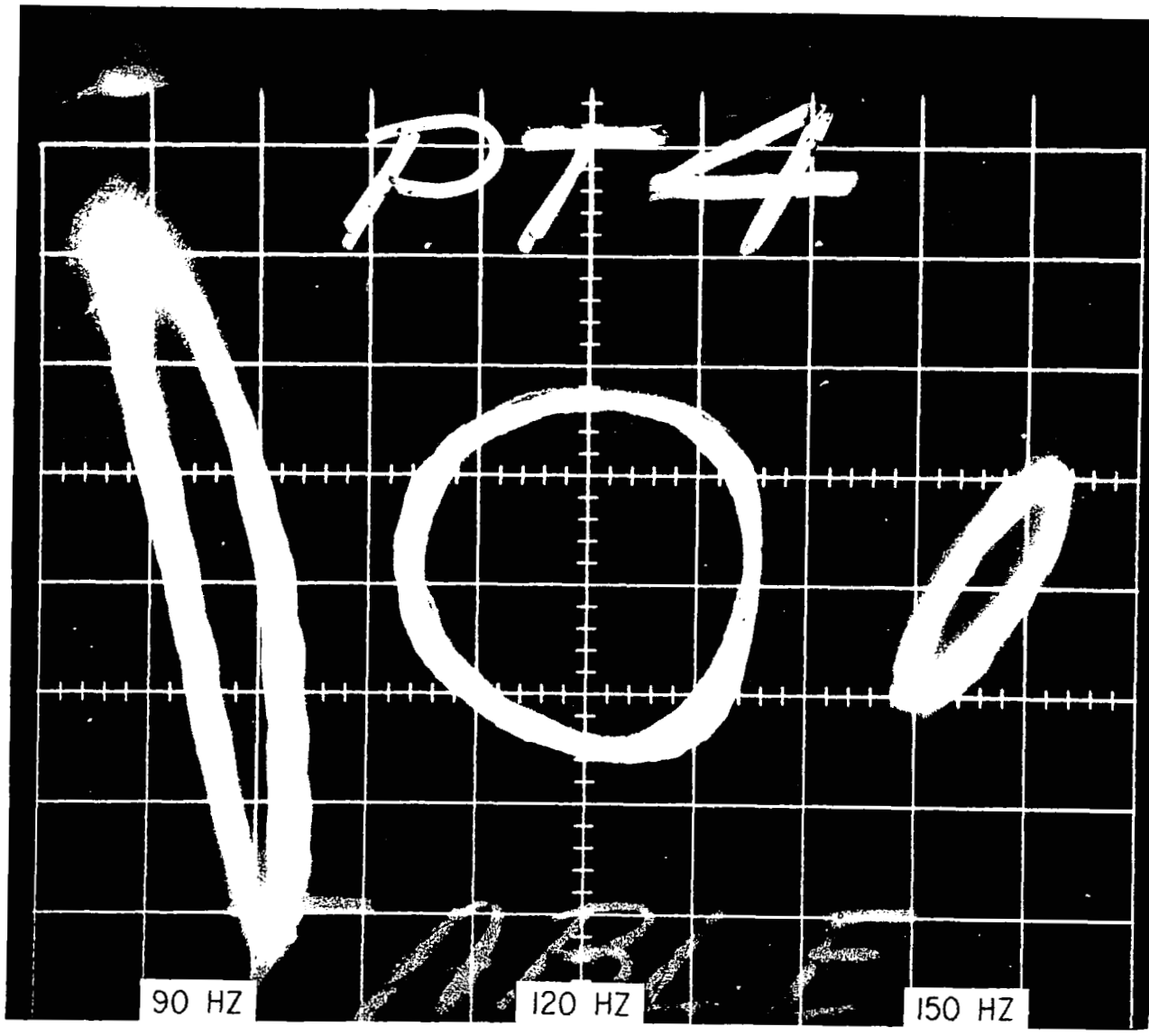

Fig. 28 Lissajous Patterns Indicating 90° Phase Shift at 120 Hz

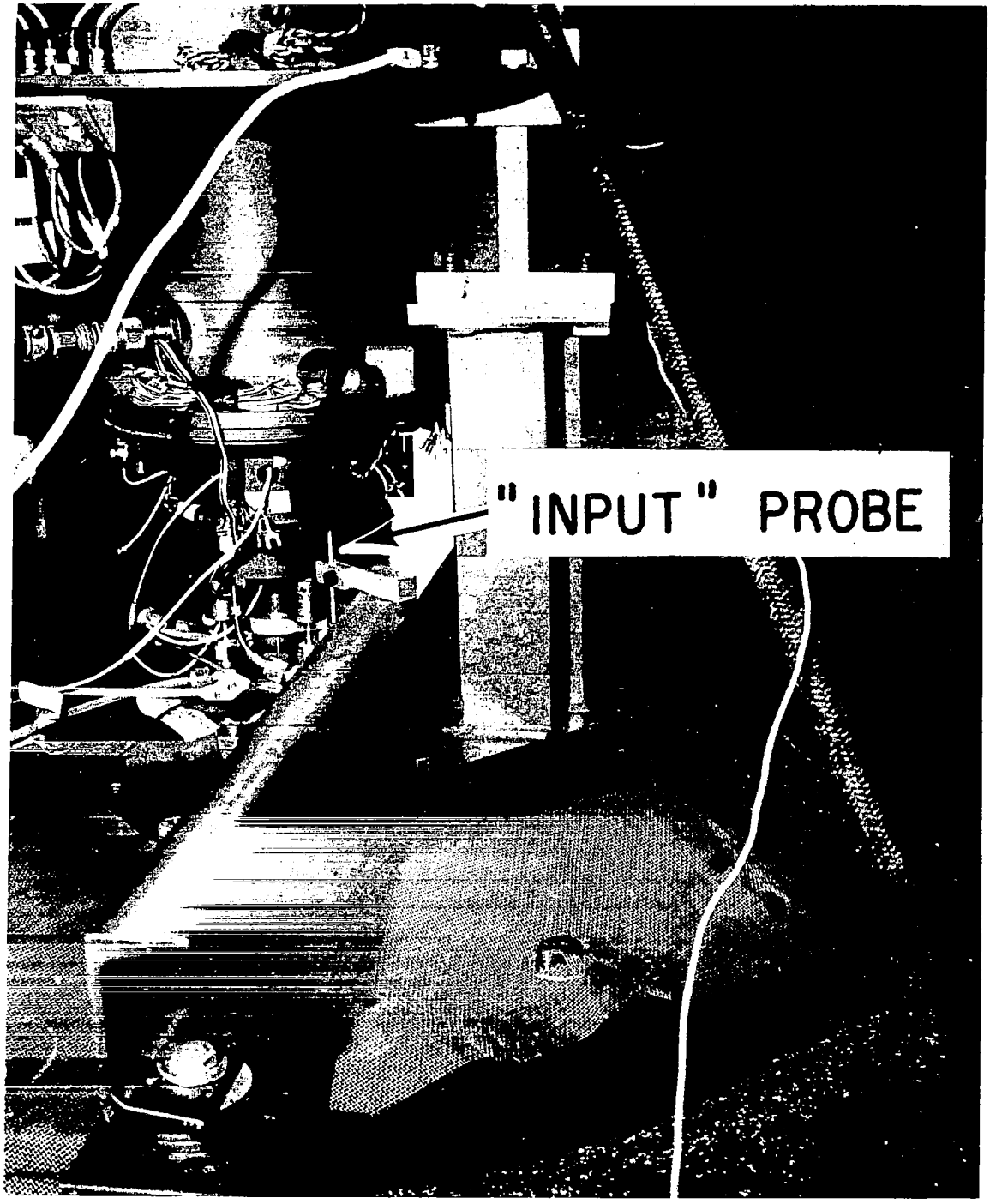

Figure 29. Test Setup to Measure Phase Shift

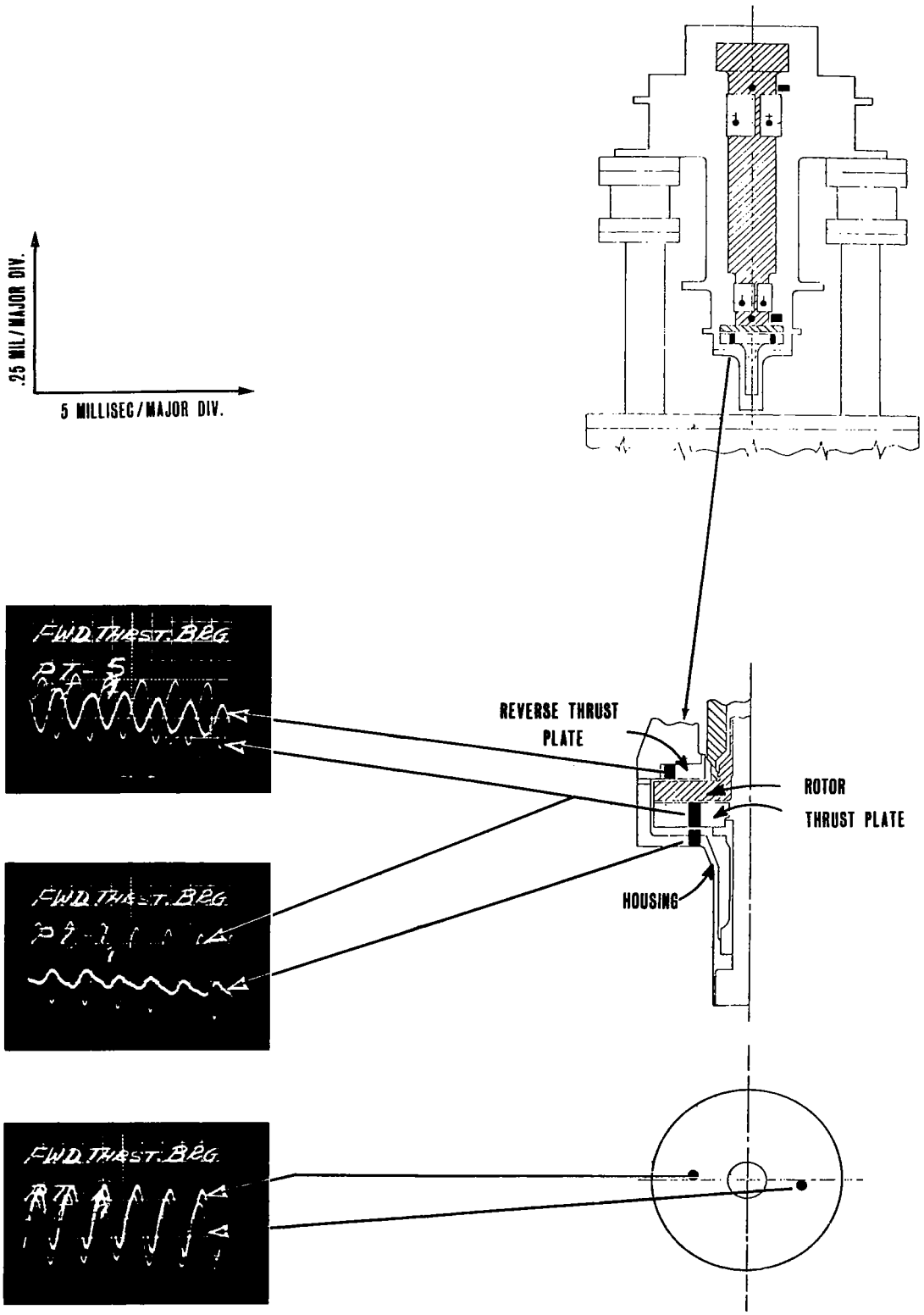

Fig. 30 Measured Modal Behavior at 605 Hz

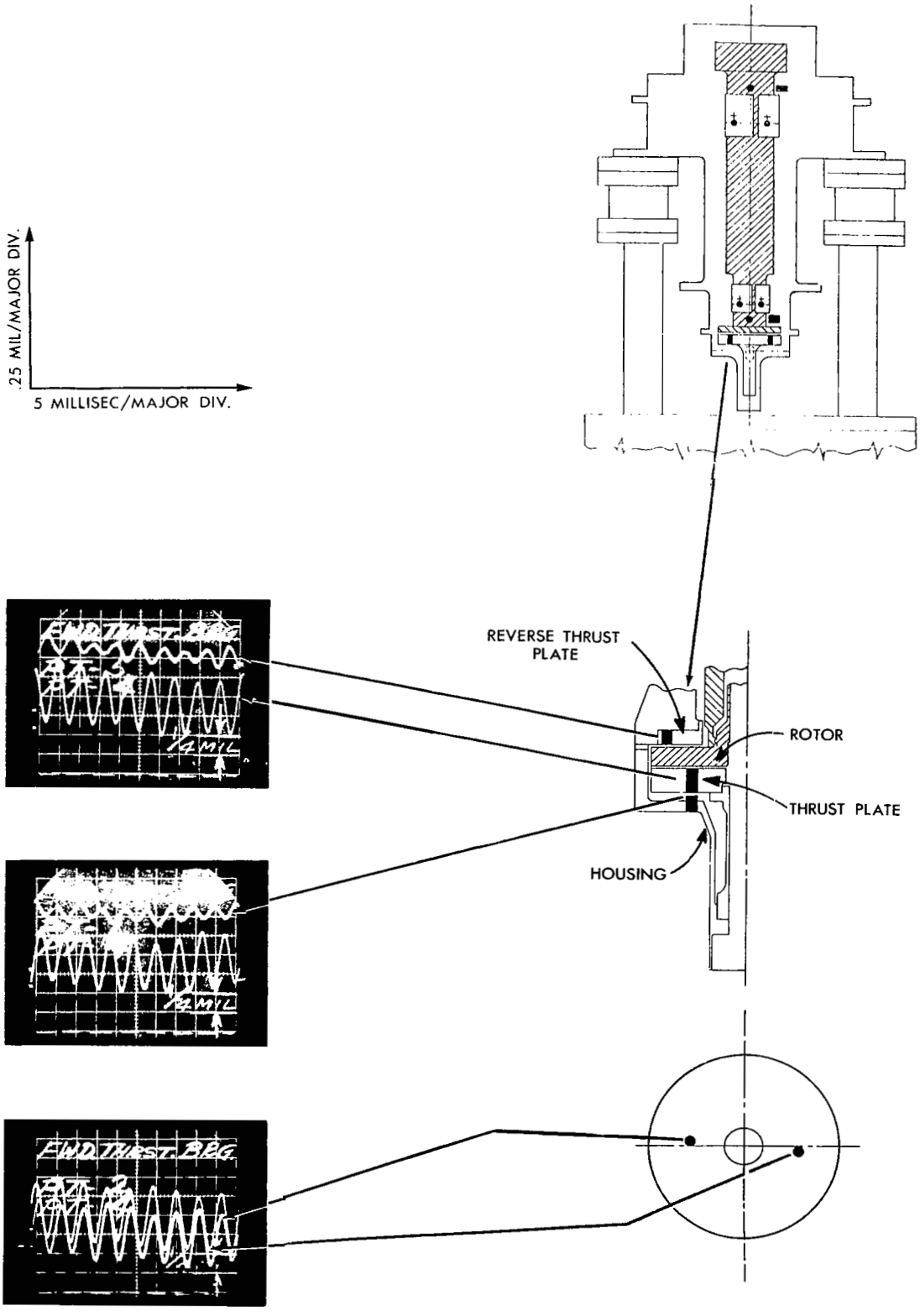

Fig. 31 Measured Modal Behavior at 870 Hz

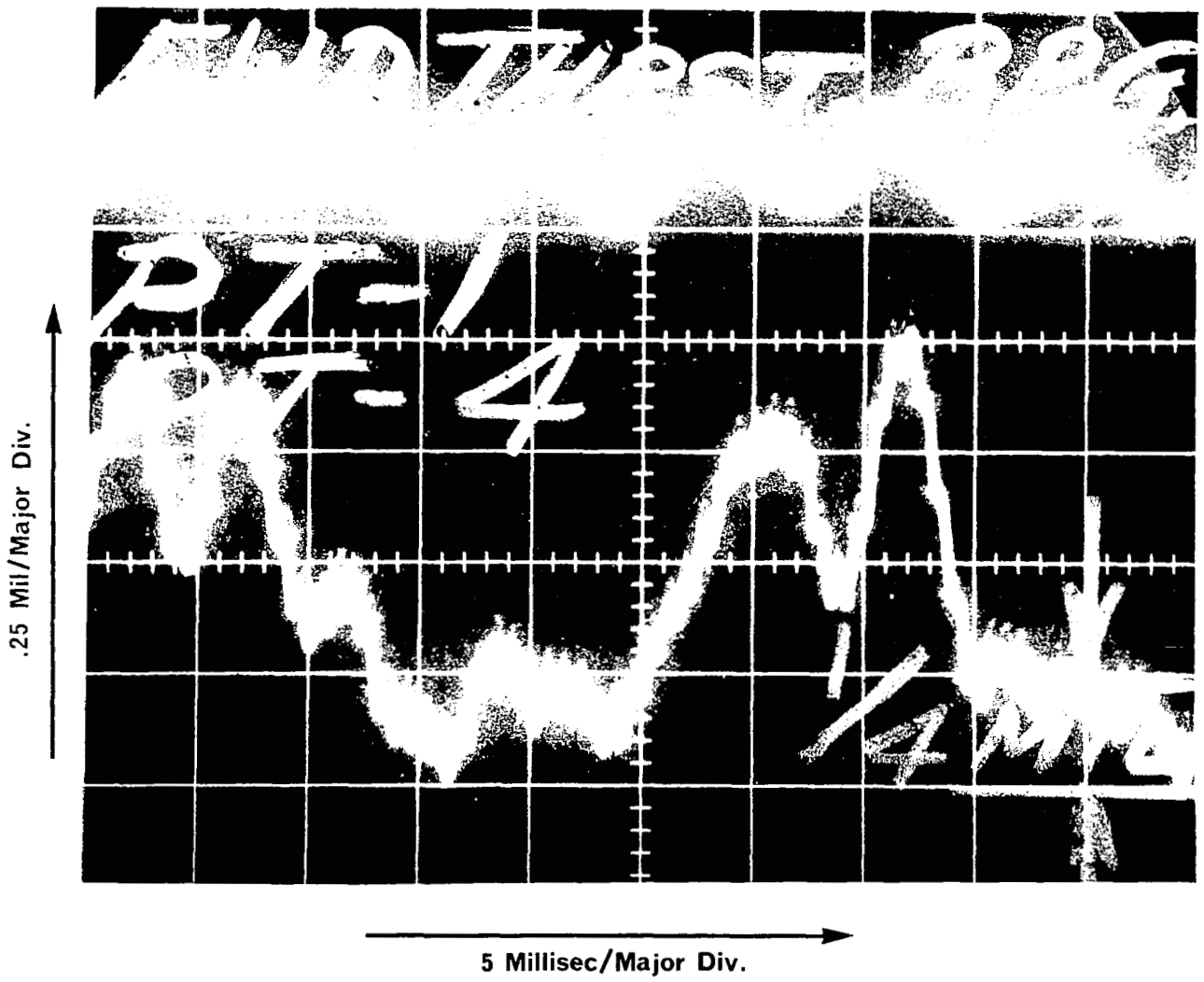

Fig. 32 Response of Thrust Bearing Gas Film at 17 Hz

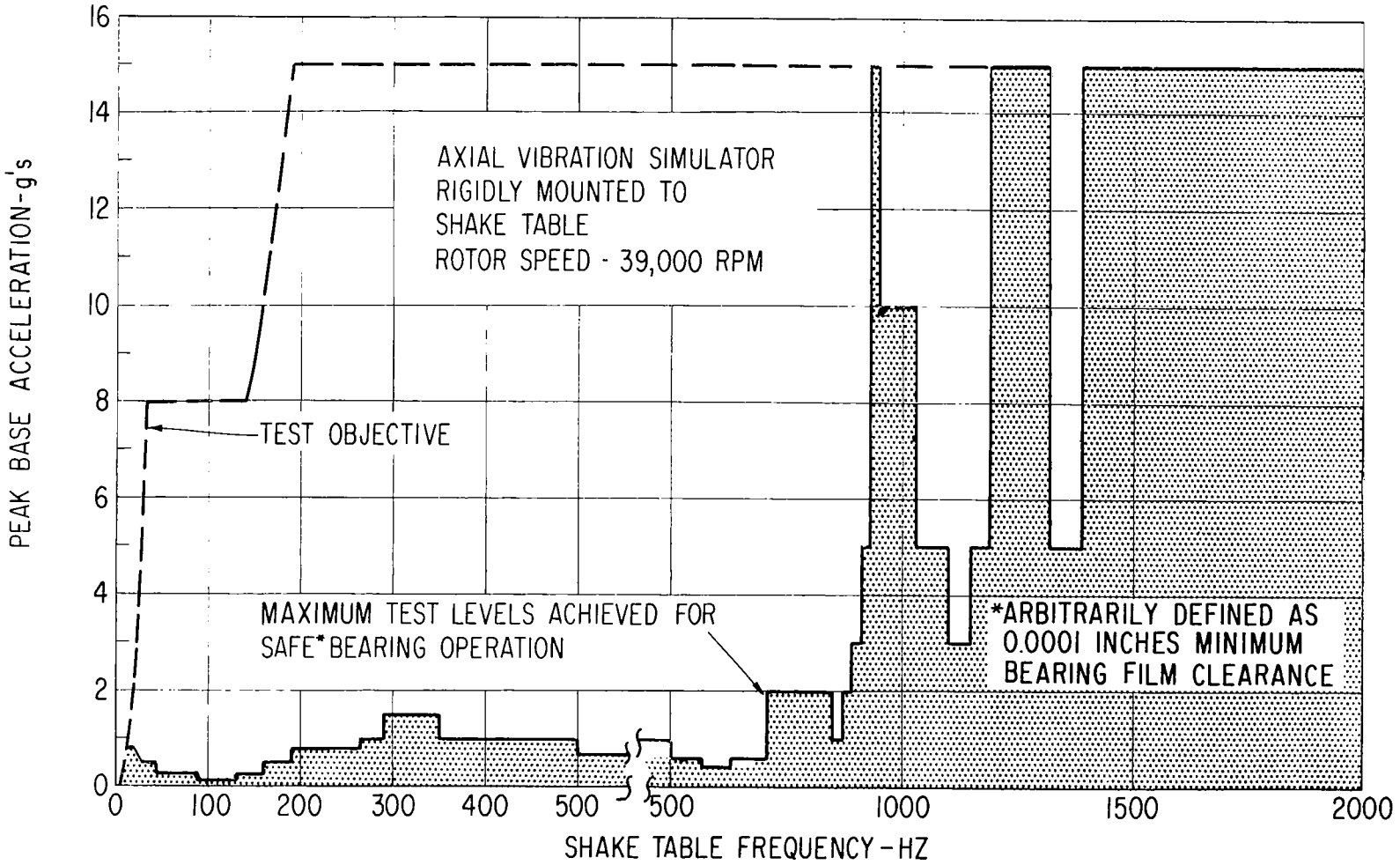

Fig. 33 Maximum Axial Vibration Levels for Safe* Operation of the Simulator When Rigidly Mounted on Vibration Table (Shaft Rotating at 39,000 rpm)

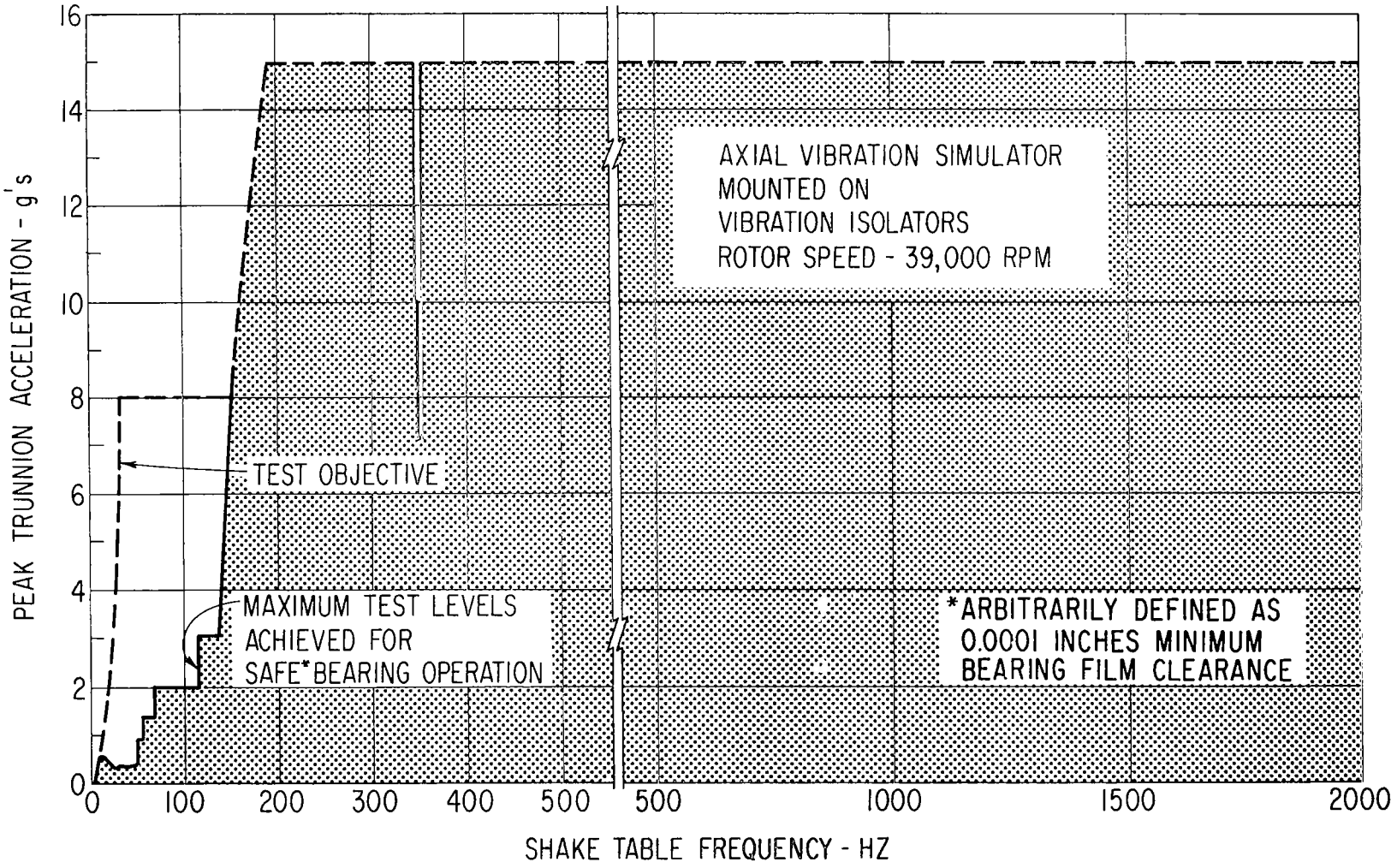

Fig. 34 Maximum Axial Vibration Levels for Safe* Operation of the Simulator When Mounted on Shock and Vibration Isolators (Shaft Rotating at 39,000 rpm)

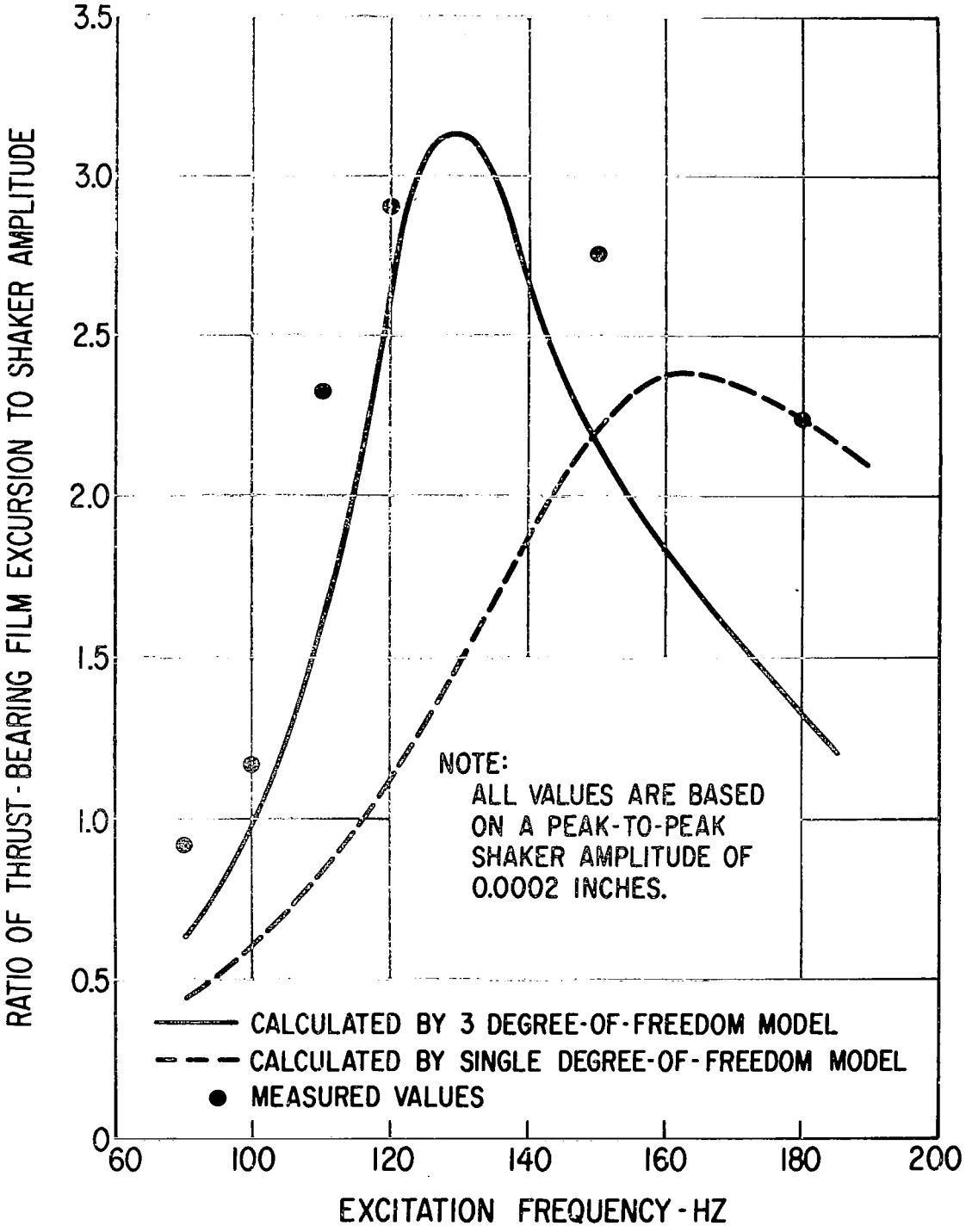

Fig. 35 Calculated and Measured Thrust Bearing Film Response to Axial Vibration About Region of First Resonance (Simulator Rigidly Mounted)

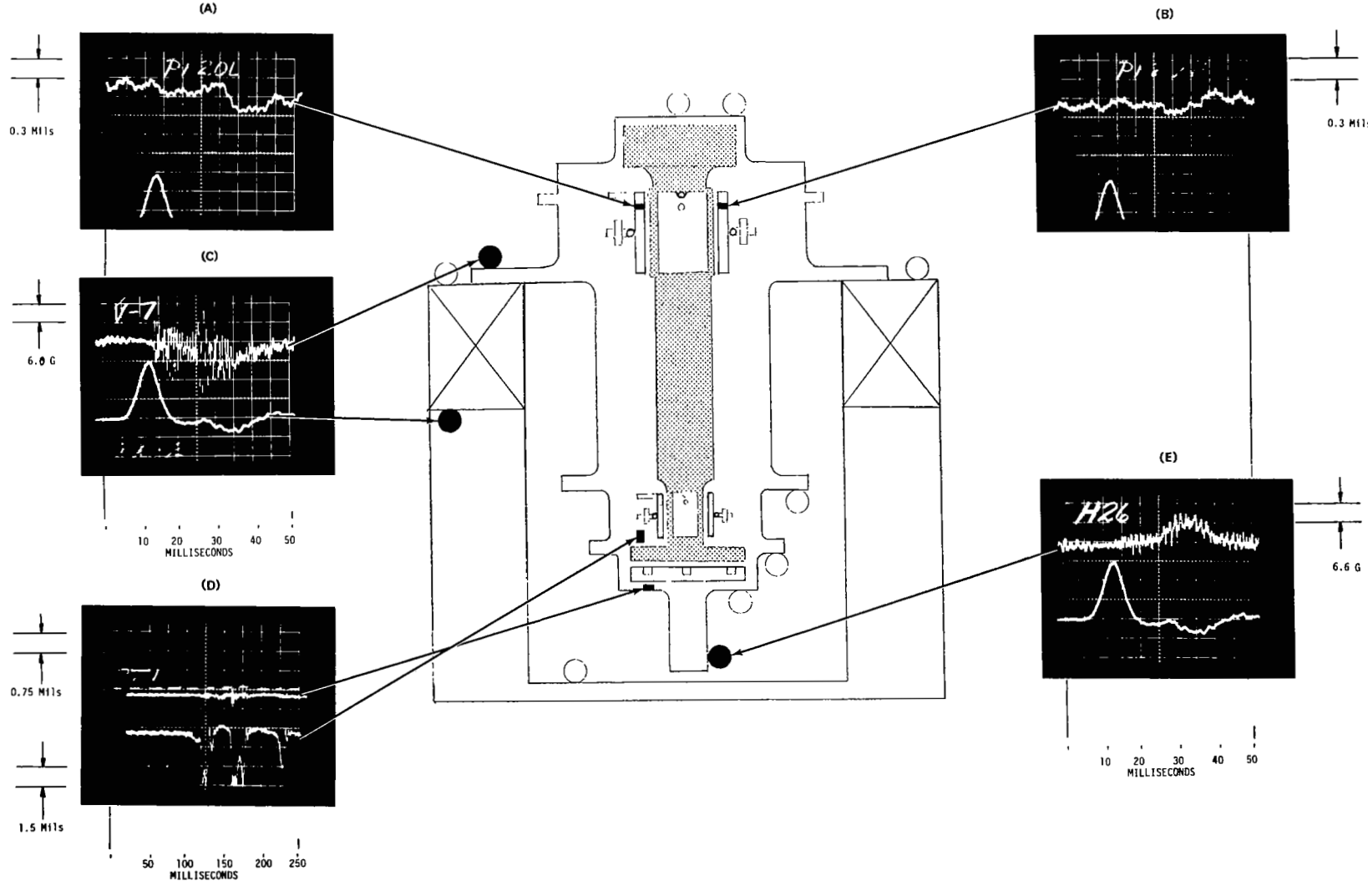

Fig. 36 Data Displays for Axial Shock Test of the Simulator When Mounted on Isolation Mounts (Shaft Rotating at 39,000 rpm)

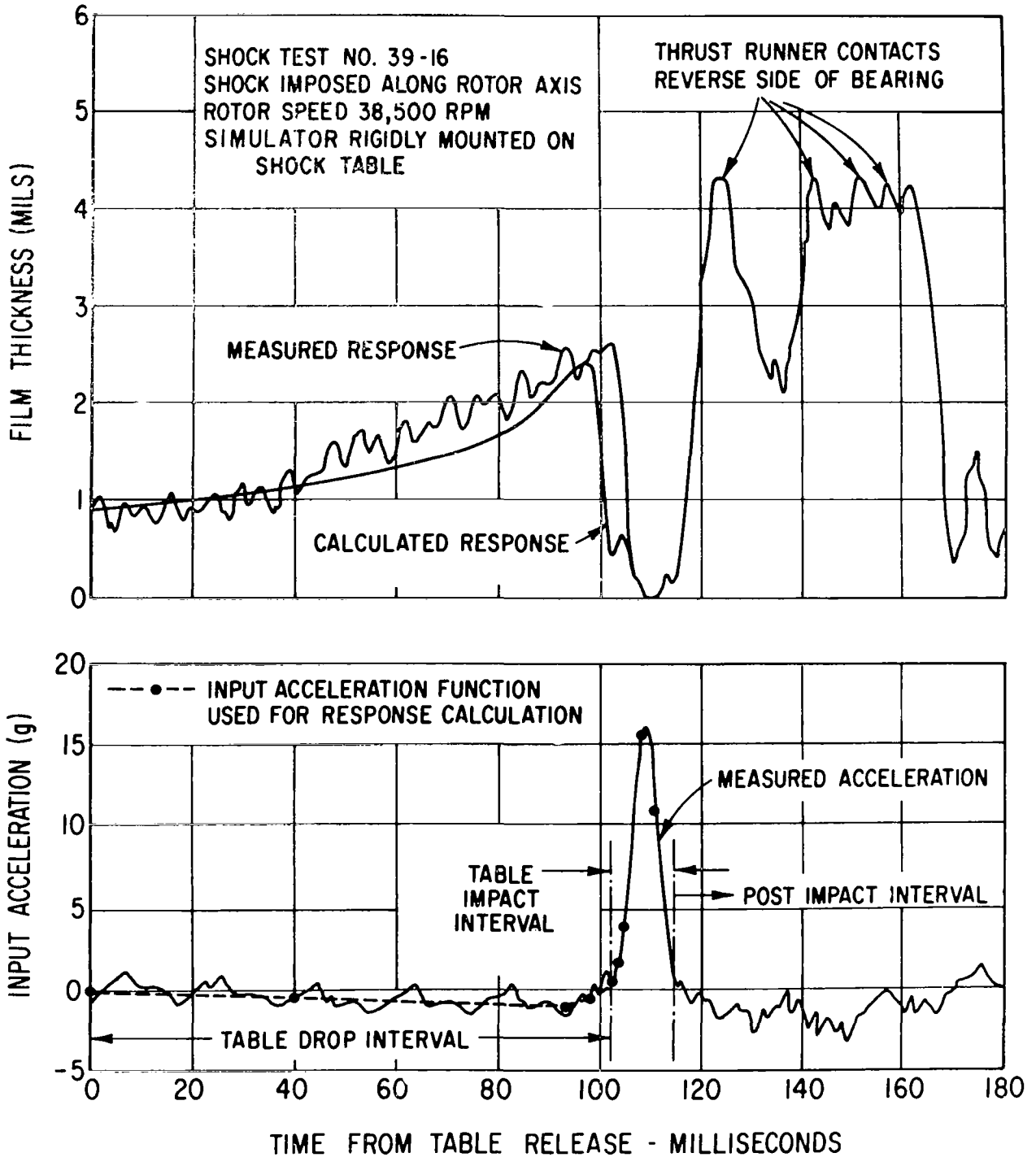

Fig. 37 Calculated and Measured Thrust Bearing Film Response to Axial Shock (Simulator Rigidly Mounted, Single-Degree-of-Freedom Analysis Model)

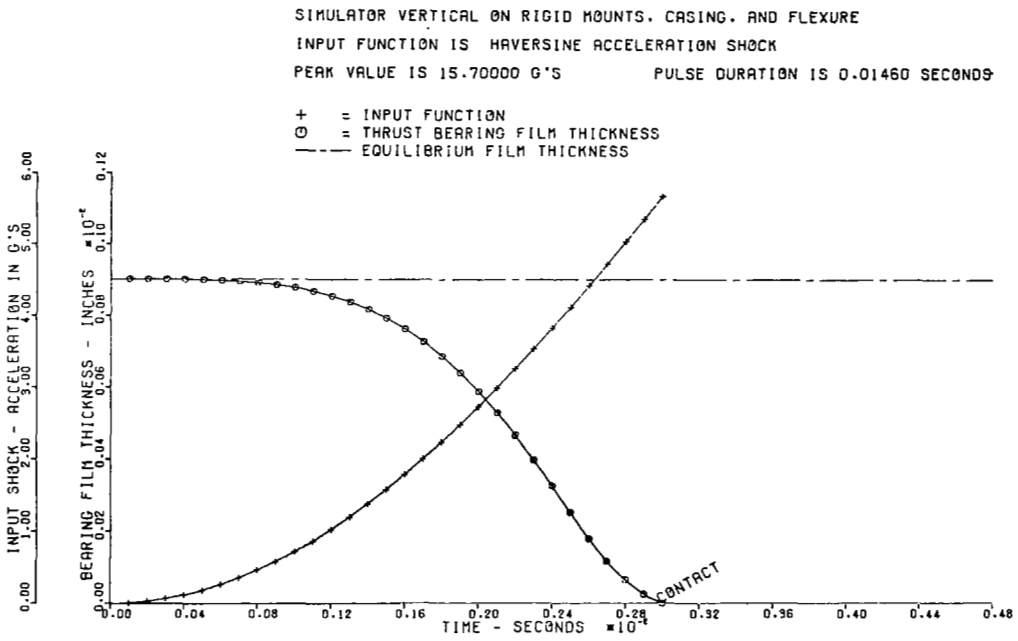

(A) UNDAMPED GAS FILM

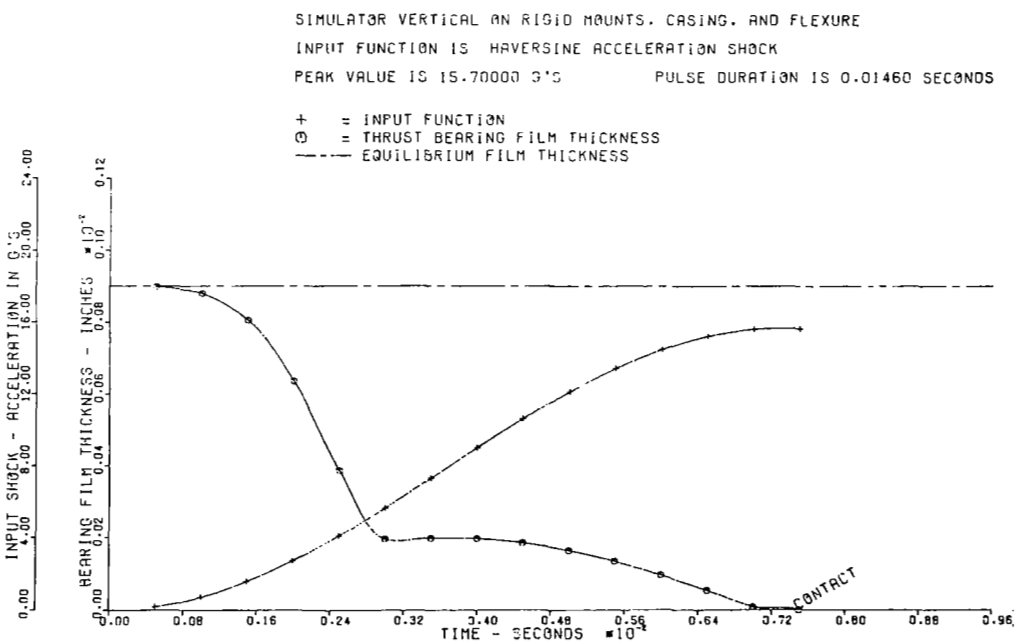

(B) DAMPED GAS FILM

Fig. 38 Calculated Response of Thrust Bearing Gas Film to a Haversine Approximation of the Axial Shock Pulse to Illustrate Effects of Film Damping

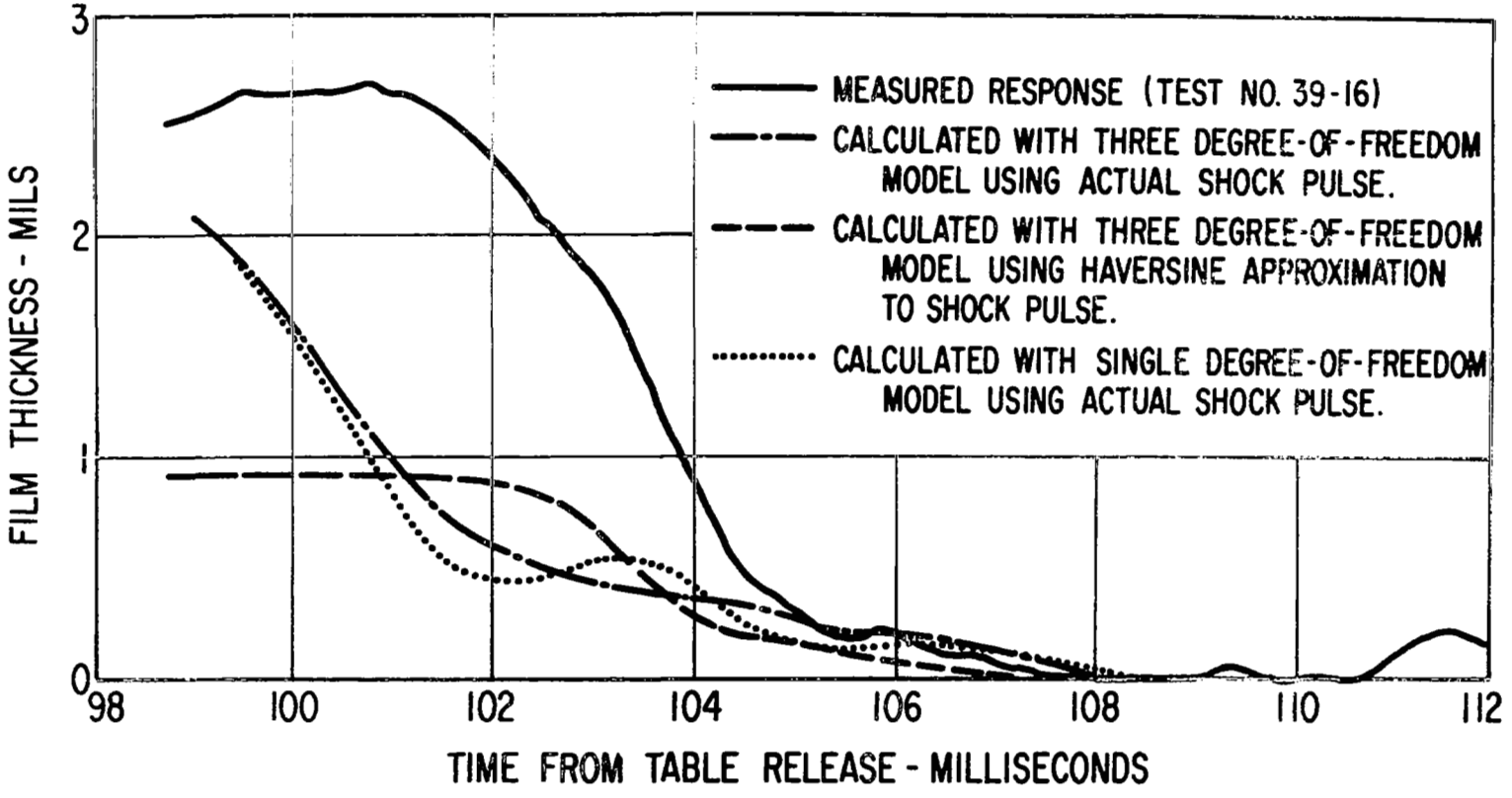

Fig. 39 Calculated and Measured Shock Response During Collapse of The Thrust-Bearing Gas Film

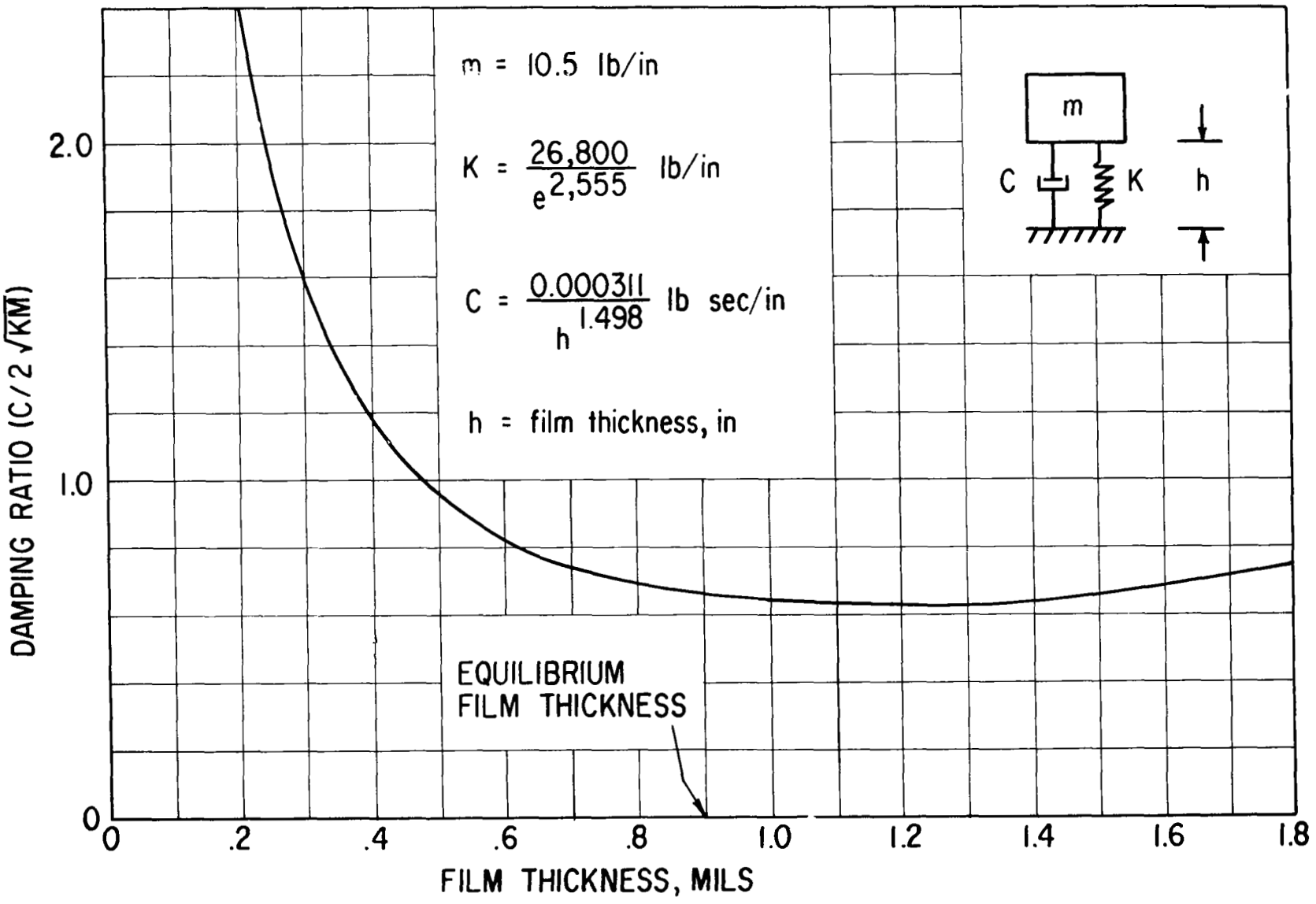

Fig. 40 Damping Ratio of the Thrust-Bearing Gas Film Versus Film Thickness

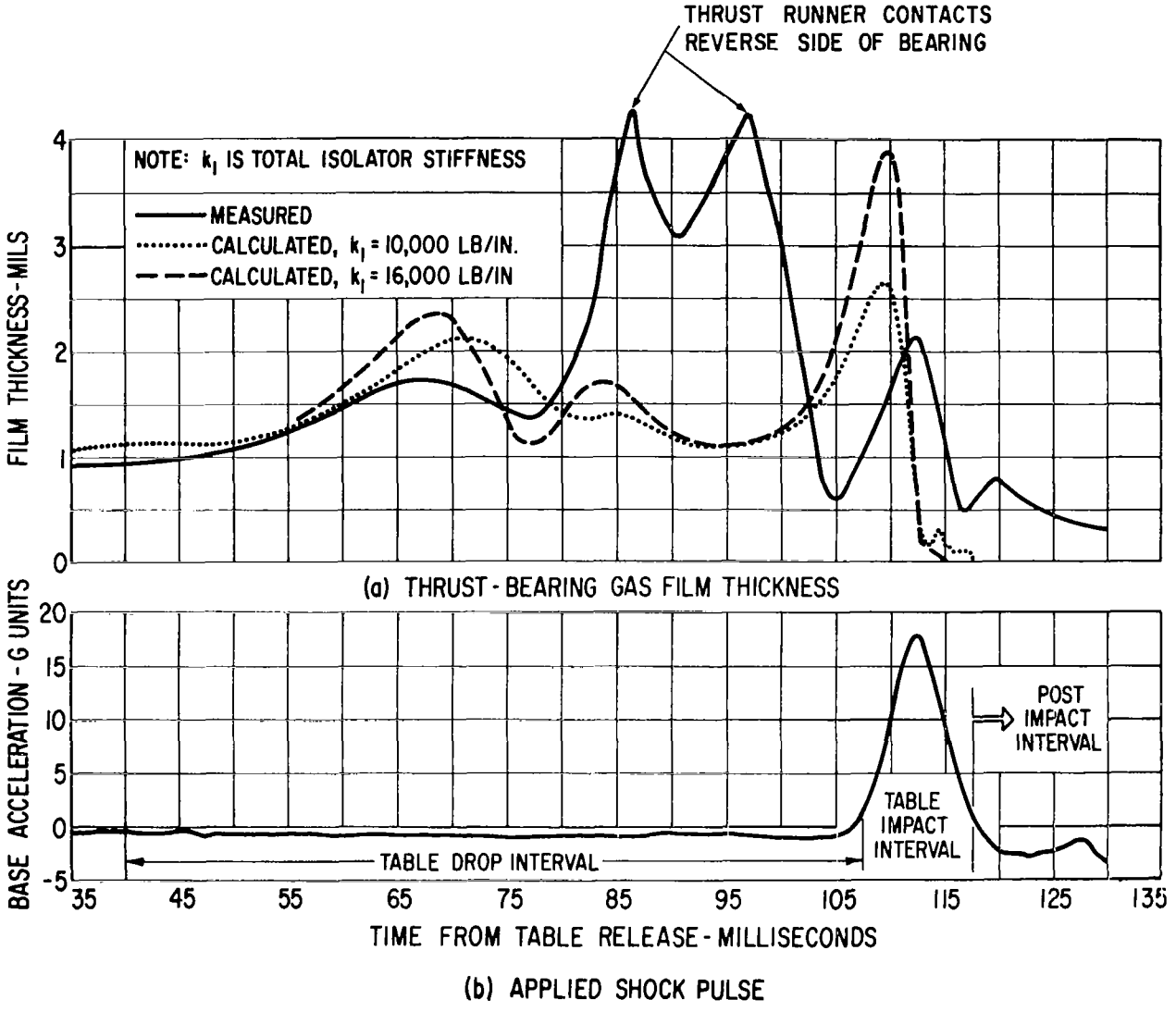

Fig. 41 Calculated and Measured Thrust-Bearing Gas Film Response To Axial Shock (Simulator Mounted on Isolators, Shafting Rotating at 39,000 rpm)

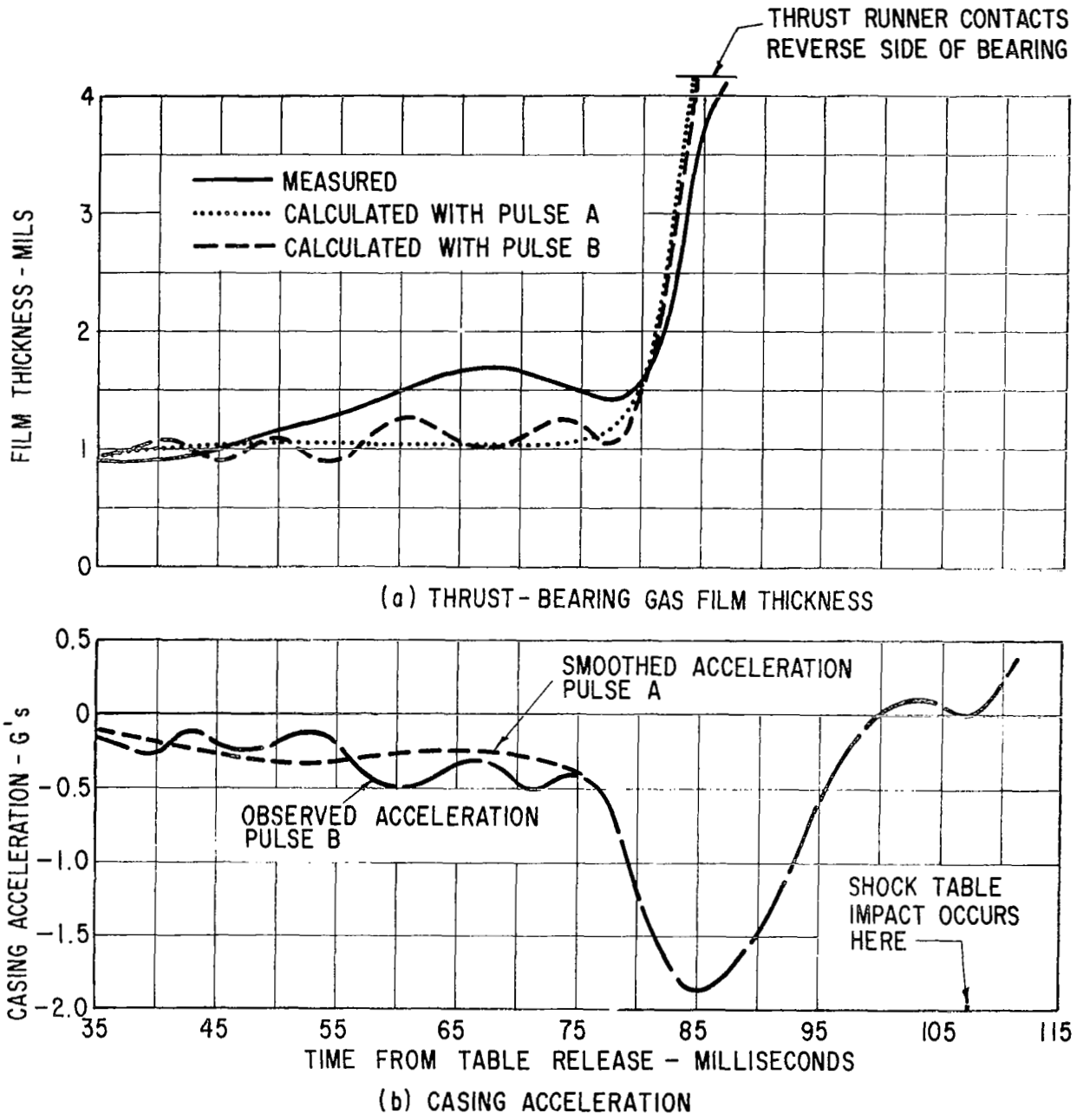

Fig. 42 Calculated and Measured Thrust-Bearing Gas Film Response to Axial Shock (Simulator Mounted on Isolators, Calculated Values Based on Acceleration of Simulator Casing)

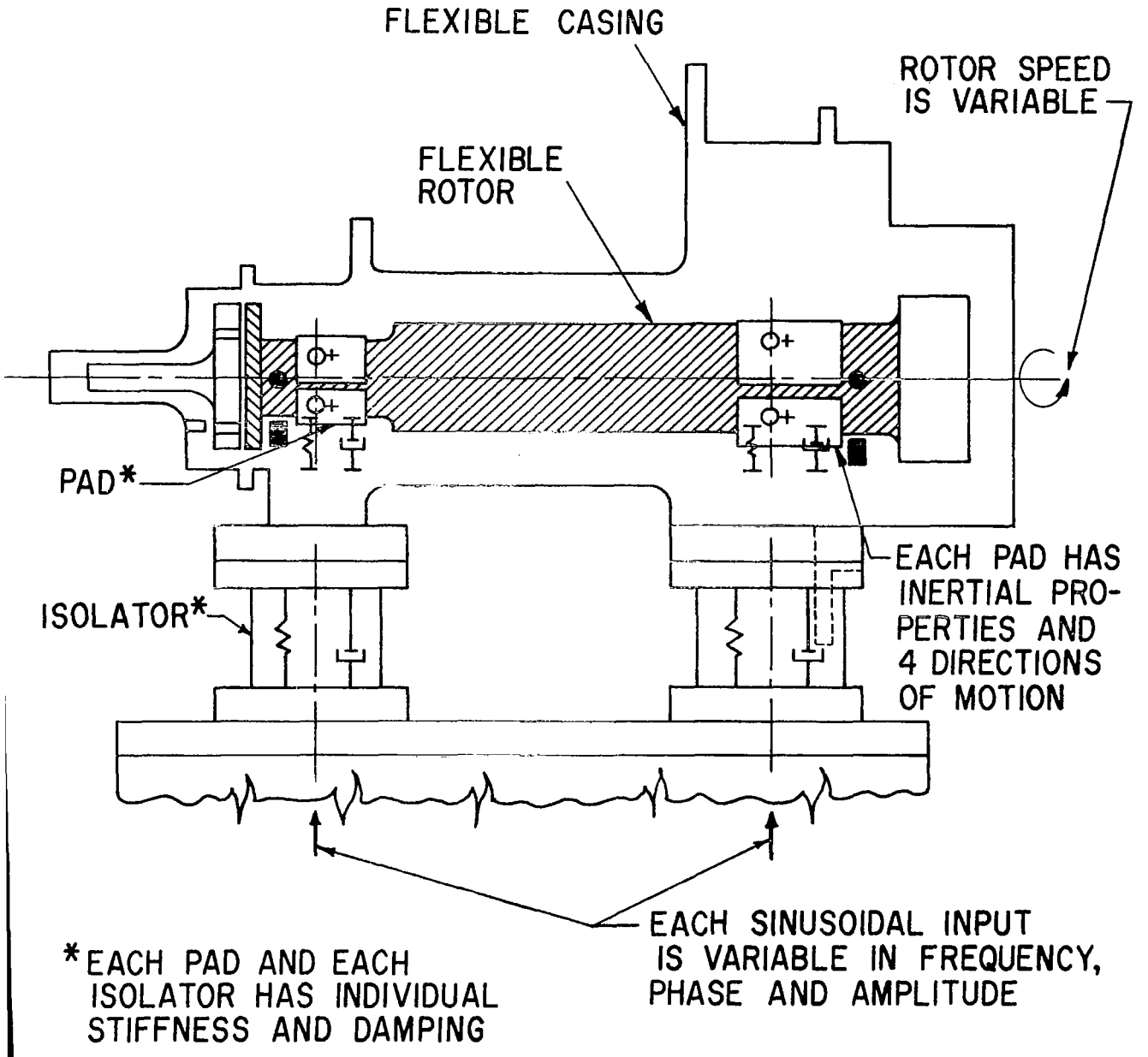

Fig. 43 Parameters of Computer Program Used to Calculate Transverse Vibration Response

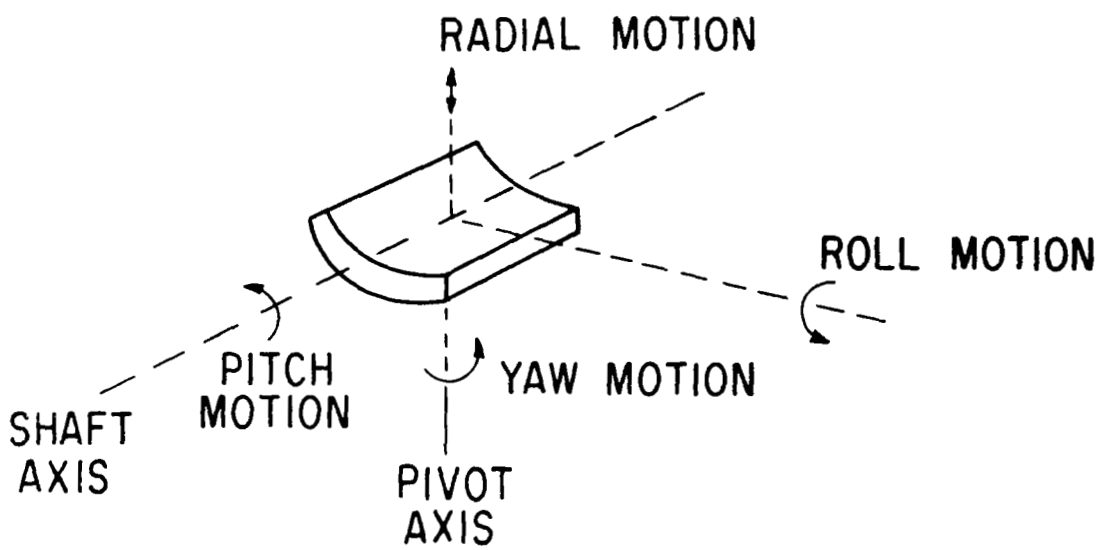

Fig. 44 Definitions of Journal Bearing Pad Motions

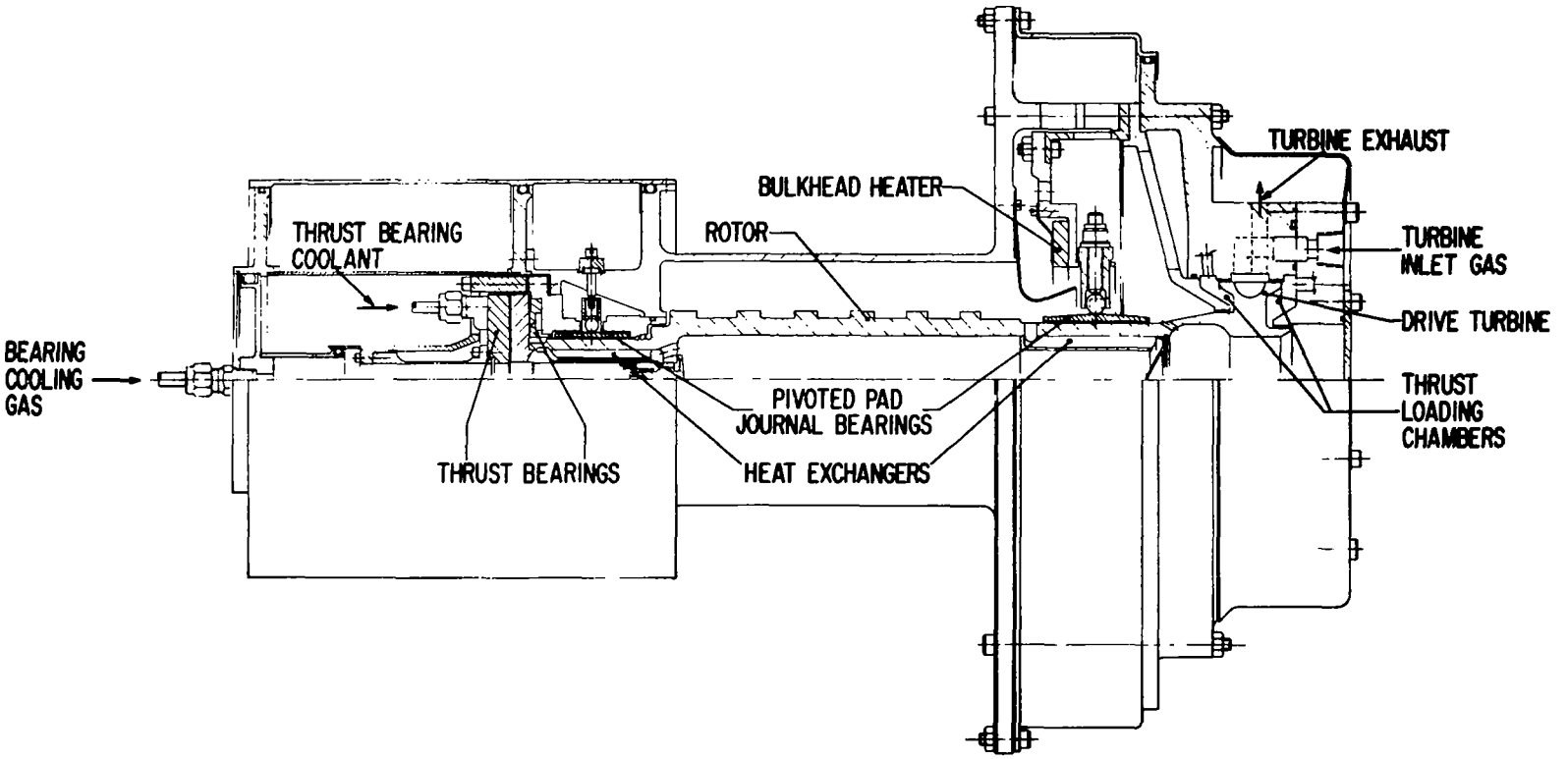

Fig. 45 Cross-Sectional View of Rotor-Bearing System Simulator

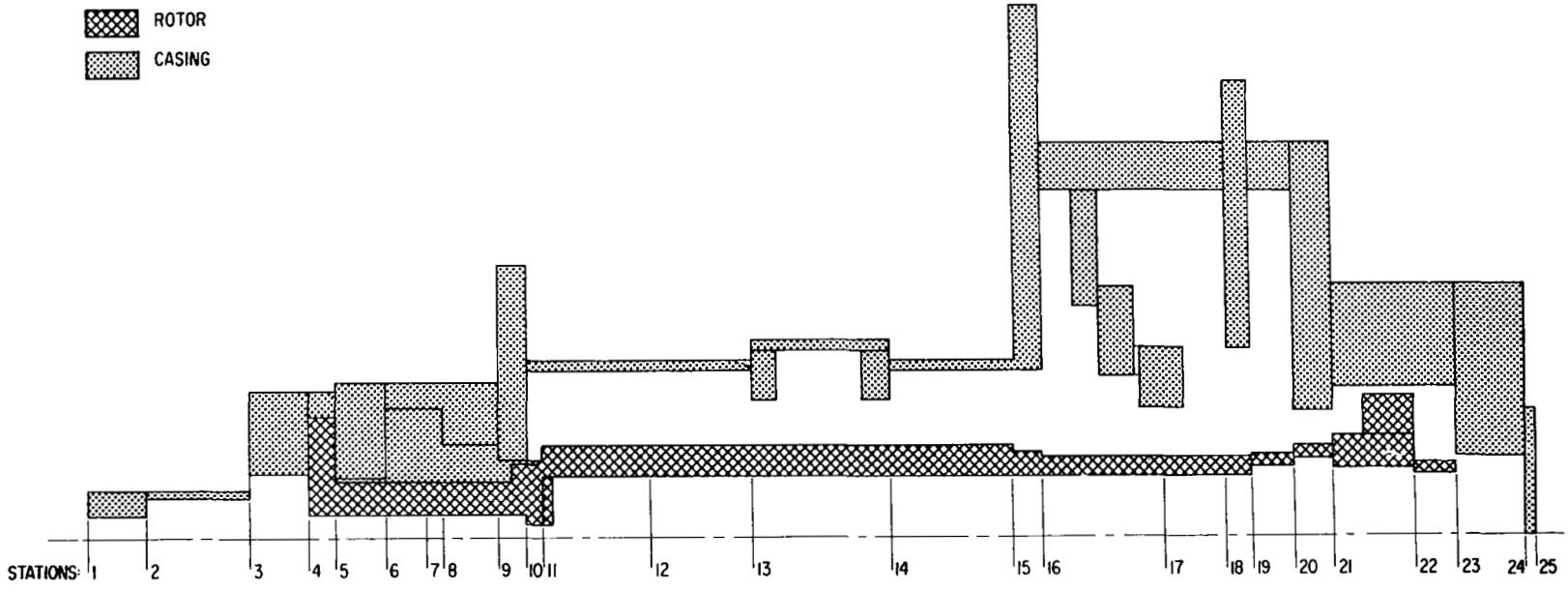

Fig. 46 Model of Rotor and Casing Used in Computer Program to Calculate Transverse Vibration Response

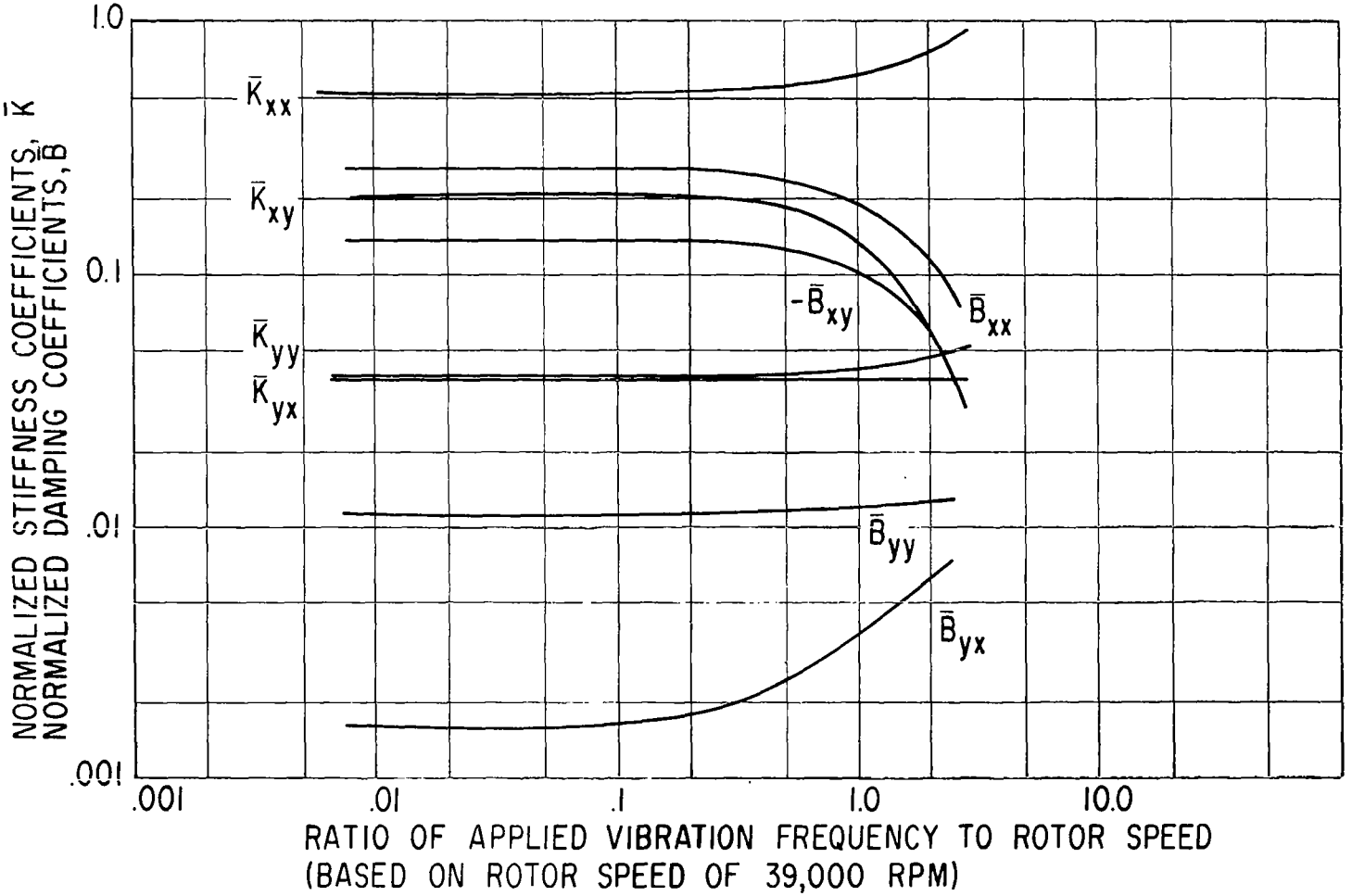

Fig. 47 Frequency Dependence of Normalized Journal-Bearing Stiffness and Damping Coefficients

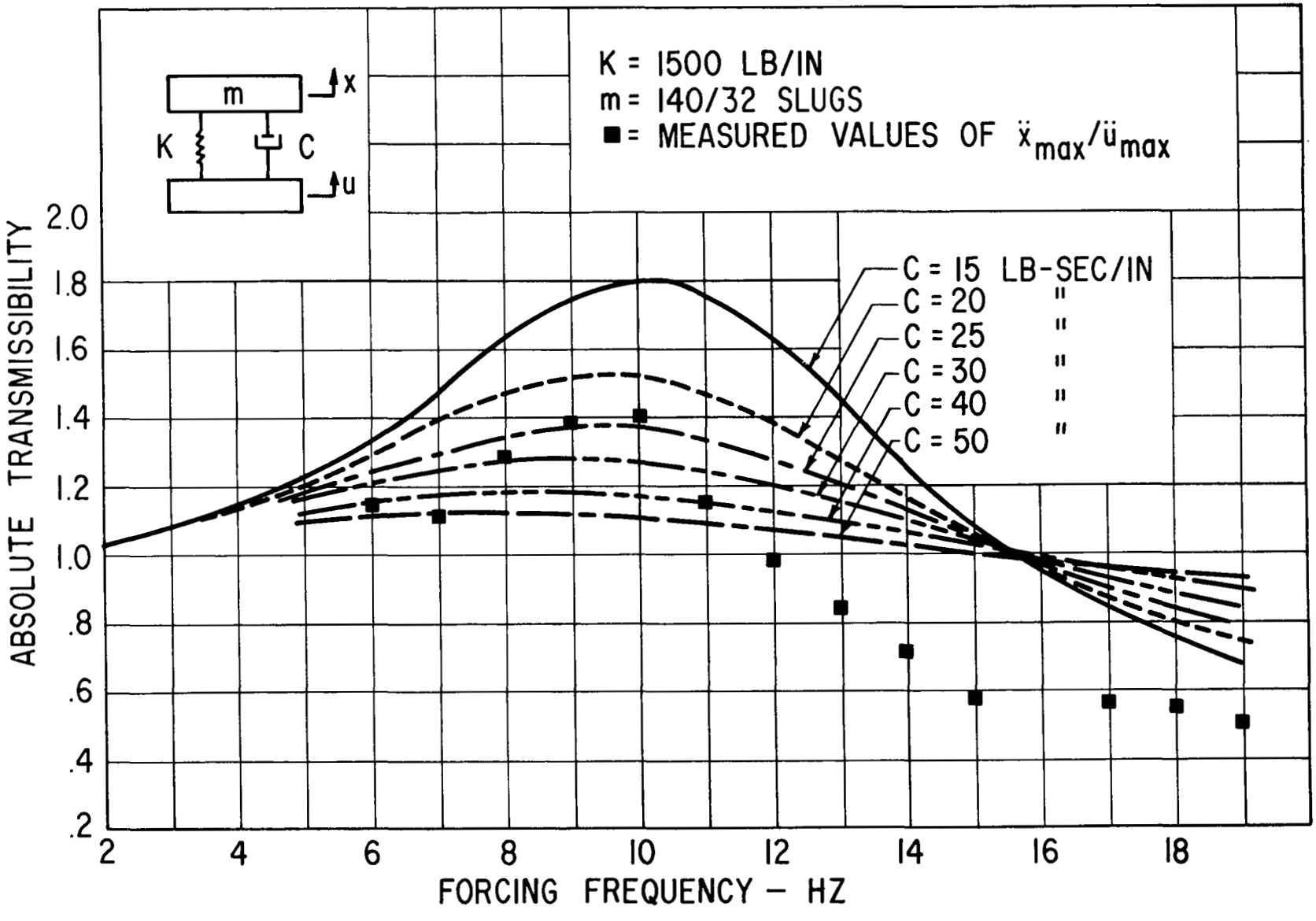

Figure 48 Method of Determining Isolator System Parameters Showing Effect of Damping

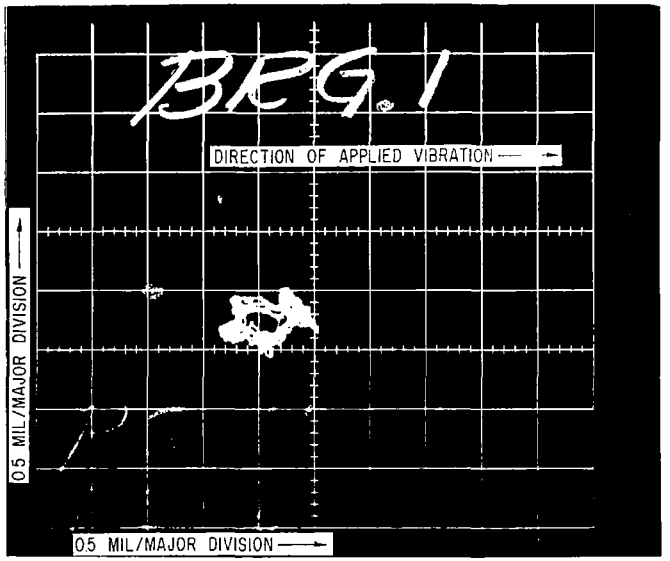

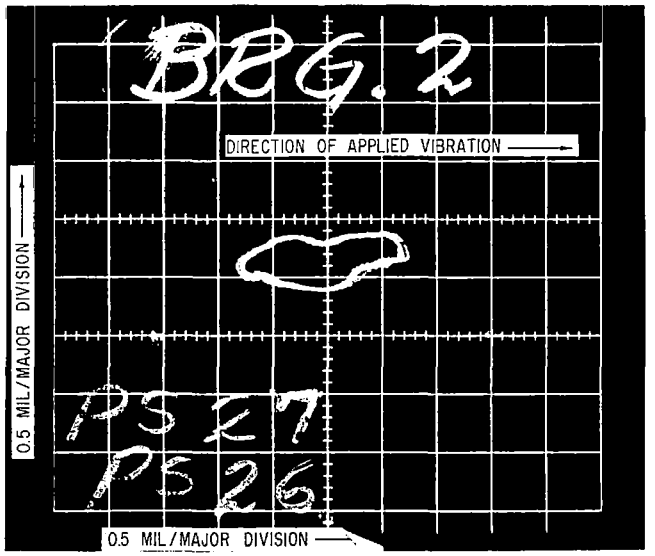

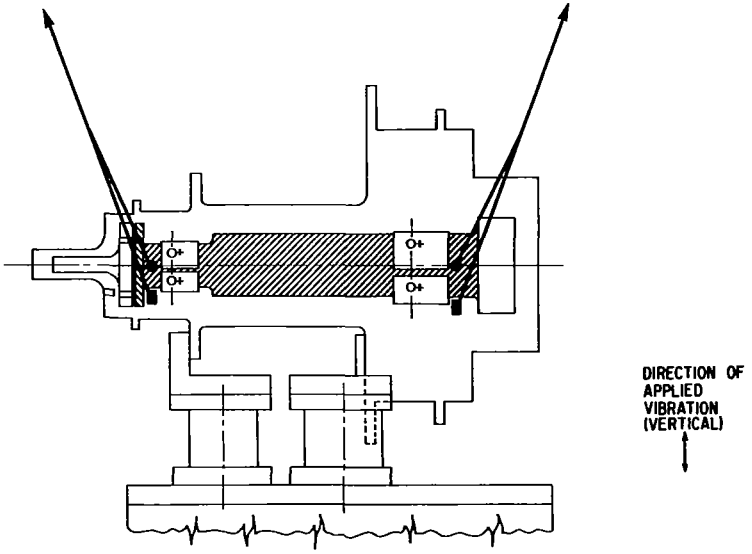

Fig. 49 Measured Orbits of Rotor at 166 Hz During Transverse Vibration Testing

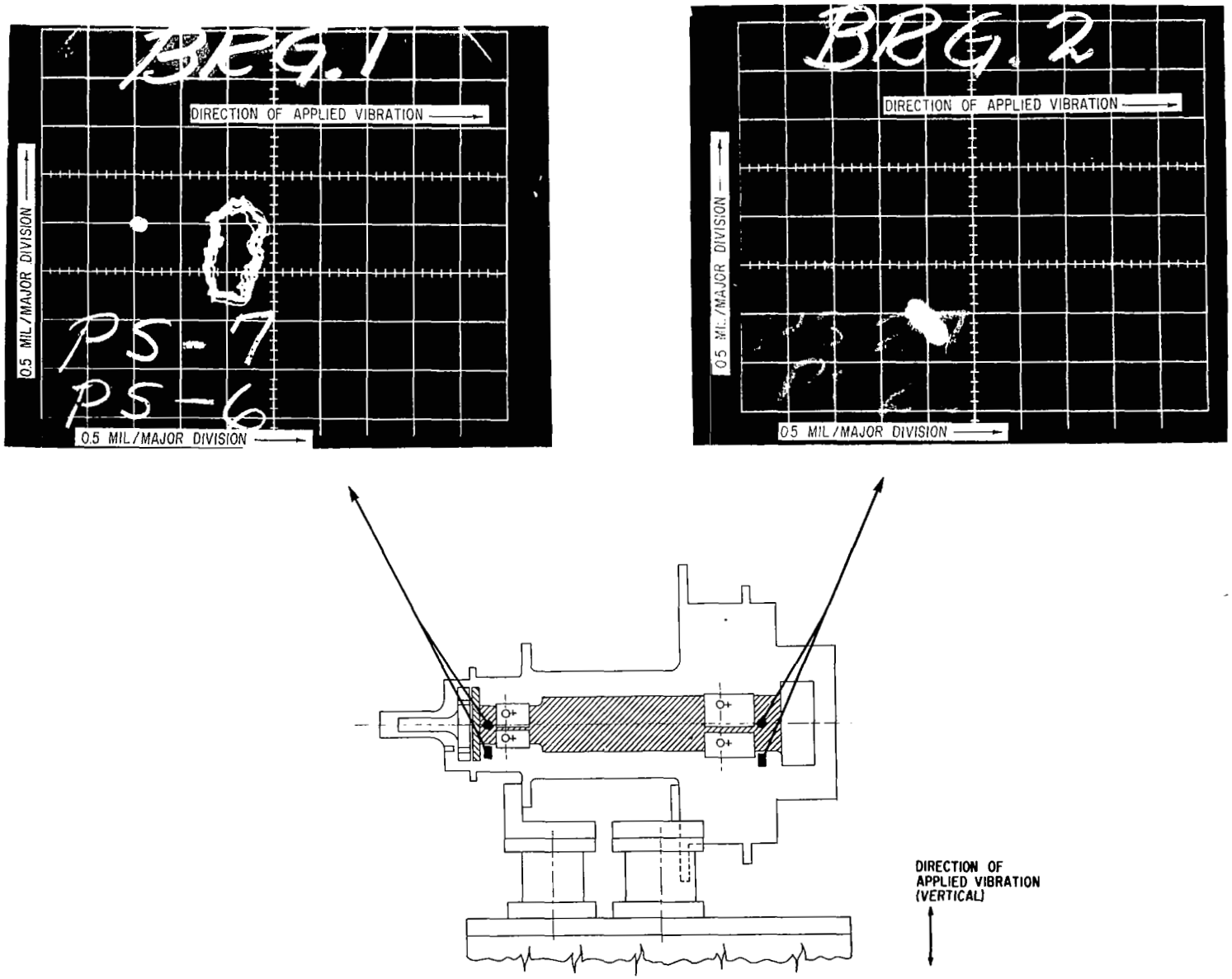

Fig. 50 Measured Orbits of Rotor at 225 Hz During Transverse Vibration Testing

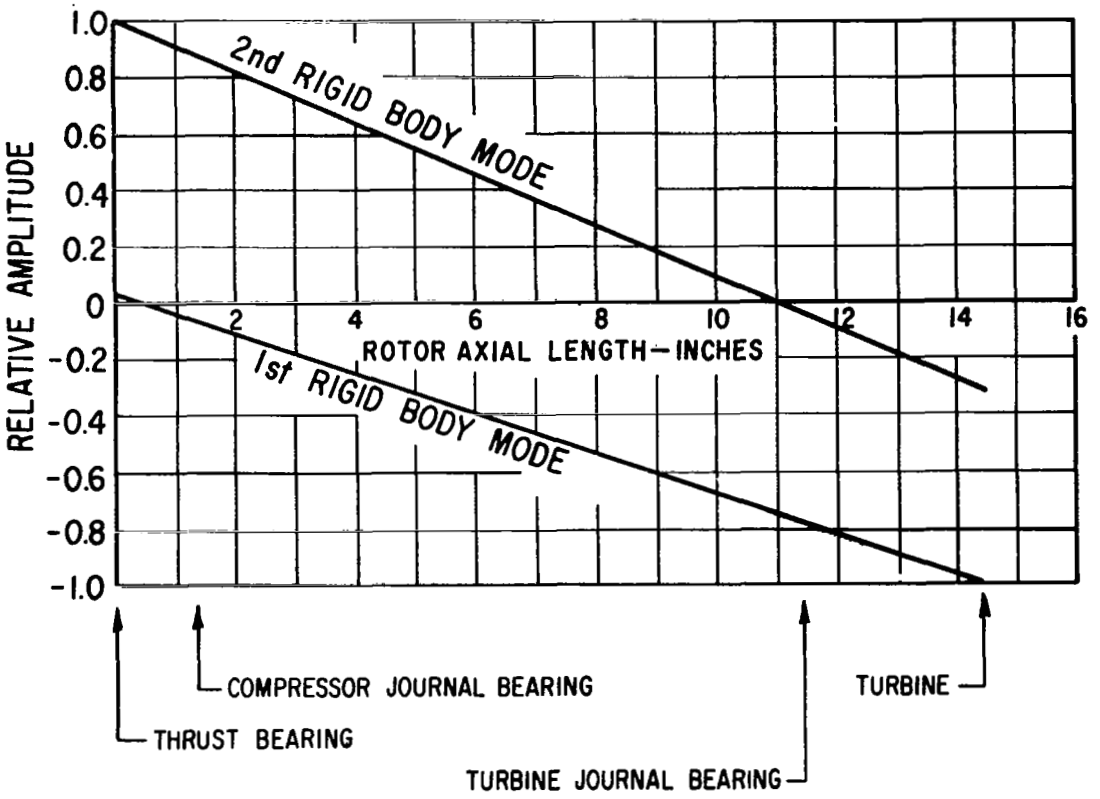

Fig. 51 Calculated Mode Shapes for the Two Rigid-Body Critical Speeds of the Rotor-Bearing System

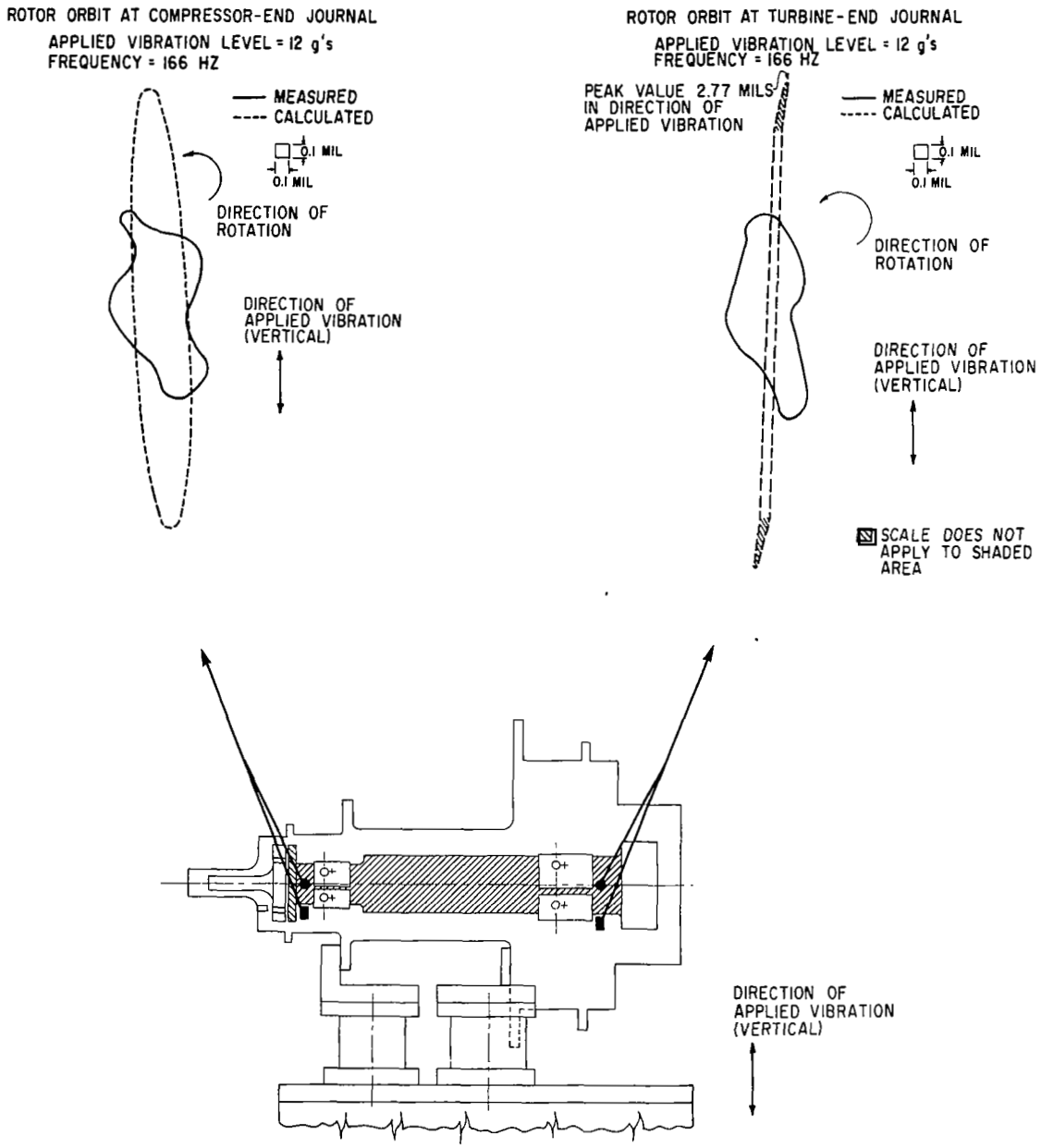

Fig. 52 Comparison Between Measured and Calculated Orbits at 166 Hz

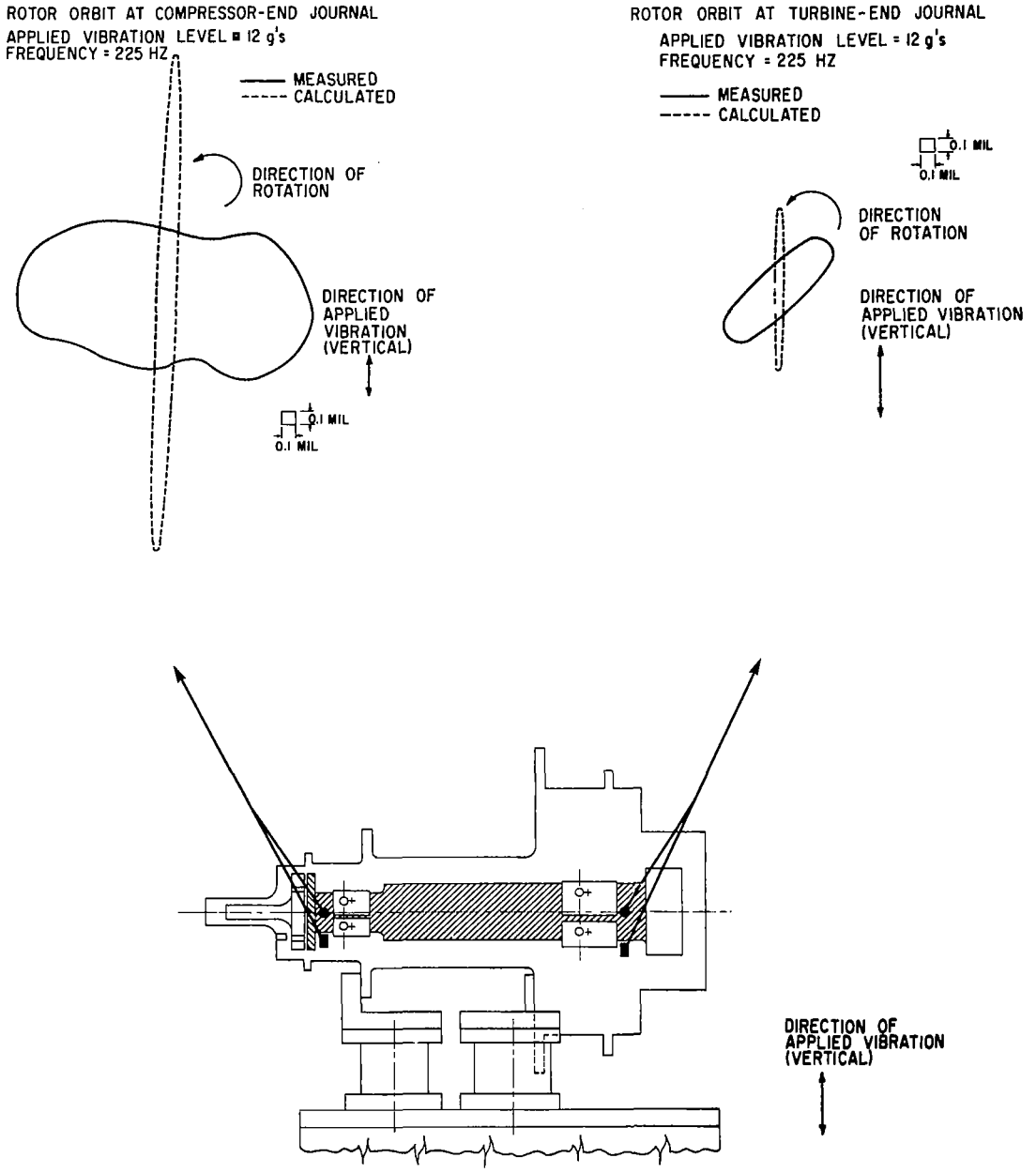

Fig. 53 Comparison Between Measured and Calculated Orbits at 225 Hz

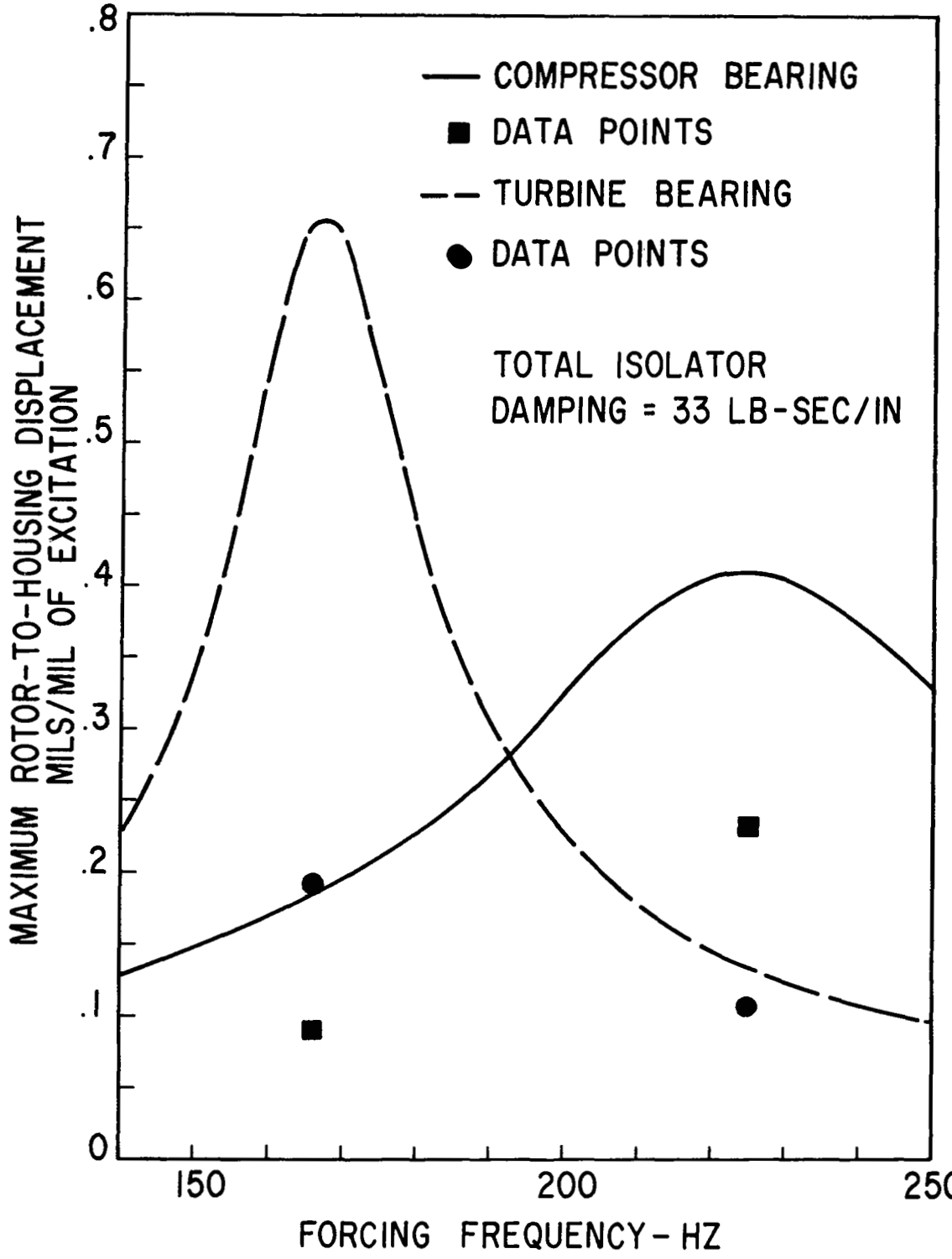

Fig. 54 Calculated Transverse Frequency Response Showing Region of First Two Rigid-Body Critical Speeds

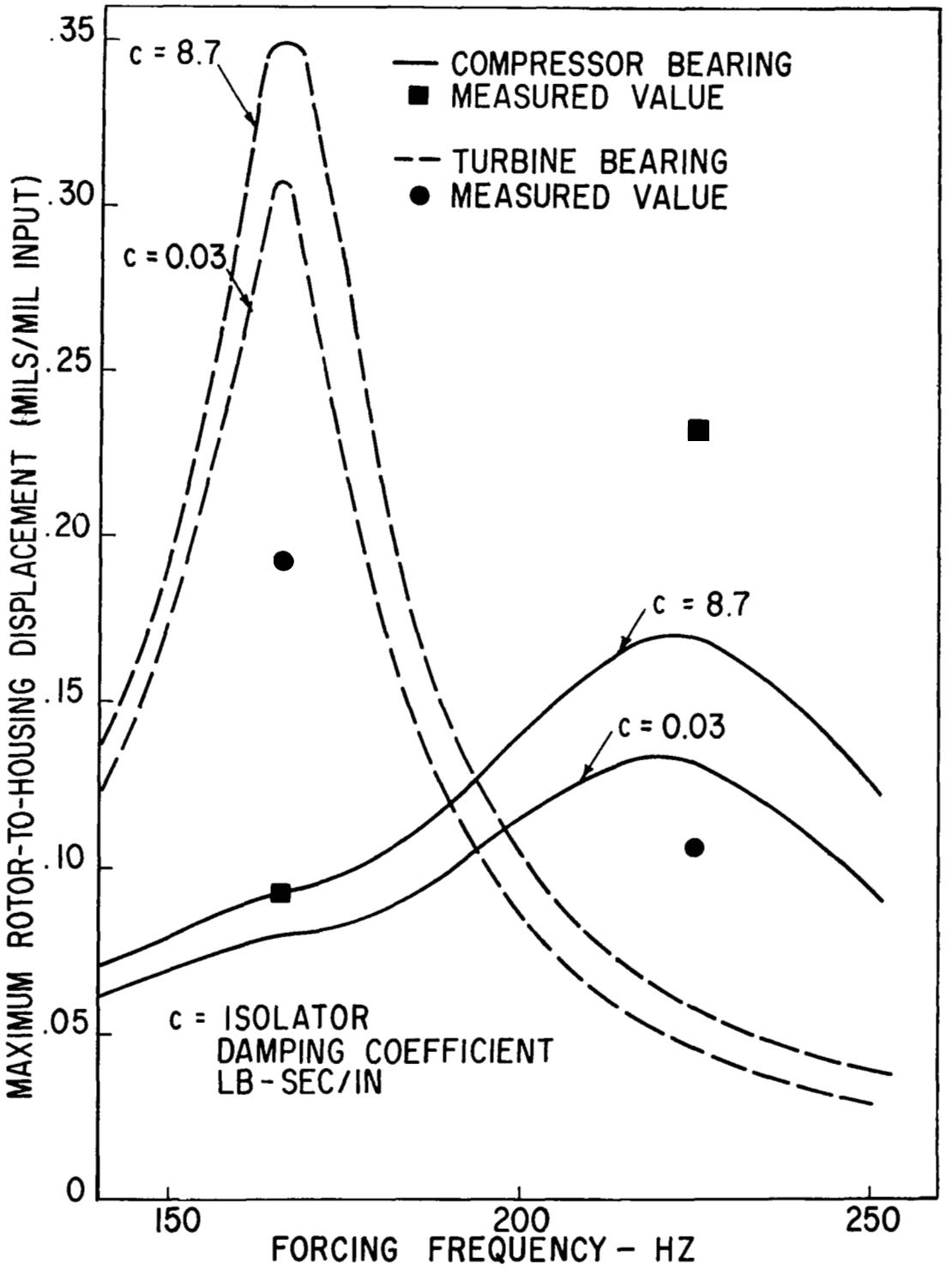

Fig. 55 Effect of Isolator Damping on Calculated Transverse Frequency Response

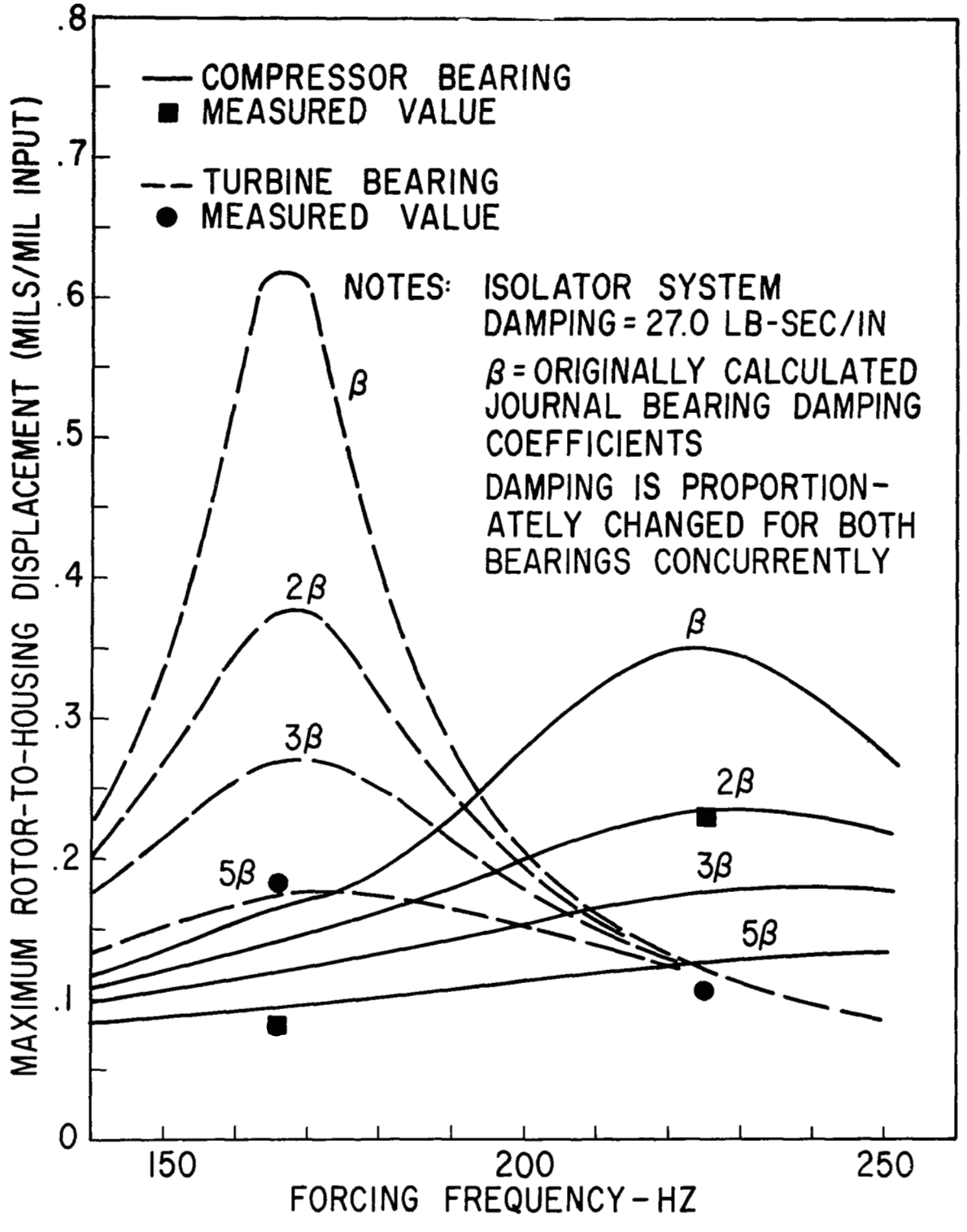

Fig. 56 Effect of Journal Bearing Damping on Calculated Transverse Frequency Response

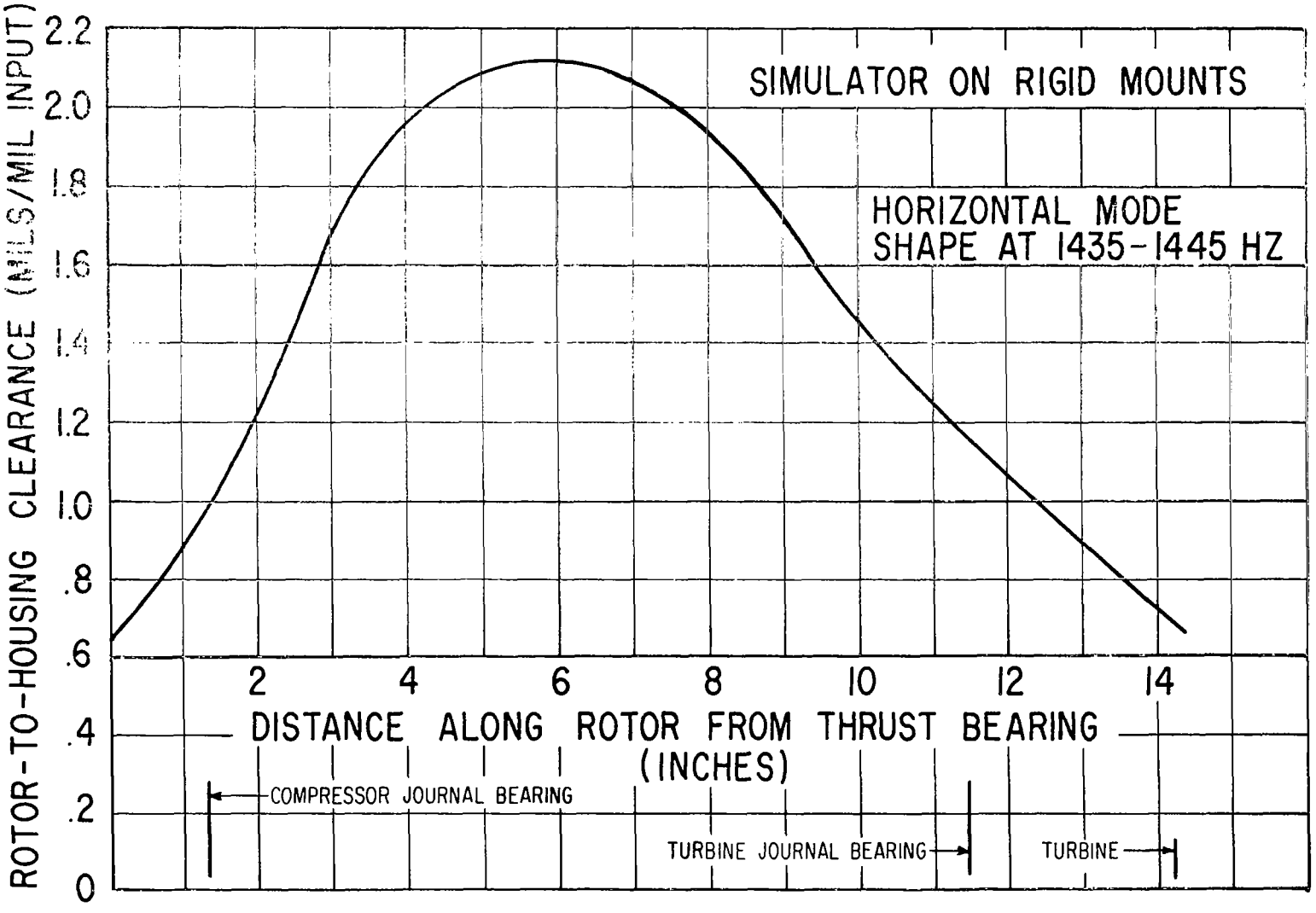

Fig. 57 Mode Shape of Casing at First Natural Bending Frequency

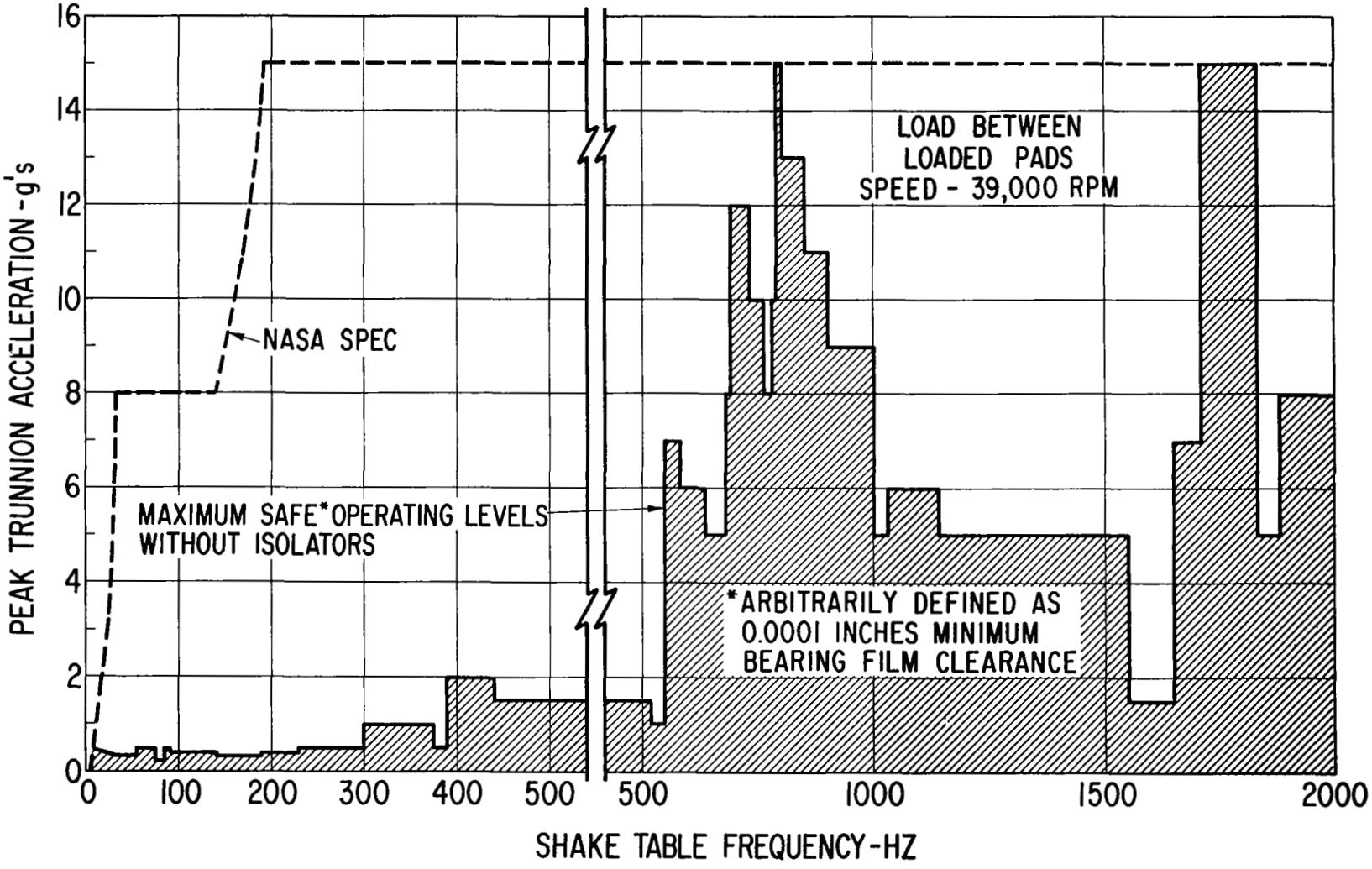

Fig. 58 Maximum Transverse Vibration Levels in the T1 Direction for Safe* Operation of the Simulator When Rigidly Mounted on Vibration Table (Shaft Rotating at 39,000 rpm)

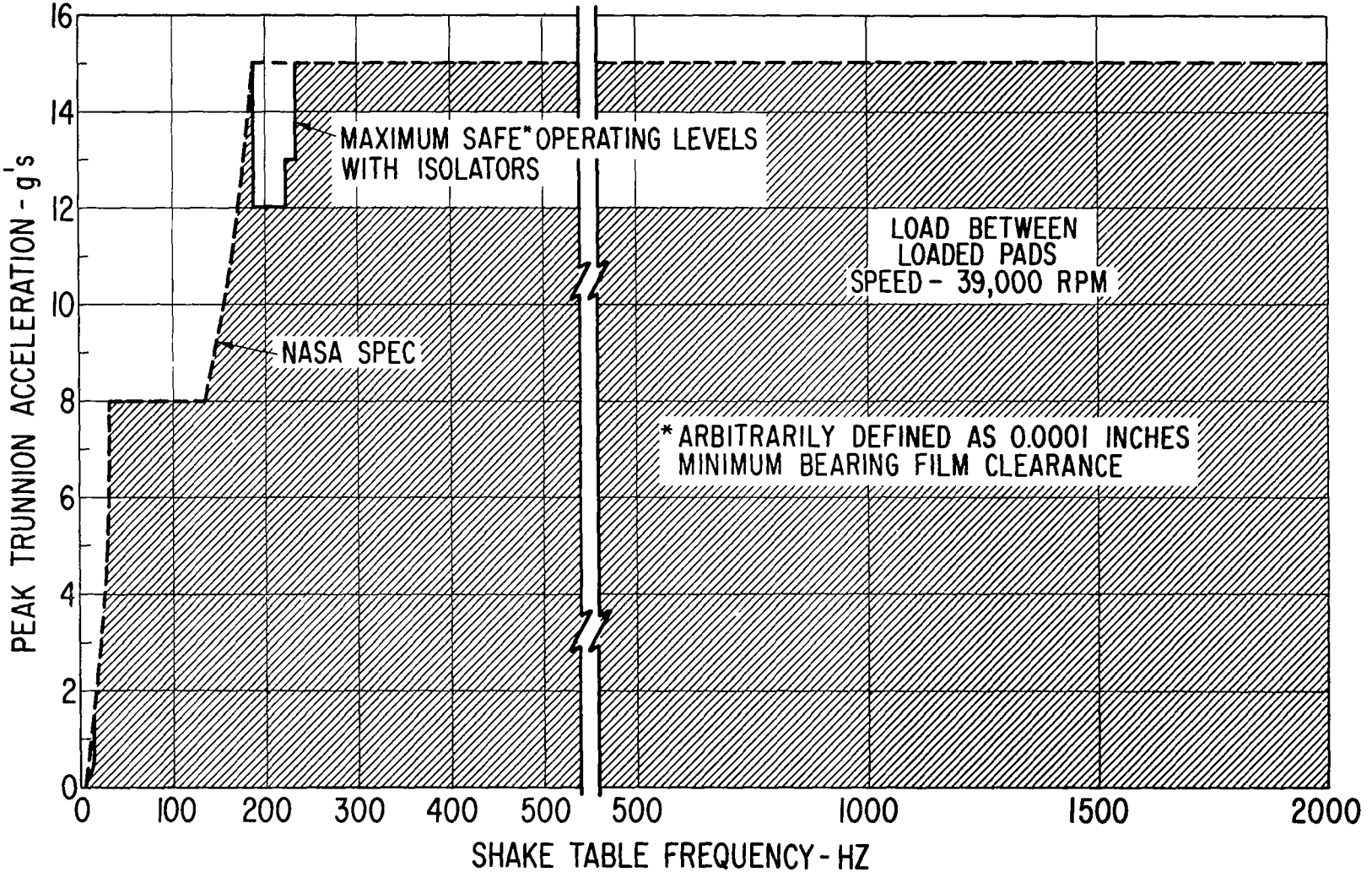

Fig. 59 Maximum Transverse Vibration Levels in the T1 Direction for Safe* Operation of the Simulator When Mounted on Vibration Isolators (Shaft Rotating at 39,000 rpm)

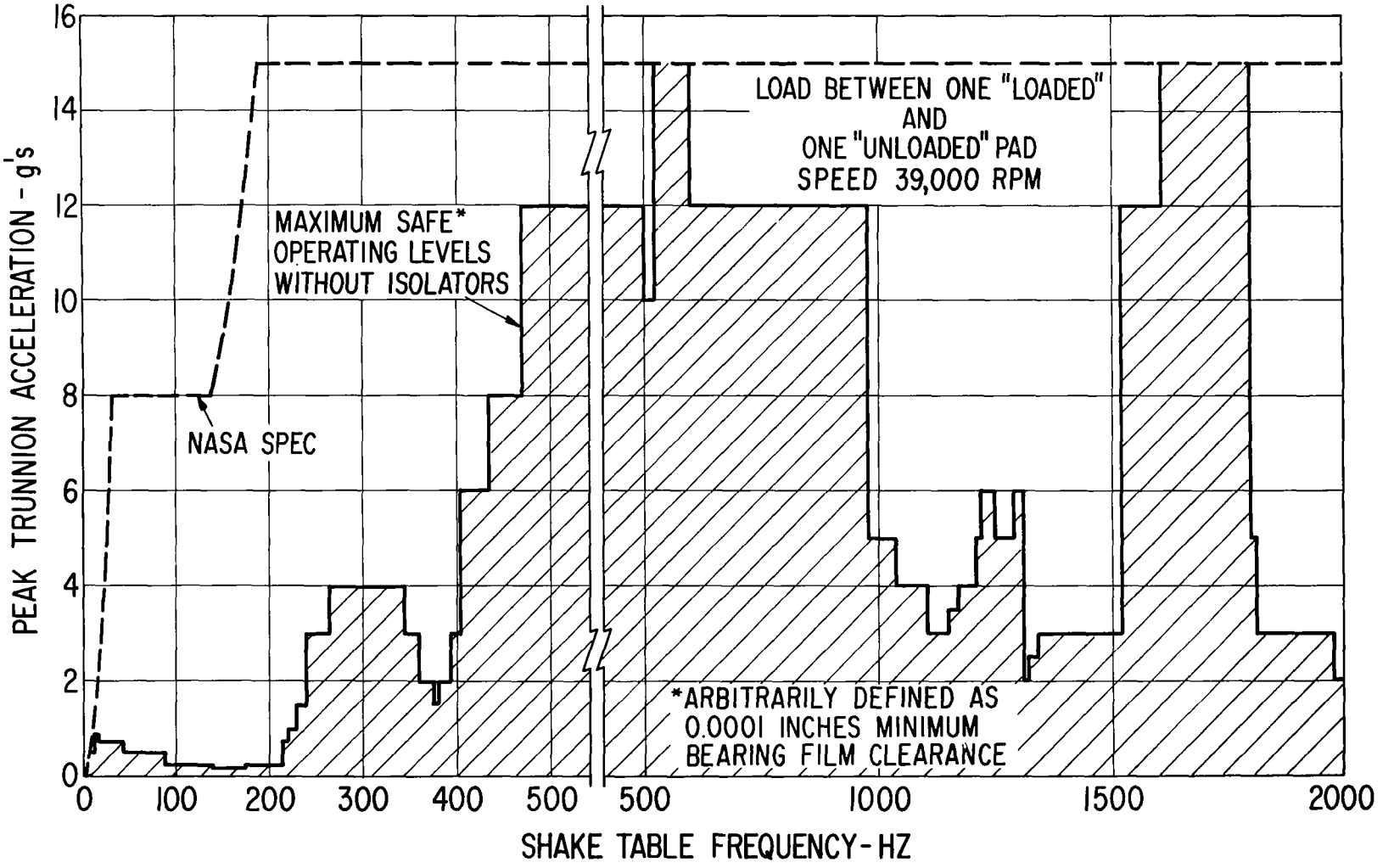

Fig. 60 Maximum Transverse Vibration Levels in the T2 Direction for Safe* Operation of the Simulator When Rigidly Mounted on Vibration Table (Shaft Rotating at 39,000 rpm)

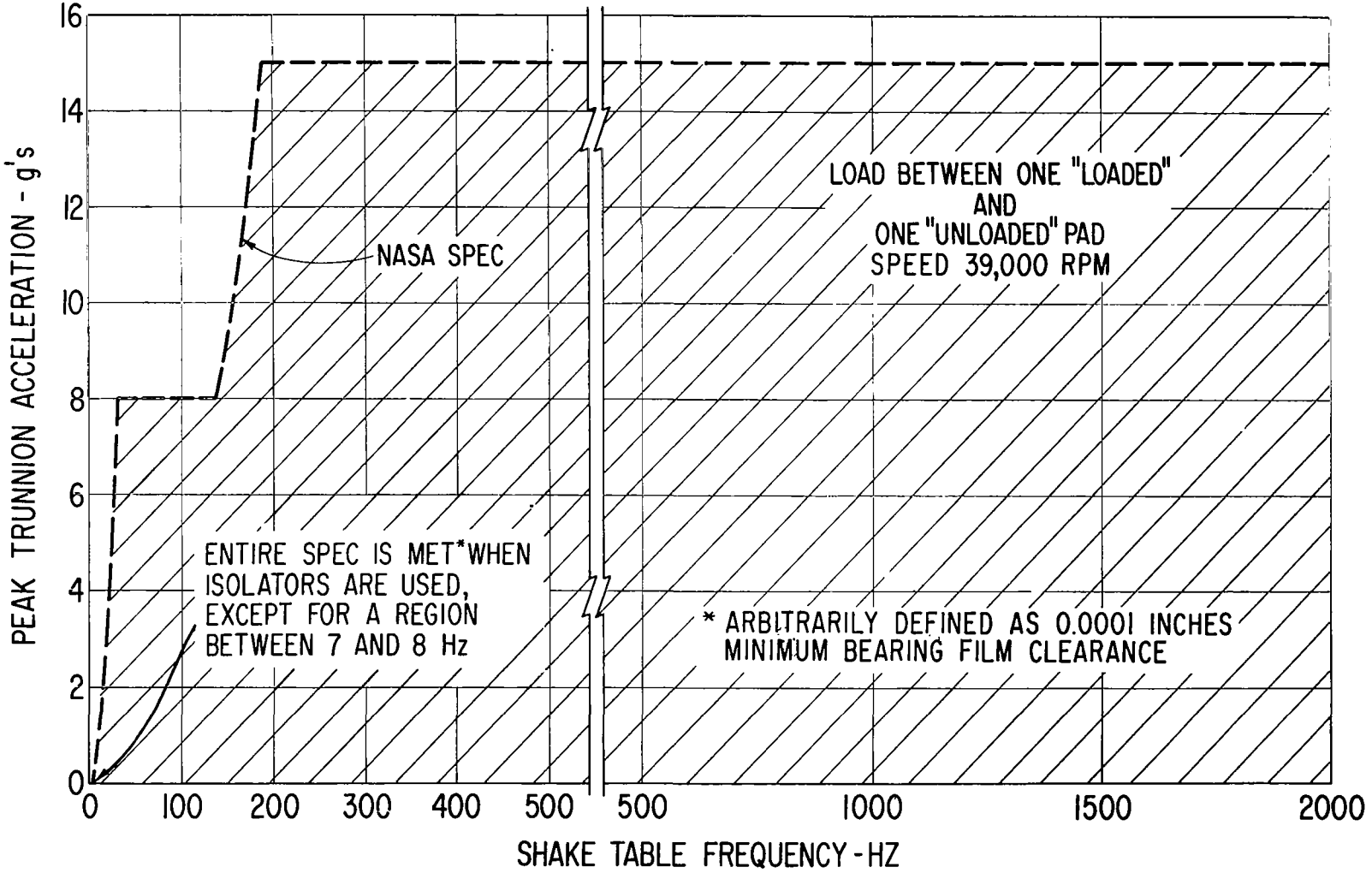

Fig. 61 Maximum Transverse Vibration Levels in the T2 Direction for Safe* Operation of the Simulator When Mounted on Vibration Isolators (Shaft Rotating at 39,000 rpm)

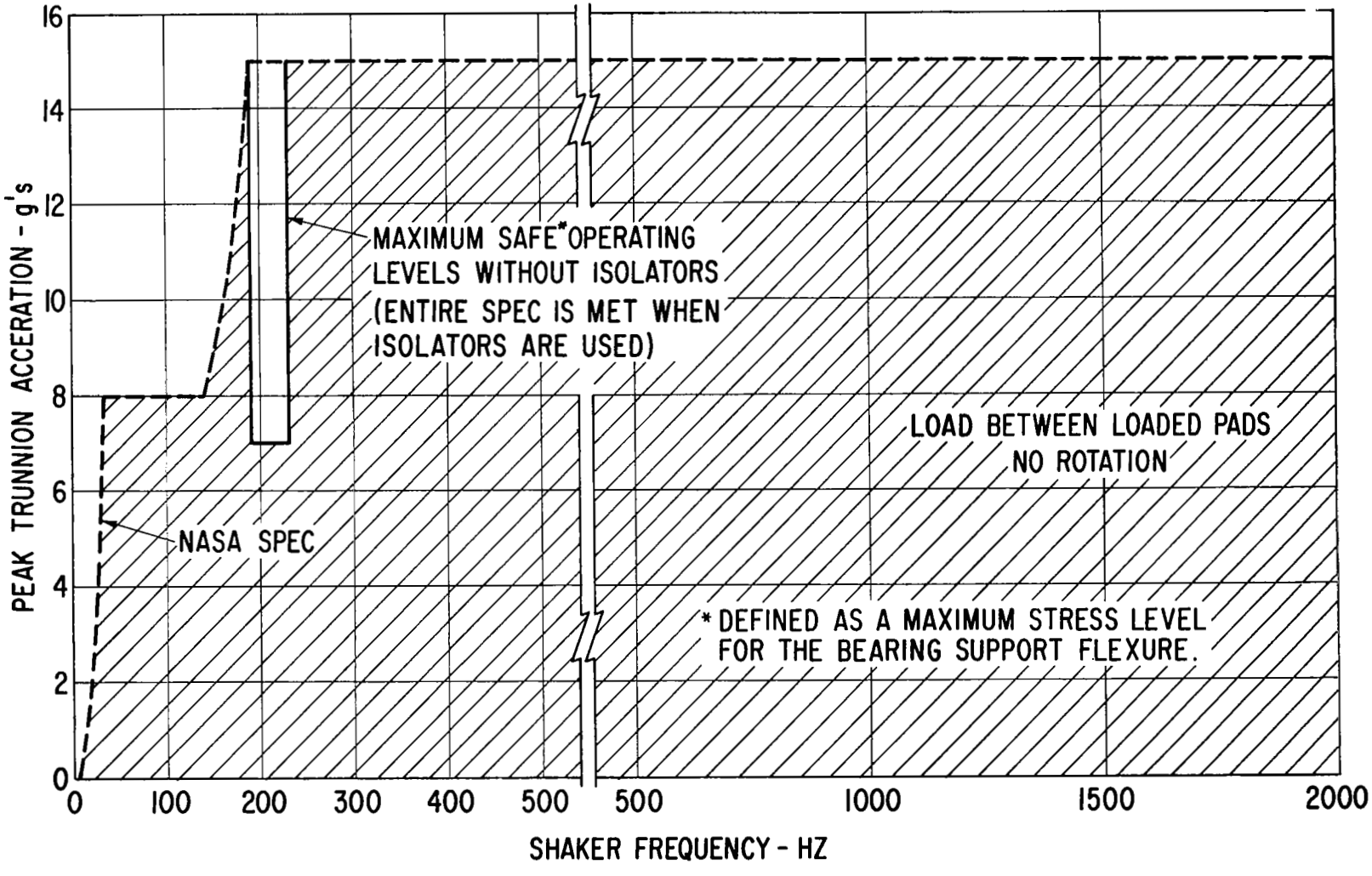

Fig. 62 Maximum Transverse Vibration Levels in the T1 Direction for Safe* Operation of the Simulator With Nonrotating Shaft, and With and Without Vibration Isolators

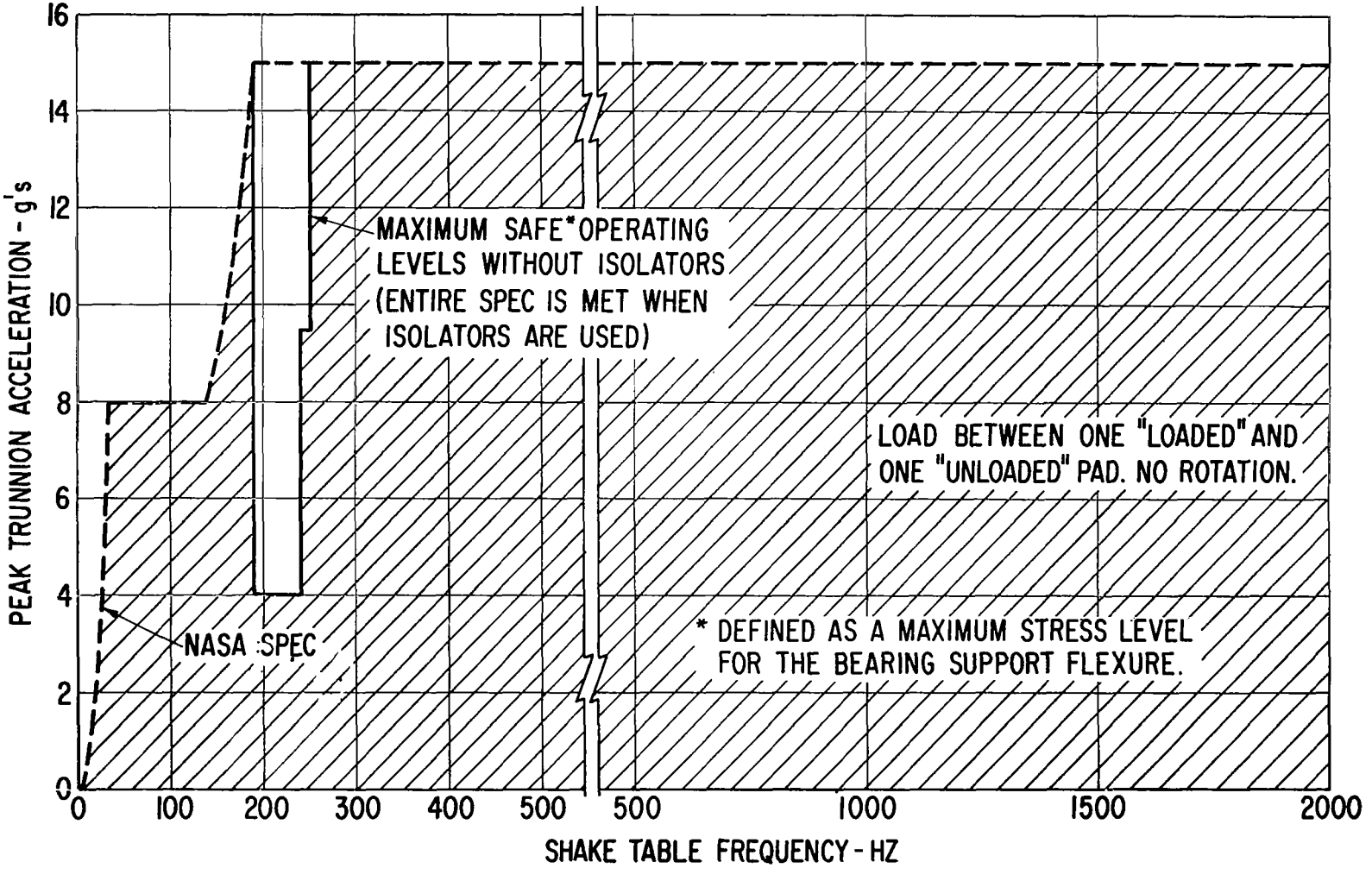

Fig. 63 Maximum Transverse Vibration Levels in the T2 Direction for Safe* Operation of the Simulator With Nonrotating Shaft, and With and Without Vibration Isolators

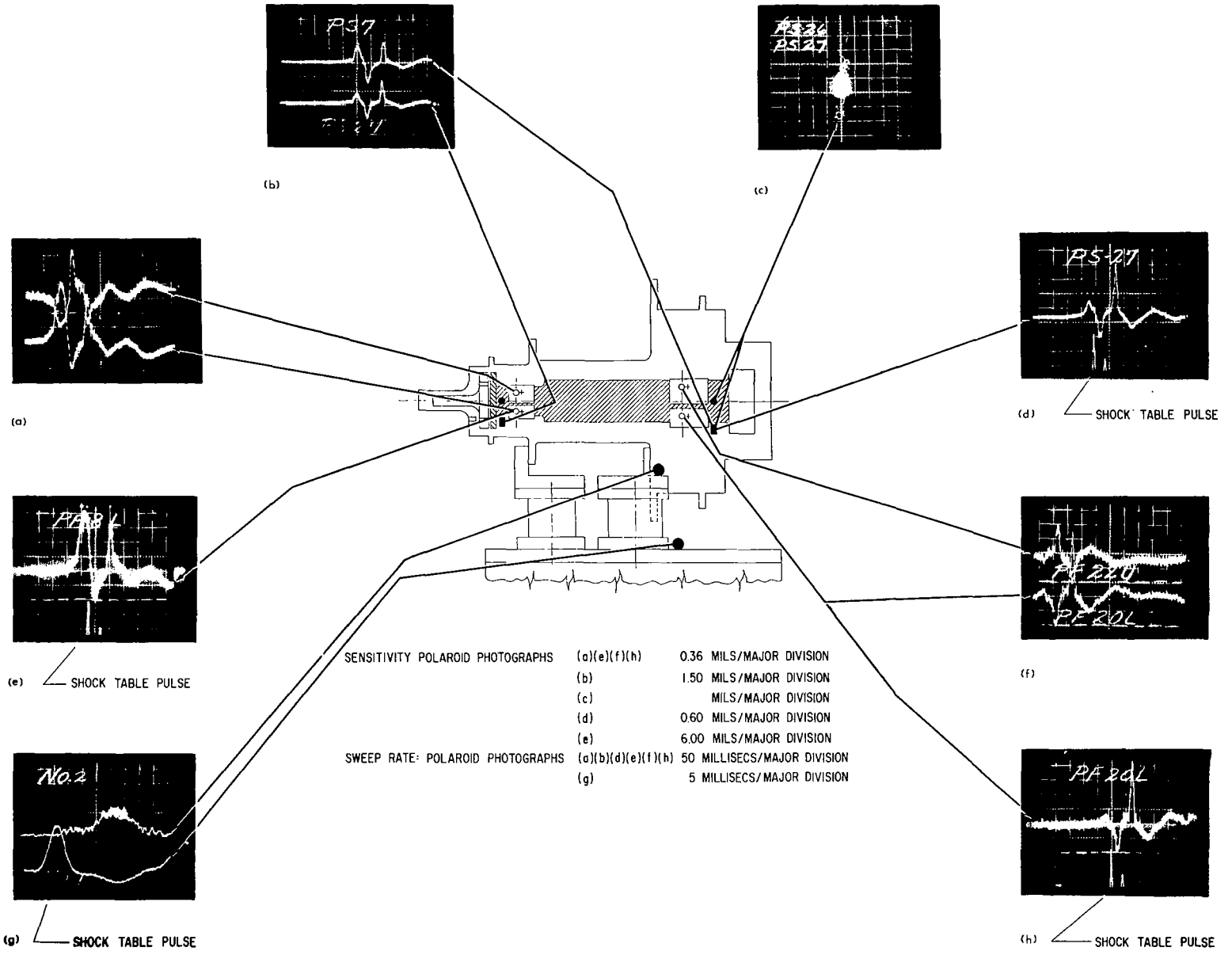

Fig. 64 Data Displays of Transverse Shock Responses With Simulator Mounted on Vibration and Shock Isolators (Shaft Rotating at 39,000 rpm)

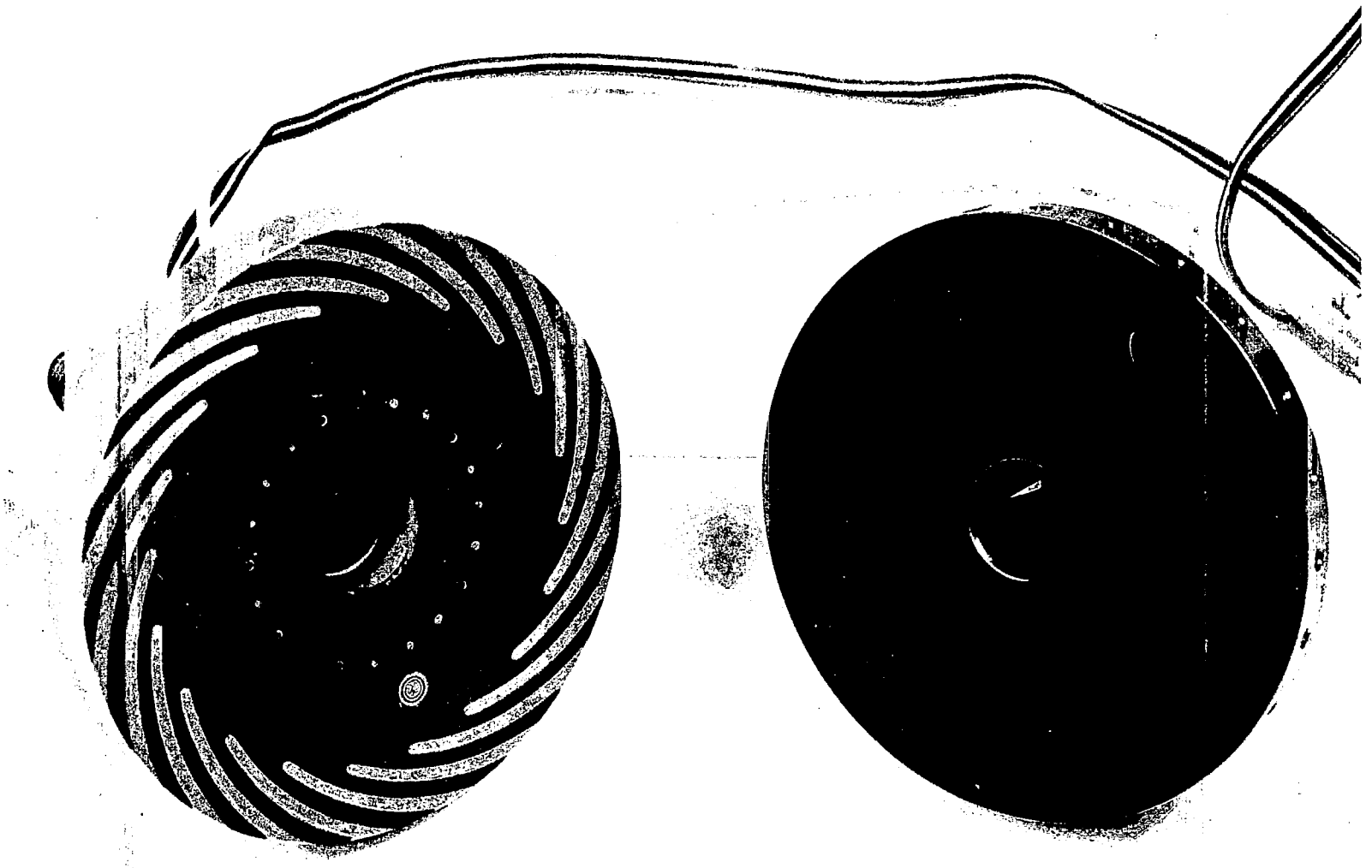

Fig. 65 Forward Thrust Plate and Runner, Inspection 1, After Cleaning

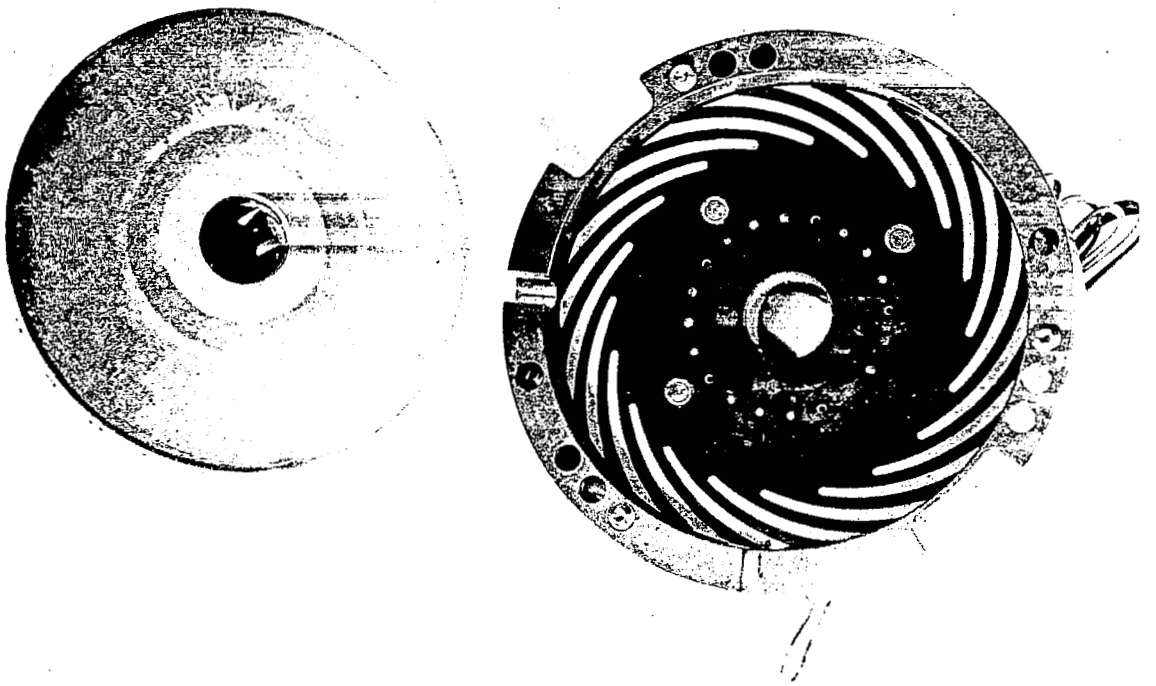

(a) Before Cleaning

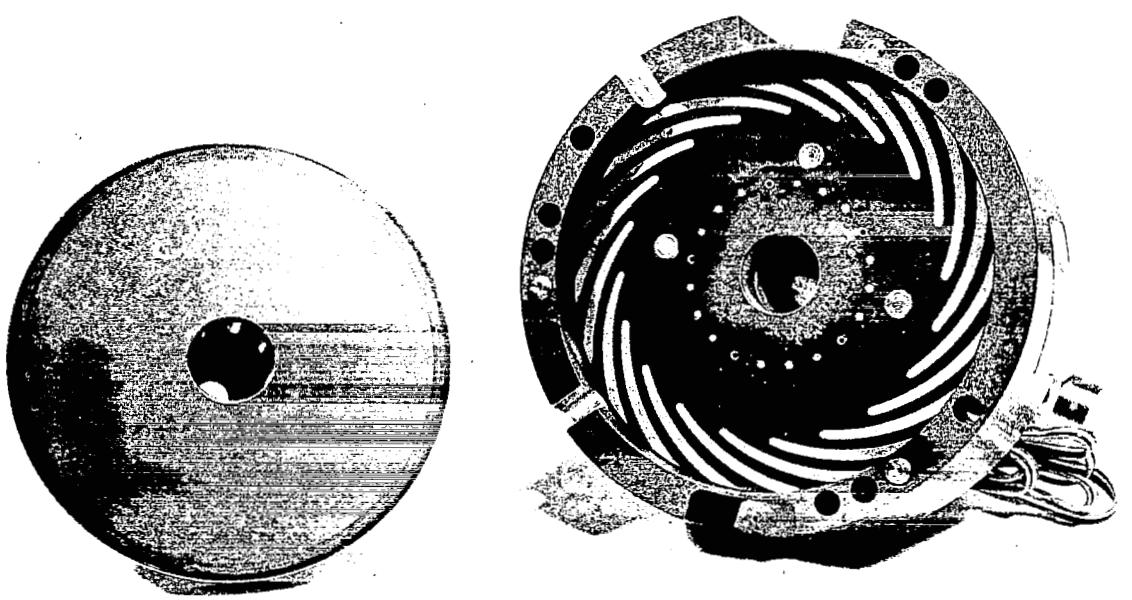

(b) After Cleaning

Fig. 66 Forward Thrust Plate and Runner, Inspection 2

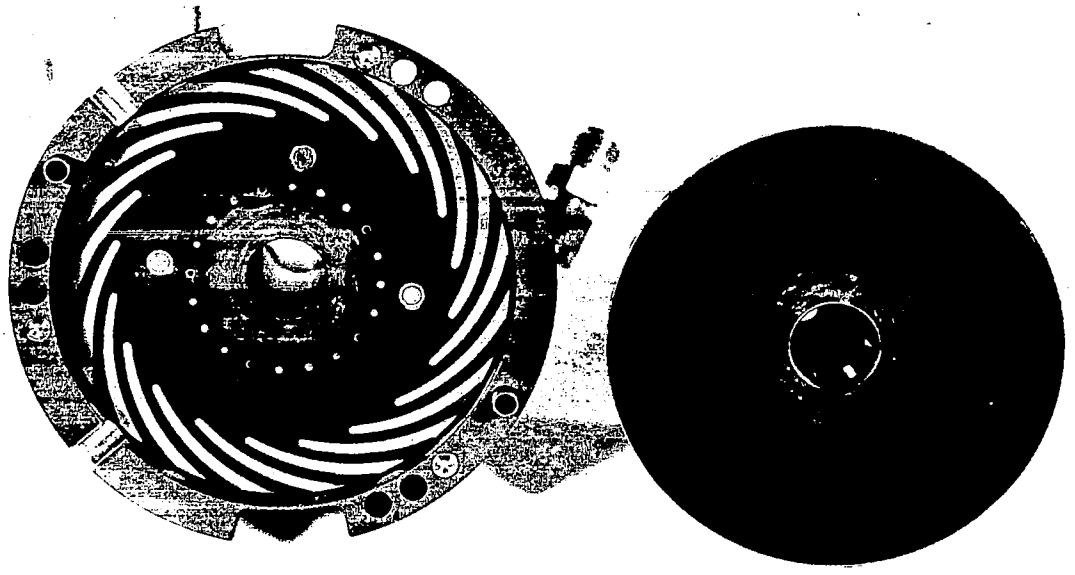

(a) Before Cleaning

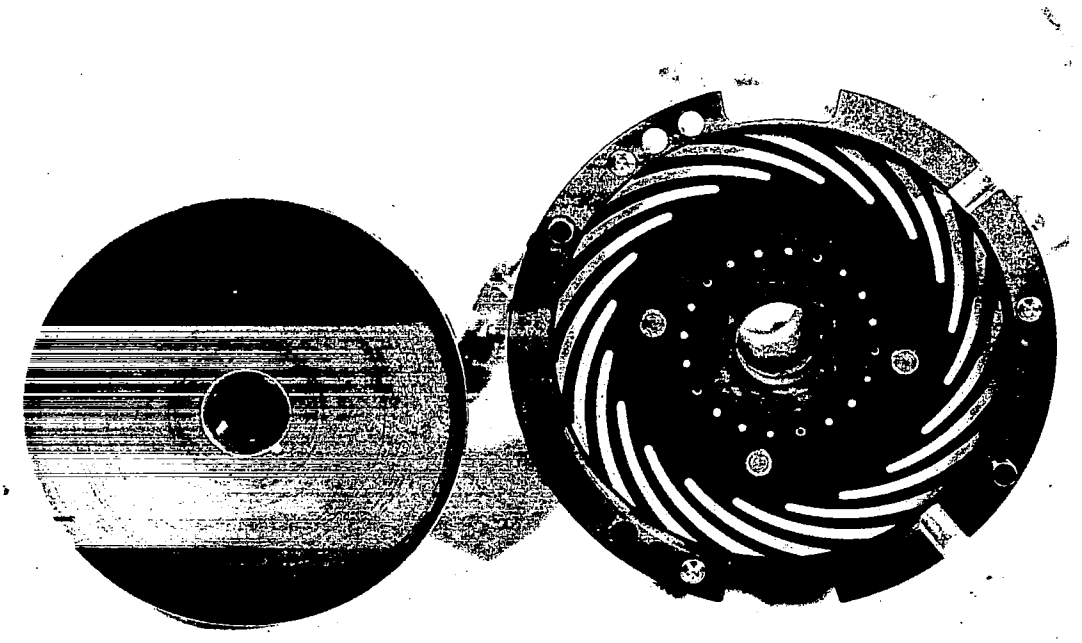

(b) After Cleaning

Fig. 67 Forward Thrust Plate and Runner, Inspection 3

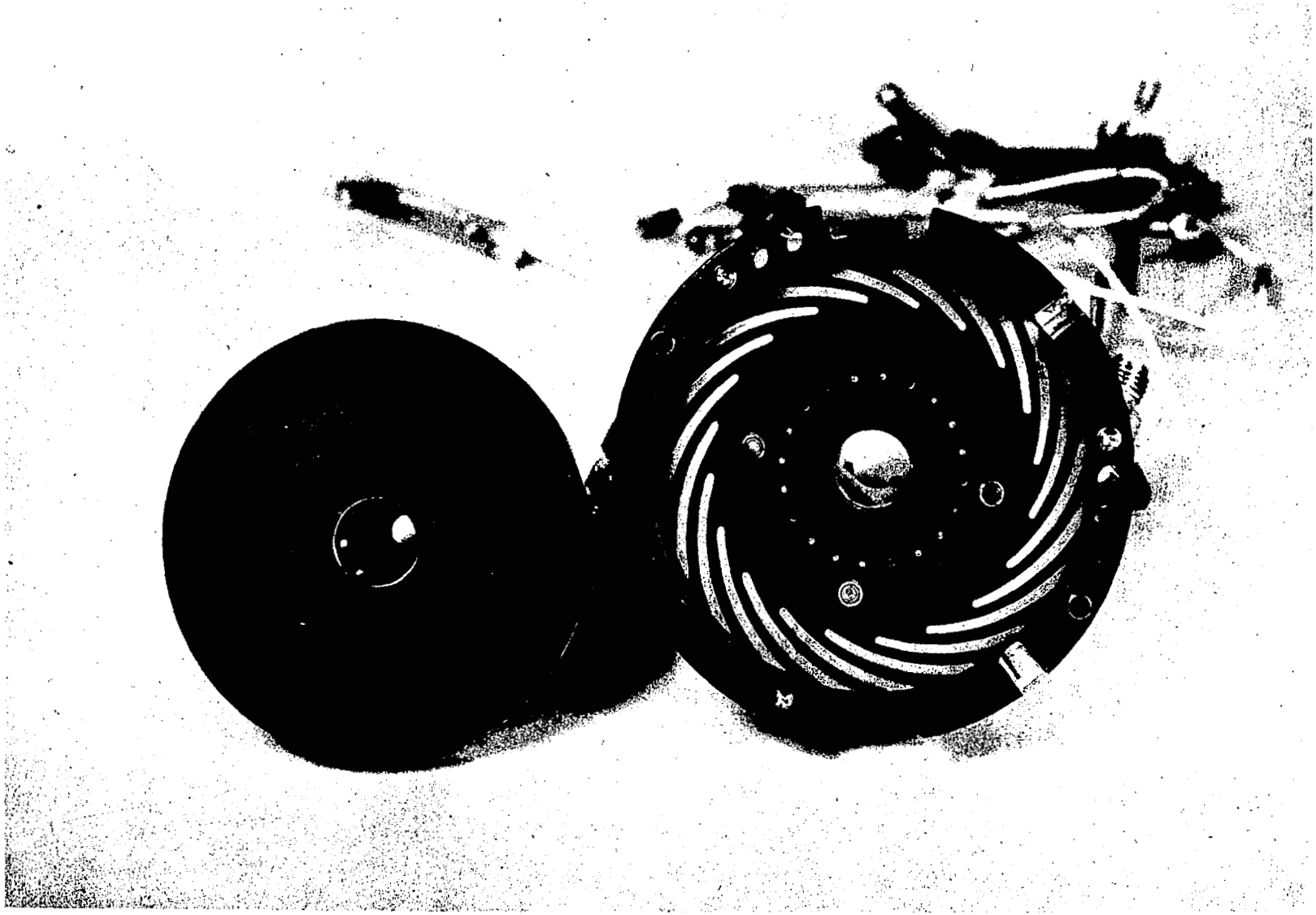

Fig. 68 Forward Thrust Plate and Runner, Inspection 4, Before Cleaning

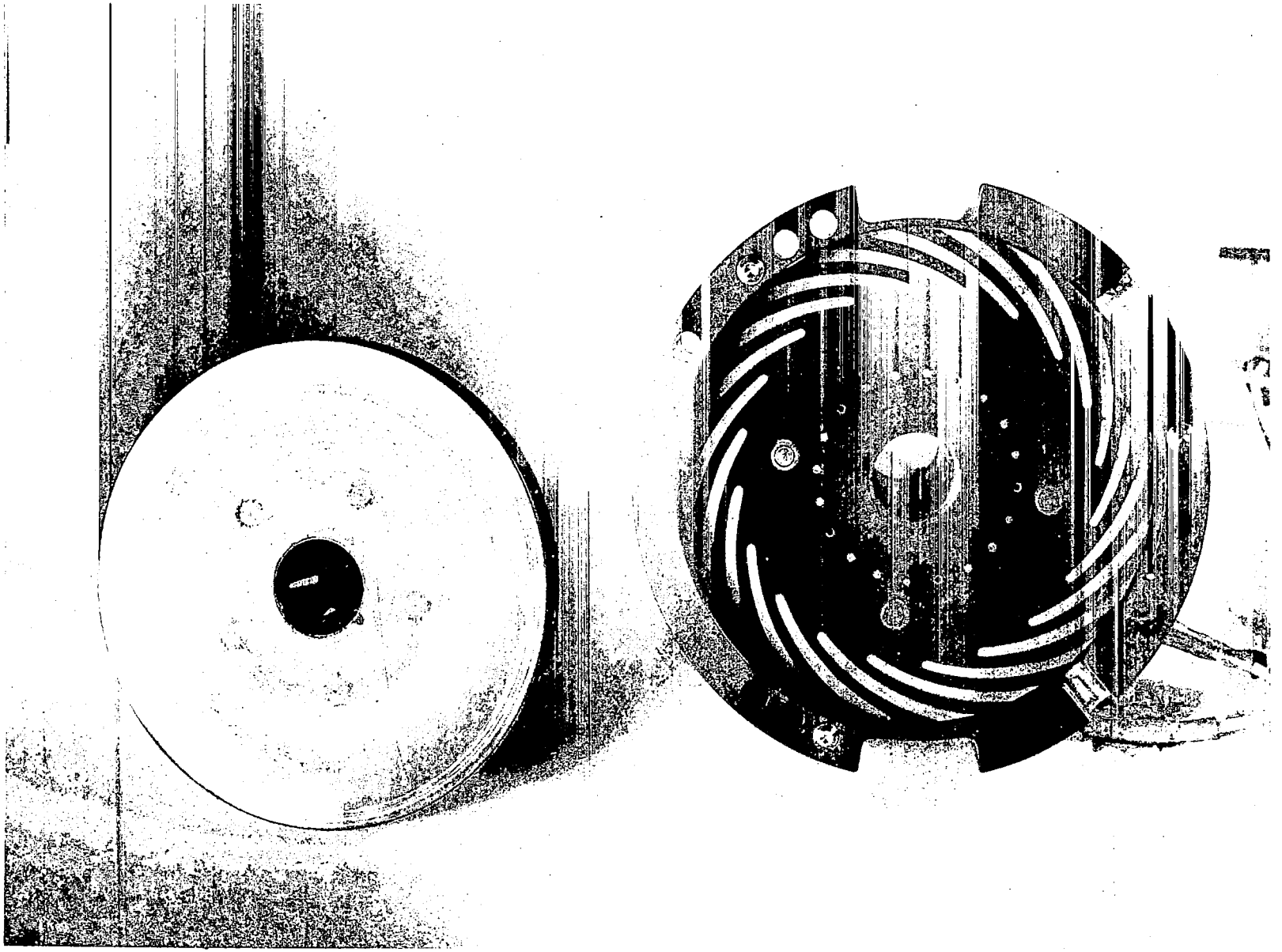

Fig. 69 Forward Thrust Plate and Runner Inspection 5, Before Cleaning

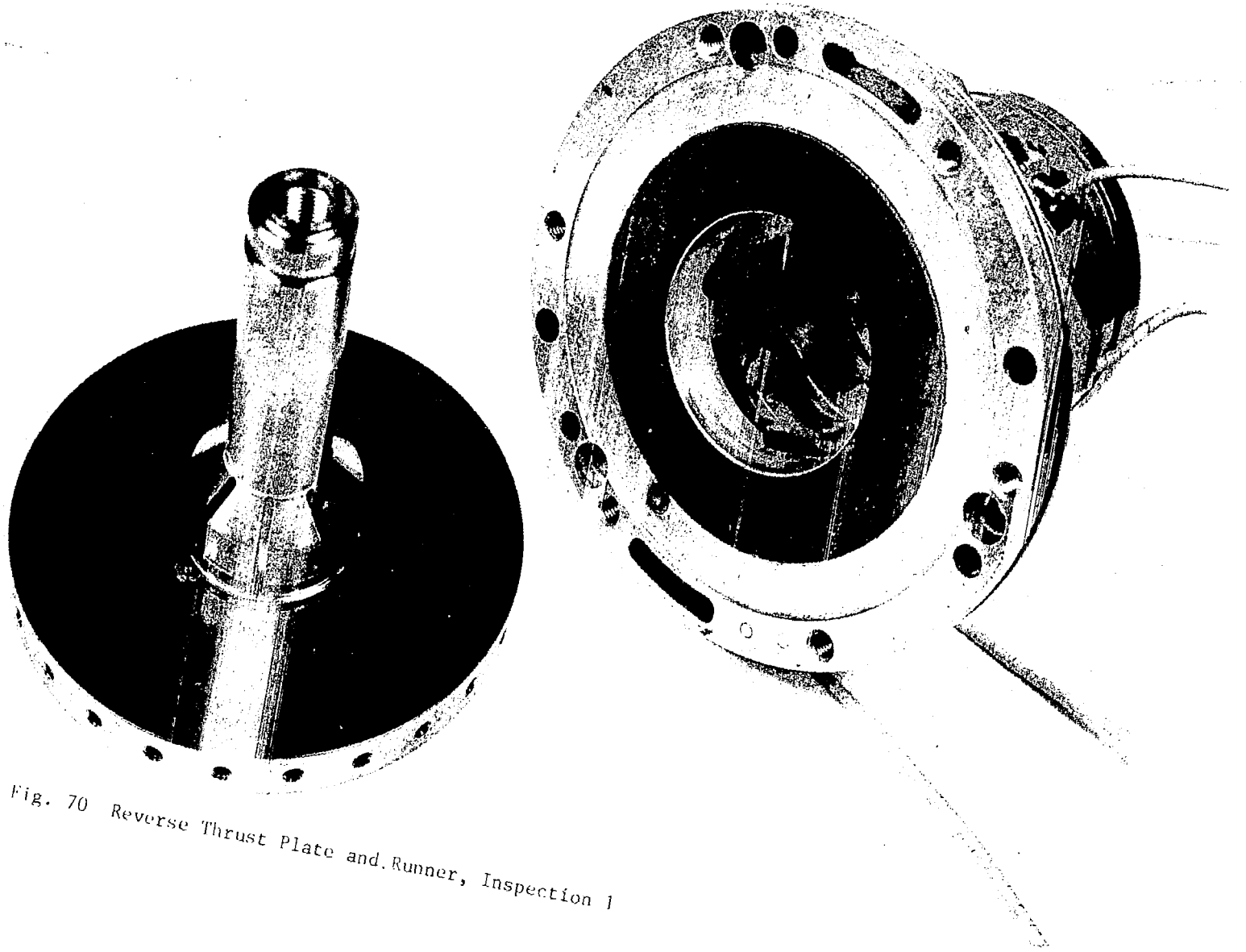

Fig. 70 Reverse Thrust Plate and Runner, Inspection 1

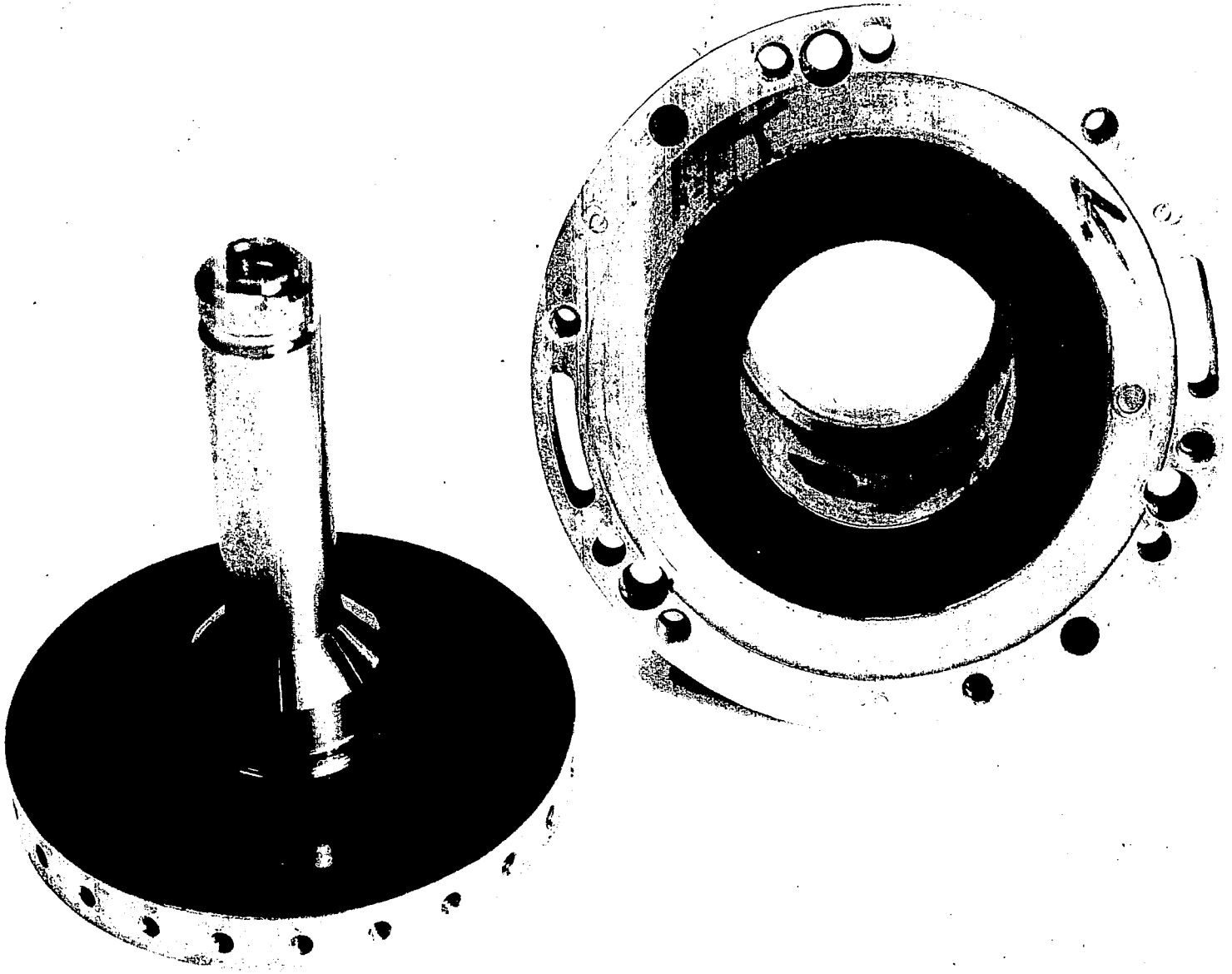

Fig. 71 Reverse Thrust Plate and Runner Inspection 5

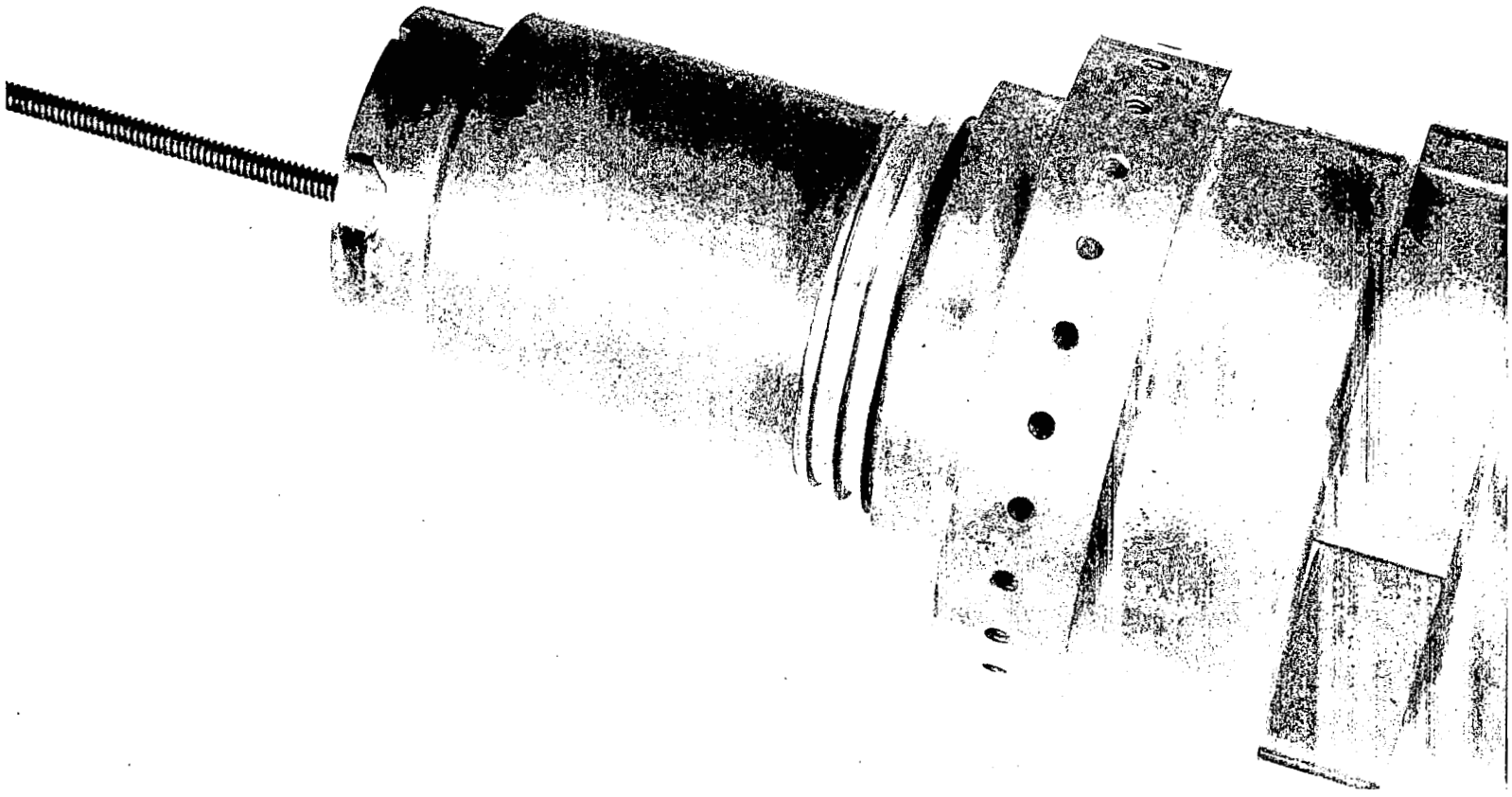

Fig. 72 Compressor Bearing Journal, Inspection 1

Fig. 73 Compressor Bearing Journal, Inspection 5

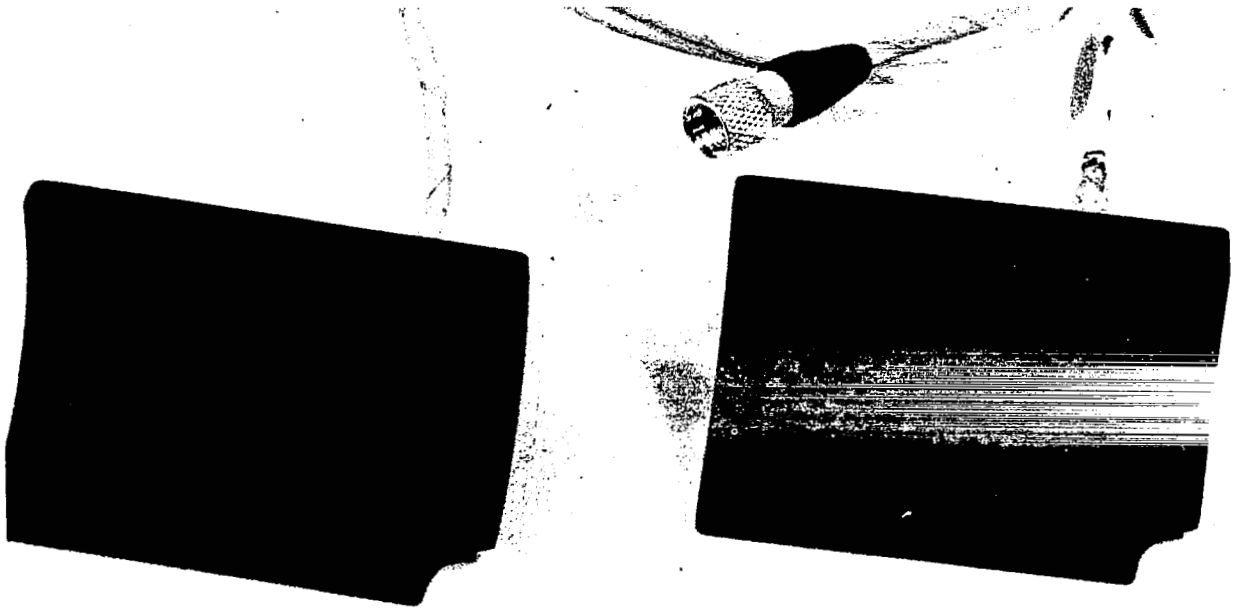

(a)

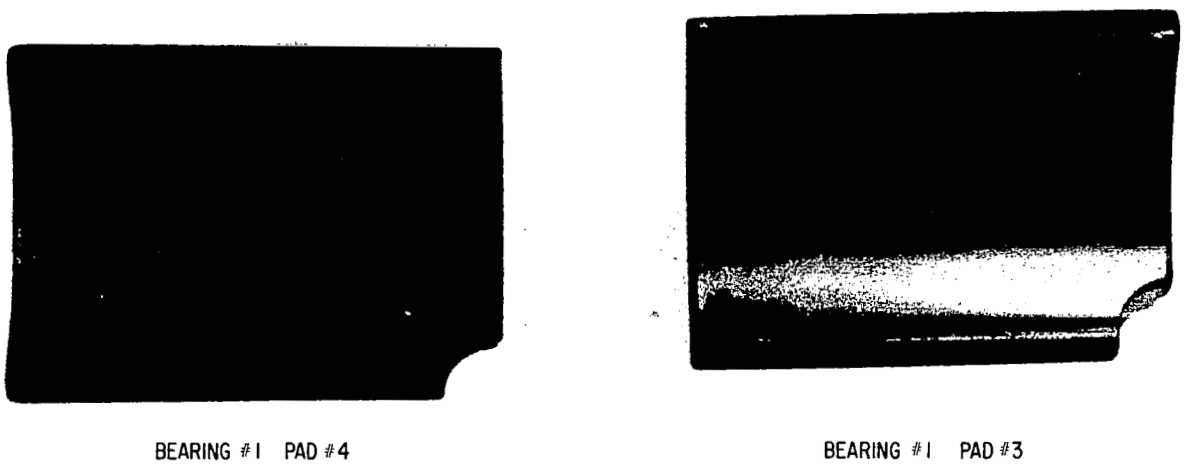

(b)

Fig. 74 Compressor Journal Bearing Pads, Face View, Inspection 1

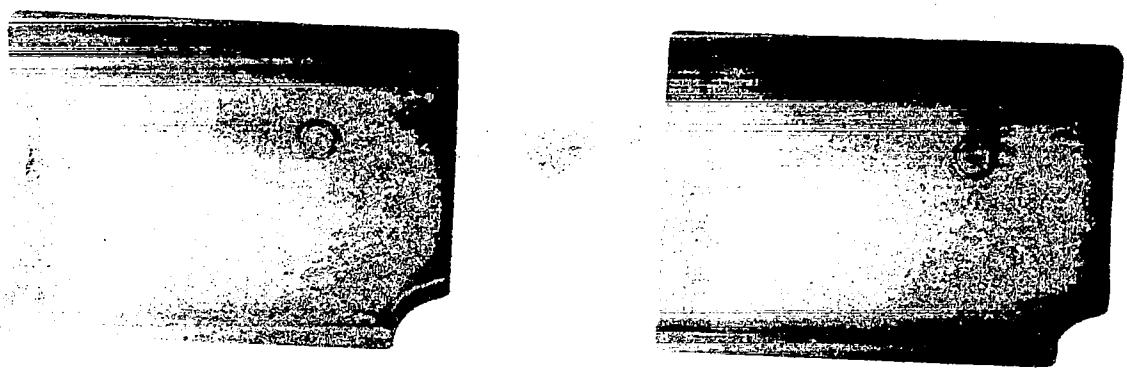

BEARING #1 PAD #1

BEARING #1 PAD #2

(a)

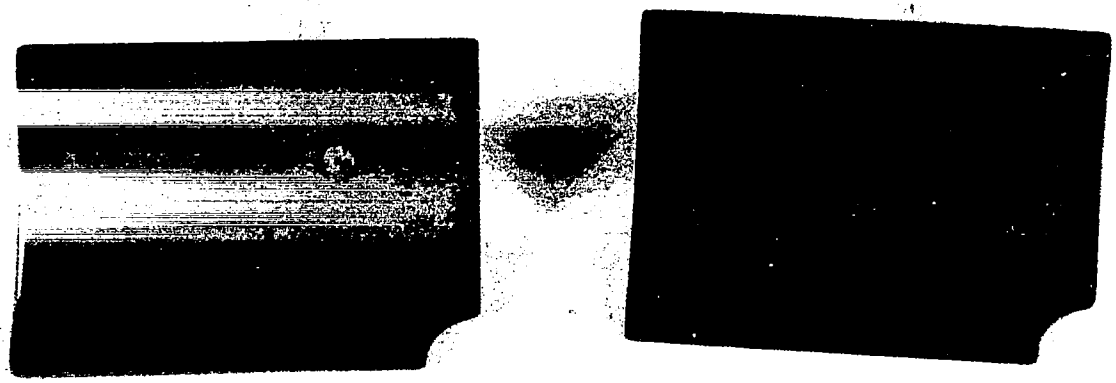

BEARING #1 PAD #4

BEARING #1 PAD #3

(b)

Fig. 75 Compressor Journal Bearing Pads, Face View, Inspection 5

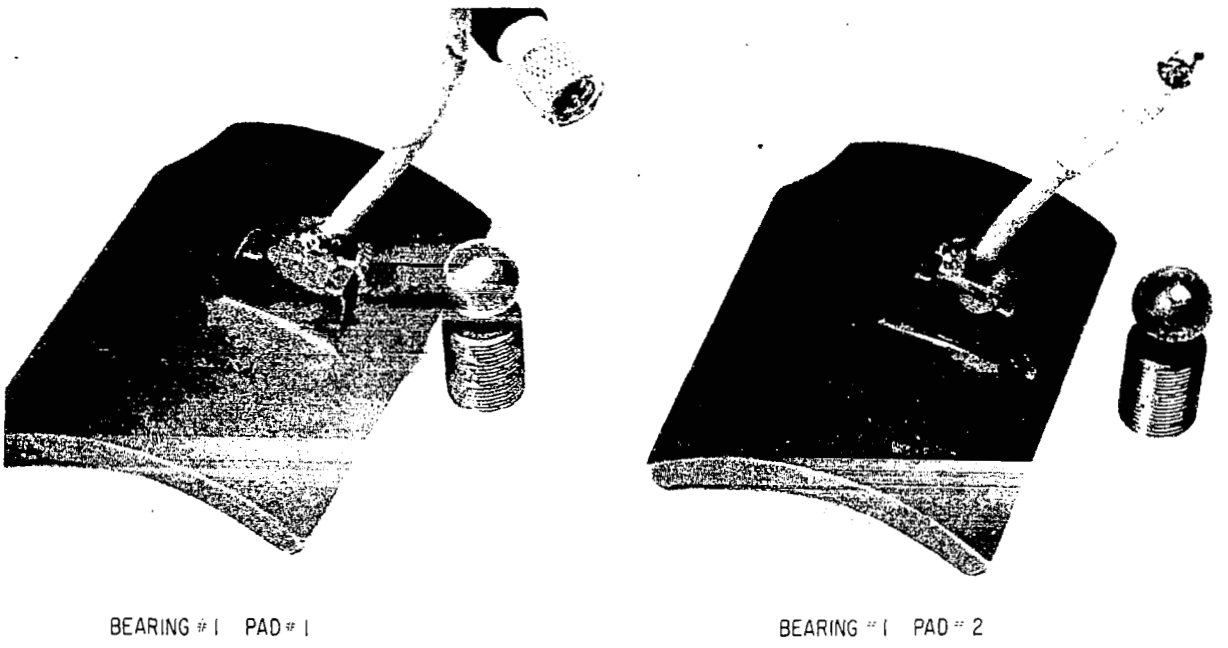

Fig. 76 Compressor Journal Bearing Pads, Rear View with Pivots, Inspection 1

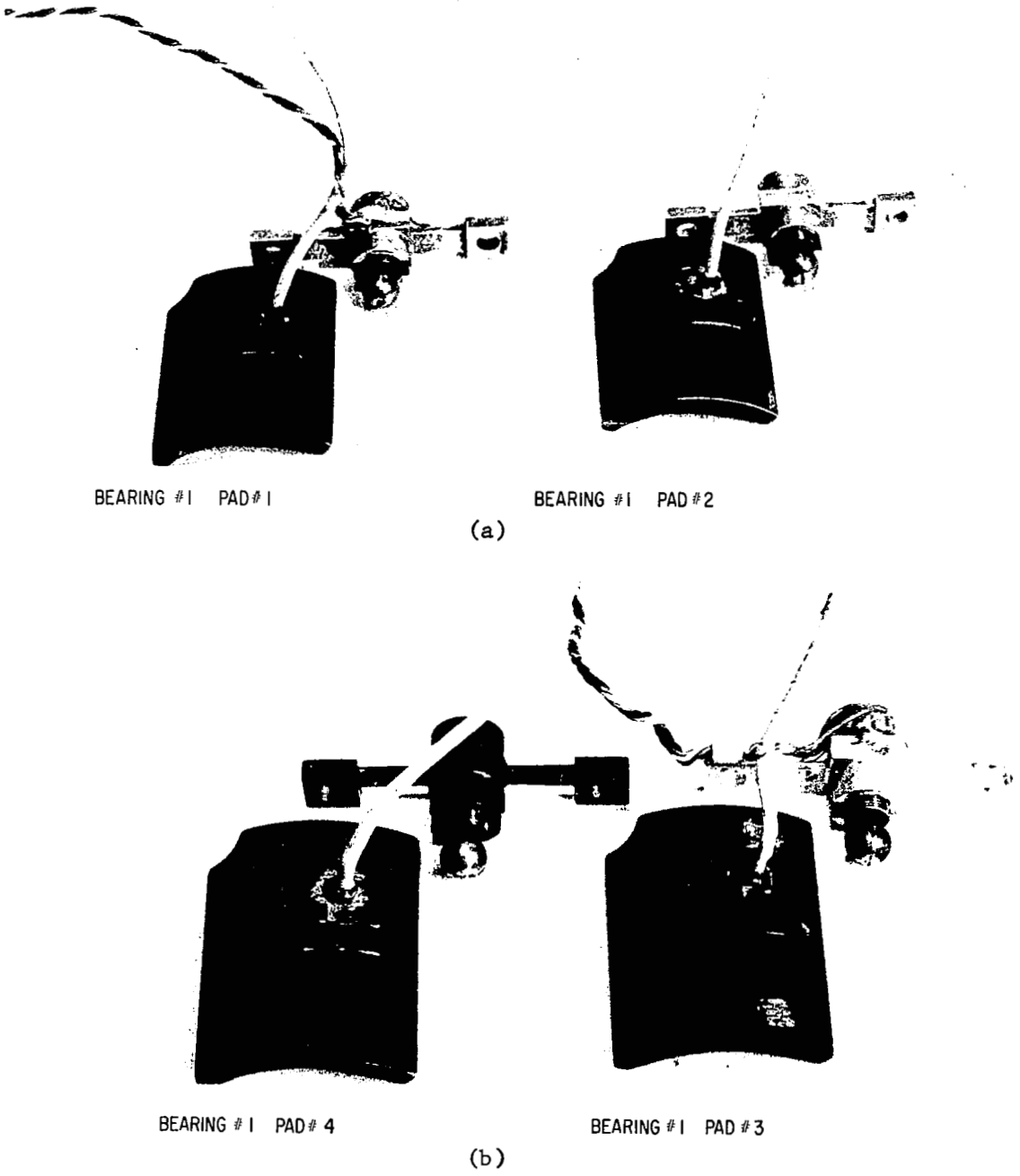

Fig. 77 Compressor Journal Bearing Pads, Rear View with Pivots, Inspection 4

(a) Socket

(b) Ball

Fig. 78 Compressor Journal Bearing Pad Pivot Surfaces, Inspection 4

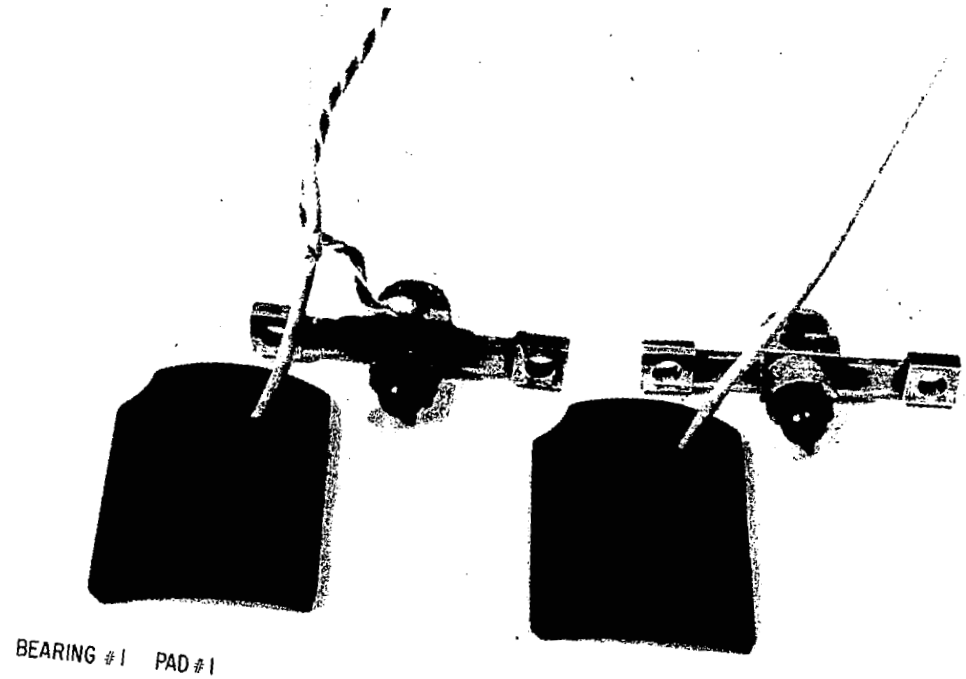

(a)

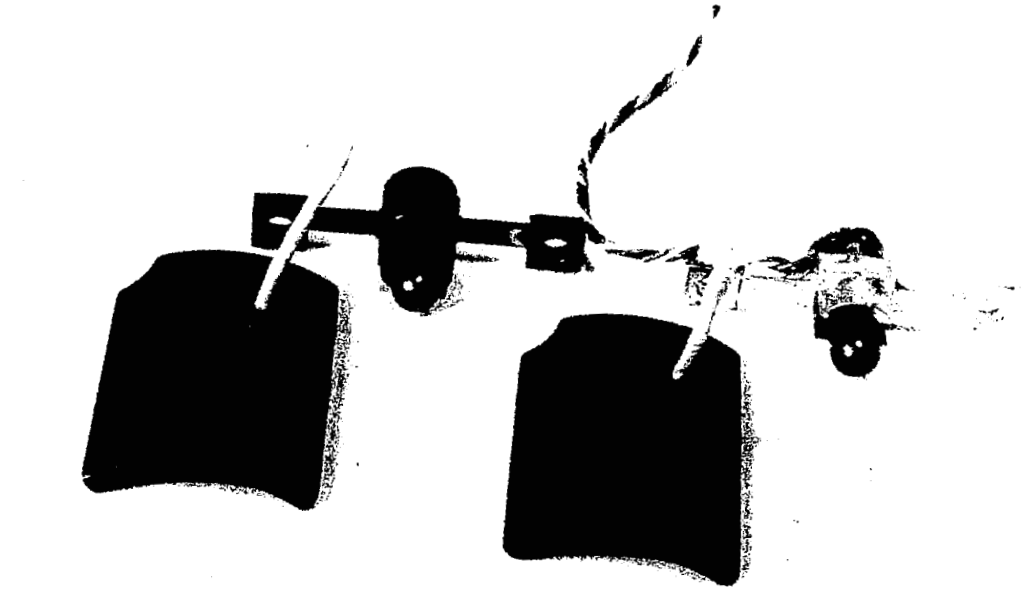

(b)

Fig. 79 Compressor Journal Bearing Pads, Rear View with Pivots, Inspection 5

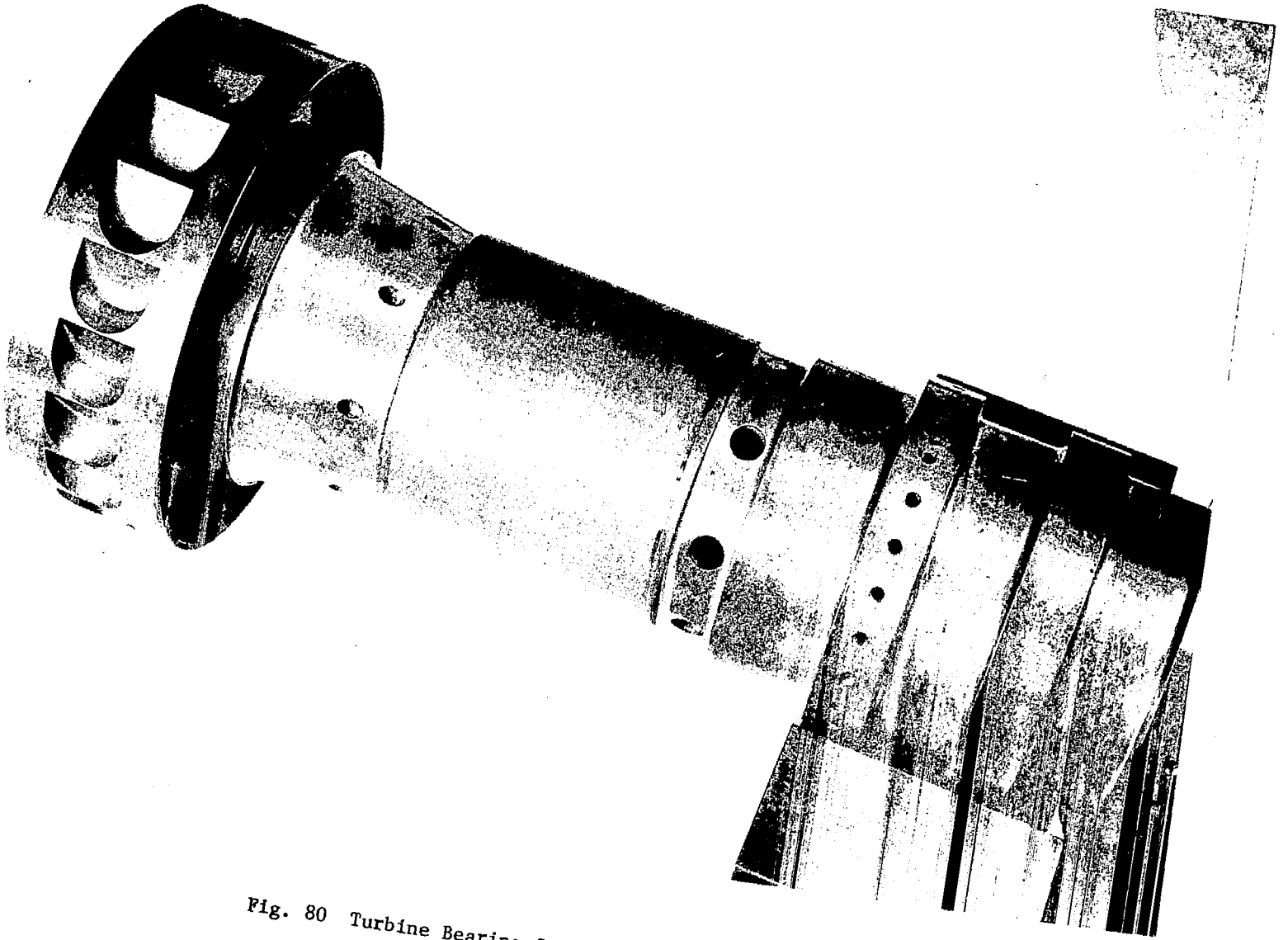

Fig. 80 Turbine Bearing Journal, Inspection 1

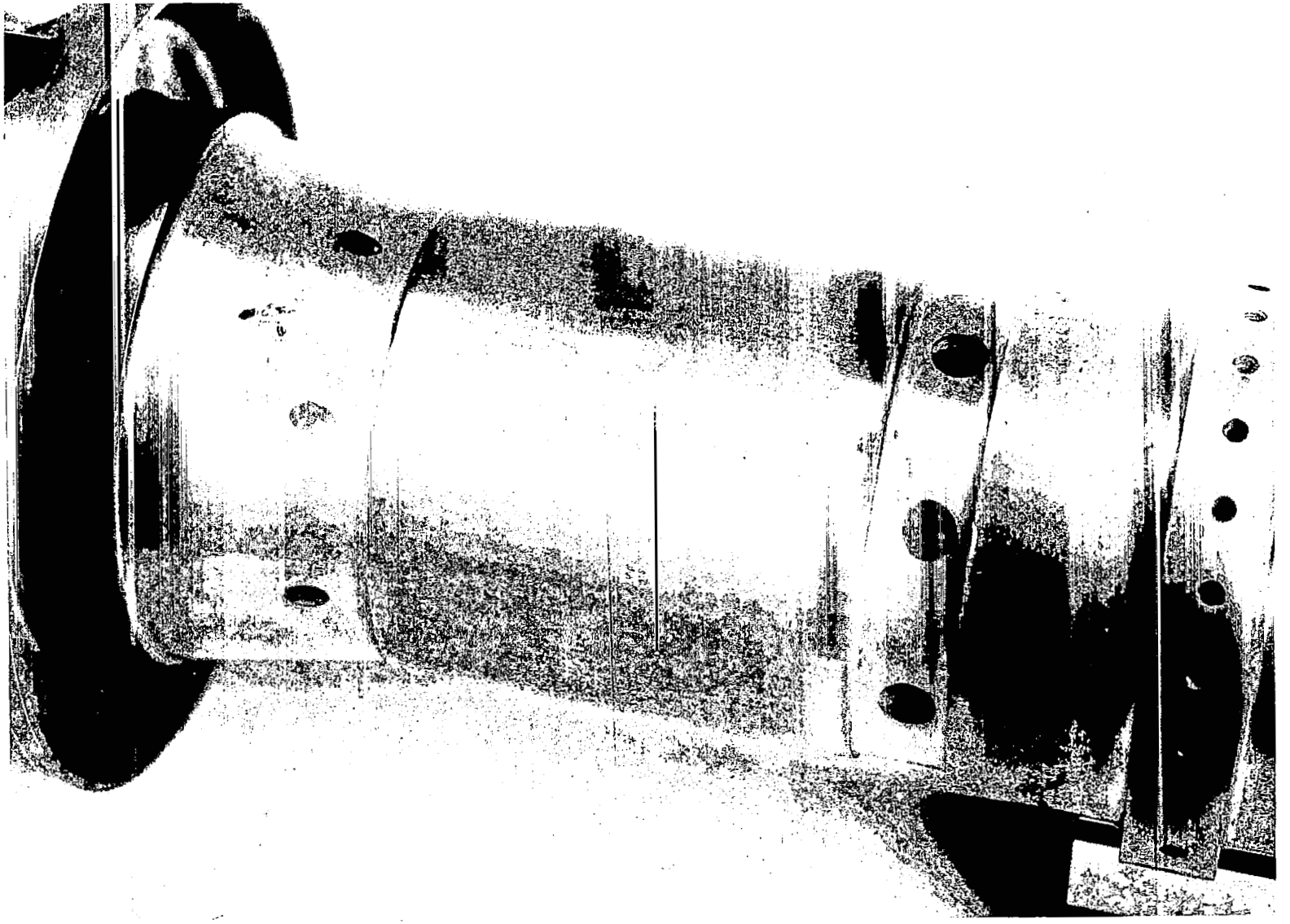

Fig. 81 Turbine Bearing Journal, Inspection 5

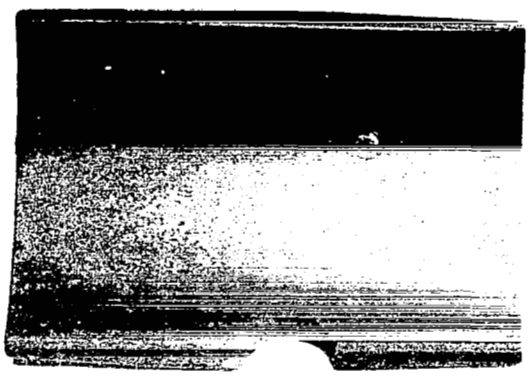

BEARING # 2 PAD # 1

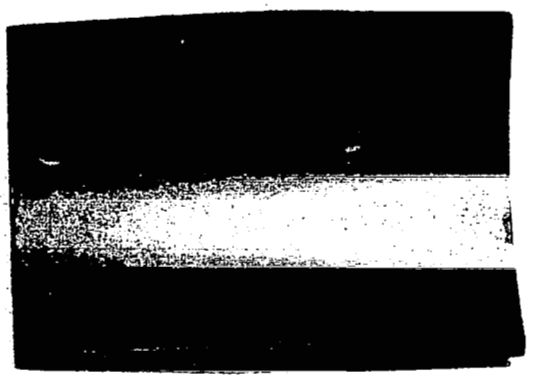

BEARING # 2 PAD # 2

(a)

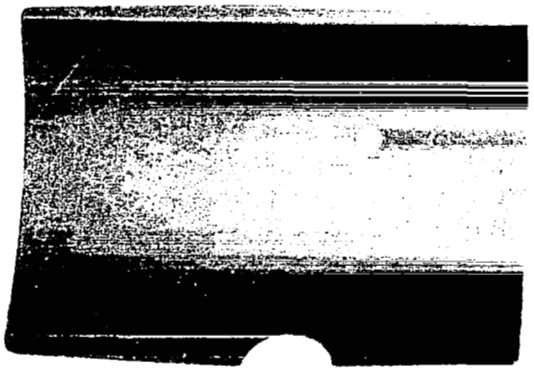

BEARING # 2 PAD # 4

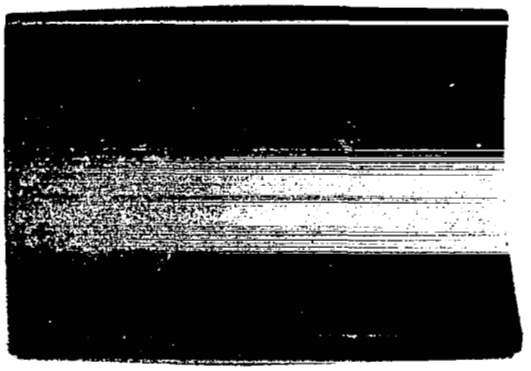

BEARING # 2 PAD # 3

(b)

Fig. 82 Turbine Journal Bearing Pads, Face View, Inspection 1

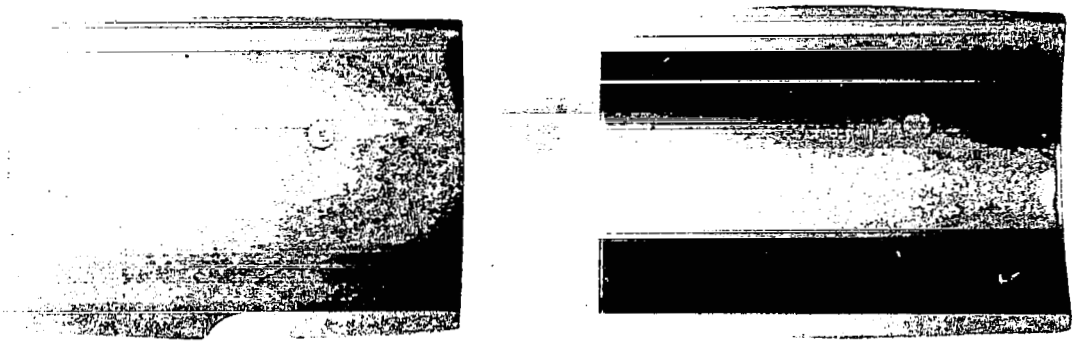

BEARING # 2 PAD # 1

BEARING # 2 PAD #2

(a)

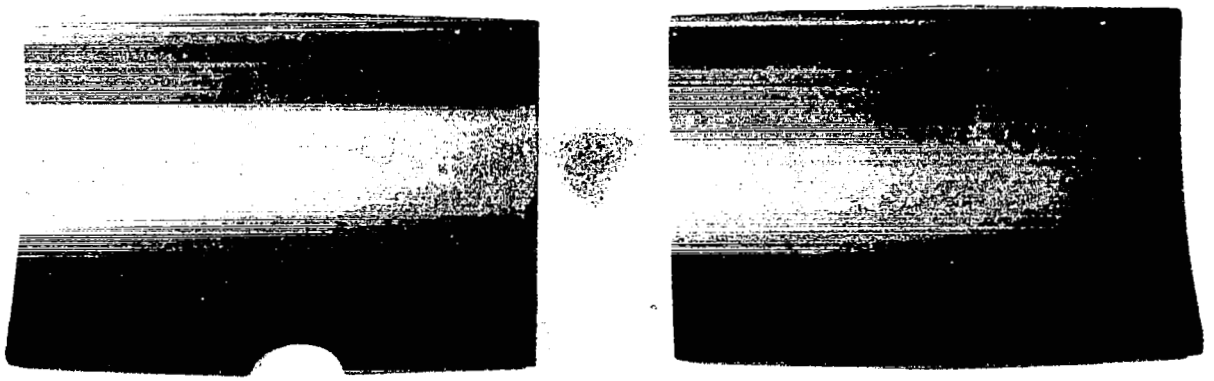

BEARING # 2 PAD # 4

BEARING # 2 PAD # 3

(b)

Fig. 83 Turbine Journal Bearing Pads, Face View, Inspection 2

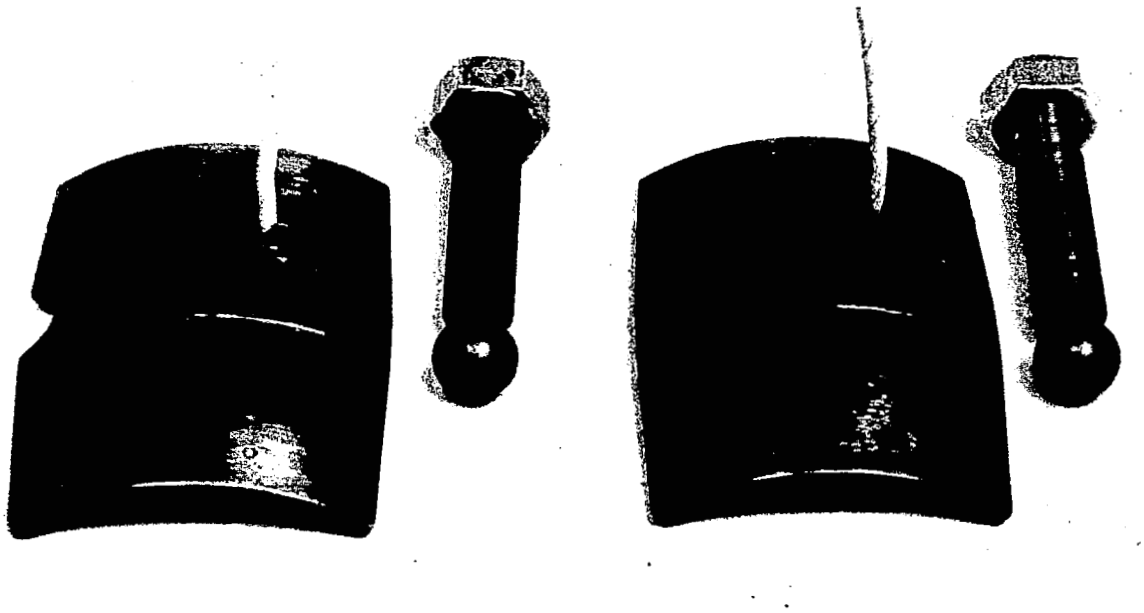

(a)

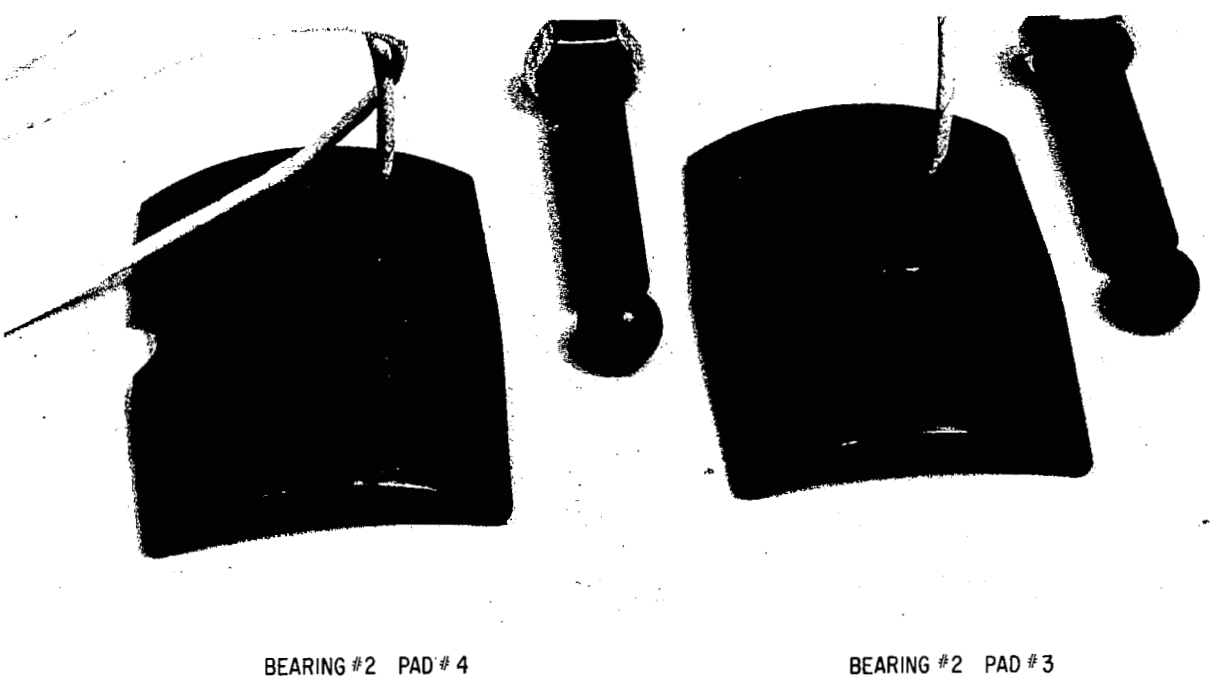

(b)

Fig. 84 Turbine Journal Bearing Pads, Rear View with Pivots, Inspection 1

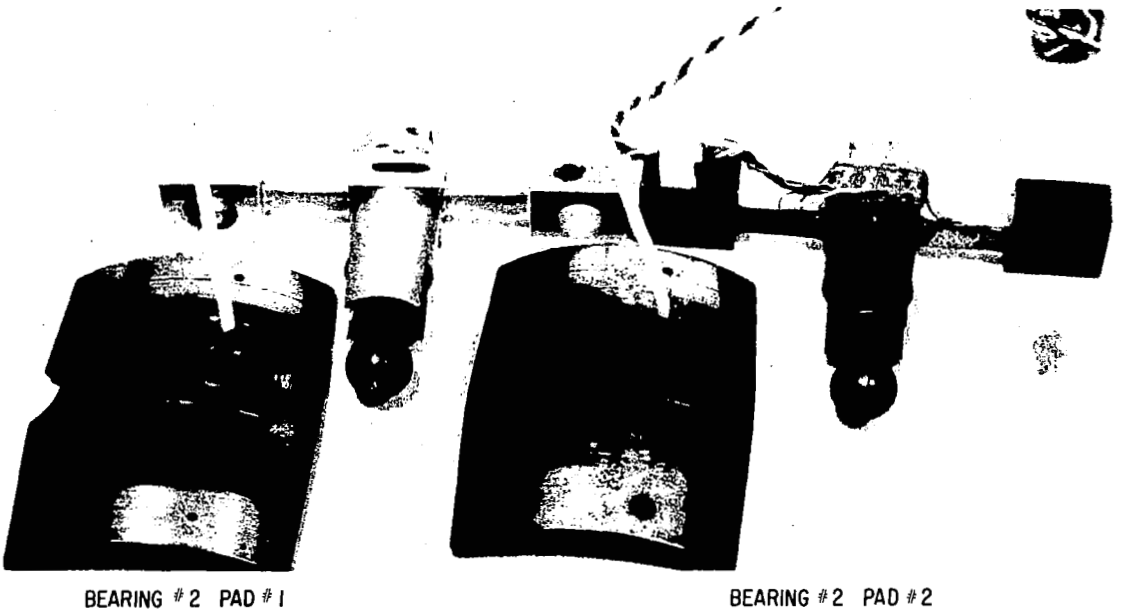

(a)

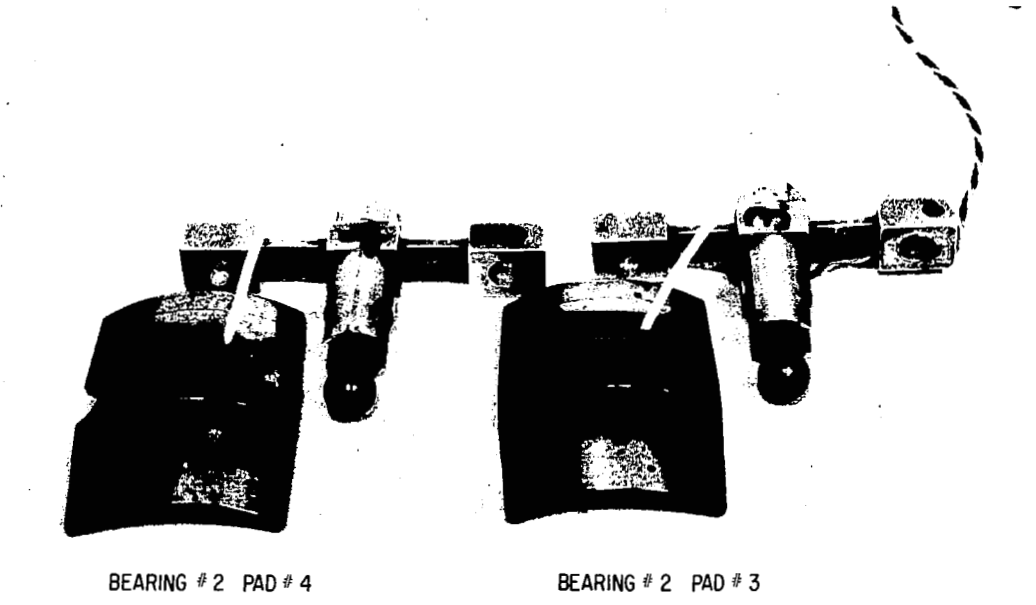

(b)

Fig. 85 Turbine Journal Bearing Pads, Rear View with Pivots, Inspection 4

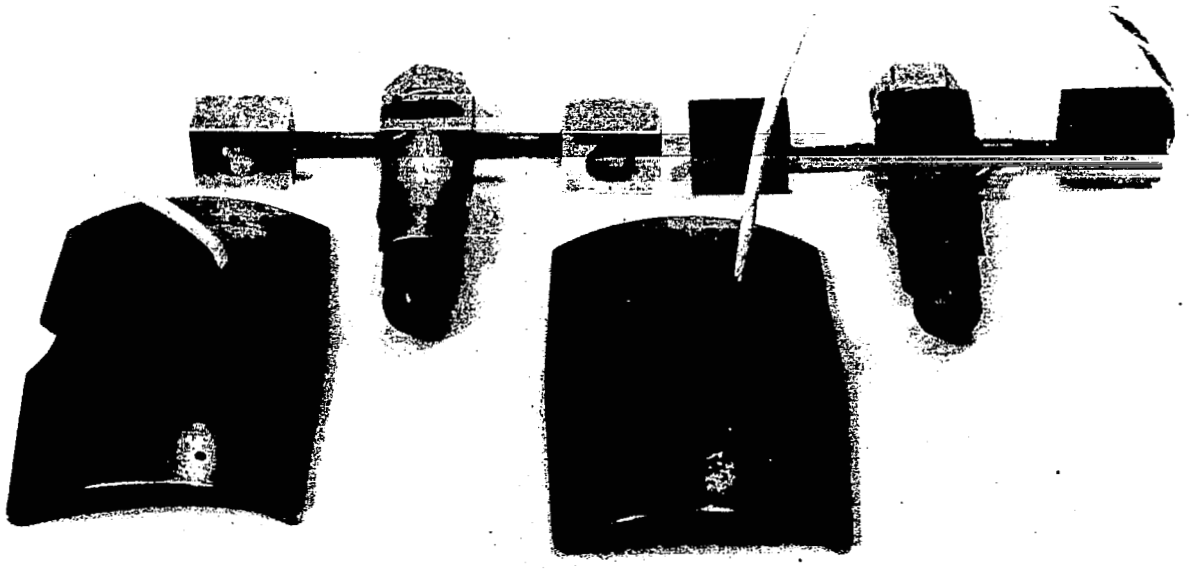

BEARING # 2 PAD # 1

BEARING # 2 PAD # 2

(a)

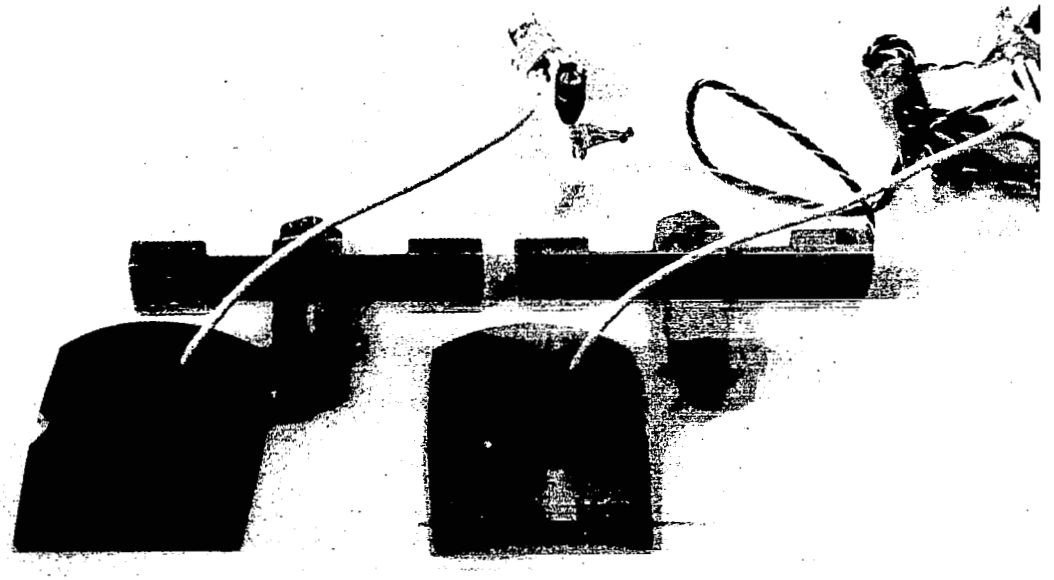

BEARING # 2 PAD # 4

BEARING # 2 PAD # 3

(b)

Fig. 86 Turbine Journal Bearing Pads, Rear View with Pivots, Inspection 5

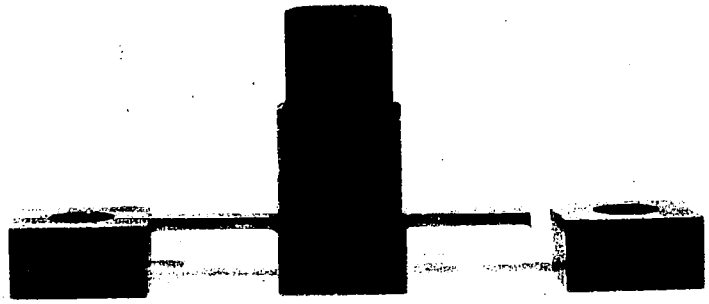

SIDE VIEW OF FRACTURED FLEXURE

A

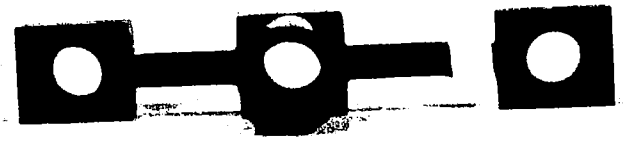

Fig. 87 Views of Fractured Flexure

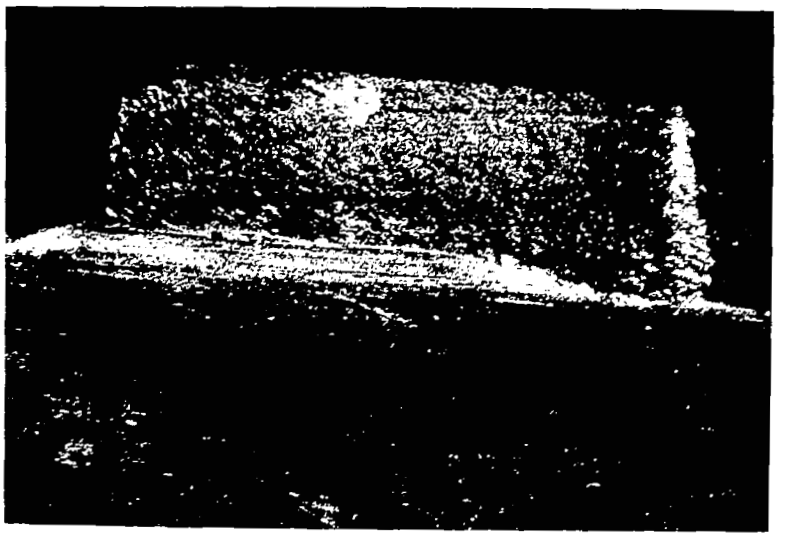

(a) Macro View - 2X

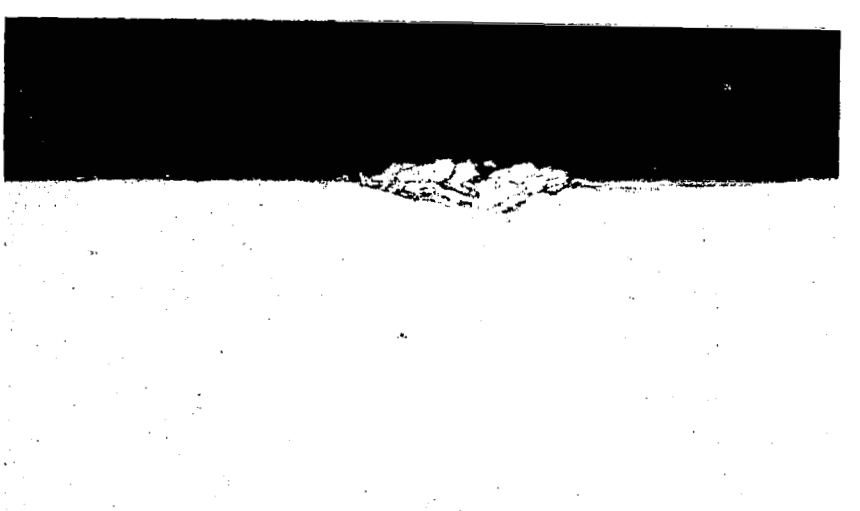

(b) Transverse View - 100X

Fig. 88 Magnified Views of Fractured Flexure Surfaces

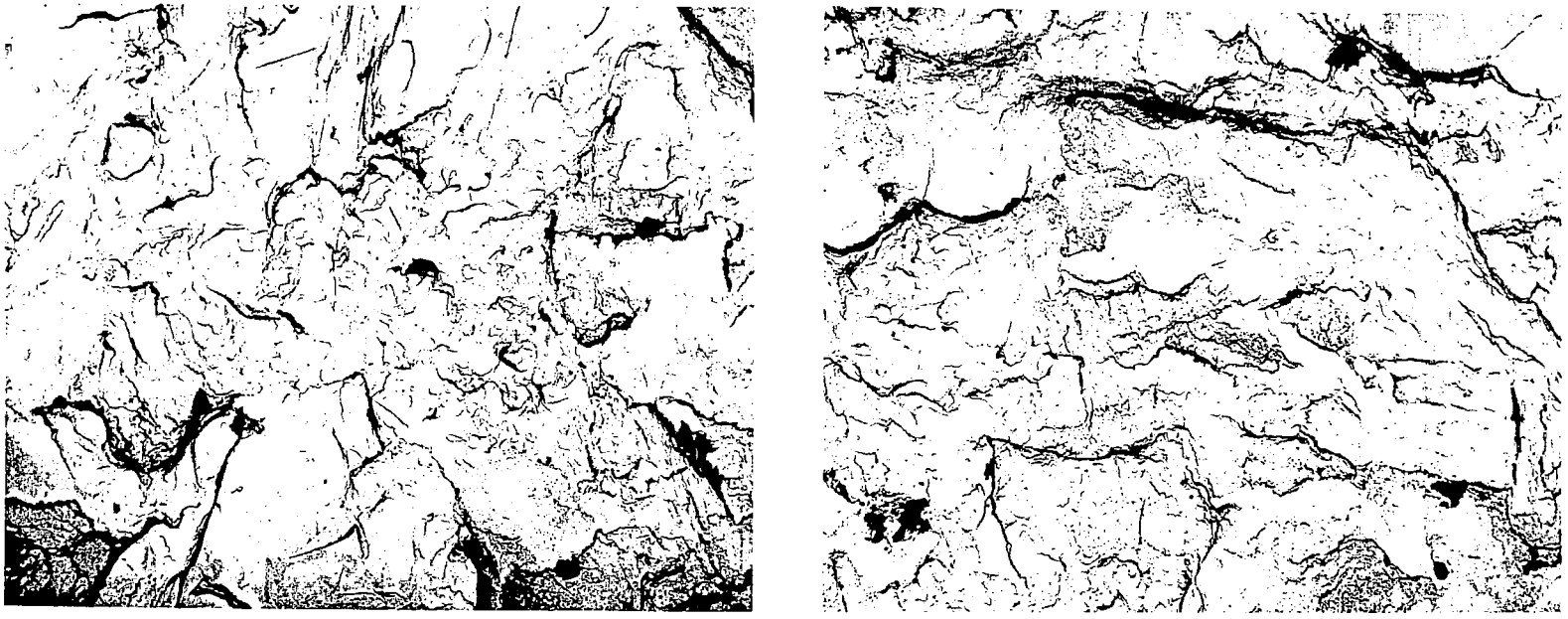

(a)

(b)

Fig. 89 Electron Micrographs of Fractured Surfaces, 6500X

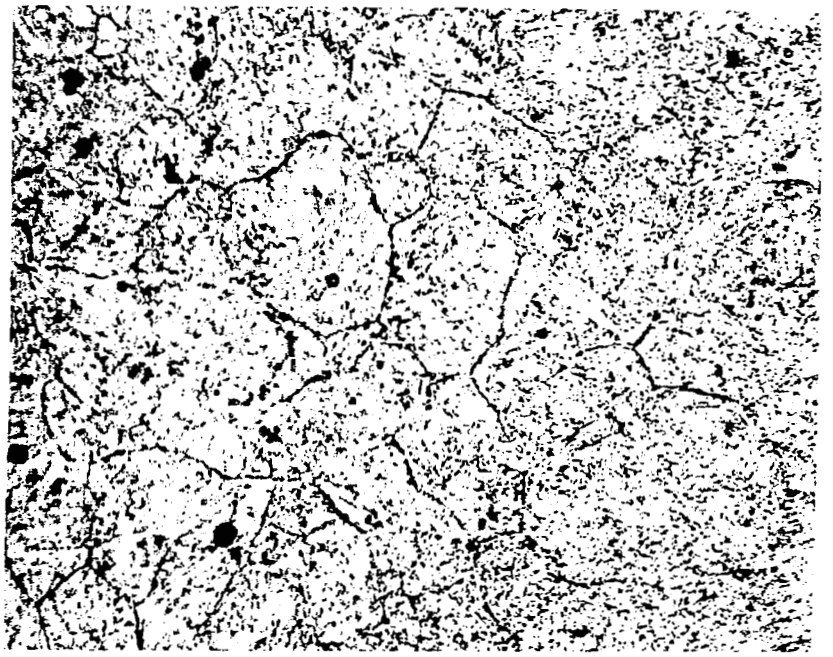

(a) Prior Austenitic Grain Size - Etchant 2% Picral - 1000X

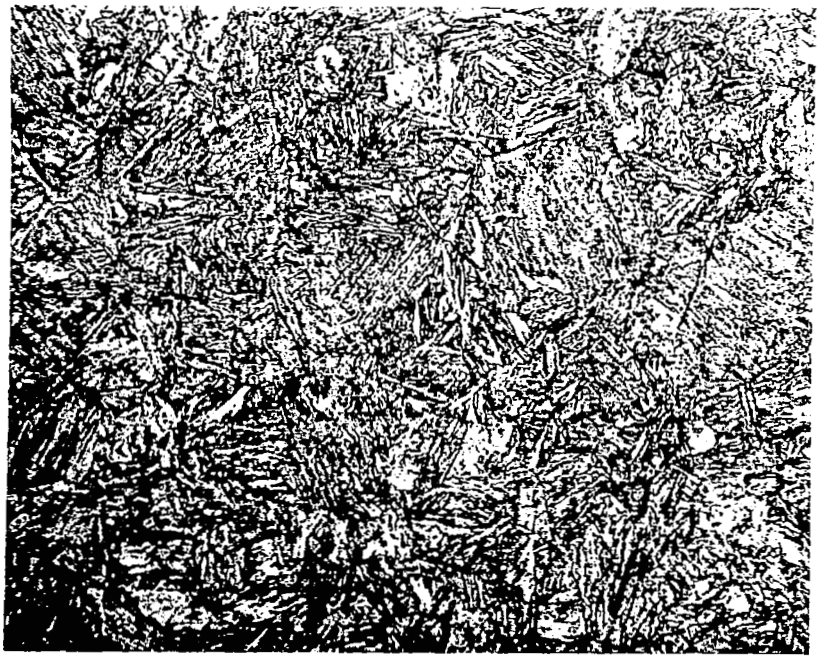

(b) Typical Microstructure - Etchant 2% Nital - 1000X

Fig. 90 Grain Structure Micrographs

NASA-Langley, 1971 —— 15 E-6160